Johannes Gutenberg-Universität Mainz
Institut für Biotechnologie und Wirkstoff-Forschung

IDENTIFICATION AND CHARACTERIZATION OF NOVEL FACTORS INVOLVED IN DIMORPHISM AND PATHOGENICITY OF FUNGAL WHEAT PATHOGEN *ZYMOSEPTORIA TRITICI*

Dissertation to attain the academic degree
Doctor Rerum Naturalium (Dr. rer. nat.)

at the Faculty of Biology,
Johannes Gutenberg University Mainz

submitted by

Alexander Yemelin
born on October 19th, 1986 in Nikolaev (Ukraine)

Mainz, April 2017

Johannes Gutenberg-Universität Mainz
Institut für Biotechnologie und Wirkstoff-Forschung

IDENTIFIZIERUNG UND CHARAKTERISIERUNG VON NEUEN DIMORPHISMUS- UND PATHOGENITÄTS-RELEVANTEN FAKTOREN IN *ZYMOSEPTORIA TRITICI*

Dissertation zur Erlangung des akademischen Grades
„Doktor der Naturwissenschaften“
(*doctor rerum naturalium*, Dr.rer.nat.)

am Fachbereich Biologie
der Johannes Gutenberg-Universität Mainz

vorgelegt von
Alexander Yemelin
geb. am 19.10.1986 in Nikolaev (Ukraine)

Mainz, April 2017

Hiermit erkläre ich, Alexander Yemelin, die vorliegende Arbeit ohne fremde Hilfe und nur unter Verwendung der angegebenen Hilfsmittel und Quellen angefertigt zu haben. Die Dissertation wurde in der jetzigen oder einer ähnlichen Form noch bei keiner anderen Hochschule eingereicht und hat noch keinen sonstigen Prüfungszwecken gedient.

Kaiserslautern, April 2017

X

Gewidmet meiner Familie

Table of contents

Summary

One of the main challenges for modern crop protection research is to minimize crop losses and to strengthen the food quality and security. Given the current trend, whereby the total area of cultivated land is decreasing year by year due to the rapid urbanization, minimizing the crop losses is an essential prerequisite to ensure the supply of the rapidly growing world population. A considerable part of devastating crop losses is attributed to phytopathogenic fungi. Therefore, for disease control and development of novel and ecologically compatible fungicides, it is essential to characterize and to understand the molecular basis of pathogenic differentiation processes in fungi.

In the current study *Zymoseptoria tritici* (teleomorph: *Mycosphaerella graminicola*) was used as a model organism, representing one of the most economically important fungal pathogens worldwide. This fungus causes *Septoria* blotch disease on wheat plants, responsible for massive crop losses every year. One of the characteristic features of this fungus is its ability to switch between two distinct growth forms, which can be induced by different environmental conditions. The fungus differentiates a yeast-like growth form, which is observed on nutrient-rich culture media. On the other hand, the fungus propagates in filamentous growth form, which is induced by nutrient deprivation or elevated temperature. The latter form is associated with pathogenicity, allowing the fungus to infect and colonize the host plant. A forward genetics approach was applied, aiming to investigate the molecular basis of the morphological transition of the wheat pathogenic fungus *Z. tritici*. A previously developed *Agrobacterium tumefaciens* mediated transformation protocol was used to generate a mutant library by insertional mutagenesis including more than 10000 random insertional transformants. A plate-based screening system was established, to identify mutant strains harbouring defects in dimorphic transition. Hence, with this approach eleven dimorphic switch deficient random mutants were recovered, ten of which exhibited a yeast-like mode of growth and one mutant predominantly growing filamentously, producing a high amount of mycelium under different incubation conditions. Sequence analysis of flanking regions for T-DNA insertions revealed potential candidate genes responsible for phenotypes observed. Relying on selection criteria defined, four transformants were characterized in detail. Three of them are non-pathogenic and one mutant exhibits a drastically impaired virulence within infection assays on whole wheat plants. Using genome walking, the T-DNA integration sites could be recovered, and the disrupted genomic loci of corresponding mutants were validated by reverse genetics approach. We present four functionally characterized genes involved in the dimorphic switch

of the fungal plant pathogen *Z. tritici*, yet not described in the literature. In addition, transcriptome analysis of selected mutant strains by RNA-Seq was performed to get first insight into regulons associated with the yeast-to-hyphal transition. The outcome of the RNA-Seq analysis provides a substantial list of target genes proposed to be implicated in regulation of dimorphic switch. Among the genes obtained, were those, whose role in the pathomorphogenic processes was previously established in other fungal pathogens. Moreover, making use of bioinformatic analysis, we also identified sets of differentially expressed genes previously not described and likely having unique role for dimorphic switch in *Z. tritici*. Based on these data, one further gene was characterized. This gene probably encodes an essential transcription factor, responsible for the coordination of meiotic division and spore formation. Based on results obtained from *in silico* analysis, its role for cellular processes in *Z. tritici* will be discussed.

Zusammenfassung

Eine der wichtigsten Herausforderungen für die moderne Pflanzenschutzforschung besteht darin, Ernteverluste zu minimieren und die Nahrungsqualität und -sicherheit zu gewährleisten. Bei gleichbleibend großer, bzw. kleiner werdender Anbaufläche ist die Minimierung von Ernteverlusten eine essentielle Voraussetzung, um die Versorgung der gleichzeitig stetig wachsenden Weltbevölkerung zu sichern. Ein Großteil der Ernteverluste, die durch biotische Faktoren hervorgerufen werden, ist auf die Schadenswirkung durch phytopathogene Pilze zurückzuführen. Daher, für einen nachhaltigen Pflanzenschutz und Entwicklung von neuen, ökologisch verträglichen Fungiziden, ist es unerlässlich die molekularen Grundlagen pathogener Differenzierungsprozesse in Pilzen zu charakterisieren.

Im Rahmen dieser Arbeit wurde *Zymoseptoria tritici* (teleomorph *Mycosphaerella graminicola*), als einer der wichtigsten Schadpilze im Getreideanbau, untersucht. Dieser Pilz verursacht *Septoria*-Blattdürrekrankheit an Weizen (*Septoria* blotch disease), welche jährlich massive Ernteausfälle zur Folge hat. Charakteristisches Merkmal dieses Pilzes ist seine Fähigkeit zur dimorphen Transition. Zum einen ist es die hefeähnliche Wachstumsform, welche man auf nährstoffreichen Kultivierungsmedien beobachtet. Zum anderen die filamentöse Wachstumsform, welche bei Nährstoffmangel induziert wird. Letztere ist mit der Pathogenität des Pilzes assoziiert und ist eine essentielle Voraussetzung für die erfolgreiche Infektion der Pflanze. Ein vorwärts-gerichteter genetischer Ansatz (*forward genetics*) wurde verwendet, um die molekulare Basis der morphologischen Transition zu untersuchen. Die zuvor entwickelte und etablierte *Agrobacterium tumefaciens*-vermittelte Transformation wurde verwendet, um eine Bibliothek mit über 10000 Transformanten durch eine insertionelle Mutagenese zu erzeugen. Desweiteren wurde ein plattenbasiertes Screening-System etabliert, das eine Identifizierung von Mutantenstämmen mit Defekten in der dimorphen Transition ermöglicht. Mit diesem Ansatz wurden elf „*dimorphic switch*“ defizienten Mutanten isoliert, von denen zehn durch ein hefeartiges Wachstum charakterisiert sind und eine Mutante, die überwiegend filamentös wächst und durch eine erhöhte Myzelformation unter verschiedenen Inkubationsbedingungen gekennzeichnet ist. Im Rahmen dieser Arbeit konnten vier Mutanten, die gemäß definierten Selektionskriterien ausgewählt wurden, im Detail charakterisiert werden. Drei von ihnen sind apathogen und eine Mutante zeichnet sich durch eine stark verminderte Virulenz gegenüber der Wirtspflanze aus. Mit dem bereits etablierten *genome walking* Ansatz konnten die T-DNA-Insertionsstellen im Genom der erzeugten *random* Mutanten lokalisiert werden. Die korrespondierenden Genloci wurden mittels gezielter

Inaktivierung der entsprechenden Gene validiert. Im Zuge dieser Arbeit werden somit vier funktionell charakterisierte Gene präsentiert, die eine wichtige Rolle in der Regulation der morphologischen Transition von *Z. tritici* spielen. Weiterhin wurde im Rahmen dieser Arbeit eine Transkriptom-Analyse mittels RNA-Seq mit ausgewählten Mutantenstämmen inklusive des Wildtypstammes unter der „*switch*"-induzierenden Kultivierungsbedingung durchgeführt, um einen tiefgehenden Einblick in die *dimorphic switch* assoziierte Prozesse zu gewinnen. Zusammen mit dem Ergebnis einer *gene enrichment* Analyse wird eine Liste von Dimorphismus-relevanten Genen präsentiert, die eine exzellente Basis für die weiterführende Untersuchung an diesem wichtigen pathogenitätsrelevanten Prozess darstellt. Gestützt auf die bioinformatische Analyse der RNA-Seq Daten wurde letztlich ein weiteres Gen charakterisiert. Dieses Gen kodiert vermutlich einen essentiellen Transkriptionsfaktor, der in anderen Pilzen für die Koordinierung von meiotischer Kernteilung und Sporenbildung zuständig ist. Basierend auf den Ergebnissen der durchgeführten *in silico* Analyse wird seine Rolle für zelluläre Prozesse in *Z. tritici* diskutiert.

List of Abbreviations

(standard abbreviations like „etc.“ or „e.g.“ are not listed)

Ø	diameter		**kbp**	kilobase pair
%	percent		**KO**	knockout
µg	microgram		**kV**	kilovolt
µl	microliter		**l**	liter
µF	microfarads		**LB**	lysogeny broth
Ω	ohm		**MAPK (-K,-KK)**	mitogen activated protein kinase (-kinase, -kinase kinase)
λ	wavelength		**MCS**	multiple cloning site
A	amp		**MM**	minimal medium
Amp	ampicillin		**ms**	millisecond
AIM	*Agrobacterium tumefaciens* induction medium		**MW**	molecular weight
A. t.	*Agrobacterium tumefaciens*		**N-deprivation**	nitrogen deprivation
ATP	adenosine triphosphate		**NCBI**	National Center of Biotechnology Information
BLAST	Basic Local Alignment Search Tool		**ng**	nanogram
bp	base pairs		**nm**	nanometre
°C	centigrade		**OD 600**	optical density, measured at a wavelength of 600 nm
cDNA	complementary DNA		**ORF**	Open reading frame
CM	complete medium		***p. a.***	pro analysis
CSPD	chloro-5-substituted adamantyl-1,2-dioxetane phosphate		**PCR**	polymerase chain reaction
DAG	Diacylglycerol		**PDA**	potato dextrose agar
DE	differentially expressed		**pH**	pondus hydrogenii
deion.	deionized		**qRT-PCR**	quantitative Real-Time PCR
DIG	digoxigenin		**Rif**	rifampicin
DMSO	dimethyl sulfoxide		**RIN**	RNA integrity number
DNA	deoxyribonucleic acid		**RNA**	ribonucleic acid
dNTPs	deoxynucleotide triphosphates		**ROS**	Reactive oxygen species
dpi	days post inoculation		**rev**	reverse
ds	double strand		**RT**	room temperature
EDTA	ethylenediaminetetraacetic acid		**SAP**	Shrink Alkaline Phosphatase
F	farads		**SDS**	sodium dodecyl sulfate
for	forward		**T_A**	annealing temperature
gDNA	genomic DNA		**TAE**	tris base, acetic acid and EDTA
h	hours		**t_E**	elongation time
HOG	High Osmolarity Glycerol		**Tris**	tris(hydroxymethyl)aminomethane
HPT* or *hph	Hygromycin B phosphotransferase gene		**UF**	ultrafiltered
Hyg	hygromycin		**rpm**	rounds per minute
IPTG	Isopropyl β-D-1-thiogalactopyranoside		**WT**	wildtype strain IPO323
Kana	kanamycine		**X-Gal**	5-Bromo-4-chloro-3-indolyl β-D-galactopyranoside

(Three-) and one-letter code of the proteinogenic amino acids according to (IUPAC) nomenclature

(Ala)	**A**	Alanine	**(Arg)**	**R**	Arginine
(Asn)	**N**	Asparagine	**(Asp)**	**D**	Aspartic acid
(Cys)	**C**	Cysteine	**(Glu)**	**E**	Glutamic acid
(Gln)	**Q**	Glutamine	**(Gly)**	**G**	Glycine
(His)	**H**	Histidine	**(Ile)**	**I**	Isoleucine
(Leu)	**L**	Leucine	**(Lys)**	**K**	Lysine
(Met)	**M**	Methionine	**(Phe)**	**F**	Phenylalanine
(Pro)	**P**	Proline	**(Ser)**	**S**	Serine
(Thr)	**T**	Threonine	**(Trp)**	**W**	Thryptophan
(Tyr)	**Y**	Tyrosine	**(Val)**	**V**	Valine

Letter code of the nucleotides/nucleobases* according to (IUPAC) nomenclature

A	Adenosine
C	Cytidine
G	Guanosine
T	Thymidine
U	Uracil
X or N	A, C, G or T

*that is, the letter code identifies the individual nucleobases. However, in this work this abbreviation is used as a synonym for nucleotides.

Explanation of the nomenclature

In the present work, the binomial nomenclature originally introduced by Linnaeus (1758) was used. The abbreviated names for genes, proteins and mutants were indicated as shown in the following example:

MYCO5	Indicates the gene from *Zymoseptoria tritici*, named *MYCO5*
Myco5p	Indicates the protein name of the corresponding gene *MYCO5*
Δmyco5	Indicates the *Z. tritici* mutant strain, which harbors an inactive gene locus *MYCO5* as result of targeted gene disruption by ATMT
Δmyco5/MYCO5	Indicates the complemented mutant *Δmyco5*, which was generated by random integration of native gene copy, including the endogenous/exogenous promoter and terminator region
IPO323::myco5-eGFP	Indicates the *Z. tritici* mutant strain, generated by integration of native gene copy fused to eGFP-encoding gene in translational in-frame manner
myco#5	Indicates the *Z. tritici* mutant strain, which was obtained from random mutagenesis program, suggested to be defective in the gene locus *MYCO5*

List of tables

List of figures

1. Introduction

1.1 General Introduction

Wheat represents one of the most important foods grain sources for the global world population. It is counted among the “big three” cereal crops, with over 700 million tons being harvested annually, along with maize (1,016 million tons) and rice (745 million tons) ("FAOStat", Retrieved 1 January 2016, Fayed *et al.*, 2015).

The widely used cultivation of wheat in the world and its popularity is particularly linked to its adaptability and high yield potential, but also to its rich nutrition value, providing an important source of essential amino acids, minerals, and vitamins.

Given the trend of the increasing world population, which according to expert estimates will probably exceed 7.9 billion people by the year 2025 (U.S. Census Bureau, “Total Midyear Population for the World: 1950-2050” International Data Base, 2010), the maintenance of sustainable food sources and their quality are of major importance (Floros, 2010). Supposing little or no change in world per caput consumption of wheat, a projection of 786 million tons of wheat will be required annually for human use in the year 2025. This underscores the need to rapidly and continuously increase production (www.fao.org). This situation, however, is further complicated by ever-smaller acreage for cultivation, particularly driven by the ever increasing urbanization tendency (McGranahan and Tacoli, 2006). To overcome these tendencies a development of various crop intensification programs are ongoing aiming to cover the supply and to ensure the food quality (Carswell, 1997). Nevertheless, the agricultural intensification is associated with negative side effects, resulting in increased susceptibility of crop plants against various pests. Furthermore, it has an adverse impact on the fertility of the soil, leading to the situation that the increase in the production rate can not constantly be maintained.

Plants face multiple stress factors throughout their life cycle which can reduce yield potential. Abiotic stress factors including drought, heat, cold, salinity of soil, nutrient stress and different weathering processes have a huge impact on world agriculture (Shrivastava *et al.*, 2015, Gill, 2013). For most major crop plants including wheat, they have been suggested in some cases to reduce the average yields by >50% (Wang *et al.*, 2003). Along with abiotic factors, the biotic factors have already become one of the most serious problems limiting the productivity of agricultural crops. Hence, plants must protect themselves from attack and invasion by a vast range of pathogens, including among others, fungi, bacteria and viruses (Hammond-Kosack and Jones, 2000). Plants implement a complex cellular and molecular

response system to withdraw these inducing stress factors and ensure survival, but often at the detriment of growth and yield (Herms and Mattson, 1992). The presence of abiotic stress can additionally have the effect of enhancing susceptibility to a biotic pest or pathogen, and *vice versa* (Atkinson and Urwin, 2012). Together, these effects reduce plant growth, development and survival (Carillo *et al.*, 2011).

For the wheat plants various pests come into consideration, wherein phytopathogenic fungi make a significant contribution to an emergence of the devastating diseases, resulting in significant losses of the global wheat production. Globally important fungal diseases of wheat are caused by obligate parasites, which include the three rusts (leaf rust, caused by *Puccinia triticina*, yellow rust caused by *Puccinia striiformis* and stem rust, caused by *Puccinia graminis*), powdery mildew (caused by *Blumeria graminis*) and bunts and smuts (caused by *Tilletia laevis* and *Tilletia tritici* respectively). Those caused by facultative parasites include leaf blotch (caused by *Zymoseptoria tritici*), glume blotch (caused by *Phaeosphaeria nodorum*, asexual form *Stagonospora nodorum*), spot blotch (caused by *Cochliobolus sativus*), tan spot (caused by *Pyrenophora tritici-repentis*) and scab (caused by *Fusarium graminearum*).

Zymoseptoria tritici, which causes *Septoria tritici* leaf blotch (STB), is a major threat to global wheat production. STB can decrease wheat yields by 50%. Reducing these losses would make it possible to meet the food demands of the rising human population (Berraies *et al.*, 2014). Numerous strategies have been developed in attempts to minimize the losses caused by plant pathogens. Traditional approaches rely on the prevention of sources of infection, vector management, modification of cultural practices, the use of resistant plant varieties obtained through conventional breeding, cross protection and chemical control (Maloy, 2005). While these methods have been successfully applied in some cases, indeed there is a need for new approaches. This is strengthened by the fact that some fungicides are being withdrawn from the market because of their undesirable effects on the environment (Soković *et al.*, 2013), whereas other are becoming ineffective due to increased emergence of fungicide-resistant isolates. New strategies for disease control are therefore urgently needed.

1.2 *Septoria* leaf blotch disease

Zymoseptoria tritici (teleomorph: *Mycosphaerella graminicola*, syn. *Septoria tritici*) is the causal agent of *Septoria* leaf blotch disease of wheat (STB). *Septoria* wheat diseases have increased in incidence over the last few decades despite the deployment of fungicide treatments and *Z. tritici* is consistently the most destructive foliar pathogen of wheat in

Europe (Jørgensen *et al.*, 1999, Hardwick *et al.*, 2001, Dean *et al.*, 2012, Jørgensen *et al.*, 2014). The economic impact of the disease is substantial since serious outbreaks result in significant crop losses (in disease-conductive climates up to 50%). Both, tetraploid durum wheat (*Triticum turgidum ssp. durum*) and hexaploid bread wheat (*Triticum aestivum*) are affected by the regularly occurring epidemics. In Europe for instance, annual losses from STB are estimated to be $400 million dollars, and similar losses are supposed for the US resulting in about $275 million dollars per year (Ponomarenko *et al.*, 2011). The increased prevalence of these diseases is considered to be due to the more frequent use of high yielding semi-dwarf rust-resistant cultivars, increased nitrogen application rates and changes to post-harvest practices (Bayles *et al.*, 1991, Kema *et al.*, 1996).

Economically the most serious threat results from infection of the top, second and third leaves which support head formation. The degree of tissue damage of the flag, the third and the second wheat leaves completely determines the potential of crop yield reduction (Shaw, Royle 1989, Shaw, Royle, 1993, Lovell *et al.*, 1997, Hunter *et al.*, 1999, Paveley, 1999, Palmer, Skinner, 2002). Although cultivars with improved resistance have been developed, their yield has to date not matched that of fungicide treated susceptible varieties and control of the disease by fungicide application (Arraiano *et al.*, 2001, Arraiano *et al.*, 2009, Orton *et al.*, 2011, van den Berg *et al.*, 2013). At the present crop protection management in terms to control the STB generally relies on host resistance, cultural practices and fungicides, such as azole fungicides (e.g. methyl benzimidazole carbamates (MBCs), demethylase inhibitors (DMIs)) or the quinone outside inhibitors (QoIs) commonly referred as strobilurins (Fraaije *et al.*, 2005, Cools and Fraaije, 2008, Torriani *et al.*, 2009, Leroux, Walker, 2011). However, the control of STB is complicated due to the extremely high levels of genetic variability/diversity of the *Z. tritici* populations enabling rapid adaptation and increased insensitivity to fungicides (Fraaije *et al.*, 2005, Stammler, Semar, 2011, Estep *et al.*, 2015). Given this trend towards the worrying resistance concerning these fungicides, there is a clear need for the development of novel plant protective agents to combat *Septoria* leaf blotch. Thus, understanding the molecular mechanisms involved in the virulence of *Z. tritici* on wheat appears essential in order to develop new plant protection strategies.

1.3 Infection cycle of *Zymoseptoria tritici* and some cytological aspects regarding infection-related morphogenesis

Z. tritici is known as a haploid, heterothallic ascomycete exhibiting (likely) a hemibiotrophic lifestyle. Taxonomically the fungus belongs to the kingdom Fungi, division *Ascomycota*,

subdivision *Pezizimycotina*, class *Dothideomycetes*, order *Capnodiales*, family *Mycosphaerellaceae* and the genus *Mycosphaerella*. The heterothallic property of the fungus, which characterizes the sexual reproduction, is linked to the presence of two cross-type idiomorphs (non-homologous alleles) at the mating type locus, which are termed MAT1-1 and MAT1-2 in analogy to many other fungi characterized (Turgeon, Yoder, 2000). The mentioned hemibiotrophic property of the fungus is, however, doubtful or at least questionable, since the fungus harbours a unique mode of stealth pathogenicity accompanied by a prolonged asymptomatic phase, also known as a latent phase (Hammond-Kosack, Rudd, 2008, Deller, 2011).

Under natural conditions, *Z. tritici* differentiates on the infected plants two types of fruiting bodies, pycnidia – bearing the asexual pycnidiospores and pseudothecia – representing the sexual reproduction organs by the formation of sexual ascospores (Figure 1).

Sexual ascospores are considered to be the primary means for the initiation of disease outbreak and are believed to be responsible for the epidemic spread of the fungus by anemochory crucial for distribution over long distances (several 100 km). Furthermore, the ascospores support the vertical gene transfer due to genetic recombination. As a consequence, this results in a high intra-population genetic variability and explains at the same time on a global scale a very similar genetic structure of isolates which were found in geographically distant regions. On the contrary, the asexual spores (pycnidiospores) may act as a secondary inoculum maintaining the spread of the disease in the field by rain splash dispersal, limited to a local area (Shaw, Royle, 1989).

The pathogenic development of *Z. tritici* can be divided into the following phases: (1) initiation of infection cycle by dimorphic switch, (2) entry of the fungus through stomata of the host plant, (3) colonization of the plant tissue and (4) formation of fruiting bodies (Figure 1; Ponomarenko, 2011, Steinberg, 2015).

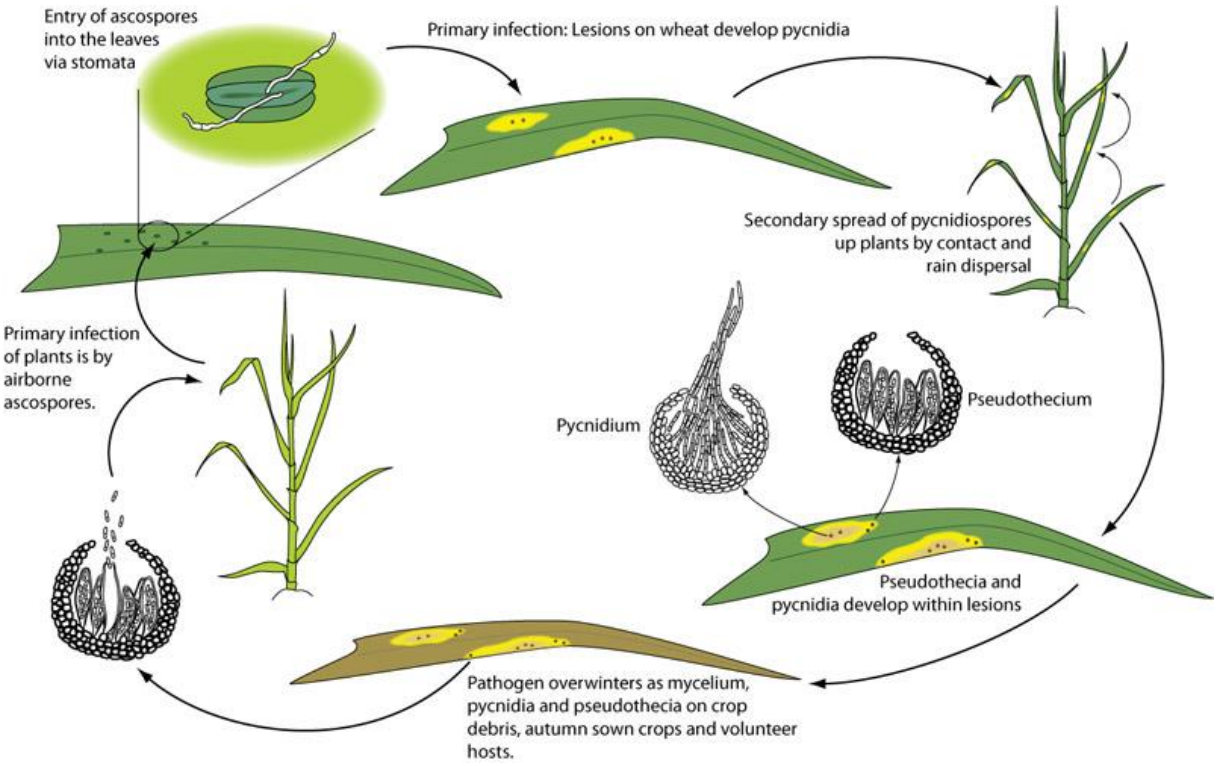

Figure 1: Infection cycle of *Z. tritici*. The figure gives an outline of central stages regarding the life cycle and infection process (adapted from Ponomarenko *et al.*, 2011).

The infection cycle is initiated by the germination of either pycnidiospores or ascospores, both of which have a pathogenic potential (Hilu and Bever, 1957, Eyal, 1987, Shipton *et al.*, 1971, Suffert *et al.*, 2013 and Morais *et al.*, 2015). They propagate on the plant leaf initially yeast-like or switch directly to hyphal growth, which is favored by nutrient deprivation condition and high relative humidity (Duncan and Howard, 2000 and Kema *et al.*, 1996). The ability of the fungus to perform the switch between two growth forms (yeast-like and filamentous), triggered by internal and/or external stimuli is referred in the literature as dimorphism, and the corresponding process as a dimorphic switch or dimorphic transition. Therefore, *Z. tritici* is considered as a dimorphic phytopathogenic fungus displaying an environmentally regulated morphogenetic transition between yeast-like and multicellular hyphal growth.

For the infection of the host plant, no specialized organs like appressoria are required, although in some cases appressoria-like thickenings of hyphae were observed (Duncan and Howard, 2000). The formation of hyphae enables the fungus to penetrate the host plant through natural openings like stomata directly. However, whether the invasion of stomata by the hyphae formed occurs randomly or as result of response to thigmotropic signal, yet unknown, remains questionable, since both scenarios were reported (Hilu, Bever, 1957, Kema *et al.*, 1996, Howard, Duncan, 2000, Shetty *et al.*, 2003).

Once the filamentous ascomycete has entered the host plant via stomata, it grows intercellular within the apoplast (Steinberg, 2015). Approximately 12-24 hours after infection of a susceptible host plant, the substomatal respiratory cavity is colonized, followed by further colonization of the palisade parenchyma and mesophyll cells (Duncan, Howard, 2000). This initial invasive colonization highlights a long latent biotrophic-like, apparently endophytic period, (Sanchez-Vallet *et al.*, 2015), which lasts depending on the susceptibility of the wheat varieties and weather conditions between 8-14 days. In the early colonization of mesophyll tissue, the biomass does not increase significantly (Kema *et al.*, 1996, Shetty *et al.*, 2003, Palmer, Skinner, 2002) and no visible symptoms of the disease are evident.

It is believed that at this stage all necessary nutrients for growth are obtained from the plant without inducing the elicitor-mediated defense mechanisms of the host. However, no feeding structures like haustories or arbuscules, mediating the uptake of nutrients or responsible for plant-pathogen communication, were observed. Along with another hypothesis, the internal nutrient storage of the fungus, such as neutral lipids and fatty acids, are used providing the fungus with required energy (Rudd, 2015). Although the plant-pathogen interaction has not been fully elucidated, recent investigations of the asymptomatic phase indicate that during the prolonged latent growth phase the fungus does not influence the host growth. This observation casts doubt on the biotrophic nature of the asymptomatic period, thereby leading to a suggestion that this organism might be a necrotrophic pathogen with a strongly delayed symptomless phase (Sánchez-Vallet *et al.*, 2015, McDonald *et al.*, 2015).

After the latent phase, the compatible interaction is initiated with a transition from the biotrophic to necrotrophic phase, induced by yet unknown trigger signals. Consequently, it comes to a sudden collapse of mesophyll tissue in the susceptible host plant, accompanied by the release of cell contents as a result of the disturbed cell wall and cell membrane integrity. This manifests first in the formation of chlorotic spots on the leaf surface, some days later, it comes to the augmented necrosis of plant cells. The leaf spots “flow” together to irregularly shaped necrosis flecks (Figure 2A). The whole process is highly reminiscent of programmed cell death, coinciding with the translocation of cytochrome c (Cyt c) from the mitochondria and RNA/DNA degradation. This allows the fungus a rapid proliferation and differentiation, which at this stage results in the detectable increase of biomass (Kema *et al.*, 1996, Duncan and Howard, 2000). In the further course of infection, it comes to a secondary colonization of the entire plant tissue, which consequently results in the formation of new pycnidia from substomatal respiratory cavities (Kema *et al.*, 1996, Figure 2B,C). The pycnidia formed differentiate mature pycnidiospores that are released by the extrusion of mucilage (cirrus)

through the stomata (Orton, 2011). The pseudothecia, in the case of a sexual reproductive cycle, were observed to be formed exclusively on the dead plant tissue and the period between the formation of pycnidia and development of mature pseudothecia can encompass several months (Hunter *et al.*, 1999).

The rapid development of necrotic spots on the leaves suggests a participation of phytotoxic secondary metabolite of the fungus (Cohen, Eyal, 1993, Kema *et al.*, 1996). However, this presumption remains elusive because to date no phytotoxin from the cultures of *Zymoseptoria tritici* could be isolated.

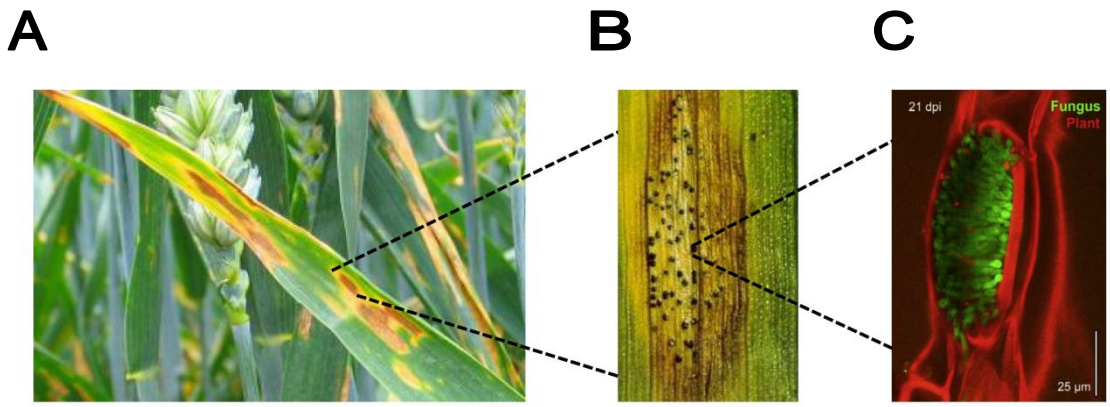

Figure 2: Development of visible disease symptoms on susceptible wheat plant infected with *Zymoseptoria tritici*. Beginning at 14 dpi necrotic lesions (A) appear on the susceptible wheat cultivar, leading in the following course of pathogenic development of *Z. tritici* to development of mature pycnidia (B). In (C) a single pycnidium is shown using confocal fluorescent microscopy; it harbours asexual pycnidiospores expressing the cytosolic eGFP. Propidium iodid was used to visualize the plant structures (adapted from Fones *et al.*, 2015).

Generally, the disease dynamics of *Z. tritici* in plant populations is essentially determined by temperature and the humidity period after infection (Shipton *et al.*, 1971). Moderate temperature of 11-25 °C but also a high relative humidity (near 100%), within the next 96 hours after the infection, positively affect the pathogenic development of *Z. tritici* (Eyal, 1987, Chungu *et al.*, 2001). There is also evidence that high light intensity reduces the probability of a successful infection, but promotes the pathogenic development *in planta* in late stages of pathogenesis (Shaw, 1991).

1.4 *Zymoseptoria tritici* as a model organism

Owing to its infection-related morphogenesis considering the dimorphic transition and due to its delayed biotrophic-like phase, the fungus has become a model organism and an important pathosystem for the study of the principles of plant-pathogen interactions in the phytopathogenic fungi. This is also favored by a number of further features that take into

account both biological and methodological aspects. Since the fungus is not an obligate fungal pathogen and doesn't couple its whole life cycle on the presence of the living host plant, its cultivation can be easily performed by *in vitro* propagation on artificial media, making its explorative investigation feasible. *Z. tritici* is considered as a dimorphic plant fungal pathogen displaying an environmentally regulated morphogenetic transition between unicellular yeast-like and multicellular hyphal growth, which seems to be essential for pathogenicity. The dimorphic yeast-to-hyphal conversion can be induced *in vitro* by incubating the fungal culture on starvation medium (like water agar or nitrogen deprivation medium) (Mehrabi *et al.*, 2006). Additionally, different experimental strains are available that are resistant to various classes of fungicides due to natural mutations and genomic plasticity. In fact, the fungus provides a powerful platform for population genetic studies, genome evolution and host specialization. A vast progress was achieved in understanding the evolutionary trends associated with the speciation and host plant adaptation making extensive use of comparative genomics (Stukenbrock *et al.*, 2011). These studies have been facilitated by the presence of genomic reference sequence available for *Z. tritici* isolate IPO323. The genome was completely sequenced in 2008, providing an essential prerequisite for more intensive applications in molecular biology. The currently available genome annotations are provided by JGI (10,933 genes), Rothamsted Research (10,688 genes) and Max Planck Institute (11,839 genes), and the predicted gene models are becoming assessed and improved by community-based curation approach. The genome contains 21 chromosomes and has a total size of 39.7 Mb, which makes this fungus having the highest number of chromosomes among the Ascomycetes. Noteworthy, the striking feature of the genome is given by the presence of a large number of dispensable chromosomes (up to eight, depending on isolate), considered to be not essential for the survival and reproduction (Goodwin *et al.*, 2011). The remaining 13 chromosomes form the so-called nuclear core chromosomes.

Techniques for genetic transformation and *KU70* disruption strains are available, resulting in frequencies of homologous recombination of transformants about 95% with no obvious effects on wildtype growth (Bowler *et al.*, 2010). This facilitates the high-throughput transformation approaches and makes the functional analysis of genes more efficient. The availability of established transformation methods, both protoplast-mediated as well as *Agrobacterium*-mediated, genome re-sequencing and improved genome annotations, facilitate both forwards and reverse genetics screens aiming to identify and functionally characterize virulence related genes (Rudd *et al.*, 2015). Recently several molecular fluorescent markers have been established, and cellular processes can be now studied, by monitoring the

organization and dynamic behavior of the microtubule cytoskeleton (Schuster *et al.*, 2015, Kilaru *et al.*, 2015).

Furthermore, the vast research progress in the understanding of *Z. tritici* biology is reinforced by the emergence and in-depth analysis of recently produced big "omics" datasets, from approaches such as RNA sequencing, comprehensive proteome and metabolome profiling studies (Lee, Rudd, Kanyuka, 2015). Given the trend by the attempts to integrate these "omics" datasets, these studies are beginning to provide potential candidate genes with crucial roles in STB disease establishment (Yang *et al.*, 2013, Kellner, 2014, Rudd *et al.*, 2015).

1.5 Known virulence factors in *Zymoseptoria tritici* and current studies

Despite the economic importance of *Z. tritici*, the molecular basis regarding the pathogenic differentiation, *in planta* growth and development has not been investigated in large detail. The remaining paucity regarding the molecular-genetic basis of pathogenicity-related determinants makes particularly the use of next generation sequencing (NGS) technologies, proteomics and metabolomics required to gain insight into different stages of the infection cycle, in order to determine novel directions and strategies for the disease control. Taking advantage of the techniques and tools developed in recent years, encompassing biochemistry, molecular and cellular biology we got a sophisticated broad arsenal of biological approaches in order to more precisely investigate the plant-pathogen interaction and pathogen-related morphogenesis of the fungus (Kilaru and Steinberg, 2015, Sidhu *et al.*, 2015).

Recent investigations by the extensive use of RNA-Seq are beginning to deliver a profound insight into the regulatory processes governing plant-pathogen interaction during the infection process. Yang *et al.*, 2013 created recently by means of dual RNA-Seq expression profiles of both *Z. tritici* IPO323 and the susceptible host plant (*Triticum aestivum*) comprising distinct phases (4, 10 and 13 days after infection) of infection course. Other findings came with the RNA-Seq study presented by Kellner *et al.*, 2014 focussing on the comparative analysis of transcriptomes derived from host and nonhost plant (*Brachypodium distachyon*) infected with reference strain IPO323. More recently Rudd *et al.*, 2015 presented a comparative transcriptome analysis using RNA-Seq spanning the entire time course of infection by comparing four *Z. tritici* strains with different levels of virulence isolated from the same field. Analysis of the transcriptional profiles revealed along with major, conserved components of infection also some heterogeneity, as several genes exhibited strongly differentiated transcriptional patterns, suggesting a considerable variation in virulence and host

specialization. Furthermore, the ongoing bioinformatic approaches make a significant contribution to understanding of the pathogenic development of *Z. tritici* by employing of structural genomic analysis of the fungus, at the same time complementing and integrating the data obtained from biochemical, histological and finally "omics" technologies. Thus, Morais do Amaral *et al.*, 2012, has provided a genome wide *in silico* analysis of secretome from *Z. tritici*, unveiling the genomic repertoire of predicted effectors and other secreted proteins suggested to function as CWDEs. Subsequent genomic comparison to other fungi harboring different lifestyles revealed exciting key features of *Z. tritici* expanding our understanding regarding the pathogenic mode of infection.

To date only a few genes encoding virulence factors have been functionally characterized. Most of them were analyzed one-by-one using reverse genetics before the genome sequence was published and they encode components of conserved signaling pathways, such as MAPK- or cAMP pathway predominantly. Figure 3 provides an overview of some major factors previously characterized regulating distinct phase transitions within infection cycle of *Z. tritici*. A complete list giving an overview of hitherto characterized genes including references is offered in Table 1 (Rudd, 2015). In the following some examples highlight the importance of these components:

For fungi, including phytopathogenic representatives, conserved signaling pathways, primarily mediated by mitogen-activated protein kinases (MAP kinases) and protein kinase A, are of major importance considering their involvement in growth, morphological development and pathogenicity related processes (Xu, 2000, Zhao *et al.*, 2007, Hamel *et al.*, 2012). In fact, the components of such conserved signaling pathways have been previously shown to have essential functions for differentiation associated processes and pathogenicity in *Z. tritici* (Kramer *et al.*, 2009).

For instance, the gene *ZtHOG1* (previously published as *MgHOG1*) encodes the MAP kinase ZtHog1p, an ortholog of the gene *HOG1* from *Saccharomyces cerevisiae*, originally found to be implicated in the regulation of osmotic stress response. *ΔZthog1* mutant (formerly published as *Δmghog1*) was previously shown to be impaired in dimorphic transition (Figure 3). The mutant is non-pathogenic, and grows on the dimorphism-inducing solid media exclusively yeast-like (Mehrabi *et al.*, 2006).

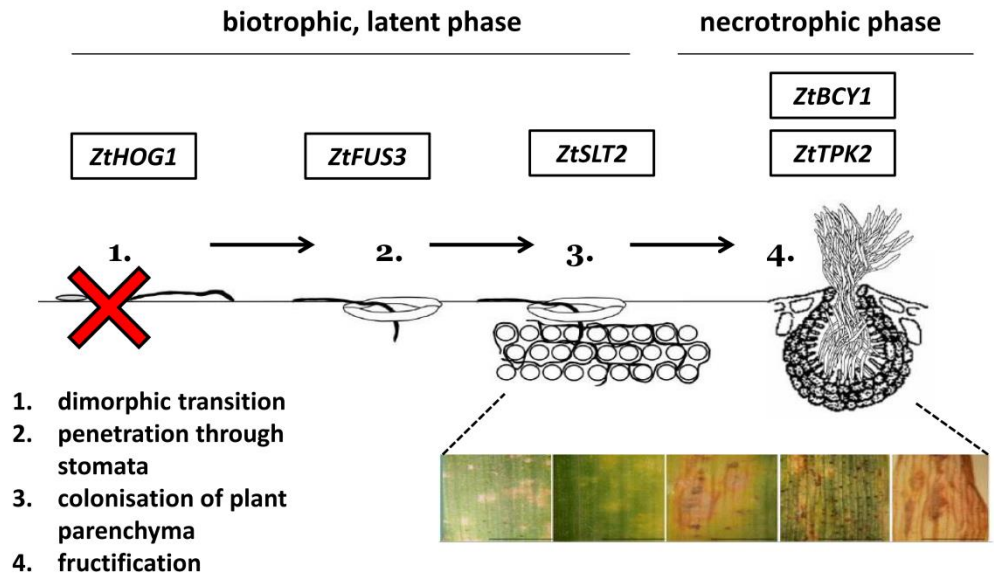

Figure 3: Distinct phases of infection cycle, characterizing the pathogenic development of *Z. tritici*. Genes encoding virulence factors previously found to be implicated in the pathogenic development of *Z. tritici* are assigned to the corresponding developmental phase (modified after Mehrabi *et al.*, 2006 and O'Driscoll *et al.*, 2015). The red cross indicates the environmentally regulated yeast-to-hyphal transition, which is essential for *Z. tritici* pathogenicity.

Generally, genetic determinants underlying dimorphic switch in *Z. tritici* are of particular interest for the plant protection research. Since filamentous growth promotes pathogenic proliferation of the fungus, *ZtHOG1* can indeed be regarded as pathogenicity factor, which is responsible for the regulation of dimorphism in *Z. tritici*. Interestingly, *ZtHOG1* is highly conserved and orthologous genes are present in a number of other phytopathogenic fungi, e.g. *Magnaporthe oryzae*, *Colletotrichum lagenarium* or *Bipolaris oryzae*. However, for most of them dimorphism does not represent a pathogenicity related factor as far as the corresponding loss-of-function mutants are pathogenic (Dixon *et al.*, 1999, Kojima *et al.*, 2004, Moriwaki *et al.*, 2006). This observation implies that ZtHog1p is essential for dimorphic differentiation, while the protein has no pathogenicity related importance for fungi with a non-dimorphic life-style.

Another pathway being involved in dimorphic transition is linked to cAMP - protein kinase A -mediated signal transduction. Mehrabi *et al.*, 2006 analyzed components of this pathway by targeted inactivation of genes encoding the catalytic subunit ZtTpk2p (formerly known as MgTpk2p) and the regulatory subunit ZtBcy1p (MgBcy1p) of the protein kinase A (Mehrabi *et al.*, 2006). ZtTpk2p was found to have an important function in regulation of mycelial growth since the corresponding gene deletion mutant failed to perform dimorphic transition on potato dextrose medium. On water agar medium, however, which is suggested to mimic natural conditions of nutrient deprivation found on the leaf surface, the filamentous growth

was observed. *ZtTPK2* defective mutant is able to penetrate the host plant through the stomata and colonize the mesophyll. However, the mutant strain displays reduced virulence and is unable to differentiate pycnidia after the latent period of infection.

Furthermore, the role of heterotrimeric G proteins and cAMP in the framework of the same pathway was observed concerning to dimorphism and pathogenicity associated processes in *Z. tritici* (Mehrabi *et al.*, 2009). Three genes were previously identified encoding G alpha-subunits (ZtGpa1p, ZtGpa2p and ZtGpa3p) and one gene encoding Gβ (ZtGpb1p) (formerly published as MgGpa1p, MgGpa2p, MgGpa3p and MgGpb1p respectively). *ZtGPA1* was found to be implicated in negative regulation of the mycelial growth since the corresponding mutant *ΔZtgpa1* formed spores with an altered morphology. When incubated on yeast glucose broth and potato dextrose solid media the mutant differentiated significantly longer spores in contrast to that of the wildtype strain IPO323. The mutant strain *ΔZtgpa3* exhibits also a clearly pronounced phenotype, forming short germ tubes without secondary or tertiary filaments. For the *ZtGPB1* and *ZtGPA3* defective mutants, a reduced intracellular concentration of cAMP was measured, indicating that products of both genes positively regulate the cAMP concentration. In all cases, the virulence of corresponding mutants was significantly reduced (Mehrabi *et al.*, 2009).

Another factor of pathogenicity, the gene *ZtSLT2* (previously published as *MgSLT2*) was previously identified, a homolog of which is known to encode a MAP kinase required for cell wall integrity in *S. cerevisiae* (Mehrabi *et al.*, 2006). Interestingly, the mutant strains disrupted in this gene were not affected in filamentation. Moreover, they were able to penetrate the host plant through stomata and to colonize the substomatal cavities. However, the mutant strains were prevented in branching and failed to colonize the mesophyll of the host plant in the course of infection, resulting in reduced virulence and lack of pycnidia formation. A similar phenotype was noticed for stains defective in gene *ZtSTE12* (previously published as *MgSTE12*, Kramer *et al.*, 2009), known to encode a transcription factor with implication in regulation of filamentous growth.

Finally, a MAP kinase encoded by *ZtFUS3* (published as *MgFUS3*) was previously characterized, being a *Saccharomyces cerevisiae* mitogen-activated protein (MAP) kinase homolog (Cousin *et al.*, 2006). Interestingly, *ΔZtfus3* mutants don't display in the early stage of their development any notable differences compared to the wildtype strain IPO323. In the late stage, however, a limited growth is apparent. Furthermore, the melanin biosynthesis is inhibited; the mutants exhibit a disoriented growth and fail to form aerial mycelium. In addition, the mutants are non-pathogenic, since the ability to penetrate leaves through the

stomata is no longer observed. As a consequence, the formation of pycnidia is disturbed, making ZtFus3p a multifunctional pathogenicity factor in *Z. tritici* (Cousin *et al.*, 2006). Targeted inactivation of *ZtSTE11* and *ZtSTE7* (previously published as *MgSTE11* and *MgSTE7*) encoding MAPKKK and MAPKK respectively, also resulted in impaired filamentous growth leading to reduced virulence, since the corresponding gene deletion mutants were likewise unable to colonize the host plant (Cousin *et al.*, 2006, Kramer *et al.*, 2009).

Table 1: Functionally characterized pathogenicity/virulence genes of *Zymoseptoria tritici* (modified after Rudd, 2015)

Gene name	Description	Reference
MgAtr4	ABC Transporter	(Stergiopoulos *et al.*, 2003)
MgFus3	Mitogen-activated protein kinase (MAPK)	(Mehrabi *et al.*, 2006)
MgSlt2	MAPK	(Mehrabi *et al.*, 2006a)
MgHog1	MAPK	(Mehrabi *et al.*, 2006b)
MgTpk2	Protein kinase A catalytic subunit	(Mehrabi and Kema, 2006)
MgBcy1	Protein kinase A regulatory subunit	(Mehrabi and Kema, 2006)
MgSTE11	MAPK kinase kinase	(Kramer *et al.*, 2009)
MgSTE50	Scaffold protein for MAPK signaling	(Kramer *et al.*, 2009)
MgSTE12	Transcription factor target of MAPK signaling	(Kramer *et al.*, 2009)
MgSTE7	MAPK kinase	(Kramer *et al.*, 2009)
MgGpa1	G-protein alpha subunit	(Mehrabi *et al.*, 2009)
MgGpa3	G-protein alpha subunit	(Mehrabi *et al.*, 2009)
MgGpb1	G-protein beta subunit	(Mehrabi *et al.*, 2009)
MgAlg2	Protein N-glycosylation	(Motteram *et al.*, 2011)
Mg3LysM	Chitin binding effector protein	(Marshall *et al.*, 2011)
MCC1	c-type cyclin	(Choi and Goodwin, 2011)
ZtWor1	Transcription factor	(Mirzadi Gohari *et al.*, 2014)
Zt80707	Unknown/Secreted	(Poppe *et al.*, 2015)
Zt89160	Unknown	(Poppe *et al.*, 2015)
Zt103264	Unknown	(Poppe *et al.*, 2015)

1.6 Dimorphism as pathogenicity-relevant process

Per definition, dimorphism refers to the ability of certain fungi to switch between unicellular yeast and multicellular filamentous growth forms in a reversible manner in response to changing environmental cues (Boyce, 2015). Dimorphism is primarily regarded as a dynamic process regulated by diverse environmental factors. The nature of these signals and the underlying regulatory mechanisms for morphogenic transition are very complex and can be regarded as a result of evolutionary adaptation processes in fungi with respect to the environmental niches they occupy (Nadal, 2008). The ability of pathogenic fungi to alter morphology during their life cycle is widespread (Gauthier, 2015). As already mentioned, *Z. tritici* is considered as a dimorphic organism that exhibits both yeast-like growth,

characterized by a budding-like mode of propagation, and mycelial form, which is required for pathogenicity (Mehrabi, 2006). However, the ability to perform morphological transition upon environmental triggers is not only restricted to this fungus. Other representatives of phytopathogenic fungi belonging to different genera are also characterized by a dimorphic growth behavior. They include for instance the hemibiotrophic fungus *Colletotrichum graminicola*, the causal agent of maize anthracnose or a basidiomycete *Ustilago maydis*, a plant pathogenic fungus responsible for corn smut. Finally, there is a range of so-called systemic dimorphic fungi, which mainly exhibit a temperature-induced phase transition and are important representatives of human pathogens. Unlike for phytopathogenic representatives, the temperature-induced transition for systemic dimorphic fungi is associated with establishment of the pathogenic yeast-like growth form, enabling systemic circulation within the bloodstream in mammals. Hence, these animal/human-pathogenic fungi exist in soil as saprobic mycelia and switch to yeast-like blastoconidial propagation when the spores are inhaled into the respiratory tract. In this case, the dimorphic switch is triggered by the temperature change experienced when moving from soil (25 °C) to host (37 °C) (Nadal *et al.*, 2008). This well-defined group of phylogenetically related mammalian pathogenic ascomycetes and basidiomycetes includes e.g. *Candida albicans*, *Histoplasma capsulatum*, *Paracoccidioides bransiliensis*, *Blastomyces dermatitidis*, *Coccidioides immitis*, *Aspergillus fumigatus*, and *Cryptococcus neoformans*. Worth mentioning in this context is the fact that distinct states of growth underlying dimorphism comprise not only yeast-like or mycelium form, but rather include other growth forms resulting in pleomorphism or polymorphism under certain conditions. The pleomorphism is characteristic for *C. albicans*, which exhibits along with the blastoconidic mode of propagation also a pseudohyphal and hyphal growth form (Sanchez-Martinez, Perez-Martin, 2001). In general terms, the ability to polymorphic development is an essential virulence factor of these human-pathogenic fungi and enables an optimal adaptation within the course of infection (Nemecek *et al.*, 2006, Klein, Tebbets, 2007). Dimorphism has often been defined as a reversible process (Romano, 1966). However, the reversibility holds true not for all dimorphic fungi. For some of them, like *U. maydis*, regaining of particular growth form requires mating process and completion of the life cycle, thus implying a link between a sexual development and virulence (Madhani, Fink, 1998, Nadal, 2008). Changes in the environment usually lead to a generation of a wide variety of detectable external/internal signals. Dimorphic fungi perceive these stimuli and undergo morphogenic transition, depending on nature of these signals as a kind of adaptation in response to changing conditions. The nature and intensity of these signals vary among the

fungal species (Nadal, 2008, Gauthier, 2015). Relying on various studies provided (mainly considering research on *S. cerevisiae* and *C. albicans*), some of the core inductive factors promoting morphogenic transition are determined by pH, temperature, cell density (quorum sensing), oxygen partial pressure and nutrient deprivation (Buffo *et al.*, 1984, Maresca, Kobayashi, 1989, Orlowski, 1991). For instance, temperature increase to 37 °C as well as addition of N-acetylglucosamine or a proline to incubation medium induce hyphal growth of *C. albicans*. Likewise, an acidic culture milieu (pH < 6.5) or cultivation under hypoxic conditions also promotes morphogenic transition towards the filamentous growth (Fonzi, 2002, Klengel *et al.*, 2005, Biswas *et al.*, 2007). An enormous progress in understanding the molecular basis of dimorphism has been achieved with the aid of reverse and forward genetics studies. However, most of molecular determinants involved in dimorphism identified so far rely on *S. cerevisiae*, which exhibits conidial propagation through budding process and pseudohyphal growth upon e.g. nitrogen deprivation. Among the fungal pathogens exhibiting true hyphal growth, *C. albicans* and *H. capsulatum* represent the best-studied pathosystems with respect to dimorphism research.

Despite the great diversity of trigger signals that induce dimorphic transition, the signaling pathways governing dimorphic (pathogenic) development, like MAP kinase- and cAMP-mediated signaling cascades, have been highly conserved in dimorphic fungi (Nadal, 2008). Inactivation of central components of these systems results in pleiotropic effects in the resulting mutants. For instance, *C. albicans*, *S. cerevisiae* and *U. maydis* employ the same signal transduction pathway, the cAMP–PKA pathway, to respond to similar environmental conditions like nutrient deprivation. However, they harbor different morphological outcomes – filamentous growth in *C. albicans*, pseudohyphal growth in *S. cerevisiae* and budding growth in *U. maydis*. On the one hand, this suggests a conservation of signaling pathways. On the other hand, the morphological variety observed underpins the diversity of downstream regulators like transcriptions factors, which can be seen as a result of evolving adaptation processes of these fungi to different environmental conditions underlying their lifestyles.

The perception of external trigger signals is primarily based on the two-component systems (histidine kinases) and heterotrimeric G-protein mediating systems, leading to activation of either cAMP-signaling pathways or downstream mitogen-activated protein kinase (MAPK) signaling cascades. There is also evidence that a "cross-talk" between cAMP and MAPK signaling pathways seems to be essential for a correct pathogenicity related morphogenesis (Hamer and Talbot, 1998, Gold *et al.*, 1994, Kruger *et al.*, 1998, Mayorga and Gold, 1999,

Kahmann *et al.*, 1999, Leberer *et al.*, 2001). In the following some examples are given to illustrate these relationships:

Previously, a hybrid histidine kinase DRK1p has been discovered, which was shown to control the shift from a non-pathogenic filamentous form to a pathogenic yeast form in dimorphic fungi (Nemecek *et al.*, 2006). It was found to function as a global regulator of dimorphism and virulence in *B. dermatitidis* and *H. capsulatum*, regulating phase transition from mycelium to yeast, expression of virulence genes, and pathogenicity *in vivo*. Disruption of *DRK1* locks the filamentous form at temperature that normally induces the phase transition to yeast-like growth form (37 °C). Furthermore, deletion of the corresponding gene causes severe alterations in the cell wall and leads to the reduced transcription of α-(1,3)-glucan synthase encoding gene (Gauthier, Klein, 2008). In *H. capsulatum*, DRK1p was found to regulate the expression of the yeast-phase specific genes *CBP1*, *AGS1* and *YPS-3*. In addition to *DRK1*, transcription factors RYP1-4p (required for yeast phase) in *H. capsulatum* promote the transition to yeast. Knockdown of *RYP1-4* induces hyphal growth at 37 °C and impaires transcription of yeast-phase related genes critical for virulence.

The molecular basis of dimorphism in *Z. tritici* is not well understood and is limited with some exceptions to the genes mentioned in previous chapter, considering the general components of signal transduction pathways, such as MAP kinases, cAMP pathway and G-proteins representing the upstream components of these signaling systems. The dimorphic transition in *Z. tritici* can be mimicked *in vitro* (Figure 4), by transferring the culture from a nutrient-rich medium, promoting yeast-like growth, to a nitrogen deprivation medium that induces a filamentous growth (Mehrabi, Kema, 2006).

Several additional factors implicated in dimorphic switch were previously identified by reverse genetics studies in *Z. tritici*. Thus, inactivation of the cyclin-encoding gene *ZtMCC* (previously published as *MgMCC*), orthologous to *Fusarium verticillioides FCC1* is associated with a delayed filamentous growth, unusual hyphal swellings, increased melanin biosynthesis, stress tolerance and reduced pathogenicity (Choi and Goodwin, 2010). Deletion of *MgMVE1* gene encoding one essential component of the regulatory complex Velvet leads to pleiotropic phenotypes including defects in yeast–mycelial transition and the effect of light on this process (Choi and Goodwin, 2011, Perez-Nadales *et al.*, 2014). However, it has no role in pathogenicity. Finally, *ZtALG2* (previously published as *MgALG2*) was identified and functionally characterized, indicating its involvement in glycosylation of secreted proteins. Deletion of *ZtALG2* led to a mutant unable to infect wheat. Furthermore, the mutant is

impaired in switching from yeast to filamentous growth and protein secretion (Motteram *et al.*, 2011).

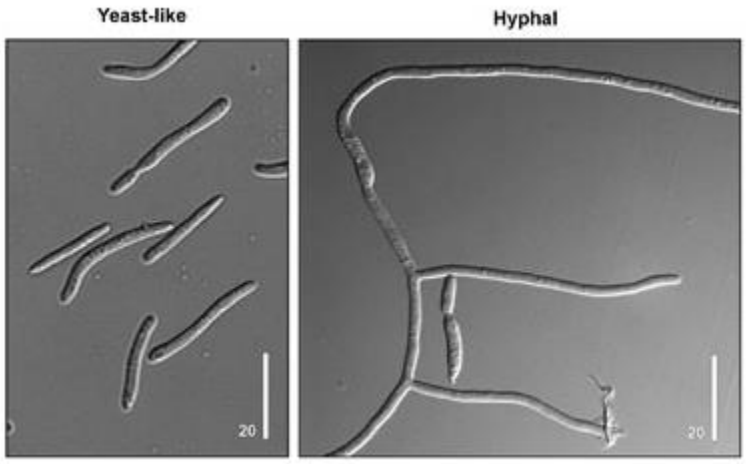

Figure 4: Dimorphic switch of *Z. tritici* induced by nitrogen deprivation. Depletion of nutrients and external nitrogen source promotes yeast-to-hyphal transition. (adapted from http://www.gerosteinberg.com). Bar scale is given in micrometers.

Consequently, these examples show that dimorphism is not only an important taxonomic feature but also a significant pathogenicity- and a virulence-related factor of many pathogenic fungi, regardless of whether they belong to phyto- or animal/human-pathogenic fungi. Generally, our understanding about the triggers, sensing and the underlying regulatory mechanisms in fungal plant pathogens governing dimorphic transition is still very limited. The experimental exploration of economically important pathogens and the emerging model systems like *Zymoseptoria tritici*, among others, will provide a deeper understanding of this interesting and critical process.

1.7 Future challenges and actuality of the current study

Generally, in spite of the mentioned situation regarding the fungicides-based control strategies in order to combat STB, there is a clear need to understand the fine tuning infection mechanisms used by this pathogen to colonize the host plant. Understanding the molecular mechanisms involved in the virulence of *Z. tritici* is essential to develop new control strategies for plant protection. Based on the recent advances and having in mind the future prospects mainly linked to the desirable discovery of the resistance breaking new compounds will include the identification and prioritization of potential drug targets and the assessment of their drugability.

At the same time relying on the present standpoint we can see a clear tendency and the future challenge of integration of "omics"-data and not at last integration of data encompassing such

criteria as predicting target drugability with information on gene essentiality, virulence factors, predicted selectivity, related fungal orthologues and assessment of structural biology accessibility.

Considering the pathogenic and developmental characteristics of *Z. tritici*, Steinberg recently formulated in his review at least three important questions. These questions represent the main current research topics concerning the fundamental developmental processes of this plant fungal pathogen which need to be addressed to improve the strategies to better control the disease (Steinberg, 2015). The questions stated in his article are: “how is the morphological transition from yeast-like growth to hyphal growth controlled during early plant infection”; “how is the transition between biotrophic and necrotrophic phase triggered” and “how does the fungus establish the biotrophic phase in a compatible interaction with wheat”? Addressing the first question, the main goal of this thesis was to unveil genetic determinants and to unravel regulation processes essential for dimorphic transition in *Z. tritici*. As mentioned above the ability of the different fungal pathogens to perform the dimorphic switch upon inducing conditions is directly coupled to their pathogenicity. Despite its importance for wheat infection, our knowledge of the requirements for dimorphic switching in *Z. tritici* is fragmentary. Interruption of this critical differentiation process within the pathogenic development could contribute to modern and innovative plant protection strategies to address this disease. Once again, it should be pointed that dimorphic transition occurs very early in the process of plant infection. During this time the fungus is most accessible for fungicide treatment. Preventing the fungus from penetrating the plant by inactivation of dimorphic switch program could therefore lead to a new generation of "preventive" fungicides acting on STB before the fungus has damaged its host plant.

1.8 Scope of the thesis

Referring to mentioned examples in previous chapters, dimorphism is concerned as a virulence/pathogenicity factor having a great impact not only for agriculture but also for medical research. Thus, facing the actual prevalence of diseases caused by dimorphic phytopathogenic and systemic dimorphic fungi, understanding the regulatory mechanisms, which govern the morphogenic transition is of high biological and therapeutical relevance. The ultimate objective of this thesis was to identify genetic determinants and to unveil molecular basis of the regulatory mechanisms of the "dimorphic switch" process in *Z. tritici*. This was achieved by extensive use of insertional mutagenesis. With the forward genetics mutagenesis approach, based on the *Agrobacterium tumefaciens*-mediated DNA

transformation method, a sustainable library of mutants was generated, followed by selective screening for switch deficient mutants. With the subsequently extended characterization of generated mutants, the use of reverse genetics and transcriptome analyses we were able to gain the first insight into the regulation process underlying dimorphic switch in *Z. tritici* and to identify novel pathogenicity factors. The latter may represent putative targets for the drug discovery with the emphasis on novel and selective mode of action. In the following figure the main tasks are listed, which were processed within this thesis:

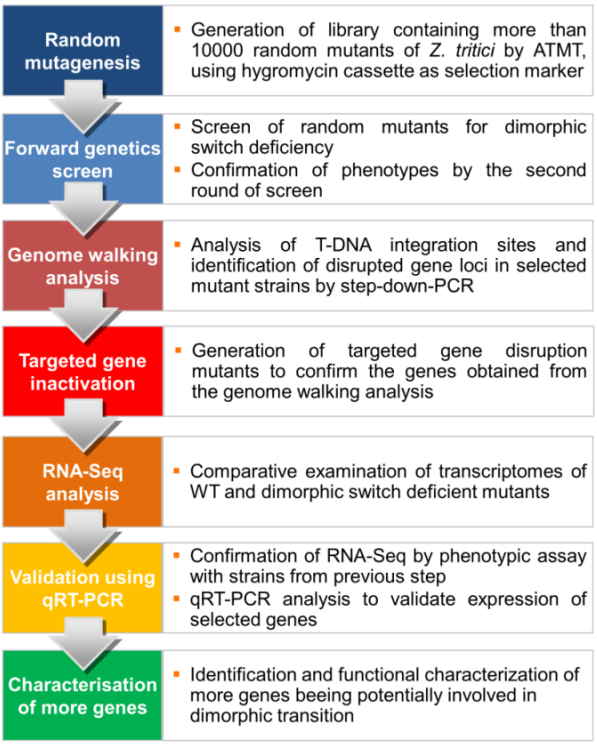

Figure 5: Flowchart representing the concept of the current thesis. The flowchart illustrates schematically sequence of core operations central to the research program of this study.

The activities undertaken in this thesis make a significant contribution to the identification of factors whose functionality is an essential prerequisite for the establishment of pathogenicity in *Zymoseptoria tritici*. The results presented in this thesis allow drawing the first conclusion to use the identified genes with their products as potential targets or as basis for the establishment of new drug screening systems. Molecular verification and validation of the putative fungicide targets should be subject of ongoing projects.

2. Material and methods

2.1 Material

2.1.1 Chemicals and media components

2.1.1.1 Water

Water was used in four different qualities. For cultivation of wheat plants, tap water was used in normal drinking quality (water hardness 4° dH). For the preparation of media and solutions, deionized water $H_2O_{deion.}$ (Seradest SD 2000 SERAL - purity water systems GmbH, Ransbach-Baumbach) was used. Solutions and buffers for use in molecular biological applications were prepared exclusively with autoclaved and ultrafiltered water H_2O_{UF} (Milli-Q®Synthesis, Quantum® EX, Q - Gard® 2, Millipore GmbH, Schwalbach). For critical applications involving RNA (such as the isolation of RNA or q-RT-PCR analysis) nuclease-free water was used (Ultra Pure™ DNase/RNase-free distilled water, Life Technologies GmbH, Darmstadt).

2.1.1.2 Solvents

Acetone (Sigma-Aldrich Chemie GmbH), acetonitrile (HPLC/MS grade) (Scharlau Chemie A.S.), DMSO *p.a.* (Sigma-Aldrich Chemie GmbH), ethyl acetate (Fisher Chemical), ethyl acetate (technical grade) (J.T. Baker), ethanol *p.a.* (EtOH) (Carl Roth), isopropanol *p.a.* (Sigma-Aldrich Chemie GmbH), methanol *p.a.* (MeOH) (Sigma-Aldrich Chemie GmbH)

2.1.1.3 Acids and alkalis

CH_3COOH *p.a.* (100%) (Carl Roth), HCl *p.a.* (32%) (Merck KGaA), HCOOH *p.a.* (99-100%) (Th. Geyer GmbH), KOH (Carl Roth), maleic acid (Merck KGaA), NaOH (Merck KGaA), trifluoroacetic acid *p.a.* (100%) (Carl Roth)

2.1.1.4 Antibiotics

Ampicillin (Sigma-Aldrich Chemie GmbH), cefotaxime sodium (Fresenius Kabi GmbH), chloramphenicol (Sigma-Aldrich Chemie GmbH), glufosinate ammonium (Sigma-Aldrich Chemie GmbH), glufosinate ammonium (Basta®) (Bayer CropScience Deutschland GmbH), hygromycin B (HygroGold™) (Invivogen), kanamycin (Sigma-Aldrich Chemie GmbH), penicillin G (SERVA/Boehringer Ingelheim), rifampicin (Sigma-Aldrich Chemie GmbH), streptomycin sulfate (Merck KGaA), tetracycline hydrochloride (Sigma-Aldrich Chemie GmbH)

2.1.1.5 Media components for liquid and solid media

Acetosyringone (Sigma-Aldrich Chemie GmbH), agarose (Biozym), Bacto Agar™ (Becton Dickinson GmbH), Bacto™ casamino acids (Becton Dickinson GmbH), Bacto™ Nutrient Broth (Becton Dickinson GmbH), Bacto™ peptone (Becton Dickinson GmbH), Bacto™ Yeast Extract (Becton Dickinson GmbH), biotin (Sigma-Aldrich Chemie GmbH), Difco™ Potato Dextrose Broth (Becton Dickinson GmbH), glucose (SHS), IPTG (MBI Fermentas), sodium (Merck KGaA), thiamine chloride (Sigma-Aldrich Chemie GmbH), tween 20 (Carl Roth GmbH & Co.)

2.1.2 Antibodies and enzymes

Anti-Digoxigenin-AP, DreamTaq™ DNA polymerase (Fisher Scientific-Germany GmbH), FastAP (Shrimp-alkaline-phosphatase) (Fisher Scientific-Germany GmbH), Lysing enzymes from *Trichoderma harzianum* (Sigma-Aldrich Chemie GmbH), Phusion® High-Fidelity polymerase (NEB (New England Biolabs Inc.)), restriction endonucleases (Fisher Scientific-Germany GmbH), NEB (New England Biolabs Inc.), RNase A (Life technologies GmbH), SapphireAmp® Fast PCR Master Mix (Takara Bio Company), T4 DNA Ligase (Fisher Scientific-Germany GmbH)

2.1.3 Reaction kits

The following reaction kits were used for molecular biological applications. The application procedures were carried out according to the manufacturer's recommendations, unless stated otherwise:

DNeasy® Plant Mini Kit (Qiagen), iTaq™ Univ. SYBR® Green One-Step Kit (Bio-Rad Laboratories GmbH), NucleoSpin® Extract II (Macherey-Nagel), GeneJET™ Gel Extraction Kit (Life technologies GmbH), GeneJET™ Gel Ex. and DNA Cleanup Kit (Life technologies GmbH), GeneJET™ Plasmid Miniprep Kit (Life technologies GmbH), Gibson Assembly® Cloning Kit (NEB), Gibson Assembly® HiFi DNA Cloning Kit (NEB), pGEM®-T Easy Vector System I (Promega), RNase-free DNase Set (Qiagen), RNeasy® Plant Mini Kit (Qiagen).

2.1.4 Solutions and buffers

2.1.4.1 Solutions

All data mentioned below relate, unless otherwise stated, to a total volume of 1 liter $H_2O_{deion.}$.

.

Acetosyringone solution (100 mM)

Acetosyringon	196	mg
DMSO	ad 10 ml	

Antibiotic solutions were prepared using sterile distilled water (or MeOH in case of Rifampicin). The solution was aliquoted in sterile 1.5 mL centrifuge tubes by filtration (filter type FP 30/03) and stored at −20 °C.

Ampicillin (Amp) solution

Ampicillin	1.0	g
H_2O_{UF}	ad 10 ml	

Cefotaxime (Cef) solution

Cefotaxime sodium	1.0	g
H_2O_{UF}	ad 10 ml	

Kanamycin (Kan) solution

Kanamycin sulfate	1.0	g
H_2O_{UF}	ad 10 ml	

Rifampicin (Rif) solution

Rifampicin	100.0	mg
MeOH	ad 10 ml	

Streptomycin (Str) solution

Streptomycin sulfate	1.0	g
H_2O_{UF}	ad 10 ml	

Antibody solution

Anti-Digoxigenin-AP	1.5	µl
Blocking buffer	ad 20 ml	

Denhardt's solution (100x)

Ficoll® 400	1.0	g
PVP	1.0	g
BSA, Fraction V	1.0	g
$H_2O_{deion.}$	ad 50 ml	

IPTG-stock solution (100 mM)

IPTG	238.0	mg
$H_2O_{deion.}$	ad 10 ml	

Alkaline Lysis Solution 1 (Storage at 4 °C)

Glucose (1 M)	2.0	ml
Na_2EDTA (0.5 M)	0.8	ml
Tris-HCl (1 M)	1.0	ml
$H_2O_{deion.}$	ad 40 ml	

Alkaline Lysis Solution 2

NaOH (10 M)	0.8	ml
SDS (10% (w/v))	4.0	ml
$H_2O_{deion.}$	ad 40 ml	

Alkaline Lysis Solution 3 (Storage at 4 °C)

CH_3COOH	5.75	ml
Potassium acetate (5 M)	30.0	ml
H_2O_{UF}	ad 50 ml	

MES-solution (1 M)

MES hydrate	19.5 g
$H_2O_{deion.}$	ad 100 ml

Na_2EDTA-solution (0.5 M)

Na_2EDTA x 2 H_2O	186.1	g
pH	8.0	

Nitrate salt solution (20x)

$NaNO_3$	120.0	g
KCl	10.4	g
$MgSO_4$ x 7 H_2O	10.4	g
KH_2PO_4	30.4	g

Nitrate-free salt solution (20x)

KCl	10.4	g
$MgSO_4$ x 7 H_2O	10.4	g
KH_2PO_4	30.4	g

Trace-element solution 1 (1000x)

$CoCl_2$	7.0	mM
$CuSO_4$	6.0	mM
$FeSO_4$	18.0	mM
H_3BO_3	180.0	mM
$MnCl_2$	25.0	mM
Na_2EDTA	135.0	mM
Na_2MoO4	6.0	mM
$ZnSO_4$	80.0	mM
pH (adjusted with 1 M KOH)	6.5	

Trace-element solution 2 (1000x)

$CuSO_4$	0.40	mM
$FeSO_4$	0.35	mM
H_3BO_3	1.60	mM
$MnSO_4$	0.60	mM
$ZnSO_4$	0.35	mM

Tris-HCl-stock solution (1 M)

Tris-HCl	121.14 g
pH	7.5

X-Gal-stock solution

X-Gal	500.0	mg

DMSO ad 10 ml

2.1.4.2 Buffers

All data mentioned below relate, unless otherwise stated, to a total volume of 1 liter $H_2O_{deion.}$.

Maleic acid buffer

Maleic acid	11.6	g
NaCl	8.8	g
pH (adjusted with NaOH)	7.5	

Blocking buffer

Skim milk powder	1.5	g
Maleic acid buffer	100.0	ml

Denaturation solution

NaCl	46.8	g
NaOH	16.0	g

Detection buffer

NaCl	5.8	g
Tris	12.1	g
pH	9.5	

Hybridization buffer

Denhardt's solution (100x)	50.0	ml
SDS (10% in water)	50.0	ml
SSPE (20x)	300.0	ml

K-buffer:

K_2HPO_4	1,15	M
KH_2PO_4	1,15	M

MN-solution:

$MgSO_4$	120	mM
NaCl	255	mM

Neutralization-buffer

NaCl	87.7	g
Tris	60.6	g
pH	7.6	

Washing buffer

Maleic acid buffer	100.0	ml
Tween 20	500.0	µl

SSPE-buffer (20x)

$Na_2EDTA \times 2\ H_2O$	7.4	g
NaCl	210.0	g
$NaH_2PO_4 \times H_2O$	27.6	g
pH	7.4	

SSPE-buffer (0,2x) + 0.1% SDS

SDS (10%)	10.0	ml
SSPE (20x)	10.0	ml

SSPE-buffer (2x) + 0.1% SDS

SDS (10%)	10.0	ml
SSPE (20x)	100.0	ml

TAE-buffer (50x)

Tris	242.0	g
Na_2EDTA-solution (0.5 M)	100.0	ml
CH_3COOH (100%)	57.1	ml
pH	8.0	

TE-buffer

Tris-HCl	10.0	ml
EDTA (0.5 M)	2.0	ml
pH	8.0	

TE+RNase-buffer

Tris-HCl	1.0	ml
EDTA (0,5 M)	0.2	ml
RNase A (100 mg/ml)	0.5	ml
pH	8.0	
$H_2O_{deion.}$	ad 100 ml	

Tris-HCl-buffer

Tris	50.0	mM
NaCl	100.0	mM
pH	7.5	

2.1.5 Culture media

All solid and liquid media for cultivation of the microorganisms used in this study were autoclaved before use with the following parameters: 20 min at a temperature of 121 °C and a

pressure of 1.1 bar. Unless otherwise specified, the required pH was adjusted with 1 M HCl or 1 M NaOH. For the production of solid media, the granulated agar (Difco™) was added (2% (w/v)) to the respective liquid media before autoclaving. All data mentioned below relate, unless otherwise stated, to a total volume of 1 liter $H_2O_{deion.}$.

2.1.5.1 Media for cultivation of *Agrobacterium tumefaciens*

AIM-medium
(Agrobacterium induction medium)

To 900 ml of autoclaved $H_2O_{deion.}$ after cooling to room temperature, the following components of the medium were added, using filter-sterilisation (NYL Filter Unit 500 ml, pore size 0.2 microns; Nalgene). For the production of AIM-solid medium, the granulated Difco Agar ™ (2 %) was added prior to autoclaving. After cooling to 55 ° C, 1 ml of the 100 mM acetosyringone solution was added.

$CaCl_2$ (1% (w/v))	1.0	ml
$FeSO_4$ (0.01% (w/v))	10.0	ml
Glucose (20% (w/v))	5.0	ml
Glycerol (50% (w/v))	5.0	ml
MES-solution (1 M)	40.0	ml
NH_4NO_3 (20% (w/v))	2.5	ml
Trace-element solution 2	5.0	ml
K-buffer	0.8	ml
MN-buffer	20.0	ml

2.1.5.2 Media for cultivation of *Escherichia coli*

LB-medium

Bacto™ Trypton	10.0	g
Bacto™ Yeast Extract	5.0	g
NaCl	5.0	g
pH	7.4	

To prepare the following selection media, the appropriate amount of filter-sterilized antibiotic-solutions were added to the autoclaved LB medium after cooling to 55 ° C. Unless indicated otherwise, the corresponding values relate to the total volume of 1 l medium.

LB-AIX-medium
LB-Medium supplemented with 1 ml ampicillin solution (100 mg/ml), 4 ml IPTG and 4 ml of X-Gal-stock solution

LB-Amp (100 mg/l)-medium
LB-Medium supplemented with 1 ml ampicillin solution

LB-Kan-medium
LB-Medium supplemented with 600 µl Kanamycin solution

LB-Rif (60 mg/l)-medium
LB-Medium supplemented with 6 ml Rifampicin solution

LB-Rif+Kan (each 100 mg/l)-medium
LB-Medium supplemented with 600 µl Kanamycin solution und 6 ml Rifampicin solution

2.1.5.3 Media for cultivation of *Zymoseptoria tritici*

Minimal medium (MM)

Biotin (0.01% (w/v))	250.0	µl
Glucose	1.0	g
Nitrate salt solution (20x)	50.0	ml
Trace-element solution 1	1.0	ml
Thiamine chloride (1% (w/v))	1.0	ml
pH	6.5	

N-deprivation medium

Biotin (0.01% (w/v))	250.0	µl
Glucose	1.0	g
Nitrate-free salt solution (20x)	50.0	ml
Trace-element solution 1	1.0	ml
Thiamine chloride (1% (w/v))	1.0	ml
pH	6.5	

PDA-medium

Potato Dextrose Broth	240.0	g

SOB-medium

Tryptone	20.0	g
Bacto™ Yeast Extract	5.0	g
NaCl	0.5	g

additionally 10 ml of 2 M Mg^{2+}-solution were added to the autoclaved SOB medium after cooling to 55 °C.

SOC-medium

SOB-medium	100.0	ml
Glucose-solution (2 M)	2.0	ml

(was added filter-sterilized to SOB medium)

V8-medium

Vitafit tomato juice	200.0	ml
pH	6.5	

$V8_{sel.}$

V8-medium supplemented with 150 µg/ml Hygromycin B, 350 µg/ml Cefotaxime and 200 µg/ml Streptomycin sulfate.

The appropriate amount of filter-sterilized antibiotic-solutions were added to the autoclaved V8 medium after cooling to 55 ° C. Unless indicated otherwise, the corresponding values relate to the total volume of 1 l medium.

YEG-medium

Glucose	10.0	g
Yeast extract	10.0	g
pH	6.5	

Water agar (pH 6.5)

For preparation of YEG medium, used for standardized cultivation of *Z. tritici* strains, Leiber yeast extract was used (it induces however a slight transition of WT IPO323 to filamentous growth form). Other investigations aimed to examine dimorphic switch process in *Z. tritici* were carried out with YEG medium based on the yeast extract type 695 (Hartge Ingredients GmbH & Co. KG), since no morphological transition of wildtype strain was observed when using this type of yeast extract.

2.1.6 Organisms used in this study

The organisms listed below were used for the molecular biological and biochemical analyses.

2.1.6.1 *Agrobacterium tumefaciens*

strain: *Agrobacterium tumefaciens* AGL1 (BAA-101) (ATCC, Manassas, USA)

genotype: AGL0 recA::bla pTIBo542deltaT Mop+ CbR (Lazo *et al.*, 1991)

competence: chemo-competent

This strain is resistant to rifampicin and carbenicillin.

2.1.6.2 *Escherichia coli*

strain: *E. coli* XL1-Blue (Stratagene, La Jolla, USA)

genotype: endA1 gyrA96(nalR) thi-1 recA1 relA1 lac glnV44 F' [::Tn10 $proAB^{+}$ $lacI^{q}$ Δ(lacZ)M15] hsdR17(rK^{-} mK^{+}) (Bullock *et al*., 1987)

competence: electro-competent

This strain harbours a natural tetracycline resistance.

strain: *E. coli* Top10 (Thermo Fisher Scientific, Pittsburgh, USA)

genotype: F- mcrA Δ(mrr-hsdRMS-mcrBC) φ80lacZΔM15 ΔlacX74 nupG recA1 araD139 Δ(ara-leu)7697 galE15 galK16 rpsL(Str^R) endA1 λ^-

competence: electro-competent

This strain is resistant to streptomycin.

strain: *E. coli* NEB-5-alpha ScEf sowie HiFi (NEB New England Biolabs Inc., Beverly,USA)

genotype: fhuA2 Δ(argF-lacZ)U169 phoA glnV44 Φ80 Δ(lacZ)M15 gyrA96 recA1 relA1 endA1 thi-1 hsdR17

competence: chemo-competent

This strain is resistant to streptomycin.

strain: *E. coli* NEB-10-beta ScEf sowie HiFi (NEB New England Biolabs Inc., Beverly,USA)

genotype: Δ(ara-leu) 7697 araD139 fhuA ΔlacX74 galK16 galE15 e14- Φ80 Δ(lacZ)M15 recA1 relA1 endA1 nupG rpsL (Str^R) rph spoT1 Δ(mrr- hsdRMS-mcrBC)

competence: electro-competent

This strain is resistant to streptomycin.

2.1.6.3 *Zymoseptoria tritici*

The wildtype strain *Z. tritici* IPO323 (CBS Fungal Collection, Utrecht, NL) was used as a recipient strain for *Agrobacterium tumefaciens* mediated transformation within both random mutagenesis and targeted gene inactivation experiments. It also served for isolation of genomic DNA in order to amplify the desired genome regions, for RNA isolation in terms of gene expression studies, and as a reference strain within phenotypic characterization experiments. The cultivation of the *Z. tritici* strains was performed by default, unless otherwise specified, either in YEG liquid medium at 18 ° C and 120 rpm for 3-5 days or on YEG solid medium (2% agar) under aerobic condition at 18 °C for 7 days. The liquid cultures were inoculated from cultures that were kept on solid medium for maximal two weeks. To prepare the spore solutions, the strains were cultivated as described above, harvested by transferring them into 50 ml falcons, followed by centrifugation at 4,000 rpm for 5 min at RT. The supernatant was discarded and the resultant pellets resuspended in the same volume of $H_2O_{dest.}$. If needed, the spore suspensions were adjusted to appropriate concentration using cell counting chamber (Neubauer improved, Carl Roth GmbH & Co.). For long-term storage the glycerol cultures were prepared: densely grown cultures in YEG-fluid medium (3-5 days

at RT) were mixed with sterile glycerol (100%) in a ratio 1:1 and they were finally stored at -80 °C. To recover a strain, a small amount of cells was streaked out onto a YEG agar medium and incubated at 18 °C for 7–14 days.

2.1.6.4 Plants and seeds

The STB susceptible wheat cultivar *Triticum aestivum* (Gramineae) cv. Riband was used for *in vivo* infections assays. The wheat seeds were kindly provided by Dr. A. Sesma-Galarraga (John Innes Centre, Norwich; UK). The cultivation of plants was carried out in plastic pots, filled with the standard soil ED73. The seeds were pregerminated in Petri dishes containing some water for 4 days in the dark and afterwards the seedlings were planted and grown for 10 days prior the infection. The growth was employed at 22 °C, 80% relative humidity and with 16:8 h light/dark cycles in Versatile Environmental Test Chamber (SANYO).

2.1.7 Vectors used in this study

pAJF-GFP (length: 4372 bp | confers resistance to ampicillin)

This vector is based on the plasmid pBluescript® II KS (-), in which additionally *eGFP* gene was inserted, which stays under control of the *toxA* promoter from *Pyrenophora tritici-repentis*. The plasmid was kindly provided by Dr. A. J. Foster.

pAJF-EFA1-GFP (length: 5113 bp | confers resistance to ampicillin)

Similarly, this plasmid is based on pBluescript®II KS (-). However the e*GFP* gene stays under control of a strong constitutive promoter of the elongation factor 1α (*EFA1*) derived from *M. oryzae* (MGG_03641.8). The plasmid was kindly provided by Dr. A. J. Foster.

pCAMB0380 (length: 6812 bp | confers resistance to kanamycin)

This plasmid belongs to pCambia series vectors. It was used as a high-copy binary vector for fungal transformation using ATMT. As binary plasmid it can be replicated in both *E. coli* and in *A. tumefaciens*. With its small size and adequate Mulitple Cloning Site (MCS) for inserting of gene costructs, the plasmid is particularly suitable as a good basis for the construction of own vectors. During ATMT the DNA fragment located in the vector between the two flanking T-DNA regions (left- and right-border repeats) is transferred into the genome of *Z. tritici*. Furthermore, the vector carries the kanamycin resistance gene (encoding aminoglycoside phosphotransferase) for selection of bacterial transformants.

pCAMB-BAR (*Sal*I) (length: 7747 bp | confers resistance to phosphinothricin and kanamycin)
This vector is based on the plasmid pCAMB0380. The bialaphos resistance cassette was cut with restriction enzyme *Sal*I from the plasmid pCB1635 and ligated into the plasmid pCAMB0380 cut with *Sal*I. The vector was kindly provided by Dr. A. J. Foster.

pCAMB-HPT(*Sal*I) (length: 8268 bp | confers resistance to hygromycin and kanamycin)
A pCAMB0380-based vector, containing the hygromycin resistance gene *HPT* from pCB1003 (Carroll *et al.*, 1994) cloned as *Sal*I fragment into the *Sal*I site of the vector. The bacterial hygromycin B phosphotransferase (*HPT*) gene is expressed under the control of the strong constitutive *Aspergillus nidulans trpC* promoter, forming the *HPT* cassette as selectable marker conferring the hygromycin resistance.

pCB1636 (length: 4417 bp | confers resistance to hygromycin and ampicillin)
This vector is based on the pBluescript II SK (-) (Stratagene, La Jolla, USA) and is a high copy plasmid for cloning and amplification in *E. coli*. Selection based on ampicillin resistance as well as blue-white screen through the *lacZ* gene can be used to identify recombinant bacterial clones for further analysis. pCB1636 contains a hygromycin resistance cassette (Sweigard *et al.*, 1997).

pGEM®-T Easy (length: 3017 bp | confers resistance to ampicillin)
This vector was obtained from Promega (Mannheim, Germany) and was used for cloning of multiple PCR-products obtained from genome walking method. This vector is suitable for blue/white selection and carries an ampicillin resistance gene. It is a linearized cloning vector, which provides at both ends 3'- thymidine residues. This allows an efficient ligation with PCR products generated by Taq polymerase, which in its turn produces the terminal 5'-adenosine residues.

pJet1.2/blunt (length: 2974 bp | confers resistance to ampicillin)
This vector was obtained from the CloneJET Cloning Kit (Fisher Scientific GmbH, Schwerte). The vector contains a lethal restriction enzyme gene *eco47IR* conferring positive selection for recovery of blunt-ended PCR products. As a result, only bacterial cells with recombinant plasmids are able to form colonies.

2.1.8 Oligonucleotides used in this study

All oligonucleotides used in this study are listed in Supplementary (Table S1-S6). All primers were designed using the program Primer3 implemented in the software package Geneious ver. 8.1 and were obtained from Eurofins-MWG-Operon (Ebersberg, Germany). The melting temperature of the primers used was determined by TM calculator program of Finnzymes, (Espoo, Finnland). The primers, which were used in the context of Gibson assembly method were designed using the NEBuilder® Assembly Tool (NEB, New England Biolabs Inc.). The following guidelines and rules for designing of efficient primers were followed:

- For gene disruption experiments, the primer pairs were selected such that if possible, regions ranging from 500-1000 bp and flanking the gene region to be manipulated, were amplified. This should contribute to a higher efficiency of homologues recombination within transformation process of *Z. tritici*. When designing primers, special care was taken to ensure that during the recombination event the neighboring gene sequences are not manipulated.
- The primer pairs for the preparation of the DIG-labeled DNA probes for the Southern Blot analyzes were designed so that the amplified DNA probes had a size of 250 bp to 400 bp and if possible, hybridized to a portion of the coding sequence of the gene of interest.
- Primers suited for gene expression analysis within the quantitative "real-time PCR" (qRT-PCR, see 2.2.8) were designed under consideration that they anneal to sequences in exons on both sides of an intron. With such primers, any product amplified from genomic DNA would result in a larger amplicon compared to that amplified from intron-less cDNA. This approach should allow differentiation between the amplified product from cDNA and an amplified product derived from contaminating genomic DNA. Visualization of such differences was performed using the gel electrophoresis with amplified product.
- For colony PCR in terms of identification of recombination events in the generated transformants, the corresponding primers were designed outside of flanking regions of the gene to be inactivated. In case one would anticipate the similarly sized amplification products, when comparing an inactivated gene locus with the corresponding native gene locus, an additional reverse primer hybridizing with the portion of *HPT* sequence region was created.

2.2 Molecular biological methods

2.2.1 Isolation and preparation of nucleic acids

2.2.1.1 Minipreparation of plasmid-DNA from *Escherichia coli* – cells

Isolation of the plasmid DNA from *E. coli* for preparative purposes was carried out using the GeneJET™ Plasmid Miniprep Kit according to manufacturer's instructions. Isolation of the plasmid DNA for analytical purposes was conducted by means of conventional alkaline lysis protocol according to Sambrook and Russell (2001). *E. coli* cultures with plasmids were inoculated into 5 mL LB medium containing for the selection – depending on the resistance gene of transformed plasmids – an appropriate antibiotic and grown for 16 h at 37 °C in a shaking incubator at 220 rpm. Concentration of the isolated plasmid DNA was estimated photometrically by UV/VIS spectroscopy using NanoDrop ND-1000 (NanoDrop Technologies, Rocky River, USA) according to the manufacturer's user manual (2.2.1.4).

2.2.1.2 Isolation of genomic DNA from *Zymoseptoria tritici*

To obtain genomic DNA (gDNA) from *Zymoseptoria tritici* strain, 50 ml of YEG medium in 100 ml Erlenmeyer flask was inoculated with a fresh *Z. tritici* culture from YEG medium (prior to inoculation grown for 7 days at 18 °C) and incubated at 22 °C and 120 rpm for 3-5 days. Prior gDNA extraction, the YEG culture was pelleted by centrifugation for 5 min at 4,000 rpm and 4 °C (Centrifuge JF Laboratory). The supernatant was decanted and the resultant pellet flash-freezed in liquid nitrogen, followed by lyophilization. The lyophilized spore cells were ground in liquid nitrogen to a fine powder, which was then used as starting material for the isolation of genomic DNA using DNeasy® Plant Mini Kit (Qiagen) according to the manufacturer's recommendations. Prior further proceeding with the isolated gDNA the spectrophotometric measurement of concentration and purity was performed as described (2.2.1.4). For long-term storage the gDNA was stored at -80 °C, until needed.

2.2.1.3 Isolation of RNA from *Zymoseptoria tritici*

For the transcriptome analysis using RNA-Seq as well as qRT-PCR, the total RNA was isolated from target *Zymoseptoria tritici* strains grown for 7 days at 18 °C as axenic cultures on N-deprivation media. Additionally, for further qRT-PCR experiments, the total RNA from reference strain IPO323 was extracted from axenic culture grown on YEG agar medium for 7 days at 18 °C as well as from infected plant leaves, encompassing several time points (1 dpi, 4 dpi, 10 dpi, 14 dpi and 28 dpi) during plant infection.

Prior inoculation, the strains were cultivated for 3-4 days in YEG liquid medium at 22 °C. Spore suspensions were prepared by harvesting the spores using centrifugation for 5 min at 4,000 rpm. For inoculation of solid media, the pellets were then resuspended in sterile water, followed by adjusting the spore concentration to 10^6 spores/ml for each strain and then evenly spreading on plates using a Drigalski spatula. For qRT-PCR studies used for examination of gene expression *in planta*, the susceptible wheat cultivar Riband was infected with the wildtype strain IPO323 by spraying. The concentration was adjusted to 10^7 spores/ml by resuspending them in 0.2% gelatine solution.

Regardless of the nature of the starting material, the samples (cultures on cellophane or infected plant leaves) were first flash-frozen in liquid nitrogen, lyophilized and then ground to a fine powder using liquid nitrogen. RNA isolation was performed using RNeasy® Plant Mini Kit from Qiagen, according to manufacturer's instructions. Following the RNA-isolation, DNaseI digestion was conducted in order to remove any residual genomic DNA. For this, the RNase-free DNase Set was used according to manufacturer's protocol. Successful removal of gDNA was verified by qRT-PCR (in this case the qRT-PCR was employed without reverse transcriptase). The qualitative and quantitative assessment of isolated RNA was performed as described (2.2.1.4). The isolated RNA was stored at -80 ° C.

2.2.1.4 Concentration and quality measurements of nucleic acids

Quantification of nucleic acids was performed by spectrophotometrical analysis (UV/VIS) using NanoDrop ND-1000 (NanoDrop Technologies, Rocky River, USA). The ratio of absorbance at 260 nm and 280 nm was used to assess the purity of DNA and RNA. A ratio of ~1.8 is generally accepted as "pure" for DNA; a ratio of ~2.0 for RNA. To examine the integrity of the total RNA isolated, a quantitative and qualitative measurement on the Agilent 2100 bioanalyzer (Agilent Technologies) using the RNA 6000 Nano Kit (Agilent Technologies) was conducted according to manufacturer's protocol. For qualitative measure of RNA quality, the RIN (RNA Integrity Number) values were calculated. For the transcriptome analysis (RNA-Seq) and expression studies by qRT-PCR, only RNA samples with a minimum RIN value of 7.0 were used.

2.2.2 Polymerase chain reaction (PCR)

2.2.2.1 Polymerase chain reaction (PCR) with genomic and plasmid DNA

Polymerase chain reaction (PCR) was used for selective amplification of DNA fragments from genomic DNA of *Z. tritici* and plasmid DNA from *E. coli*. Depending on the purpose of analysis (preparative or analytical), the PCR reactions were employed using different DNA polymerases. Thus, for the production of amplicons for subsequent ligation into the cloning vector pGEM-T easy, DreamTaq™ DNA polymerase (Table 2) was used. Amplification of DNA fragments for Gibson-assembly was performed using Phusion® High-Fidelity DNA polymerase (Table 3). In both cases, PCR was carried out by default in the thermocycler GeneAmp PCR System 9700 (Applied Biosys - system, Carlsbad, USA). The pipetting and programming scheme of the respective PCR were set up following the general manufacturer's instructions.

PCR-reaction set-up using DreamTaq™ DNA polymerase

10x reaction buffer	5.0 µl
$MgCl_2$ (25 mM)	1.0-5.0 µl (optional)
forward Primer (5 pmol/µl)	2.0 µl
reverse Primer (5 pmol/µl)	2.0 µl
dNTP-Mix (10 mM)	1.0 µl
template-DNA (gDNA/plasmid-DNA)	x µl (= 50-100 ng)
DreamTaq® polymerase (1u/µl)	1.0 µl
H_2O_{UF}	ad 50 µl

Table 2: PCR-program used for DreamTaq™ DNA polymerase amplification

program segment	number of cycles	temperature [°C]	time
Initial denaturation	1	95	2 min
Cyclic amplification	30 - 35	95	30 s
		$\mathbf{T_A}$	30 s
		72	$\mathbf{t_E}$ min
Final extension and hold	1	72	10 min
		4	∞

($\mathbf{T_A}$ = annealing temperature; $\mathbf{t_E}$ = time for the elongation)

PCR-reaction set-up using Phusion® High-Fidelity DNA polymerase

5X Phusion HF	10.0 µl
forward Primer (5 pmol/µl)	2.0 µl
reverse Primer (5 pmol/µl)	2.0 µl
dNTP-Mix (10 mM)	1.0 µl
template-DNA	x µl (= 50-100 ng)

(gDNA/plasmid)	
Phusion® High-Fidelity DNA polymerase (1u/µl)	0.5 µl
H_2O_{UF}	ad 50 µl

Table 3: PCR-program used for Phusion® High-Fidelity DNA polymerase amplification

program segment	number of cycles	temperature [°C]	time
Initial denaturation	1	98	1 min
Cyclic amplification	30 - 35	98	15 s
		T_A	30 s
		72	t_E min
Final extension and hold	1	72	10 min
		4	∞

($\mathbf{T_A}$ = annealing temperature; $\mathbf{t_E}$ = time for the elongation)

2.2.2.2 Colony-PCR

The colony PCR was modified in accordance with protocol published by Tendulkar *et al.*, 2003 and served as the preselection method in terms of selecting *Z. tritici* - transformants prior to Southern Blot analysis. For ultra-fast preparation of gDNA from *Z. tritici* transformants, a small part of a growing *Z. tritici* colony was transferred using a sterile pipette tip to a 1.5 ml reaction vessel and suspended carefully in 100 µl of sterile H_2O_{UF}. The cells were then broken by treating them for 1.5 min at 900 W in a microwave oven. The cell debris were then pelleted by centrifugation for 1 minute at 13,200 rpm and 2 µl of the resultant supernatant was used as template for the following PCR using SapphireAmp® Fast Mix:

PCR-reaction set-up using SapphireAmp®-Polymerase

SapphireAmp®Fast Mix	12.5 µl
forward primer (5 pmol/µl)	2.0 µl
reverse primer (5 pmol/µl)	2.0 µl
template-DNA (gDNA/plasmid-DNA)	2.0 µl
H_2O_{UF}	ad 25 µl

The reaction parameters of the programming scheme used for amplifying DNA in the GeneAmp PCR System 9700 were broadly in line with the program parameters employed for PCR using Phusion® High-Fidelity DNA polymerase, except for a few modifications: the annealing temperature was lowered by 5 °C and the number of cycles has been increased by 5-7 cycles.

2.2.2.3 Generation of DIG-labeled hybridization probe

To generate DNA probe that hybridizes to the DNA of the genomic region of interest, a PCR was performed using DreamTaq® DNA polymerase (MBI Fermentas, St. Leon-Roth) and DIG-labeled dUTPs. The generated gene inactivation constructs were used as a template for the PCR. By incorporation of the digoxigenin (DIG) conjugated dUTP, the amplified probes were labeled allowing the subsequent detection within the Southern Blot analysis. The PCR program used corresponded to the following scheme:

PCR-reaction set-up for generation of DIG-labeled DNA-probes

10x reaction buffer	5.0 µl
$MgCl_2$ (25 mM)	1.0-5.0 µl (optional)
forward primer (5 pmol/µl)	2.0 µl
reverse primer (5 pmol/µl)	2.0 µl
dNTP-Mix (10 mM)	1.0 µl
DIG-11-dUTPs (1 nmol/µl)	1.5 µl
template-DNA (plasmid-DNA)	x µl (= 50-100 ng)
DreamTaq® polymerase (1u/µl)	1.0 µl
H_2O_{UF}	ad 50 µl

2.2.2.4 Genome walking analysis and recovery of T-DNA integration sites using step-down PCR

The DNA from the site of the T-DNA insertion was recovered using a step-down PCR-based approach, as previously described (Zhang and Gurr, 2000), by two nested rounds of amplification using the gene-specific primers gspBa, gspB, gspAa, gspA and adapter-specific primers PP1 and PP2 (see Table S2). The principle of the genome walking technique is summarized in Figure 6. First, genomic DNA was isolated from investigated strains (2.2.1.2) and cut by endonucleases derived from two enzyme-sets (**set 1:** *Spe*I, *Nhe*I, *Xba*I; **set 2:** *Xma*I, *Ngo*MIV, *Bsp*EI).The digested gDNA was then purified using NucleoSpin® Extract II kit (Macherey-Nagel) in order to avoid the contamination with restriction enzymes and ligated with the adaptors specified for each of the mentioned restriction enzyme sets, following the four step ligation program shown in Figure 6. Subsequently, step-down PCR was performed using gene-specific primers binding to the ORF of the *HPT* cassette (gspAa, gspA, for the left-site amplification and gspBa and gspB, for the right-site amplification) and adaptor-specific primers assigned as PP1 and PP2 (remain the same either for left- or right-site amplification). The gsp primers hybridizing within the coding region of the *HPT* are shown in Figure 6.

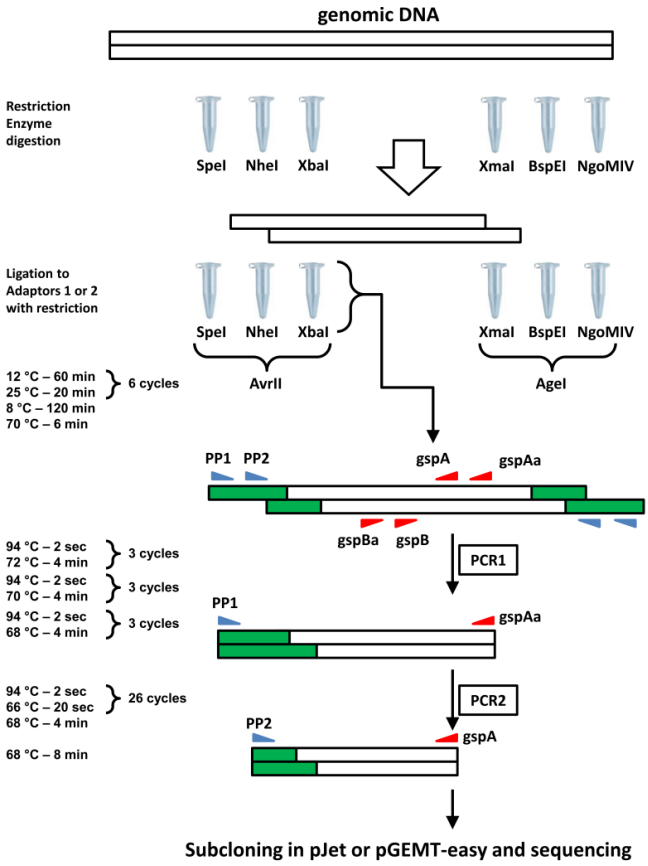

Figure 6: Principle of "step down" genome walking approach used in this study, according to Zhang and Gurr 2000. Green bars denote adapters. Genomic DNA was restricted with one of six different enzymes (*Spe*I, *Nhe*I, *Xba*I, *Xma*I, *Bsp*EI, *Ngo*MIV), ligated to adaptors and further restricted by *Avr*II (set 1) or AgeI (set 2). Exemplarily, "stepdown" PCR was performed with primers PP1 and the gene-specific primer gspAa, followed by amplification using internal primers PP2 and gspA in the second round of PCR.

The primary PCR reaction (PCR1) uses the outer adaptor primer (PP1) and the outer gene-specific primers (gspAa and gspBa). The product of the primary genome walking was then diluted (1:100) and used as a template for a secondary PCR with the nested adaptor (PP2) and nested gene-specific primers (gspA and gspB). The amplicons obtained were finally cloned into pGEM-T easy or pJET vectors (Promega) and sequenced using universal primers (M13 -20, T7 and M13 rev -49).

2.2.3 Restriction of DNA and gel electrophoresis

2.2.3.1 Restriction of DNA

The restriction of bacterial and fungal DNA was carried out according to the general guidelines of Sambrook and Russell (2001). Depending on the restriction enzyme used in respective case, specific incubation conditions were followed according to the manufacturer's recommendations. In general, the incubation time was 1.5 hours at the optimal temperature

for respective enzyme and the reaction was stopped by heat inactivation, precipitation of the DNA or by the addition of DNA gel loading buffer. When using FastDigest™ restriction endonucleases, the mixture was incubated at the appropriate temperature for 30 min.

Restriction reaction for analysis purposes

DNA	x µl (250-500 ng)
enzyme buffer (10x)	2.0 µl
restriction enzyme	1.0 µl
H_2O_{UF}	ad 20 µl

Restriction reaction for cloning purposes

DNA	x µl (1.5 µg)
enzyme buffer (10x)	10.0 µl
restriction enzyme	2.0 µl
H_2O_{UF}	ad 100 µl

To prevent undesirable re-ligation of vectors opened after restriction reaction for cloning purposes, 3 ul SAP (shrimp alkaline phosphatase) or FastAP were added to restricted DNA, enabling the dephosphorylation of free 5' - DNA ends of backbone vector. The reaction set-up was incubated for 20 min at 37 °C. A subsequent denaturing and thus inactivation of the enzymes was carried out for 15 min at 65 ° C.

Restriction reaction set-up for Southern Blot analysis

DNA	x µl (7 µg-10 µg)
enzyme buffer (10x)	30.0 µl
restriction enzyme	5.0 µl
H_2O_{UF}	ad 300 µl

2.2.3.2 Agarose gel electrophoresis with DNA

The agarose gel electrophoresis was carried out according to Sambrook and Russell (2001). TAE buffer was used to dissolve the agarose, as well as a running buffer. By default the separation of DNA was performed in 1% agarose gel using standard gel chamber (BioRad) at constant voltage of 80-100 V. To determine the DNA fragment sizes, GeneRuler™ DNA Ladder 1 kb was used. For visualization, the gels were stained for 10 s in an ethidium bromide solution (5 µg/ml), and rinsed with water for 20 minutes to reduce background, followed by gel documentation using QUANTUM Model 1100 (PEQLAB GmbH) and UV irradiation (365 nm).

2.2.3.3 Isolation of DNA-fragments from agarose gels

After DNA electrophoresis, the separated (desired) DNA fragments derived from PCR and/or from restriction analyses were excised from the gel with a clean scalpel and purified using the NucleoSpin® Extract II kit (Macherey-Nagel) according to the manufacturer's instructions.

2.2.4 Ligation and DNA cloning methods

2.2.4.1 Ligation

T4 DNA ligase (MBI Fermentas) was used with the appropriate buffer to join the DNA between the 5'-phosphate and the 3'- hydroxyl-group of adjacent nucleotides of the vector and *insert*-DNA. Usually a molar vector:insert ratio of 1:3 was used to achieve a high ligation efficiency. The ligation reaction was carried out for 3 h at 22 °C and was subsequently stopped by heat inactivation (10 min at 65 °C). Ligations in the linearized pGEM-T easy® vector were performed according to the manufacturer's instructions (Promega) over night at 4 °C. The ligated products were then transformed into competent bacteria.

Standard ligation reaction set-up:

vector (backbone)	x µl (ca. 50 ng)
insert-DNA-fragment	x µl (3 to 6-fold for amount of inserted fragments)
ligase buffer (10x)	2.0 µl
T4-DNA-ligase	1.0 µl
H_2O_{UF}	ad 20 µl

Alternatively, a ligation reaction was performed in GeneAmp PCR System 9700 (Applied Biosystems, Carlsbad, USA), making use of graduated programming scheme, aiming to ensure a better annealing of the sticky ends. The cycle program used for ligation reaction is shown in Figure 7.

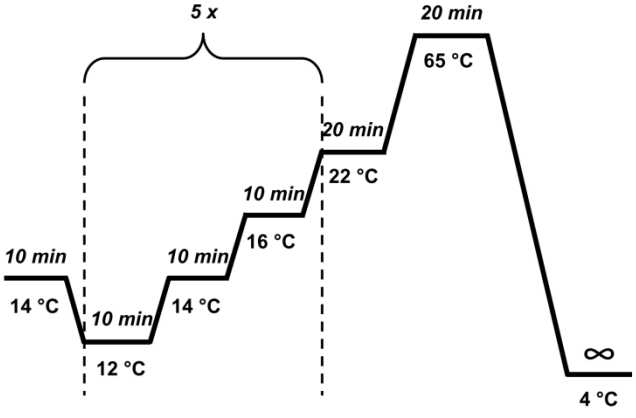

Figure 7: Schematic representation of cycle program used for ligation reaction

2.2.4.2 Dephosphorylation of DNA

To avoid the re-ligation of plasmids opened after restriction for cloning purposes, the DNA fragments were incubated in the presence of Shrimp Alkaline Phosphatase (SAP) or FastAP for 20 min at 37 °C, enabling the dephosphorylation of free 5' - DNA ends. For inactivation of the enzyme, heat denaturation was performed by incubating the reaction mix for 15 min at 65 °C. Following the gel electrophoresis the DNA fragments were finally purified according to gel extraction protocol to avoid any contamination by alkaline phosphatase.

2.2.4.3 DNA precipitation

Both ethanol or isopropanol were used to precipitate DNA (Sambrook and Russell, 2001). For ethanol precipitation, 0.1 volume 3 M sodium acetate and 2 volumes absolute ethanol were added to a given amount of DNA containing solution and incubated for 10 min at -70 °C, followed by centrifugation at 13,000 rpm at 4 °C for 30 min. The resulting pellet was washed with 70% ethanol, air dried and re-dissolved in a given volume of water or TE buffer. For isopropanol precipitation, 0.7-1.0 volume 100% isopropanol were added to a given quantity of DNA depending on the salt concentration and subsequently pelleted by centrifugation at 13,000 rpm at room temperature. Likewise, the pellet was air dried and re-dissolved in a given volume of water or TE buffer.

2.2.4.4 General strategies for construction of transformation vectors

Construction of vectors used for transformation was performed using two different approaches: either by means of classical restriction enzyme- and ligase-dependent cloning or using Gibson Assembly® approach. The principle of Gibson Assembly® (NEB, New England BioLabs® Inc.) approach is shown in Figure 8. In contrast to conventional restriction enzyme ligase-dependent cloning, this technique allows joining of multiple fragments simultaneously, in order to assemble the desired transformation construct. This is achieved by the concerted action of a 5'-exonuclease, a DNA polymerase and a DNA ligase, which promote the assembling of multiple overlapping DNA molecules in a single isothermal reaction. T5-exonuclease chews back nucleotides from the 5' end, and creates single-stranded DNA in the ends of all sequences, thus facilitating the subsequent annealing. DNA polymerase fills the gaps and Taq-ligase finally seals the nicks. T5-exonuclease is heat-labile and can be inactivated during the 50 °C incubation (Gibson *et al.*, 2009). Prior assembling reaction the overlapping fragments were generated by PCR using Phusion® High-Fidelity DNA polymerase and appropriate primers with overhangs (2.2.2.1). The generated amplicons

were separated using gel electrophoresis (2.2.3.2) and purified using NucleoSpin®Extract II reaction kit (Macherey-Nagel) according to the manufacturer's manual (2.2.3.3). The primers were designed using online tool NEBuilder™ provided by NEB. The detailed assembly strategies as well as descriptions for particular transformation constructs are listed in supplementary materials. Generally, for construction of binary vectors used for targeted gene inactivation, the vector pCAMB0380 was used as backbone, to introduce the transformation construct in the MCS enclosed by left- and right borders. Regardless the method used for assembly, the transformation constructs suited for targeted gene inactivation contained homologous recombination sequences on either side of the selection marker (*HPT*) in the T-DNA region of the final transformation vector. In contrast, complementation experiments, aiming to restore the normal phenotype in the mutant strains, rely on random ectopic integration of the gene of interest in the genome of corresponding mutant using either endogenous (native) or heterologous (*gpdA*, constitutive promoter from *Aspergillus nidulans*) promoters. As backbone vector pCAMB-BAR was employed, since it contains *BAR*-cassette conferring glufosinate ammonium resistance, allowing transformation of hygromycin resistant strains. For construction of transformation vectors used for protein localization studies by fluorescent microscopy, either pAJ-GFP or pCAMB-GFP-BAR was used as backbone vectors. All generated transformation plasmids were verified either by sequencing or restriction analysis prior further usage within ATMT.

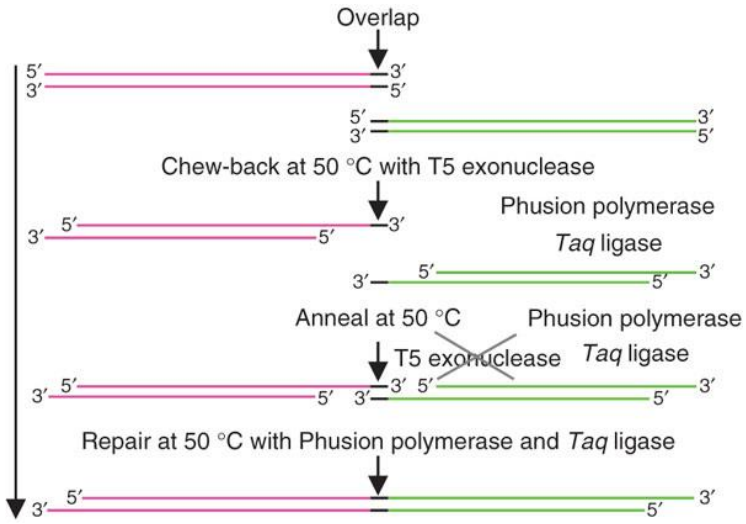

Figure 8: Principle of the Gibson DNA assembly. Gibson Assembly is based on three enzymatic activities employed in a single-tube isothermal reaction. The three required enzyme activities are: T5 exonuclease, Phusion DNA polymerase, and Taq DNA ligase. The exonuclease is responsible for "chew back" of DNA from the 5' end. This results in formation of single-stranded regions that can anneal. The DNA polymerase re-synthesizes the strands and the DNA ligase covalently combines the adjacent segments to one fragment. Hence, the resulting product is different DNA fragments joined into one (picture adapted from Gibson *et al.*, 2009).

2.2.4.5 Sequencing of the DNA

DNA-constructs used in this work were sequenced by GATC Biotech AG, Cologne. The DNA sequencing was performed with the purpose of sequence verification for both, the generated gene inactivation vectors, as well as for the identification of the extracted DNA-fragments obtained from the genome walking analysis and subsequently ligated to one of the defined standard vectors (pJet or pGEM-T easy). The sequencing was carried out using the standard vector primers M13 -20, T7 and M13 rev -49.

2.2.5 Transformation

2.2.5.1 Transformation of *Escherichia coli*

2.2.5.1.1 Production of electro-competent *Escherichia coli* cells

For the preparation of competent *E. coli* cells, the strain XL1-Blue was first cultivated on an LB agar plate without antibiotic (incubation at 37 °C for 48 h). A single grown colony was transferred to 10 ml tube containing 5 ml LB medium and incubated for 16-18 h at 37 ° C in an orbital shaker at 220 rpm. Two milliliters of this culture were used to inoculate 500 ml LB medium containing 20 mM glucose in a 1000 ml Erlenmeyer flasks with 4 baffles, followed by the incubation in the orbital shaker (220 rpm) at 37 °C, until the culture reached OD 600 nm of 0.6 to 0.8. Afterwards, the culture was placed on ice and kept cold for the duration of the procedure. The cells were pelleted at 4,000 rpm (centrifuge GR 422, Jouan S.A.) for 15 min at 4 °C and the supernatant was discarded. The cell pellet was resuspended in 200 ml ice cold 10% (v/v) glycerol. The centrifugation step was repeated once more, with the same parameters. The supernatant was discarded, the recovered cell pellet resuspended in 50 ml of 10% (v/v) glycerol and recentrifuged at the same speed for 10 min at 4 °C. The competent cells were subsequently resuspended in 2 ml ice cold 10% (v/v) glycerol and aliquoted to 80 µl in pre-chilled 1.5 ml microcentrifuge tubes, followed by snap-freezing in liquid nitrogen. The electro-competent cells were finally stored at -80 °C. During the entire process each step was carried out quickly and the cells were always kept cool on ice during the various washing operations. To verify the competence of cells, a transformation with a control plasmid (pUC18) was carried out. A good transformation efficiency is characterized by $>1\times10^8$ colony forming units (cfu)/µg of pUC18 DNA.

2.2.5.1.2 Transformation of *Escherichia coli* cells by electroporation

The transformation of *E. coli* cells was conducted according to the protocol of Fiedler and Wirth, 1988. The 80 ul aliquots of electro-competent *E. coli* XL1-Blue cells were first thawed on ice, mixed with 2.5 µl of the ligation product and transferred into pre-chilled 1 mm electroporation cuvettes (PeqLab, Erlangen).

The cells were electroporated in a Gene Pulser II by an electrical pulse (capacity 25 µF, resistance 200 Ω, voltage 1.25 kV). The time constant was in the 4-5 ms range. For regeneration of the electroporated cells, 500 µl SOC medium was added, followed by incubation at 37 °C for 1 h in an orbital shaker (220 rpm). Finally, the transformed cells were plated on the selection medium (LB medium with the appropriate antibiotics, depending on the resistance gene) and incubated for 16-18 h at 37 °C. For further analysis of transformants, plasmid DNA from individual colonies was isolated (2.2.1.1) and verified by restriction analysis (2.2.3.1).

2.2.5.1.3 Transformation of the chemo-competent *Escherichia coli* cells

For the transformation of vectors constructed by Gibson Assembly® method, the chemo-competent *E. coli* NEB 5-alpha cells were used. 50 µl aliquots of these cells were thawed on ice and sequentially mixed with 2.5 µl, containing 50-100 ng of the assembled product (transformation vector DNA). The cells were incubated for 30 min on ice and then heat-shocked at 42 °C for 1 min. The cells were placed on ice for 5 min, followed by adding 950 µl SOC medium and incubation for one hour in orbital shaker (220 rpm) at 37 °C. Finally, 50-100 µl of the mixture was spread on selection plate containing appropriate antibiotic, depending on resistance gene, and incubated for 16 h at 37 °C.

2.2.5.1.4 Identification of *Escherichia coli* transformants

Individual colonies, grown on the selection plates, were transferred into 5 ml LB liquid medium supplemented with appropriate antibiotic in sterile 14 ml tubes (PP Tube) and incubated in a shaking incubator (orbital shaker, Thermo Forma, Marietta, USA) at 37 °C and 220 rpm for 16 hours. Plasmid DNA from the grown cultures was then isolated as described (2.2.1.1), and subsequently verified by restriction analysis (2.2.3.1).

When using the blue-white selection system, based on the pGEM-T easy® vector, only the plasmid DNA obtained from white colonies was analyzed by restriction analysis. In these cells the vector-encoded *lacZ* gene was inactivated by insertion of a cloning DNA-fragment into the *in-frame* multiple cloning site (MCS) of the coding gene sequence. The disruption of

the *lacZ* gene in its turn prevents the conversion of X-Gal into a blue dye indigo, giving the colonies a white appearance.

2.2.5.2 Transformation of *Zymoseptoria tritici*

2.2.5.2.1 Transformation of chemo-competent *Agrobacterium tumefaciens* cells

An aliquot of the chemically competent *A. tumefaciens* AGL1 cells in a 1.5 ml tubes was thawed on ice and ~2 µg of plasmid-DNA (vectors constructed for gene inactivation, complementation and protein localization experiments) was added and gently mixed. The cells were heat-shocked by incubating the mix for 5 min at 37 °C and immediately placed on ice for 2 min. The cells were then transferred into a sterile 14 ml tube and mixed with 400 µl LB medium, followed by incubation for 3-4 h at 28 °C in a shaking incubator at 220 rpm. Subsequently, 100 µl and 300 µl of the cell suspension were plated on prewarmed selection medium $LB_{Rif+Kan}$ (2.1.5.2) and the plates were incubated for 3 days at 28 °C in the dark.

2.2.5.2.2 Transformation of *Zymosetporia tritici*

Transformation of conidia and selection of hygromycin-resistant transformants of *Z. tritici* were performed using *Agrobacterium tumefaciens*-mediated transformation protocol (ATMT) (de Groot *et al.*, 1998, Zwiers *et al.*, 2001). Several colonies of the transformed *A. tumefaciens* AGL1 strain (from the previous step) were used to inoculate 5 ml $LB_{Rif+Kan}$ liquid medium, followed by incubation for 16 h at 28 °C and 220 rpm in the orbital incubator. Thereafter, the grown culture was centrifuged for 5 min at 6,000 rpm and the resultant pellet resuspended in 1 ml AIM-liquid medium. The cell suspension was diluted in a sterile 14 ml tube with further 4 ml of AIM-medium and subsequently incubated for 6-8 h at 28 °C and 220 rpm in the orbital shaker. Four-day old YEG cultures of the wildtype strain *Z. tritici* IPO323 were centrifuged at 4,000 rpm and 4 °C for 5 min (centrifuge GR 422, Jouan S.A.), the supernatant decanted and the resultant pellet resuspended in the same volume of $H_2O_{dest.}$. Using the cell counting chamber (Neubauer improved, Carl Roth GmbH & Co., Karlsruhe), the spore density was determined and adjusted with $H_2O_{dest.}$ to 10^7 spores/ml and $5x10^7$ spores/ml. After the incubation period, 200 µl of induced AGL1 cells were mixed with 200 µl of the conidia suspensions prepared and applied by evenly spreading onto a sterile filter (cellulose nitrate, NC45 ST), which was placed on AIM-agar plate.

After drying, the plates were incubated for 48 h at 28 °C in the dark. The filters were then transferred to selection medium, followed by incubation at 18 °C for several weeks. Selection of hygromycin resistant transformants was performed using 150 mg/l hygromycin gold

(Invivogen) on V8 agar medium, while selection of glufosinate ammonium resistant transformants produced within complementation of null mutants of *Z. tritici* was performed with 200 mg/l BASTA® (glufosinate ammonium) on MM. Selection in both cases included 200 mg/l streptomycin and 350 mg/l cefotaxime. After 2 to 3 weeks, hygromycin/glufosinate ammonium-resistant colonies appeared on the selective medium, and every isolated colony was first inoculated once more on $V8_{sel.}$ or MM (supplemented with 200 mg/l BASTA®) for repeated selection and then transferred for subsequent subculture in fresh YEG medium. Identification of mutants and analysis of recombination events upon ATMT was achieved by means of colony-PCR, using the appropriate screen primers (Table S5), and by Southern Blot analysis as described (2.2.6).

2.2.6 Southern Blot

Southern (1975) Blot analysis was conducted to examine the recombination events in the generated *Z. tritici* transformants. It followed, except for a few variations of procedure listed below, the general protocol according to Sambrook and Russell (2001).

2.2.6.1 Isolation and restriction of genomic DNA

Genomic DNA (gDNA) from investigated strains of *Z. tritici* was isolated (2.2.1) and 5-10 µg was digested by the appropriate restriction enzyme (5-10 U), as previously described (2.2.3.1). The restricted gDNA was then precipitated either by the addition of 0.7 vol 100% isopropanol at RT or alternatively by treatment with 10% (v/v) 3M sodium acetate and 200% (v/v) EtOH *p.a.* and subsequent incubation at -20 °C (see 2.2.4.3). The dried pellets were resuspended with 30 µl H_2O_{UF}, mixed with LoadingDye (1x) and loaded along with a DIG-labelled DNA size reference (DIG-marker III or VII, obtained from Roche Diagnostics GmbH) on a 1% (w/v) agarose gel. Separation of the DNA fragments via gel electrophoresis was conducted at a constant voltage of 80 V, achieving a field strength of 12 V/cm^2.

2.2.6.2 DNA transfer on Nylon membrane

After the gel electrophoresis, the nucleic acids were transferred to a nylon membrane by a capillary blot. First, the DNA in the gel was depurinated and denatured, to achieve an efficient transfer to the membrane. To this end, the gel was incubated for 15 min in 0.25 M HCl under gentle shaking condition, to induce the strand breaks. After a brief washing with $H_2O_{deion.}$, the gel was placed in denaturation buffer and incubated under gentle shaking for 30 min to induce denaturation of the double-stranded DNA under alkaline conditions. Following the

renaturation, the gel was incubated twice for15 min in neutralization solution. Between each buffer change, the agarose gel was briefly rinsed with $H_2O_{deion.}$. Finally, the gel was rinsed with 10X SSC and the DNA fragments were blotted on nylon membrane (Hybond N, GE Healthcare Life Sciences) as described by Southern, 1975 and Sambrook and Russell, 2001. The gel was blotted overnight by capillary transfer to a nylon membrane. Two gel blotting papers (GB 005; Schleicher & Schuell) were soaked with neutralizing solution and placed on a flat surface. The gel was laid on the wet gel blotting papers. A nylon membrane was placed on top of the gel and covered with two soaked gel blotting papers. A stack of dry paper towels was laid on top to draw the liquid and transfer the DNA onto the nylon membrane.

2.2.6.3 Nucleic acid hybridization

After the transfer, the membrane was air-dried and exposed to UV-light (120 mJ/cm^2) to prevent a loss of DNA from the membrane during hybridization. Hybridization was conducted with DIG-labeled probes (2.2.2.3). The membrane was pre-hybridized once in 10 ml hybridization buffer (per 100 cm^2) for 4 h at 60 °C. Hybridization was followed with 0.2-0.4 µg DIG-labeled probe in 3.5 ml hybridization buffer (per 100 cm^2) for 14-16 h at 60 °C. Prior to addition to the hybridization solution the DIG-labeled probe was denatured for 5 min at 95 °C and chilled on ice.

2.2.6.4 Detection step

The membrane was washed twice with SSPE (2x) + 0.1% SDS for 15 min and twice in SSPE (0.2x) + 0.1% SDS for 15 min at 60 °C. The following steps were done at room temperature: the membrane was incubated for 1-2 min in DIG-wash buffer, then blocked in 40-50 ml blocking buffer for 1 h. Anti-DIG antibody (1 µl) was suspended in 10 ml blocking buffer and the membrane was incubated in this solution for 45 min. Subsequently, the membrane was then washed twice in DIG-wash buffer for 15 min and incubated in detection buffer for 2-3 min.

For the detection, the substrate CSPD (25 mM) 1:2 (10 µl/10 ml) diluted in detection buffer was added to the membrane, followed by incubation for 15 min at 37 °C. After the incubation the CSPD solution was completely removed. The membrane was placed in a hybridization bag and sealed, and exposed to X-Ray film (Hyperfilm™ MP, GE Healthcare Life Sciences) inside an X-Ray cassette for 1h followed by developing of the film using AGFA CP 1000 (Typ CP 1000, Agfa-Gevaert) according to manufacturer's recommendations.

2.2.7 Transcriptome analysis using RNA-Seq

In order to investigate the gene expression profiles associated with the dimorphic transition, two generated dimorphic switch deficient mutants *Δmyco5* and *Δmyco56* were selected for transcriptome analysis using RNA-Seq. IPO323 and *ZtHOG1* null mutant served as control strains. Prior to RNA isolation, spore solutions of the strains were prepared with a final concentration of $1x10^6$ spores/ml each, and plated evenly on N-deprivation-agar plates covered with sterile cellophane. The plates were incubated for 7 days at 18 °C in order to obtain the synchronous cultures. Total RNA extraction was performed using the RNeasy Plant Mini Kit (Qiagen Sciences) following manufacturer's instructions. Prior to RNA extraction, the samples (cellophane with fungal biomass) were lyophilized followed by grounding to a fine powder using liquid nitrogen. In each case the RNA was extracted from three biological replicates. The quality and integrity of the isolated RNA were determined using a Bioanalyzer 2100 (Agilent). All samples had a 260 nm/280 nm ratio between 1.8 and 2.1 and a 28S/18S ratio within 1.7–2.0. The RNA concentration was assessed by ND-1000 NanoDrop spectrophotometer (NanoDrop Technologies). Library preparation was performed by GENterprise Genomics (Mainz, Germany) using 1.5 µg of total RNA for each strain. The samples were sequenced in a 150 bp paired-end run on an Illumina HiSeq 2500 (IMSB, Mainz, Germany). For the library preparation the TruSeq RNA Sample Prep Kit v2 (Illumina, Inc., CA) was used according to manufacturer's recommendations.

2.2.8 qRT-PCR analysis

qRT-PCR analysis was used for validation of RNA-Seq data, as well as to examine expression of selection genes *in planta* and during the axenic growth. For this purpose, cDNAs from RNA-seq samples (for each strain-pool) were used in a qRT-PCR experiment using the iQ SYBR Green Supermix Kit (Bio-Rad) with gene-specific primers and an annealing temperature of 59 °C. The procedure of total RNA extraction for all types of samples is described in 2.2.1.3. The PCR was conducted on a CFX96 Real-Time PCR Detection System (Bio-Rad). Transcript levels were measured from 2 biological replicates with 3 technical replicates each, according to Livak method, as a special case of Pfaffl method (Livak and Schmittgen, 2001, Pfaffl, 2001). *ß-tubulin* (*Zt99044*) was used as a constitutively expressed control gene (house-keeping gene). To compare the relative abundance of target gene transcripts, the average Ct value was normalized to that of *ß-tubulin* for each of the samples as $2^{-\Delta Ct}$, where $2^{-\Delta Ct} = (Ct_{(\text{target gene})} - Ct_{(\textit{ß-tubulin})})$. For instance, the fold changes of transcripts for selected genes from investigated mutants *(Δmyco56, Δmyco5* and *ΔZthog1*) compared to those

in wildtype strain IPO323, both exposed to switch-inducing growth condition, were calculated as $2^{-\Delta\Delta Ct}$, where $2^{-\Delta\Delta Ct} = [(Ct_{(target\ gene)} - Ct_{(ß\text{-}tubulin)})_{\ mutant\ under\ switch\text{-}inducing\ condition}] - [[(Ct_{(target\ gene)} - Ct_{(ß\text{-}tubulin)})_{\ IPO323\ under\ switch\text{-}inducing\ condition}]$. Primers used for quantitative real-time PCR are listed in the Table S6.

2.3 Methods for phenotypic characterization of *Zymoseptoria tritici* strains

2.3.1 Conidiogenesis

The assessment of the differences/similarities regarding the conidiogenesis in YEG liquid medium of the mutant strains compared to the wildtype strain *Z. tritici* IPO323 was performed as previously described (Kramer *et al.*, 2009). 300 µL of the prepared spore suspension of each strain (2.1.6.3) were adjusted to 10^7 spores/ml and then evenly plated on V8 agar medium using a Drigalski spatula and incubated for 5 days at 18 °C. Three homogeneously grown agar blocks (8 mm Ø) were used to inoculate 50 ml of YEG liquid medium in 100 ml Erlenmeyer flasks and the cultures were subsequently incubated for 72 h at 22 °C and 120 rpm. The corresponding spore production rates were determined microscopically using the cell counting chamber (Neubauer improved, Carl Roth GmbH & Co).

2.3.2 Biomass production

To compare the biomass production of the mutants with the wildtype strain *Z. tritici*, the liquid cultures in 50 ml YEG medium were prepared by inoculating as described (2.3.1) and incubated for 72 h and 120 rpm at 22 °C. After the incubation period, the liquid cultures were withdrawn in preweighted 50 ml centrifugation tubes (agar blocks used as inoculum were removed with a sieve) and centrifuged at 4,000 rpm for 5 min at RT. The supernatant was discarded and the resulting pellets washed once with deionized water and lyophilized. The dry weight of the cultures was determined by subtracting the tare weight.

2.3.3 Examination of vegetative growth behaviour on different media

In order to investigate the growth behaviour and phenotypes of the generated mutants (compared to wildtype), macroscopic appearance of the strains was monitored on different cultivation media. For each strain, the spore suspensions of various concentrations (5 of 1/10 dilutions of a dilution series, where 10^8 spores/ml represented the starting concentration) were prepared, as described (2.1.6.3) and 1.7 µl of each spore suspension was applied in triplicates on the defined agar plates. YEG and N-deprivation media served as the basis media and were

supplemented with different stress mediating components: NaCl, Sorbitol, H_2O_2, SDS, Congo Red (CR) in order to analyze the sensitivity of investigated strains to ionic and non-ionic osmotic stress, oxidative stress and cell wall stress respectively. Unless stated otherwise, the agar plates with applied cultures were finally incubated for 7 days at 18 °C. Additionally, the incubation was performed at 27 °C, in order to assess the temperature sensitivity.

2.3.4 Spore germination test

Germination studies of pycnidiospores of *Z. tritici* strains were conducted on microscopic slides covered with a thin layer of either water agar or water agar amended with 0.00025% (w/v) biotin and 0.001% (w/v) thiamine chloride. The incubation was performed in a moisture chamber for 72 h in the dark. The spores were directly microscopically analysed and the percentage of germinated spores of each strain was determined.

2.3.5 Pathogenicity assays

The pathogenicity assay was performed in order to assess the effect of gene inactivation on the disease development. The susceptible host plant was infected with wildtype and generated mutant strains. Inoculation, incubation and examination of intact plants were carried out as previously described (Kramer *et al.*, 2009), however with some modifications. Seven days solid medium cultures were used to inoculate 50 ml of YEG fluid medium in 100 ml flasks. The cultures were incubated at 18 °C under shaking condition (120 rpm). Conidia of investigated strains were harvested from 4-day-old YEG submerged cultures by pelleting them for 5 min at 4,000 rpm and resuspending to $1x10^7$ conidia/ml in 0.2% gelatine. Ten-day old seedlings of the susceptible wheat line *cv. Riband* were used for plant infection assays by brushing the spore solution on the marked area of the second plant leaf. The infected plants were placed into bags together with 100 ml of water. The infected plants were incubated at 22 °C with a 16-h light/8-h dark cycle at 80% humidity and examined 21 days after inoculation.

2.3.6 Micro-/Macroscopic analysis and photographic documentation of results

For stereomicroscopic analysis of the investigated strains the binocular Zeiss Stemi 2000-C (Carl Zeiss Microscopy GmbH) was used, which was mounted with the digital camera Canon PowerShotG10 to take the photographs. Light microscopic and fluorescence microscopic analyses were employed on Zeiss Axioskop 2 (Carl Zeiss Microscopy GmbH), equipped with CCD Videocamera Sony MC-3255P. For fluorescence detection of eGFP and FITC, a filter set with excitation at 470/40 nm and emission at 535/50 nm was used. For DAPI analysis the

excitation at 380/30 nm was employed and the emission was detected using 420 nm filter set. Pictures were acquired and edited using the AxioVision image analysis software ver. 4.8.2. Additionally, confocal laser scanning microscopy was performed using a Leica TCS SP5 II (Leica Microsystems) with an HCX PL APO lambda blue 63.0 x 1.20 Water UV objective lens. For the excitation of eGFP, an argon laser of 488 nm (15% strength) was used and the fluorescence emission was detected within the range 496 to 556 nm. The digitization of X-ray films as well as documentation of infected wheat plants was conducted with Epson Perfection V750 Pro flatbed scanner, using the corresponding scanning software for digital editing.

2.3.7 Spore Lysis Test

The strains selected for examination were grown in YEG as described (2.1.6.3). The conidial cells of each strain (4 ml adjusted to 10^7 spores/ml) were pelleted by centrifugation at 4,000 rpm, washed three times in an isotonic buffered solution (0.15 M Na_2HPO_4, 0.08 M citric acid, 1.4 M KCl; pH 5.8) and finally resuspended in 4 ml of this isotonic buffer. Each suspension was then treated with 30 mg of lysing enzymes from *Trichoderma harzianum* (Sigma) and incubated at 30 °C for 3 h with a slight stirring. The kinetics of protoplast release and lysing rate were monitored and determined by enumerating the remaining intact yeast-like conidia (or filaments in case of *Δmyco5* mutant strain) using cell counting chamber (Neubauer improved, Carl Roth GmbH & Co.).

2.4 Bioinformatic analysis and data mining

2.4.1 RNA-Seq data analysis considering expression of known pathogenicity related genes

The deduced amino acid sequences of significantly regulated genes were interrogated with the known pathogenicity proteins from different pathogenic fungi. For this purpose, a custom database was implemented containing the published pathogenicity factors, based on data obtained from the pathogen-host interaction (PHI) database (Urban, 2014). The interrogation against the custom database was performed using the local BLASTp search with a minimum *cutoff*-value of e10-29.

2.4.2 Multiple sequence alignment and phylogenetic analysis of *Zymoseptoria tritici* protein sequences

Phylogenetic analysis on the basis of the deduced *Z. tritici* protein sequences corresponding to the genes *MYCO1*, *MYCO4*, *MYCO5* and *MYCO56* was conducted together with the

respective homologues from other fungal pathogens, using the Geneious version 8.1 workbench package (http://www.geneious.com, Kearse *et al.*, 2012). All fungal protein sequences were retrieved from NCBI database. The alignment of protein sequences was performed using MUSCLE or ClustalW (Edgar, 2004, Larkin *et al.*, 2007), considering "BLOSUM" as a cost matrix with gap open cost and gap extend cost of 10 and 0.1 respectively. In each case *Saccharomyces cerevisiae* was included as taxonomic out-group. The phylogenetic tree was constructed using "neighbor-joining"-algorithm based on the "Jones–Taylor–Thornton (JTT)" - model. The statistical accuracy of the tree was tested by bootstrap analysis including 10^5 replicates.

2.4.3 Gene ontology and gene enrichment analysis

Gene ontology and gene enrichment analysis of differentially expressed genes provided by RNA-Seq analysis were performed using the tools Blast2GO Pro, TopGO and REVIGO (Conesa *et al.*, 2008, Alexa *et al.*, 2016, Supek *et al.*, 2011). The Blast2GO analysis tool was used for functional annotation analysis by retrieving descriptions of gene function based on the standardized vocabulary of the Gene Ontology bioinformatics initiative. The outcome of BlastGO analysis was then used to refine/update the GO annotation obtained from JGI. The resulting GO terms were further processed within TopGO analysis using Fisher's Exact Test in order to obtain a list of significantly enriched GO clusters, considering a corrected P-value of 0.05. Top 50 GO clusters for each investigated strain were then subsequently used for REVIGO online analysis (http://revigo.irb.hr) by discovering over-represented gene ontology (GO) categories of the differentially expressed (DE) genes ($p < 0.05$) and generating a global description of biological processes. This was achieved by grouping the related terms based on semantic similarity and removing of existing redundancies. Default parameters were used and the redundancy threshold (allowed similarity) was set to 0.7 (medium). The resultant enriched GO clusters, specific for each strain, were visualized as tree maps using the implemented R package *ggplot*.

2.4.4 Homology modelling and structure comparison

Three-dimensional model structures of deduced protein sequences obtained from JGI server for the genes *MYCO1*, *MYCO4*, *MYCO5* and *MYCO56* were generated by the Phyre2 free online homology modelling server, which constructs protein models based on homology modelling (Protein Homology/analogY Recognition Engine V 2.0) (Kelley *et al.*, 2015). Phyre2 uses the alignment of hidden Markov models via HHsearch to significantly improve

accuracy of alignment and detection rate. This incorporates a new *ab initio* folding simulation called "Poing" to model those regions of proteins, which have no detectable homology to known structures (Kelley *et al.*, 2015). The Phyre2 confidence score represents the probability (0 to 100%), that the match between an input sequence and a specific template delivers a true homology.

Molecular graphics and analytical data were obtained using the UCSF Chimera package, v.1.10.2 (Chimera). Chimera was developed by the Resource for Biocomputing, Visualization, and Informatics at the University of California, San Francisco (http://www.cgl.ucsf.edu/chimera). Prior the structure-based alignment the required alignment of homologous protein sequences for each protein was performed by MUSCLE or ClustalW analysis implemented within Geneious ver. 8.1 software package, using "BLOSUM" as cost matrix with "gap open cost" 10 and "gap extend cost" 0.1. The homologous protein sequences were retrieved by BLASTp analysis considering the following fungal organisms:

Aspergillus nidulans FGSC A4 (*A.n.*), *Aspergillus fumigatus* A1163 *(A.f.)*, *Blastomyces dermatitidis* SLH14081 *(B.d.)*, *Candida albicans* WO-1 (*C.a.*), *Coccidioides immitis* RS (*C.i.*), *Colletotrichum graminicola* M1.001 (*C.g.*), *Fusarium graminearum* PH-1 (*F.g.*), *Histoplasma capsulatum* NAm1 *(H.c.*), *Magnaporthe oryzae* 70-15 (*M.o.*), *Neurospora crassa* OR74A (*N.c.*), *Paracoccidioides brasiliensis* Pb03 (*P.b.*), *Sphaerulina musiva* SO2202 (*S.m.*), *Talaromyces marneffei* ATCC 18224 (*P.m.*), *Ustilago maydis* (*U.m.*), *Zymoseptoria ardabiliae* STIR04_1.1.1 *(Z.a.*), *Zymoseptoria brevis* ZBREZB163 *(Z.b.*) and *Zymoseptoria pseudotritici* STIR04_2.2.1 (*Z.p.*) and *Saccharomyces cerevisiae* (*S.c.*).

The structure represented as PDB file format was obtained from the preceding Phyre2 analysis. Consequently, structural models and homologous structures were aligned using the "*Match* → *Align*" function of Chimera. Images of protein models coloured by sequence conservation were generated using the Render by Conservation tool with default settings in Chimera. A corresponding colour key was generated for each rendering.

2.4.5 RNA-Seq data processing

For data processing in terms of transcriptome assembly and differential expression analysis, RNA-Seq processing pipeline based on TopHat-Cufflinks-Cuffdiff was used. First, the raw paired-end RNA-Seq reads were quality checked using FastQC (http://www.bioinformatics.babraham.ac.uk/projects/fastqc/), where necessary trimmed and were merged using FLASH 1.2.9 (http://sourceforge.net/projects/flashpage/?source=dlp). The merged paired reads were aligned to the reference genome using TopHat v1.3.3 (Trapnell *et*

al., 2009), run with standard options. As input parameters for TopHat v1.3.3 the reference genome build Zymoseptoria_tritici.MG2.30.dna.genome.fa.gz provided by EnsemblGenomes (ftp://ftp.ensemblgenomes.org/pub/fungi/release-30/fasta/zymoseptoria_tritici/dna/), and the annotation file Mgraminicolav2.FilteredModels1.gff based on filtered gene models provided by JGI server (http://genomeportal.jgi-psf.org/Mycgr3/Mycgr3.home.html, last accessed March 2015) were used. The fragment length parameter was set to 200 bases with a standard deviation of 100 bases. The Integrative Genomics Viewer (IGV; Robinson *et al.*, 2011, Thorvaldsdóttir *et al.*, 2013) was then used to visualize the assembled transcripts. Cuffdiff was finally employed in order to calculate the expression levels (expressed in FPKM values), using the standard annotation ".gff" file with the tophat aligned ".bam" file for each strain. To explore the processed RNA-Seq data and to visualize the differential expression patterns, the CummeRBund 2.0 analysis and visualization package for Cufflinks high-throughput sequencing data implemented in R/Bioconductor was used. The abundances were reported as normalized fragments per kb of transcript per million mapped reads (FPKM). All P-values obtained were adjusted using Benjamini-Hochberg procedure for false discovery rate from multiple-hypothesis testing. Genes with the corrected P-value (= q-value) of ($\leq$ 0.05) and a greater than 2.5 fold change in transcript levels were considered as differentially expressed, unless otherwise stated. Heatmaps of gene expression profiles were generated using R (www.R-project.org) based on significant expression changes (log10 FPKM plus 1).

2.4.6 Retrieval of target sequences and basic analysis

The gene sequences as well as deduced protein sequences were obtained from the database of JGI Mycosphaerella graminicola v.2 and interrogated against NCBI database entries to find orthologs in other organisms. Parameter values for BLAST 2.2.26 were set to default. Prediction of transmembrane helices in the query sequences was performed using TMHMM 2.0 and TargetP 1.1. Subcellular and nuclear localization of proteins were predicted by MultiLoc and cNLS Mapper respectively, using deduced amino acid sequences (Höglund *et al.*, 2006, Kosugi *et al.*, 2009).

3. Results

3.1 Generation of a transformant library by *Agrobacterium tumefaciens* mediated transformation

In order to elucidate the molecular basis of regulatory mechanisms associated with the dimorphic switch in *Z. tritici*, a mutant screen for the identification of genes involved in dimorphism was established. Based on random insertional mutagenesis (representing a forward genetics approach), a sustainable and durable library of transformants was created, aiming in a subsequent phenotypic exploration to selectively screen transformants affected in dimorphic transition upon inducing conditions. The mutagenesis program was conducted by *Agrobacterium tumefaciens*-mediated transformation (ATMT), representing a stable and reliable transformation method, which was previously established and approved in different reverse genetics studies with *Z. tritici* (Kramer *et al.*, 2009). Using pCAMB-HPT(*Sal*I) as a transformation vector (Kramer *et al.*, 2009, Figure 9C), containing hygromycin phosphotransferase gene (*HPT*) as a resistance marker derived from *Escherichia coli* under control of upstream *trpC* promoter from *Aspergillus nidulans* and downstream *NOS* terminator from *Agrobacterium tumefaciens*, a transformant library comprising about 10000 strains was generated by means of insertional mutagenesis. The transformants were subsequently subjected to a plate-based screening system, in order to identify dimorphic switch deficient candidate strains. For the screening system, choice and establishment of a suitable incubation medium is a valuable prerequisite for the cost- and time-efficient screening of generated "random" transformants. The following criteria were defined in order to find the appropriate medium suitable for screening purposes: 1) the medium should mimic the natural conditions regarding the nutrient availability on the leaf surface (i.e. lack of nutrients) 2) the medium should enable rapid, straight forward and unambiguous identification of mutants with defects in morphological transition 3) ensure a rapid growth of *Z. tritici* resulting in the sufficient biomass for downstream cultivation, considering the second round of the screening program. Among the solid media tested (potato dextrose agar (PDA), V8, water agar, nitrogen deprivation medium (N-deprivation medium) and minimal medium), N-deprivation medium was found to meet all three criteria. Therefore, the initial screen for dimorphic switch deficient mutants was performed by cultivating the generated random mutants on N-deprivation medium. The selected switch-deficient mutants were subsequently cultivated on water agar, likewise representing a strong switch inducing medium

but a poor nutrition medium for appropriate cultivation, to confirm their inability to perform the morphological transition (yeast-to-hyphal conversion).

3.2 Analysis of the frequency and mode of the T-DNA integration in the genome of *Zymoseptoria tritici*

One of the main parameters describing the quality of the transformation system is given by the transformation efficiency, which in its turn is primarily determined by the frequency and nature of genomic T-DNA integration. Thus, analyzing the T-DNA integration pattern concerning the insertion copy number and genomic integration mode of T-DNA, Southern Blot analysis was performed with 100 randomly selected transformants proved to be resistant to hygromycin B at 200 µg/ml (Figure 9B). To determine the percentage of multiple integration of the T-DNA and a "randomized" distribution of integration sites especially regarding the potential occurrence of so-called "hot spots" (genomic sites with bias towards T-DNA insertion, which has been reported in the case of some fungi) the isolated genomic DNA of transformants was fragmented with *Hind*III and probed with DIG-labelled *HPT*-fragment. Overall, a nearly 72% frequency of the presumably single-locus integration of the T-DNA was observed (Figure 9D). This observation is consistent with reports previously published in other fungi (Abuodeh *et al.*, 2000, Takahara *et al.*, 2004, Muench *et al.*, 2011). However, these conclusions should be considered with caution since the fragmentation of genome sequence by restriction enzyme can result in fragments of the same size, making it impossible to determine the exact number of T-DNA integrations. Additionally, the resulting fragments can vary drastically in size, being out of the visible size range suitable for appropriate detection within Southern Blot analysis. Fragmentation with *Hind*III was conducted in order to circumvent this problem, since according to the statistical distribution of restriction sites for *Hind*III in the genome sequence, 90% of the fragments would result in a size ranging from 0-7 kbp, by a mean size of approx. 3.2 kbp and standard deviation of approx. 3.5 kbp across 21 chromosomes of IPO323 genome (Figure S1). Furthermore, the T-DNA construct also harbors a *Hind*III-restriction site, leading to a better distribution of small-sized fragments (Figure 9A). The distribution pattern observed, which didn't display any biases towards detected hybridization signals within the Southern Blot analysis, as well as the theoretical knowledge about the distribution of generated restriction fragments, lead to the conclusion that in fact, no locus-specific preference for the T-DNA integration occurred. Considering this assumption, the ATMT approach appeared to be a suitable transformation

system offering a T-DNA transferability of genome-wide coverage, since a randomized distribution of integration sites could be achieved under defined conditions (Figure 9B).

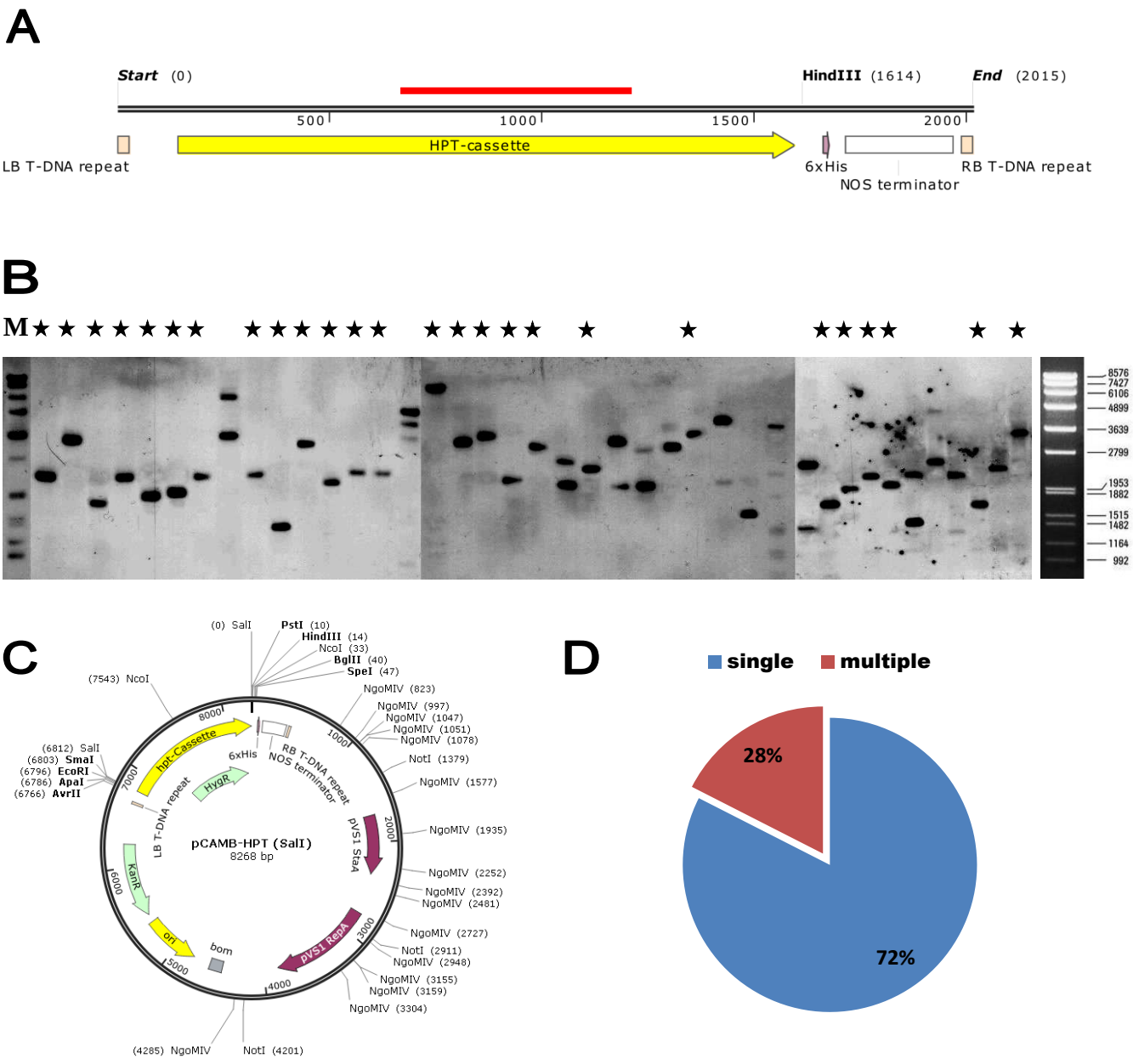

Figure 9: Analysis of *Z. tritici* random mutants generated by *Agrobacterium tumefaciens*-mediated transformation (ATMT). (A) Map of T-DNA construct used for genomic integration, containing *HPT* cassette (promoter+ORF+NOS terminator) flanked by left- and right-borders. *Hind*III restriction enzyme was used for the restriction of genomic DNA derived from the random mutants prior to the following Southern Blot analysis. The red bar indicates the location of probe used for hybridization. **(B)** Southern Blot analysis of 40 representative random transformants of *Z. tritici*. Genomic DNA of respective strains was restricted with *Hind*III. Black asterisks represent most likely a single T-DNA integration event; two or more hybridization signals indicate that most likely two or multiple T-DNA integrations in the recipient genome at different sites might have occurred. M: DNA Molecular Weight Marker VII, DIG-labeled (Roche Applied Biosciences). **(C)** Map of pCAMB-HPT (*Sal*I)-vector used for ATMT. **(D)** Pie chart showing the relative percentage of occurred T-DNA integration events in the generated random mutants (the estimated percentage refers to 100 randomly selected transformants).

3.3 Identification and characterization of "dimorphic switch" - deficient transformants

The outcome of the random mutagenesis approach resulted in 11 insertional mutants, exhibiting “dimorphic switch” deficiency and providing a recovery frequency of 0.11% when extrapolating from the total number of transformants screened. All of them remained mitotically stable, maintaining the hygromycin B resistance. Five successive passages of these transformants on YEG medium without hygromycin did not result in the loss of integrated T-DNA containing the *HPT* cassette. Thus, after five subcultures the transformants grew on V8 containing 200 µg/ml hygromycin B, suggesting that the *HPT* gene was stably integrated. The integration/insertion of *HPT* cassette was additionally confirmed in all mutants by colony-PCR (data not shown).

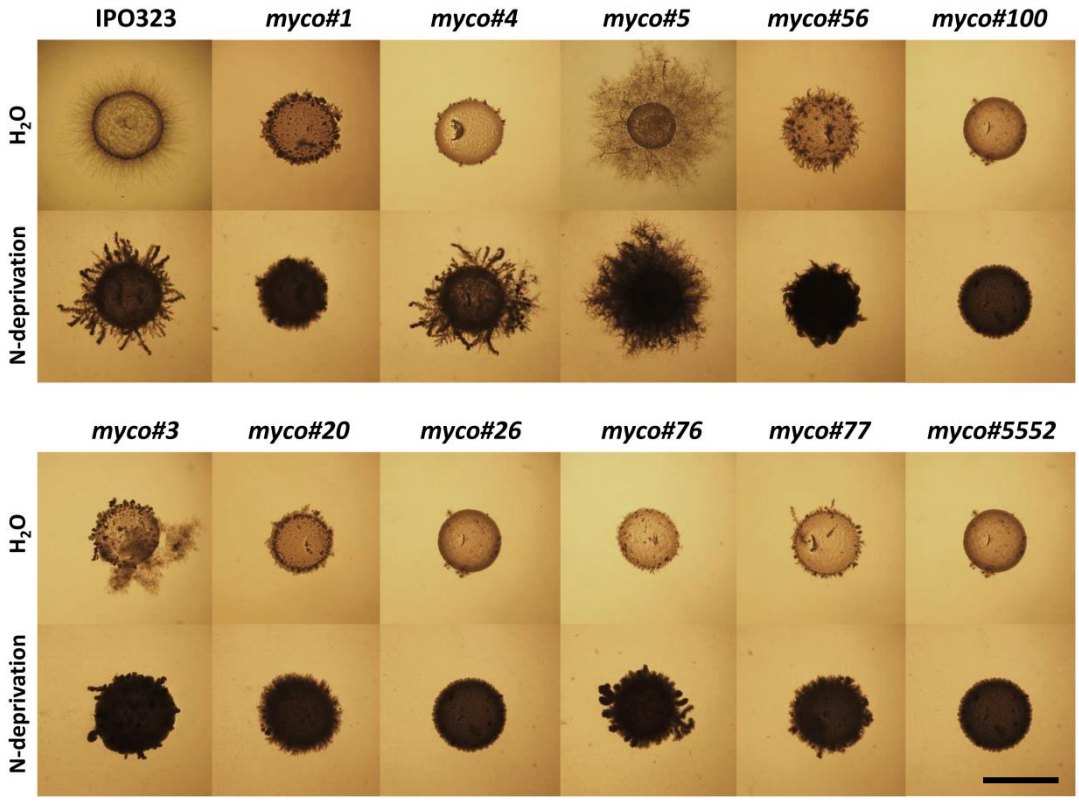

Figure 10: Analysis of *Zymoseptoria tritici* random mutant strains. The figure shows generated mutant strains (1.5 µl; 1×10^8 spores/ml) grown on water agar medium and nitrogen starvation medium (N-deprivation) after 21 days of incubation at 18 °C. N-deprivation medium was used as screening medium. Water agar (H_2O), which provides no external nutrition source was used for second round of screening. The wildtype strain IPO323 grows filamentously and forms mycelium on N-deprivation medium and water agar medium. The strains *myco#1*, *myco#3*, *myco#20*, *myco#26*, *myco#56*, *myco#76*, *myco#77*, *myco#100* and *myco#5552* show an extreme reduction in mycelium formation on both screening media. The *myco#4* mutant grows poorly on H_2O medium showing a drastically reduced mycelium formation, however beeing able to switch to filamentous growth on N-deprivation medium. In contrast, *myco#5* displays a hyperfilamentation phenotype under tested cultivation conditions, exhibiting a severely increased filamentous growth. Scale bar corresponds to 1 cm.

Ten of the recovered mutants were growing predominantly yeast-like under switch-inducing conditions (Figure 10). One mutant, designated *myco#5*, appeared to be locked in one growth stage producing a high amount of mycelium even on complete medium. Hence, nine random mutants, which were designated *myco#1*, *myco#3*, *myco#20*, *myco#26*, *myco#56*, *myco#76*, *myco#77*, *myco#100*, *myco#5552*, exhibited a yeast-like propagation under switch-inducing condition by incubating them on N-deprivation medium or water agar at 18 °C (Figure 10). In the case of *myco#4*, one striking feature was apparent: within the first 7 days of cultivation on N-deprivation medium, the mutant strain grew exclusively yeast-like (data not shown). However, when following the prolonged incubation period of 21 days, the morphological conversion starting at 14 days of incubation from yeast-like towards filamentous growth was evident, indicating a delayed mode of transition compared to that of wildtype strain IPO323. Interestingly, when *myco#4* was grown on water agar, no visible formation of hyphae could be observed, even when the cultivation time was extended to 21 days. Furthermore, the growth was very sparse, resulting in a significantly reduced colony density compared to wildtype (Figure 10).

For the random mutant *myco#5*, a predominantly filamentous growth was detected, regardless of the cultivation condition. Thus, incubating the mutant strain on the YEG standard medium at 18 °C, which normally supports the yeast-like propagation of the wildtype strain, revealed contrary to the wildtype a filamentous growth accompanied with the formation of aerial mycelium. Interestingly, a very similar growth behavior was noticed in YEG liquid medium, resulting in the enhanced mycelium formation, which was not observed in the wildtype strain IPO323 and other strains (data not shown).

3.4 Molecular identification of T-DNA tagged gene loci

Genome walking analysis was performed in order to examine the T-DNA integration sites and to identify genes potentially associated with an observed deficiency in morphological transition. The putative disrupted gene loci were identified for all insertional switch deficient mutants obtained. The T-DNA integration sites were recovered by “step-down” amplification of genomic DNA fragments acquired by endonuclease restrictions from two enzyme sets, followed by an adaptor ligation using a modification of the method previously described by Zhang and Gurr (2000). This approach allowed the amplification and isolation of DNA fragments in a range between 500 bp to 5 kb, followed by DNA-sequencing. Using BLASTn, a comparison of the sequences flanking the T-DNA with fungal genome sequence provided by JGI (Zymoseptoria Sequencing Project, Broad Institute of Harvard and MIT,

http://www.broadinstitute.org/) revealed significant similarities, allowing the identification of the T-DNA integration sites precisely and to localize the corresponding disrupted gene loci (Figure 11).

Prior to genome walking analysis selected mutants were subjected to Southern Blot analysis to evaluate the T-DNA integration frequency in the mutants investigated. This was achieved in analogy to previous analysis with randomly chosen mutants by restriction of isolated gDNA with endonucleases *Hind*III, *Psp*OMI and *Not*I. Similarly to *Hind*III the selected endonucleases were analyzed for the restriction pattern of gDNA concerning the restriction fragment distribution and were found to be suitable for Southern Blot analysis. The resulting fragmentation was examined by probing with PCR-amplified *HPT* cassette fragment. Hence, in case of *myco#1*, *myco#3*, *myco#4*, *myco#5*, *myco#26*, *myco#56*, *myco#76*, *myco#100* and *myco#5552* single hybridization signals were detected, indicating only single genomic sites of T-DNA insertion. For the mutant strains *myco#20* and *myco#77* several hybridization signals were observed, suggesting multiple genomic T-DNA insertion sites (data not shown). Overall, among the T-DNA insertions sites detected, two (in case of *myco#3* and *myco#56*) were located within open reading frames (ORFs) of annotated genes, while the remaining nine genes (*myco#1*, *myco#4*, *myco#5*, *myco#20*, *myco#26*, *myco#76*, *myco#77*, *myco#100* and *myco#5552*) were positioned in the intergenic regions (Figure 11). The significant insertion bias towards predicted promoter and terminator regions goes along with previous reports for *Magnaporthe oryzae* (Meng *et al.*, 2007). Furthermore, neither deletion of small regions in the recipient genome through microhomology nor truncation of T-DNA on both termini were detectable, both events which were previously described in plants (Kleinboelting *et al.*, 2015). The JGI database IDs for the predicted genes derived from genome walking analysis as well as further information concerning homology analysis and genomic coordinates of T-DNA insertions sites are shown in Table 4.

Figure 11: Results of genome walking analysis of recovered T-DNA disrupted gene loci. Predicted T-DNA insertion sites for each random mutant within putative genomic loci containing annotated genes are shown. DNA sequences obtained from genome walking PCR are illustrated as red lines aligned to a corresponding genomic locus; arrow heads determine the sequencing direction. Restriction enzymes used to obtain each of the DNA fragments prior to sequencing are indicated. Genes are named in concordance with JGI annotation by their Protein ID. The asterisks indicate the start position of the region matching the partial sequence of *HPT* cassette, thus pointing to the site of T-DNA integration for each mutant strain-specific locus. In case when the portion of *HPT* cassette was not identified, the putative genomic position of T-DNA inserted was estimated by fragment length obtained from restriction analysis and Southern Blot results. Predicted sites of T-DNA insertions are marked by vertical arrowheads.

Because some of the mutants identified had multiple copies of integrated genomic T-DNA, which hampered the precise identification of disrupted gene loci responsible for the phenotypic alteration observed, this study aimed to characterize only those mutants whose T-DNA integration event could be uniquely assigned to genes consonant with JGI annotated gene models. Generally, mutants were preferred which harbored the T-DNA insertion in the open reading frame (ORF) of the putative gene or promoter regions. Additionally, proximity to the neighbor regions was considered, thus, for instance, the location of T-DNA in the intergenic region of two approximately equally distant genes would indicate each of the genes could potentially cause the phenotypic effect observed. In this case, the additive effect or (synergistic) epistasis of both disrupted genes is unavoidable, meaning that functional analysis of both genes would be essential to evaluate the link between the disrupted locus and phenotype associated with corresponding mutant strains.

Hence, in this study, we provide detailed phenotypic characterization regarding the morphological and physiological properties of four of those interesting dimorphic switch deficient mutants. A detailed functional characterization of putatively T-DNA tagged genes assigned to these mutants was conducted and is presented in the following chapter. Only the mutant strains indicated as *myco#1*, *myco#4*, *myco#5* and *myco#56* were chosen for further functional processing since examining all of the mutants generated and provided in the list, the chosen four mutants were found to meet all criteria mentioned above for further investigation. Southern Blot analysis revealed that the random mutants selected had most probably single genomic T-DNA integrations, as far as only single hybridization signals in each case were detected. Furthermore, the hybridization pattern observed from Southern Blot analysis coincided with results obtained from genome walking analysis (data not shown).

Table 4: Summary of *Z. tritici* genes identified from T-DNA flanking sequences.

Mutant strain	T-DNA location / Protein ID (JGI)	Size nt (aa)	BLASTp match with functional annotation	Organism	BLASTp E-value (identity %)
myco#1	**Chr.3 at position 2.499.750 / ID: 70181**	**2277 (589)**	two-component response regulator SSK1p	[*Blumeria graminis* f. sp. hordei DH14]	**1e-156 (52%)**
myco#3	**Chr.11 at position 1.383.695 / ID: 63892**	**1125 (373)**	Hypothetical protein (letm1-like protein)	[*Marssonina brunnea* f. sp. 'multigermtubi' MB_m1]	**1e-37 (37%)**
myco#4	**Chr.8 at position 84.634 / ID: 87000**	**1343 (428)**	phosphoribosylamine-glycine ligase	[*Sphaerulina musiva* SO2202]	**0.0 (72%)**
myco#5	**Chr.1 at position 4.409.323 / ID: 66947**	**1441 (247)**	Hypothetical protein (Modifier of rudimentary)	[*Macrophomina phaseolina* MS6]	**2e-55 (53%)**
myco#20	**Chr.4 at position 2.507.660 / ID: 109296**	**1790 (551)**	amino acid permease	[*Trichophyton rubrum*]	**1e-154 (54%)**
	Chr.9 at position 2.068.569 / ID: 105813	**671 (120)**	Hypothetical protein (*Z. tritici* unique)	–	–
myco#26	**Chr.11 at position 1.278.735 / ID: 49268**	**498 (165)**	Hypothetical protein (DUF1768-domain containing protein)	[*Alternaria alternata*]	**2e-39 (44%)**
	Chr.11 at position 1.278.804 / ID: 77057	**1730 (480)**	Zinc finger RING protein	[*Macrophomina phaseolina* MS6]	**8e-87 (36%)**
myco#56	**Chr.8 at position 1.351.161 / ID: 110503**	**2931 (743)**	RNA-binding post-transcriptional regulator cip2	[*Aspergillus lentulus*]	**4e-166 (54%)**
myco#76	**Chr.12 at position 1.278.989 / ID: 50731**	**310 (76)**	DUF1242-domain-containing protein	[*Sphaerulina musiva* SO2202]	**1e-39 (88%)**
myco#77	**Chr.3 at position 1.655.698 / ID: 27490**	**600 (200)**	copper homeostasis protein CutC	[*Flavobacterium cauense*]	**6e-48 (53%)**
	Chr.15 at position 502.425 / ID: 97690	**1524 (434)**	Hypothetical protein (*Z. tritici* unique)	–	–
myco#100	**Chr.6 at position 967.563 / ID: 109795**	**2133 (582)**	Patatin/Phospholipase A2-related protein	[*Macrophomina phaseolina* MS6]	**2e-139 (51%)**
myco#5552	**Chr.2 at position 1.195.392 / ID: 36801**	**1258 (396)**	Methionine synthase, vitamin-B12 independent	[*Purpureocillium lilacinum*]	**0.0 (75%)**
	Chr.2 at position 1.195.392 / ID: 103147	**1054 (289)**	Delta(12) fatty acid desaturase	[*Pyrenophora tritici-repentis* Pt-1C-BFP]	**3e-134 (70%)**

The gene and protein sequences were retrieved from the *Z. tritici* completed genome v.2 database at http://genome.jgi-psf.org/Mycgr3/Mycgr3.home.html. For each random mutant the T-DNA insertion site identified by genome walking approach as well as the best BLASTp match with provided E-value and corresponding organism are shown.

3.4.1 Identification of T-DNA insertion site in targeted mutant strains and functional gene sequence analysis of *MYCO1*, *MYCO4*, *MYCO5* and *MYCO56*

A detailed sequence analysis of the amplified flanks in case of mutant *myco#1* revealed that the T-DNA integration occurred in the 5'-UTR region (at 327 bp) of the annotated gene with the Protein ID 70181 according to JGI Institute database or MYCGR3_70181 according to Ensemble (Figure 12A). The precise location of T-DNA insertion was determined on chromosome 3 at genomic position 2.499.750 (Table 4, Figure 11). BLASTp analysis of the deduced protein sequence indicated that this gene encodes a homolog of Ssk1p, a known regulator within the *HOG1*-pathway in fungi (Saito, 2004, Bahn *et al.*, 2006, Jacob *et al.*, 2015), based on similarity to the *Magnaporthe oryzae* homologous protein with significant E-value of 1.24e-153 and 99% identity. Myco1p is a predicted 589 amino acid protein harboring a *Response_Reg* domain (Pfam ID: PF00072) located between amino acids 329–406.

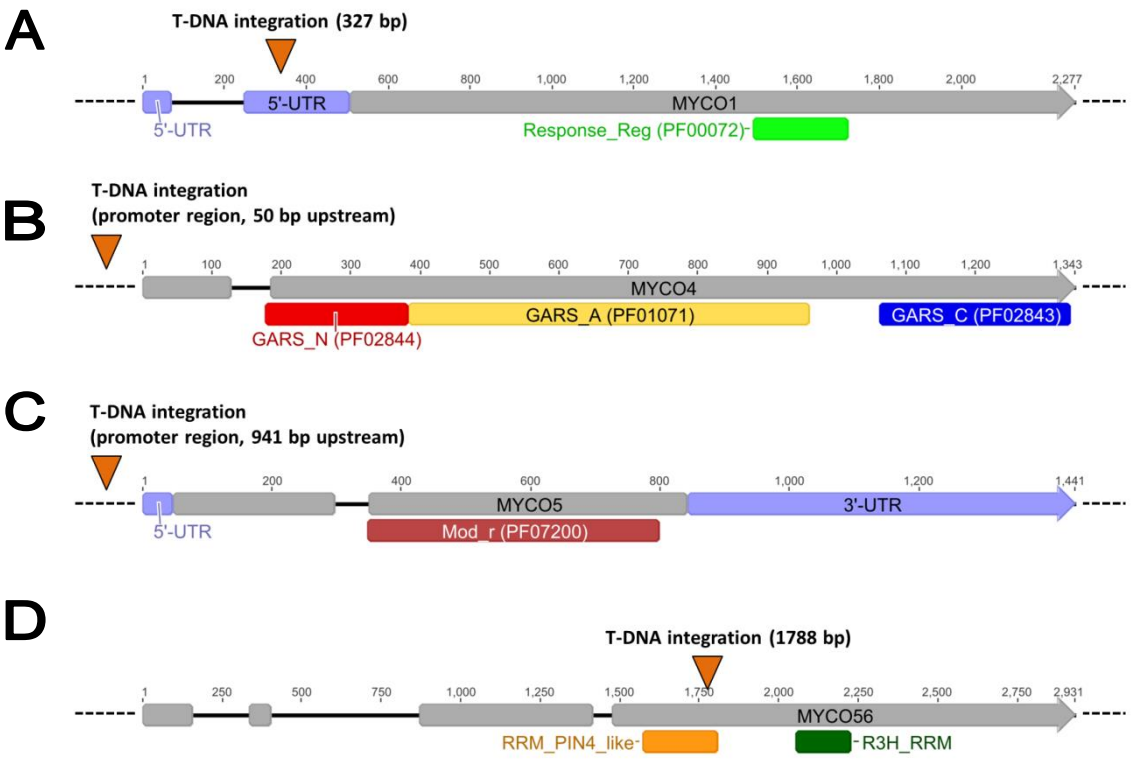

Figure 12: Structural analysis of target genes. The figure illustrates the structure of the predicted target genes *MYCO1* (A), *MYCO4* (B), *MYCO5* (C) and *MYCO56* (D) affected by random mutagenesis. T-DNA location sites (*HPT*-integration) assigned in the corresponding gene loci are indicated. The numbers over the bars indicate the length of the annotated genes according to JGI gene models. The highlighted bars represent the functional domains of each gene, determined by Pfam database interrogation using InterProScan and mapped to the corresponding gene model. Introns are indicated as black lines joining gene exons, the latter represented as gray bars. Dash lines depict flanking regions of the genes. Orange triangles mark identified position of T-DNA insertion for each target gene. UTR: untranslated region.

For the *myco#4* mutant, the genomic T-DNA insertion location was identified on chromosome 8 at genomic position 84.634 (Figure 12 B), about 50 bp upstream of a predicted gene (JGI Protein ID: 87000; Ensembl: MYCGR3_87000) with high similarity to the bifunctional *Saccharomyces cerevisiae* ADE5,7 (46% amino acid identity) required for the second and fifth step of *de novo* purine nucleotide biosynthesis (Table 4, Figure 11). This gene was previously functionally characterized in the yeast *S. cerevisiae* and *C. albicans* encoding a bifunctional enzyme possessing phosphoribosylglycinamide synthetase (aminoimidazole ribotide synthase/glycinamide ribotide synthase) activities (Jones and Fink, 1982, Jezewski *et al.*, 2007). The similarity is largely confined to the region where the predicted functional domains are located. These domains include *PRibGlycinamide_synth_N* (PF02844), *PRibGlycinamid_synth_ATP-grasp* (PF01071) and *PRibGlycinamide_synth_C-dom* (PF02843). However, we noticed an absence of functional domains *AIRS* (PF00586) and *AIRS_C* (PF02769) typically present in other fungi including the yeast homolog, indicating that the *Z. tritici* counterpart is monofunctional (Figure S2). In our prescreening the random mutant lacking the functional gene exhibited a poor vegetative colony growth on poor-nutrient media like N-deprivation and water agar, providing a nutrient-less medium. When grown on YEG standard complex medium a very similar phenotype to wildtype was observed. Also, no defects in spore morphology were visible when comparing to the wildtype strain IPO323. However when grown on MM or N-deprivation medium the colonies of *myco#4* mutant exhibited a sparse growth compared to wildtype, prohibiting a considerable biomass increase, thus indicated auxotrophic properties of the mutant.

In case of *myco#5*, sequence analysis of the *HPT*-insertion region using BLASTn against the genome sequence of *Z. tritici* (provided by JGI server) revealed that T-DNA was integrated in the promoter region on chromosome 1 at position 4.409.323, 941 bp upstream of the predicted ATG translational initiation codon of the annotated gene with JGI Protein ID 66947 (MYCGR3_66947). *MYCO5* is predicted to encode a hypothetical protein comprising a *mod_r* domain (PF07200) (Figure 12C). The similarity between the likely orthologues is mostly confined to the C-terminal of the proteins. The presence of *mod_r* domain appears to be a common feature of proteins which show homology to Modifier of rudimentary (*mod_r*) proteins of *Drosophila melanogaster*. Proteins of this family harbour generally acidic residues at the N-terminal half, whereas the C-terminal half has a basic character. One member belonging to this family is Vps37p, being along with Vps23p and Vps28p part of the endosomal sorting complex ESCRT-I which represents a protein complex involved in cellular protein trafficking and sorting at the multivesicular body (MVB) (Hurley *et al.*, 2010). In

addition, the mammalian homolog of Vps37p interacts with Tsg101p (PF05743) through its *mod_r* domain and its function was previously shown to be essential for lysosomal sorting of EGF receptors (Lu *et al.*, 2003, Stuchell *et al.*, 2004).

In the *myco#56* random mutant, T-DNA integration occurred on chromosome 8 at the genomic position 1.351.161, 1788 bp downstream of the start codon within the ORF of the gene with JGI Protein ID 110503 (MYCGR3_110503) (Table 4, Figure 11, Figure 12D). The most similar previously characterized protein found in the NCBI "nr"-database was the *Schizosaccharomyces pombe* protein Cip2p (Acc. No. NP_592895.1; E-value: 3e-41), which shares 32% of its amino acids with Myco56p. In *Z. tritici* the predicted protein is a 743 amino acids protein with an *RRM_6* domain (PF14259) located between amino acids 295–365 and an *R3H* domain (PF01424) located between amino acids 469-510. *RRM* domains were previously reported to be typically present in proteins involved in RNA processing. A prominent example is given by a functional triade, consisting of Csx1p, Cip1p and Cip2p, previously shown to play a crucial role in controlling gene expression during oxidative stress in *S. pombe* (Rodriguez-Gabriel *et al.*, 2003). Cip1p and Cip2p counteract the function of Csx1 to control the stability of cellular mRNAs upon intermediate oxidative stress (Martin *et al.*, 2006). Cip2p also harbors an *R3H* motif suggested functioning in sequence-specific binding to single-stranded nucleic acids (Grishin, 1998). Performing a BLASTp search, the sequence homology of Myco56p to its homologs was as expected confined predominantly across the *RRM* domain and *R3H* domain.

3.4.2 Phylogenetic analysis and further extended characteristics of identified candidate genes in *Zymoseptoria tritici*

In order to determine the relationship of deduced amino acid sequences of identified genes with homologs derived from other fungal species a phylogenetic analysis was performed, taking closely and distantly related species into consideration, comprising both, filamentous and systemic dimorphic fungi. At least 16 orthologous genes from other organisms for each target gene examined were selected to construct phylogenetic trees. The orthologue sequences were originating among others from the closely related fungi such as *Zymoseptoria brevis*, *Zymoseptoria pseudotritici*, *Zymoseptoria ardabiliae, Sphaerulina musiva, Magnaporthe oryzae, Neurospora crassa*, *Aspergillus oryzae*, *Colletotrichum graminicola*, as well as distantly related systemic dimorphic fungi, e.g. *Candida albicans*, *Histoplasma capsulatum*.

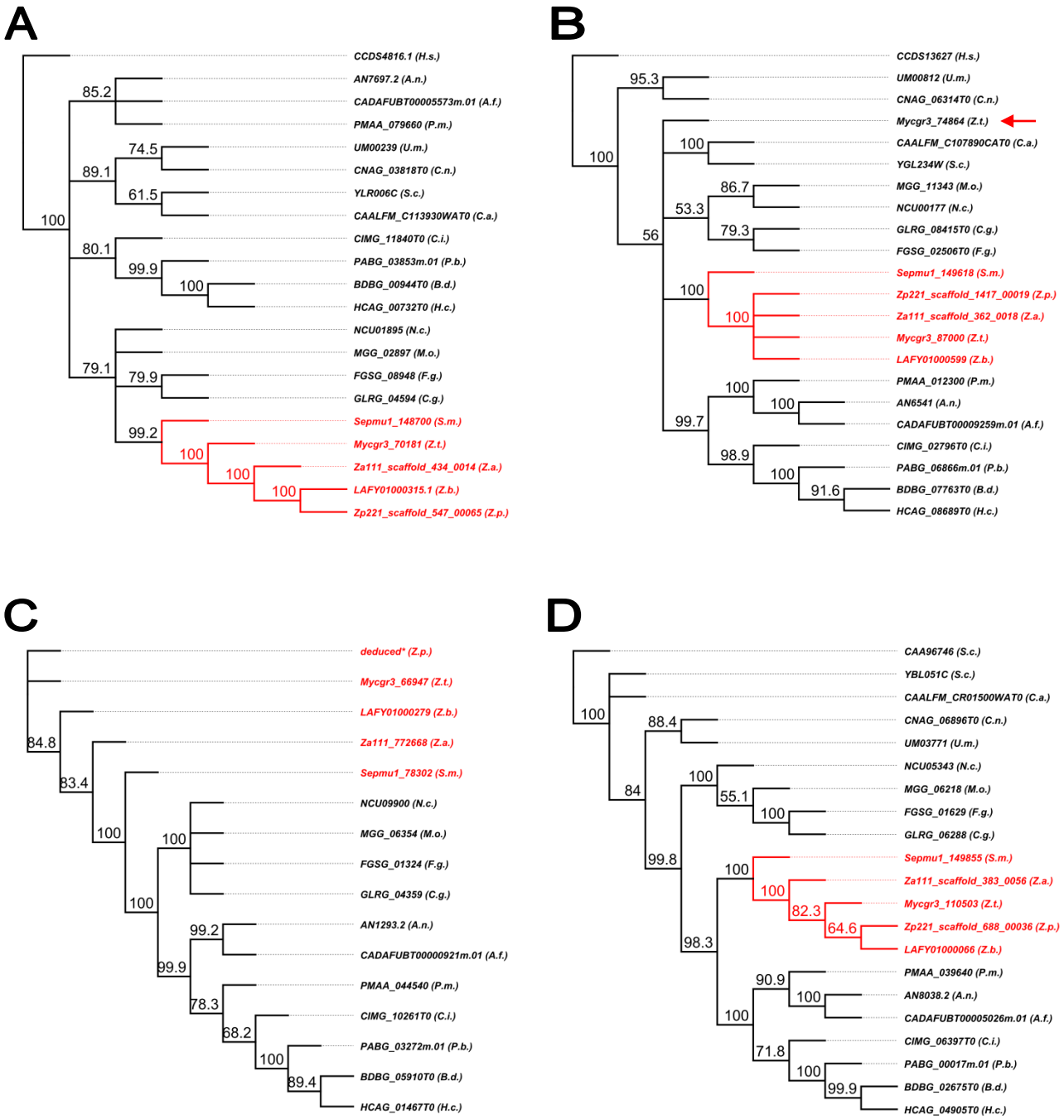

Figure 13: Phylogenetic trees of *Zymoseptoria tritici* (*Z.t.*) candidate genes with the corresponding predicted homologs from different fungi. The tree construction is based on amino acid sequence alignments performed by MUSCLE program. The trees represent the phylogenetic relationships of **(A)** Myco1p, **(B)** Myco4p, **(C)** Myco5p and **(D)** Myco56p with orthologs in other fungi, including *Aspergillus nidulans* FGSC A4 (*A.n.*), *Aspergillus fumigatus* A1163 *(A.f.)*, *Blastomyces dermatitidis* SLH14081 *(B.d.)*, *Candida albicans* WO-1 (*C.a.*), *Coccidioides immitis* RS (*C.i.*), *Colletotrichum graminicola* M1.001 (*C.g.*), *Fusarium graminearum* PH-1 (*F.g.*), *Histoplasma capsulatum* NAm1 *(H.c.*), *Magnaporthe oryzae* 70-15 (*M.o.*), *Neurospora crassa* OR74A (*N.c.*), *Paracoccidioides brasiliensis* Pb03 (*P.b.*), *Sphaerulina musiva* SO2202 (*S.m.*), *Talaromyces marneffei* ATCC 18224 (*P.m.*), *Ustilago maydis* (*U.m.*), *Zymoseptoria ardabiliae* STIR04_1.1.1 *(Z.a.*), *Zymoseptoria brevis* ZBREZB163 *(Z.b.*) and *Zymoseptoria pseudotritici* STIR04_2.2.1 (*Z.p.*). *Saccharomyces cerevisiae* (*S.c.*) and *Homo sapiens* (*H.s.*) were used as outgroup. The phylogenetic trees were constructed using "neighbour-joining"-algorithm based on the "Jones-Taylor-Thornton (JTT)" - model. The statistical accuracy was tested by bootstrap analysis including 100000 replicates. Deduced*: target gene identified by advanced BLAST and Mauve analysis in *Z.p.* Red arrow indicates the deduced protein possessing *AIRS* domain (Protein ID: 74864), which is not present in the "monofunctional" Myco4p.

If available, the orthologues sequences of *Homo sapiens* or *Saccharomyces cerevisiae* were used as outgroup for the construction of rooted phylogenetic trees. As expected, the results indicate that in each case the deduced proteins across the *Zymoseptoria* species were grouped together in one phylogenetic clade suggesting their origin from a single progenitor species (Figure 13). For *MYCO5*, no orthologs in genomes of *Candida albicans* and *Histoplasma capsulatum* were found, indicating apparently an affected synteny between *Z. tritici* and systemic dimorphic fungi as a consequence of a possible loss of genetic information due to evolutionary adaptation processes. Relying on the latest genome annotation of the closely related *Zymoseptoria pseudotritici*, no orthologous sequences could be identified when performing BLAST analysis. However, when conducting a genome-wide mapping of the gene sequence against the entire genome sequence of *Z. pseudotritici* provided by JGI, the existence of homologous gene was apparent. Furthermore, an augmented analysis using Mauve (Darling *et al.*, 2004) revealed a high conservation of the genomic locus, supporting the synteny across *Zymoseptoria* species (data not shown). For the Myco4p the homologous protein sequences were clustered in three distinct clades dependent on the occurrence or absence of the additional functional domains. As expected, the protein sequences from the closely related species *Z. tritici*, *Z. brevis*, *Z. ardabiliae*, *Z. pseudotritici* and *Sphaerulina musiva* were classified together in one group, reflecting their relatedness based on the presence of three predicted domains *GARS_N*, *GARS_A* and *GARS_C* (Figure S2). For the other related fungal species (e.g. *C. albicans*, *M. oryzae*, *N. crassa*, *A. oryzae* and *F. oxysporum*) two additional domains *AIRS* and *AIRS_C* were predicted, consonant with the bifunctionality of the enzyme previously reported for most of the fungal organisms. An orthologous protein from *H. sapiens* was found in a separate branch, based on the observation that the protein contains along with aforementioned functional domains an additional motif (*Formyl_trans_N*) located in the C-terminus. This observation goes along with previous reports, indicating that the human protein is trifunctional.

3.4.3 Three-dimensional structure prediction of the deduced protein sequences

To approve the results obtained from BLASTp search, regarding the protein homology especially of Myco5p and Myco56p, Phyre2 supported modeling was performed. With this approach, we aimed to deduce the potential function of the proteins from its structural information by three-dimensional modeling and thereby to verify or complement the results obtained by BLASTp analysis. By inferring the modeled structure, we exploited the assumption that evolutionary the three-dimensional structure is more closely associated with

potential function than would be expected on the basis of primary sequence conservation. Despite the fact that sequence similarity across different species can be quite low, the structural homology can be well supported, suggesting similar or at least related functional activity. Running Phyre2 in the "intensive mode" revealed for both (Myco5p and Myco56p) several template hits reported previously. In the case of Myco5p, the final model of the protein modeled 72% residues with a well-supported confidence score of > 90%. As a basis for the modeling of protein structure, two templates were selected, relying on the heuristics to maximize confidence, alignment coverage and percentage identity. The amino acids 62 to 240 of the deduced Myco5p protein sequence were aligned to a chain C of the Srn2p protein (PDB-ID: 2P22) in yeast, being an assembly component of the ESCRT-I heterotetramer core. The alignment coverage spanning the amino acids 62 to 240 comprised 166 aligned residues, with 17% of identical amino acids and the corresponding model was computed at 99.87% confidence, indicating a 99% chance that Srn2p is a true structural homolog. Meanwhile, the sequence region of Myco5p spanning amino acids 2-87 was modeled based on the homology with chain C of the Smnp (PDB-ID: c4nl6C) protein at 74.84% confidence score, relying on the 86 aligned amino acid residues, 19% of which were identical.

In case of Myco56p, only 21% of residues of provided query sequence were modeled at >90% confidence, indicating that no existing protein structure templates (hidden Markov models) with a significant similarity to Myco56p are present in the Phyre2 database of HMMs of known protein structures. Thus, 73% of the sequence were predicted to be disordered and were therefore modeled *ab initio*, resulting in a quite reduced structural reliability, since disordered regions cannot be meaningfully predicted. The best template hit could be assigned to Ref2p, an mRNA export factor, showing only 14% of identity at 99.6% confidence and spanning 127 aa residues (from 241 to 368) within the generated alignment with Myco56p query sequence. The obtained result for Myco56p should be regarded with caution. Therefore the information referring to homology comparison, to retrieve the homologs for Myco56p, was relying on results obtained from preceding BLASTp analysis.

Using UCSF Chimera, a sequence conservation analysis was performed based on the preliminary alignment analysis of corresponding protein sequences by MUSCLE (the same as was used for construction of phylogenetic trees; data not shown). The resulting alignment was finally mapped on the protein structure provided by the aforementioned Phyre2 analysis. In both cases, Myco1p and Myco4p, the rendered residues of the proteins (colored in blue) indicate a high structural conservation, since the most conserved regions covered the whole

protein sequence in accordance with the preceding alignment analysis, thereby suggesting the functional conservation of the proteins (Figure 14).

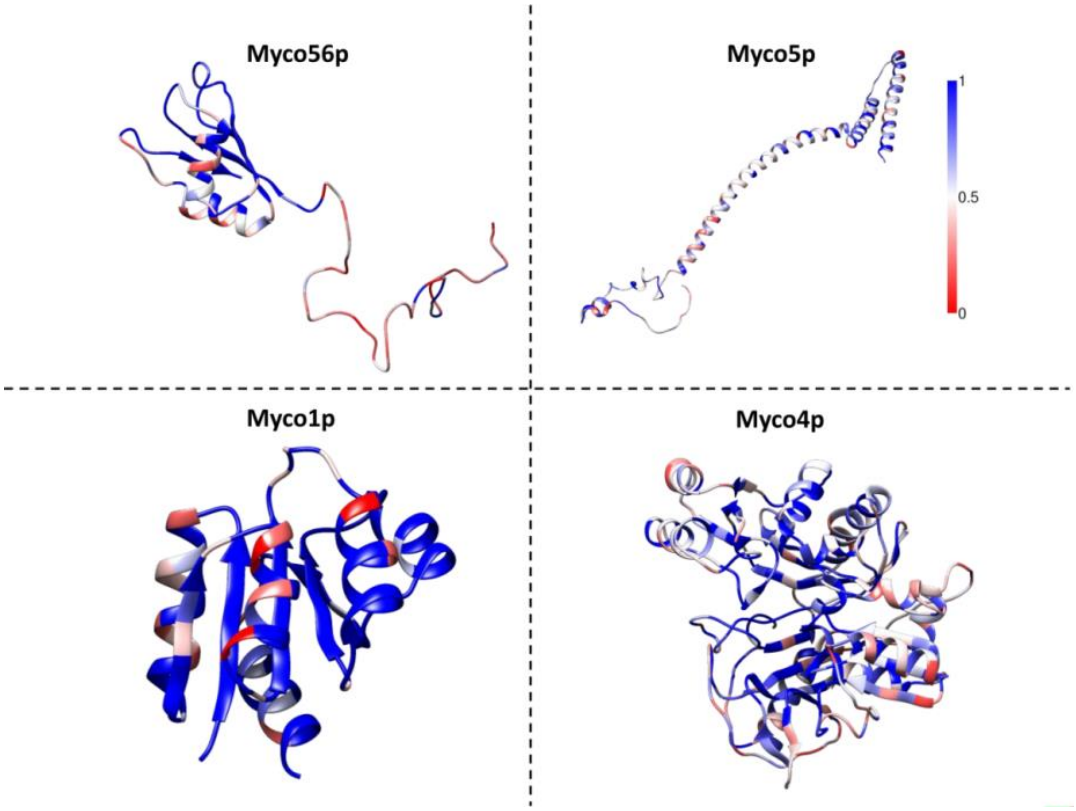

Figure 14: Three-dimensional structural analysis with target protein sequences deduced. The predicted 3D structures of Myco1p, Myco4p, Myco5p and Myco56p with residues color-coded according to their conservation in the alignment are shown. In the present case, the most conserved regions are coloured in blue and the less conserved ones in red. The figure was prepared using UCSF Chimera version 1.10.2.

For the Myco5p the structural conservation is confined to the second half of the protein sequence including the C-terminus. According to preceding Pfam analysis, this region was predicted to contain a *mod_r* domain, ranging from amino acid 82 to 234. Analyzing the second structure of primary protein sequence by EMBOSS garnier (Rice *et al.*, 2000), this domain is found to contain beta-sheet structures for the first half the protein sequence and for the remaining part exclusively the Alpha-helices, both arranged in a serial manner (data not shown). Contrarily, in the case of Myco56p, the structural conservation was confined to the first half of the protein sequence, including N-terminus of the protein and the region enclosing functional domains *RRM_6* (PF14259) and *R3H* (PF01424) previously identified. This observation coincides with the 3D protein model obtained from Phyre2 analysis, signifying a well fitted structural conservation for the first half of the protein (N-terminal), whereas the

second part was predicted to be disordered and therefore was modeled with a reduced structural reliability.

3.4.4 Verification of random mutants by targeted gene inactivation and initial phenotypic characterization

In order to validate the genome walking results and to evaluate the postulated involvement of the selected genes in dimorphic transition, directed gene inactivation and complementation *Z. tritici* mutants were generated based on homologous and heterologous recombination respectively. The success of targeted gene replacement using the *HPT* containing transformation construct was validated by screen-PCR and Southern Blot analysis (Figure S3B-D, S4B-D, S5B-D and S6B-D). For the generated complementation strains the genomic reintegration of intact native gene copy was evaluated by screen-PCR using *BAR*-cassette-specific primers. In all four cases, the physiological properties of strains generated by targeted gene disruption (in the following indicated as *Δmyco1*, *Δmyco4*, *Δmyco5* and *Δmyco56*) were confirmed, as they exhibited the same phenotype as the corresponding random mutants. One mutant strain for each target gene was selected for further biological characterization. Genomic complementation of the targeted inactivation mutants with the corresponding native gene alleles also inferred an expected linkage between respective genes and the observed phenotype, as far as the wildtype habitus could be recovered. These results imply that the genetic mutations/inactivation resulting in the observed phenotypes corresponded to respective genes identified. As expected, on the switch-inducing medium (N-deprivation medium), the mutant strains *Δmyco1*, *Δmyco4* and *Δmyco56* showed an impaired ability for filamentous growth, likewise consistent with observed phenotypes of corresponding random mutants. This observation was also supported by results obtained from germination assays, indicating a drastically reduced percentage of germinated spores of *Δmyco1*, *Δmyco4* and *Δmyco56* along with the reference strain *ΔZthog1*, whereas *Δmyco5* exhibited enhanced germination ability (Figure S7). Interestingly, a different degree of pigmentation was apparent, when comparing the resulting phenotype of *Δmyco56* on N-deprivation agar medium and minimal medium (MM), the later including nitrogen in inorganic form as nitrate ($NaNO_3$). The mutant strain is darkly pigmented in its appearance when cultivated on N-deprivation medium, whereas a non-pigmented phenotype is noticed on MM (Figure 15). On a macroscopic scale, in case of *Δmyco4* strain, the yeast-to-hyphal transition was observed, but it appeared in a delayed manner after two weeks of incubation under defined conditions (N-deprivation medium, 18 °C) compared to the wildtype strain IPO323, which accomplished

conversion to mycelial growth form after one week of incubation. Furthermore, the growth of *Δmyco4* under nutrient deprivation provided by minimal, N-deprivation and water agar media was strongly reduced, as we noticed only a poor colony development associated with a low spore density. However, incubation of the mutant on YEG restored these growth defects and a very similar phenotype to that of wildtype was apparent. On the water agar, all of these mutants except for *Δmyco5* were found to grow yeast-like, even if the incubation period was prolonged up to 21 days. An interesting phenotype was observed in case of the *MYCO5* deficient mutant showing an increased mycelia production under different incubation conditions, including growth on YEG-agar medium, where the wildtype strain grows yeast-like. Apart from that, the growth rate of the mutant colonies on standard media tested (YEG) showed no significant difference to that of the wildtype strain IPO323, albeit a morphological alteration considering the conidial colony morphology was apparent. Hence, on YEG medium *Δmyco1* and *Δmyco4* along with wildtype exhibit typical circularly shaped colonies with smooth surface texture, showing entire margins/edges (Figure 15). In contrast, *Δmyco56* displays irregularly formed colony with wrinkled-rough surface and undulate-curled edge in appearance signifying disoriented growth behaviour.

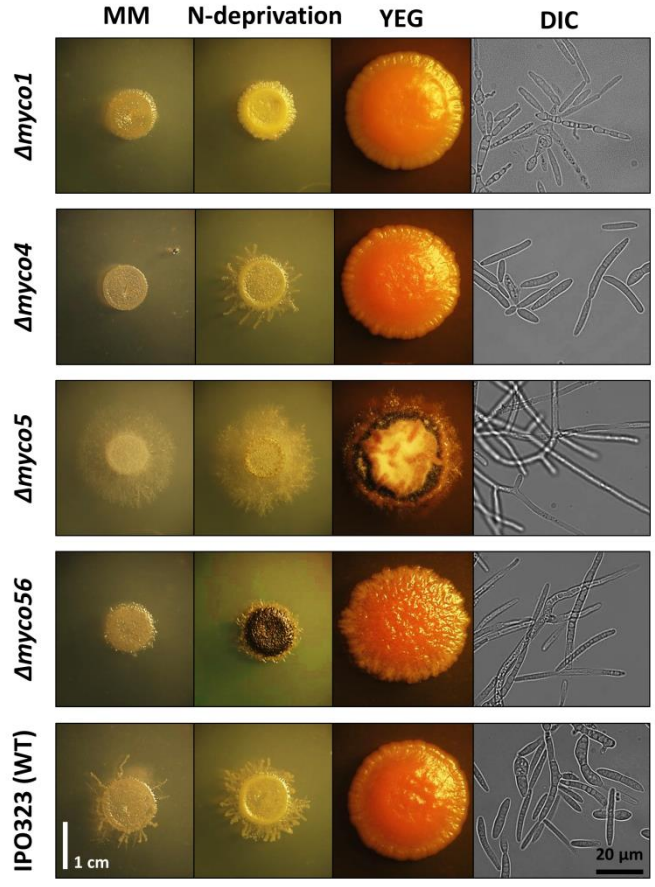

Figure 15:
Representative phenotypes of selected mutants (*Δmyco1*, *Δmyco4*, *Δmyco5* and *Δmyco56*) compared to the reference strain IPO323. The observed phenotypes of the respective mutants are illustrated as macroscopic analysis of colony development after 21 days incubation on minimal medium (MM), N-deprivation and YEG medium and as light microscopic images (DIC) showing the spore morphology after 3 day incubation in YEG liquid medium. The images showing the colony growth on different media consider the real relation regarding the colony sizes.

Meanwhile, *Δmyco5* exhibits irregularly shaped colony morphology, however being fluffy in appearance due to enhanced mycelium formation. Furthermore, melanised regions of the colony are visible, indicating potentially enhanced aging of the culture.

On the microscopic scale, significant differences concerning spore morphology were detected as well. Thus, *Δmyco5* displayed two distinct conidia types upon incubation in YEG culture, including type III yeast-like pycnidiospores (according to Stukenbrock *et al.*, 2011) indistinguishable from that of the wildtype strain and those which harbored an aberrant morphology growing as hyphae and representing at the same time the vast majority of the observed conidia (Figure S8). There was a noticeable difference in morphology of conidia produced by *Δmyco56* and wildtype when cultivated under the same condition. Thus, *Δmyco56* formed exclusively pseudohyphal-like conidia, which may be referred as elongated type I conidia (according to Stukenbrock *et al.*, 2011) undergoing the microcyclic conidiation at the apices. Either in complete medium (YEG) or nitrogen deprivation medium, the conidia appeared elongated, being up to three times longer relative that of the wildtype and displayed a pseudohyphal-like growth form. This conidial morphotype was characterized by a budding-like propagation of pycnidiospores in the unipolar fashion. The conidia were produced in chains (2 – 3 conidia attached at apices to each other), showing only rarely a lateral branching (Figure S8). For the *Δmyco4* mutant no significant differences in spore morphology were observed; thus the shape, length and the conidial propagation pattern were similar to that observed in the case of the wildtype. Meanwhile, *Δmyco1* forms conidia, which are morphologically very similar to those of *ΔZthog1* mutant previously characterized (Mehrabi *et al.*, 2006). Hence, the spores were found to have an aberrant morphology compared to the conidia of the wildtype strain IPO323, as they were significantly shorter and harbored irregular apical and subapical swellings.

3.4.5 Dimorphic switch as determinant factor for pathogenicity

Plant infection assays were employed in order to examine the effect of inactivation of the target genes on the virulence-related processes and generally to test whether dimorphic switch provides a critical step in the pathogenic development of the fungus. Expectedly, the virulence to susceptible wheat cultivar Riband was significantly affected in all mutant strains selected compared to the wildtype IPO323 (Figure 16). The mutant strains *Δmyco1*, *Δmyco4* and *Δmyco5* were found to be non-pathogenic or at least showing a drastically reduced virulence, as no or a very reduced amount of necrotic lesions were found after the latent phase of

infection on the host plants. Hence, *Δmyco4* displayed a significant reduction of infectivity on wheat plants (cv. Riband). A very intriguing phenotype was observed in the case of *Δmyco5*. Although this mutant predominantly grows in filamentous form, no typical symptoms of

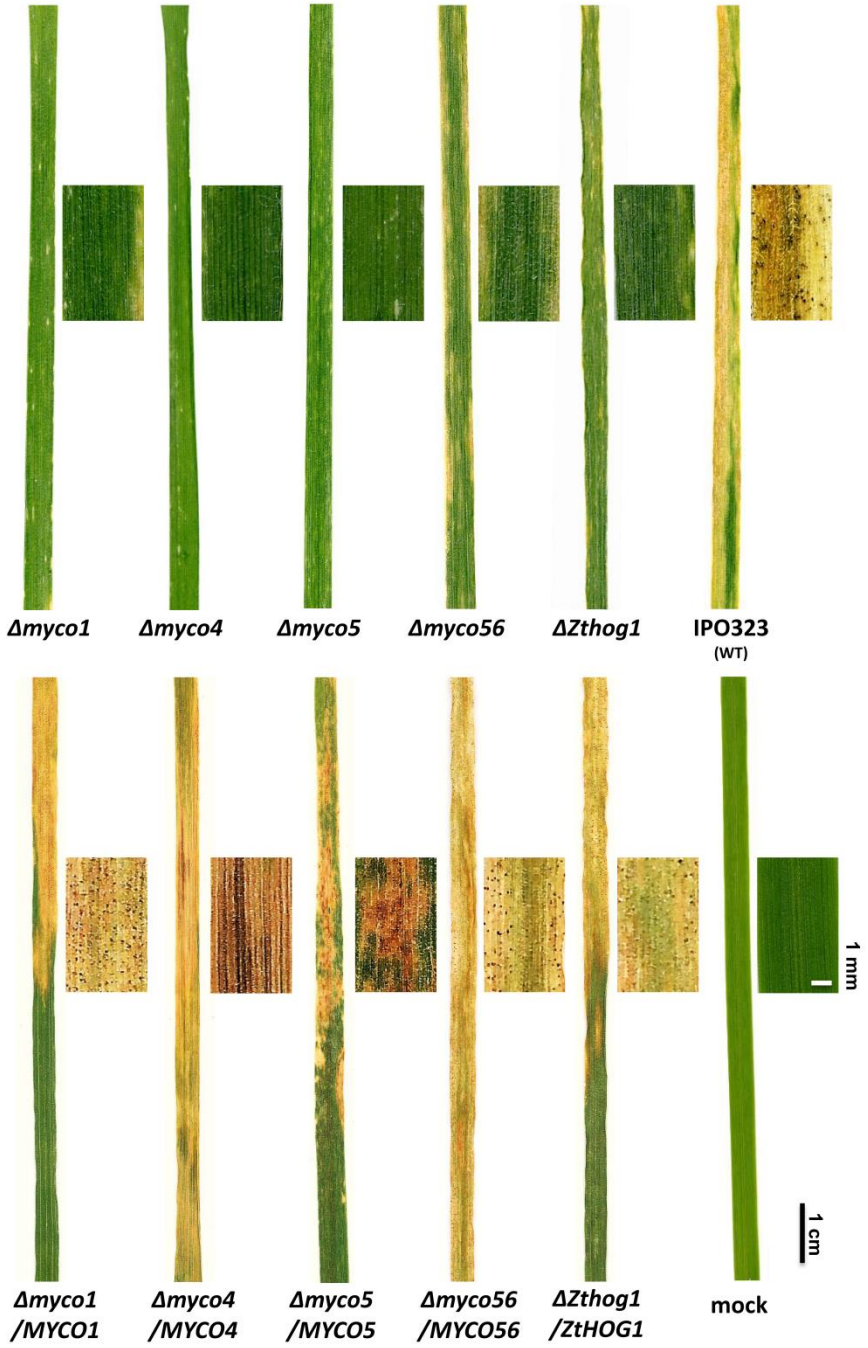

Figure 16: Plant infection assay with selected mutant strains. Effects of the gene inactivation on disease development in the susceptible wheat cv. Riband after 21 days after inoculation (21 dpi) are shown. WT IPO323 and *ΔZthog1* are regarded as references and mock as negative control, meaning plant leaves were sprayed with water only. The incubation of infected plants was performed with the following parameters: temperature: 22 °C, humidity: 80%, Lightcycle: 16 h / 8 h. *Z. tritici* strain *Δmyco5* was found to be non-pathogenic while *Δmyco4* and *Δmyco56* strains along with *ΔZthog1* are drastically reduced in virulence. Meanwhile, typical symptoms of successful infection were observed for WT IPO323, forming mature pycnidia 21 dpi. Full virulence to the loss-of-function mutants *Δmyco1*, *Δmyco4*, *Δmyco5* and *Δmyco56* was completely restored by retransformation of the strains with respective functional full-length gene copies.

successful colonization of the plant developed (Figure 16). *Δmyco1* was drastically impaired in virulence and exhibited a *ΔZthog1*-like phenotype (Mehrabi, 2006), giving only rarely chlorotic lesions on inoculated leaves, but provoking no necrosis of plant tissue.

Meanwhile, the mutant strain *Δmyco56* caused very occasionally necrotic lesions and produced a drastically reduced amount of pycnidia after a latent period of infection. No differences regarding pathogenicity/virulence were observed between the wildtype strain IPO323 and any of the complementation mutants, generated by reintegration of intact copy of a gene into the genome of corresponding mutant strain. Collectively, these data indicate a pathogenicity related role of the genes *MYCO1*, *MYCO4*, *MYCO5* and *MYCO56* within the *Z. tritici* - wheat pathosystem and requirement of dimorphic switch ability for pathogenic development.

3.5 Transcriptome analysis of selected strains during the dimorphic transition on artificial medium

In order to investigate the impact of the target genes on the yeast-to-hyphal transition, we examined transcriptomes of the targeted mutant strains and wildtype IPO323 as reference using RNA-Seq upon switch inducing condition. RNA-seq allows analysis of gene expression on a genome-wide scale, enabling a deeper understanding of the transcriptional landscape of investigated process. For this analysis, the mutant strains *Δmyco5* and *Δmyco56* were selected, since they harbored a clearly aberrant mode of growth compared to wildtype. The wildtype IPO323 and *ΔZthog1* were used as reference strains, representing filamentous and non-filamentous growth forms under the cultivating condition. The rationale used for the choice of *Δmyco5* and *Δmyco56* was furthermore motivated by the postulated function of the respective proteins encoded by *MYCO5* and *MYCO56* and the observable attributes of the corresponding mutants lacking these genes. If assuming a Cip2p-like function for the Myco56p (Martin *et al.*, 2006) and participation of the *mod_r* protein Myco5p in the endocytic pathway (Bache *et al.*, 2004), than one would expect that both genes are likely to be involved in the global regulation processes critical for the yeast-to-hyphal transition. This may be achieved either directly by regulating the transcription activity of other dimorphic-switch related genes (in case of *MYCO56*) or indirectly by controlling the turn-over rate of transcription factors (in case of *MYCO5*). Especially due to the increased mycelium formation of the *Δmyco5* strain, we hypothesized for Myco5p a function in repression of the expression of genes required for filamentous growth. Prior to RNA isolation and further processing within RNA-Seq analysis the *Zymoseptoria tritici* mutant strains as well as WT IPO323 were incubated on cellophane-

covered N-deprivation solid medium for 7 days at 18 °C. TopHat and Cuffdiff (within Cufflinks software package) were used as open-source software tools for gene discovery and comprehensive gene expression analysis of RNA-Seq data. The RNA-Seq reads were mapped to the reference genome of IPO323 obtained from JGI using TopHat aligning tool. Detailed analysis of the distribution of reads aligned to the reference genome indicated that the sequencing depth across investigated strains was sufficient (Figure S9).

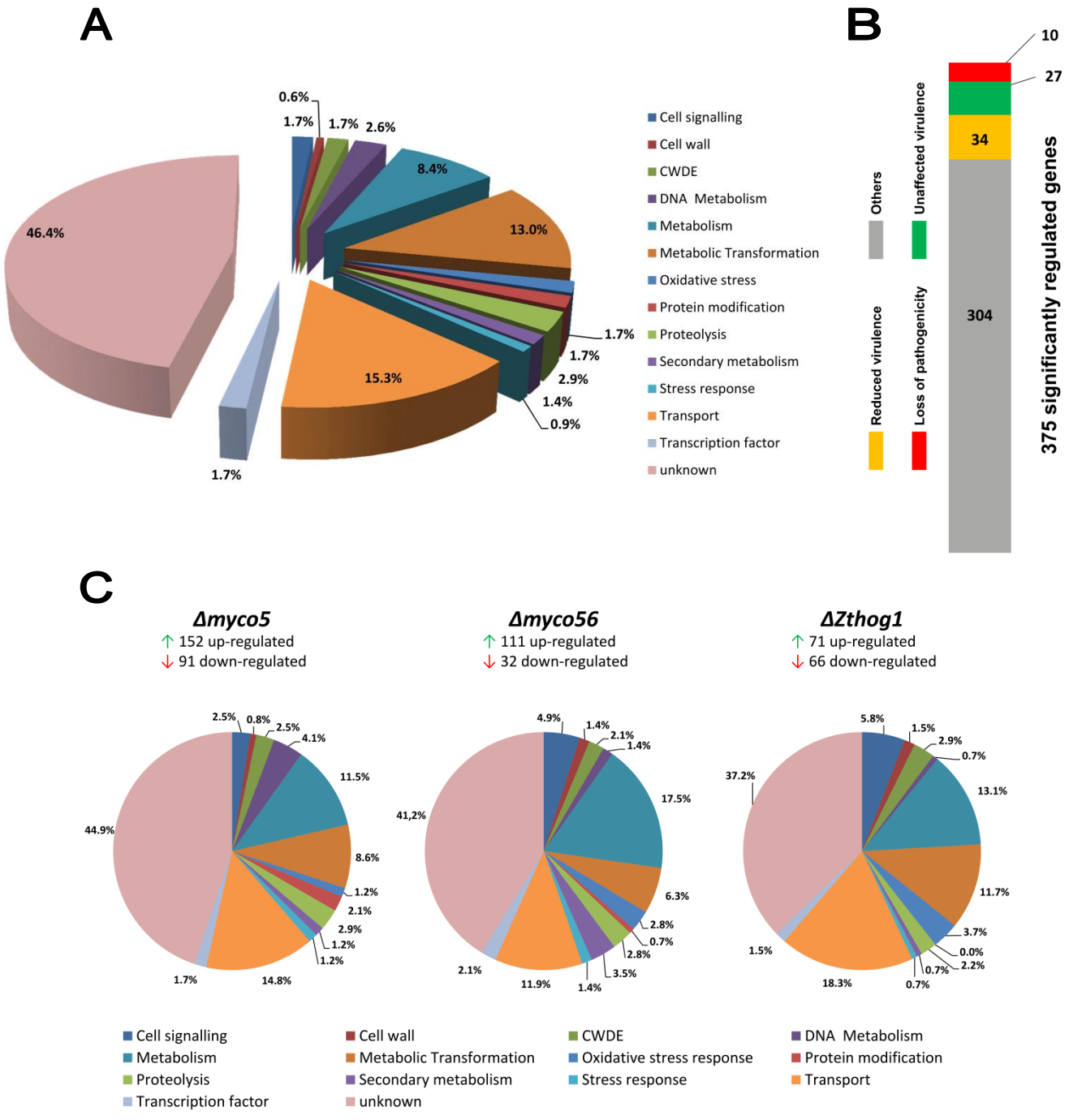

Figure 17: Transcriptome analysis of investigated strains (IPO323, *Δmyco5*, *Δmyco56* and *ΔZthog1*) cultivated under dimorphic-switch inducing condition.

(A) Pie chart representing the customized categories of the total DE genes (375) obtained from RNA-Seq analysis, which were termed in concordance with data obtained from JGI server and Blast2GO analysis. As significant only those genes were regarded, whose average expression was affected by factor 2.5x at least in one instance of pairwise comparison across all investigated strains and considering the q-value of less or equal 0.05.

(B) Identification of known pathogenicity related genes. The interrogation of deduced amino acid sequences from the set of DE genes was performed using local BLASTp (E-value cutoff of 1e-29) analysis against the implemented PHI-Base database (version 4.0, www.phi-base.org, last accessed December 19, 2015), in order to assess their potential involvement in host-pathogen interactions.

(C) Pie charts of GO categories (Biological Process) generated from RNA-seq data on total differentially expressed target genes between the investigated strains (*Δmyco5*, *Δmyco56* and *ΔZthog1*) and wildtype IPO323 as reference strain under N-deprivation condition. Each sector of the pie chart represents the procentual number of genes expressed for each biological process. Genes resulting from Cuffdiff-analysis were filtered for an absolute fold change value ≥ 2.5 and q-value threshold of 0.05.

Cuffdiff was used as a sound statistical analysis tool for quantification of aligned reads to determine the differentially expressed genes (DE genes). The DE genes resulting from CuffDiff quantification were examined and classified according to Gene Ontology (GO) functional criteria in compliance with JGI genome annotation data. To extract the maximal information from the RNA-Seq data, we first examined a total set of differentially expressed genes. Hence, a total of 375 significantly regulated genes were identified (Figure 17A), wherein as significant only those were regarded, whose average expression was affected by factor 2.5x at least in one instance of pairwise comparison across all investigated strains and considering the q-value (represents the false discovery rate of P-value) of less or equal 0.05. Classification of genes according to their biological functions yielded a total of 14 customized functional categories, which were named in accordance with annotated GO and KOG (euKaryotic Orthologous Groups) data obtained from JGI, as well as based on the results retrieved from BLASTp and InterProScan analysis. The GO data provided by JGI were reanalyzed and updated by conducting the Blast2GO analysis. Thus, BLASTp interrogation against NCBI "nr"-database complemented by GO analysis resulted in a set of 201 genes (53.6%), which could be assigned to distinct functional categories defined (Figure 17A). The most enriched category with about 15% of DE genes was represented by transport proteins, directly followed by two other comprising nearly 13% and 8% of DE genes putatively involved in metabolic transformation processes or other metabolism-related processes respectively. The remaining 174 genes (46.4%) were predicted to encode hypothetical proteins and were assigned as "unknown", since no GO annotation terms were found (Figure 17A). Furthermore, using a custom database of known virulence factors (implemented as PostgreSQL Database), most of which were obtained from PHI-Base version 4.0, we identified a set of orthologous genes, whose role in the pathogenicity related processes has

been already elucidated in other pathogenic fungi (Figure 17B). Grouping of these genes was carried out according to three criteria: "Loss of pathogenicity", "reduced virulence" and "hypervirulence or unaffected virulence". Hereafter, 10 genes were identified, whose inactivation in other pathogenic fungi leads to "loss of pathogenicity" (Figure 17B). Moreover, the number of genes, whose targeted inactivation leads to a reduced virulence and being homologs in other fungi was amounted to 34. The majority of these genes encodes on the one hand various transporters (mainly MDR transporters) and on the other hand, represents a set of the genes whose encoding products are involved in metabolic processes. Known representatives of this gene set are for instance *PTH11* from *Magnaporthe oryzae* (DeZwaan, 1999), *MEP1* from *Coccidioides posadasii* (Hung, 2005) and *SCD1* from *Colletotrichum lagenarium* (Kubo, 1996). Meanwhile, 27 differentially regulated genes were found to have homologs in other fungal species associated with hypervirulence or being assigned to unaffected pathogenicity according to PHI-Base (Figure 17B). Similarly, most of these genes encode different transporters or proteins putatively involved in metabolic processes.

Moreover, relying on the same RNA-Seq data, we analyzed the strain-specific genes displaying significantly different transcript abundances in the respective mutant compared to those of the wildtype. With this approach we attempted to dissect the transcriptome data in order to determine the transcriptional regulons of the target genes *MYCO5*, *MYCO56* and *ZtHOG1*. Likewise, only those genes were considered as differentially expressed, which displayed a minimum fold change value of 2.5 along with the false discovery rate for the P-value of ≥ 0.05 (Figure 17C). In the following the target gene-specific regulons based on RNA-Seq analysis are presented:

Addressing the transcriptional regulon of *MYCO5*:

The *MYCO5* dependent regulon comprised 143 DE genes, wherein 152 up-regulated and 91 down-regulated genes were detected (Figures 17C, S10). The common set of DE genes was greatly enriched for proteins implicated in transport (14.8%), metabolism (11.5%) and metabolic transformation (8.6%) related processes. A similar observation was made when separately examining the up- and down-regulated genes. In both cases, the most abundant genes were found to be associated with metabolism-related pathways or being involved in transport associated processes. Among the transporter-encoding genes showing decreased transcript abundance, were particularly those, whose predicted function may be linked to uptake of external glucose or other monosaccharides. Examining the expression pattern of up-regulated genes, a group of significantly expressed genes encoding several

lysophospholipases (*Zt41969*, *Zt107391*, *Zt109795*), esterases (*Zt29873*, *Zt74078*) and triacylglycerol hydrolases (*Zt81448*, *Zt105080*) was apparent, leading to suggestion that the primary energy source for filamentous growth may rely on degradation of lipid reserves. Using GO-enrichment analysis platform provided by REVIGO server, the semantically similar GO terms of differentially regulated genes were clustered, focussing primarily on "biological processes". To extract the maximal meaning of processed data, 50 of most enriched gene clusters were computed and specified for each of investigated mutant (Figure 18). According to this analysis, clustering of GO terms enriched in DEG set of *MYCO5* indicated that most of the DE genes are related to transport, such as carbohydrate transport (GO:0008643), peptide transport (GO:0015833) and inorganic ion transport (GO:0015698), as well as processes related to lipid metabolism (GO:0030258, GO:0030259) and catabolic processes (GO:0008643, GO:0019566, GO:0046373). Interestingly, in contrast to other strains investigated, three genes encoding putative FabD/lysophospholipase-like protein and two triacylglycerol hydrolases were found to have highly abundant transcripts only in the *MYCO5* deficient mutant.

At the same time three genes encoding sterol esterase (Protein ID: 29873), lipase (Protein ID: 74078) and fatty-acyl-CoA synthase (Protein ID: 39405) displayed in *Δmyco5* decreased expression relative to the wildtype strain. Relying on this observation, we speculate that the observed fluctuations in the transcription abundance of these functionally related genes may also have a significant impact on cell wall remodeling processes by modifying the glycolipid composition of the cell wall. Furthermore, based on lipase activity, the released fatty acids can be potentially converted to signaling molecules and thus may initiate intracellular signaling pathways (Bazan, 2009). Hence, assuming that the observed up-regulation of lipases encoding genes correlates with the corresponding protein level, it was logical to infer the gene expression of ß-oxidation genes, as far as lipase activity is primarily linked to the release of fatty acids, which in their turn can be fed to glyoxylate cycle. A preliminary *in silico* investigation of the *Z. tritici* genome based on the JGI provided annotation indicated the presence of 16 proteins involved in β-oxidation of fatty acids (data not shown). However, analysis of the transcriptional level of the predicted homologous genes which encode proteins with functions in ß-oxidation metabolic pathway and mitochondrial transport processes displayed no noticeable changes in expression in comparison to wildtype, supporting at the same time our hypothesis towards predominant implication of the lysophospholipases encoding genes in signaling pathways. Additionally, the transcriptional profile of *Δmyco5* revealed a set of hypha-specific gene homologs previously characterized as virulence factors

in other fungi, with significant up-regulation compared to IPO323, *Δmyco56* and *ΔZthog1*: e.g. *TEC1* (*Zt92404*) from *Candida albicans* (Schweizer *et al.*, 2000), *GEL2* (*Zt51025*) from *Aspergillus fumigatus* (Mouyna *et al.*, 2005), *MEP1* (*Zt43998*) from *Coccidioides posadasii* (Hung *et al.*, 2005).

Addressing the transcriptional regulon of *MYCO56*:

When dissecting the transcriptional regulon of *MYCO56*, a total of 111 genes were found to be up-regulated and 32 genes were down-regulated under "dimorphic switch" inducing condition (Figure S10). Most of the genes with increased transcript level having functional annotation were enriched in such biological processes like metabolism, metabolic transformation and processes related to transport activity. Similarly, most of down-regulated genes were enriched in the categories "metabolism" and "transport" (Figure S10). Furthermore, in contrast to *MYCO5* and *ZtHOG1* regulons, 3.5% of DE genes were assigned to "secondary metabolism". Hence, taking a closer look at the transcriptional profile of *Δmyco56*, four genes involved in melanin biosynthesis were found to be transcriptionally induced under investigated condition compared to wildtype, *ΔZthog1* and *Δmyco5*. They represent predicted gene homologs of *Colletotrichum lagenarium* encoding the known polyketide synthase (*PKS1*) (Takano *et al.*, 1995), 1,3,6,8-tetrahydroxynaphthalene (T4HN) reductase (*BRN2*) (Tsuji *et al.*, 2003), scytalone dehydratase (*SCD1*) (Kubo *et al.*, 1996) and 1,3,8-trihydroxynaphthalene (T3HN) reductase (*BRN1* or *THR1*) (Perpetua *et al.*, 1996) as well as *CMR1* (Tsuji *et al.*, 2000), a transcription factor encoding gene, previously shown to regulate the transcription of the melanin biosynthesis gene cluster. This observation was also supported by subsequent GO clustering analysis of the differentially regulated genes using REVIGO, indicating enriched functional categories related to melanin biosynthesis (GO:0006582), secondary metabolic process (GO:0019748), amino acid catabolic processes (GO:0006546, GO:0009071), carbohydrate metabolic process (GO:0005975) and carbohydrate transport (GO:0008643) (Figure 18). Furthermore, several genes enriched in oxidative stress response (GO:0006801, GO:0006979) were detected, showing on average increased expression in *Δmyco56* when comparing to the wildtype strain IPO323.

Addressing the transcriptional regulon of *ZtHOG1*:

The transcriptome of *ΔZthog1* comprised 137 significantly regulated genes when compared to that of wildtype strain IPO323, 71 of which displayed an increased transcriptional expression (Figure 17C, S10). Meanwhile, 66 genes were found to be down-regulated.

MYCO5

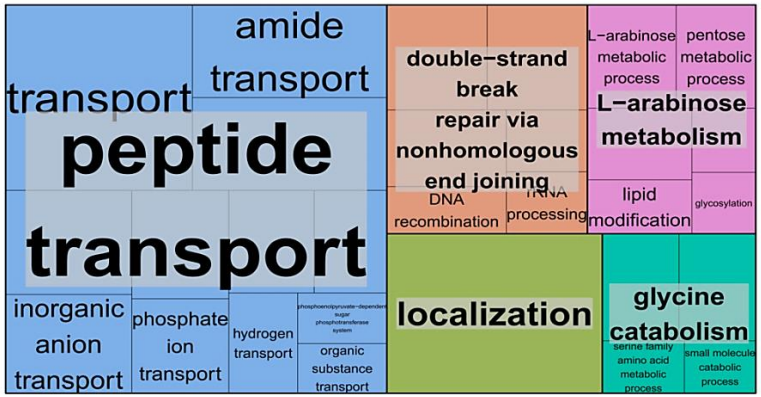

GO.ID	Term	Annotated	Significant	Expected	classicFisher
GO:0006810	transport	657	31	15.72	4.40E-05
GO:0051234	establishment of localization	658	31	15.74	4.60E-05
GO:0051179	localization	659	31	15.76	4.70E-05
GO:0044765	single-organism transport	278	14	6.65	0.0053
GO:0006857	oligopeptide transport	5	2	0.12	0.0054
GO:0015833	peptide transport	5	2	0.12	0.0054
GO:0042886	amide transport	5	2	0.12	0.0054
GO:1902578	single-organism localization	281	14	6.72	0.0058
GO:0008643	carbohydrate transport	68	5	1.63	0.0222
GO:0015698	inorganic anion transport	11	2	0.26	0.027
GO:0000726	non-recombinational repair	2	1	0.05	0.0473
GO:0006303	double-strand break repair via nonhomolo...	2	1	0.05	0.0473
GO:0006835	dicarboxylic acid transport	2	1	0.05	0.0473

MYCO56

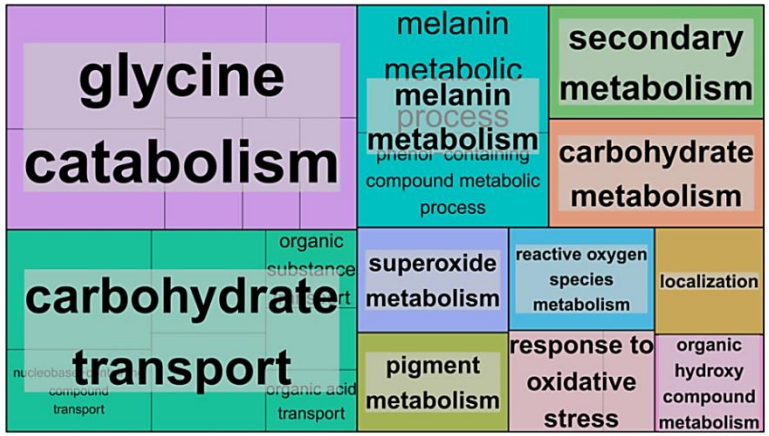

GO.ID	Term	Annotated	Significant	Expected	classicFisher
GO:0006582	melanin metabolic process	2	1	0.03	0.03
GO:0019748	secondary metabolic process	2	1	0.03	0.03
GO:0005975	carbohydrate metabolic process	207	7	3.15	0.035

ZtHOG1

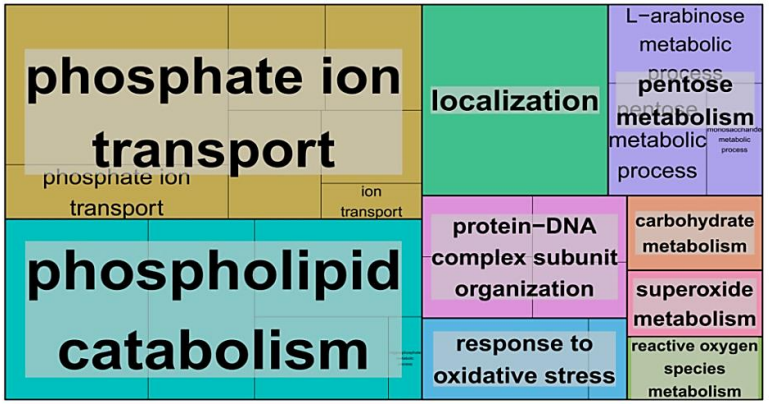

GO.ID	Term	Annotated	Significant	Expected	classicFisher
GO:0006810	transport	657	21	9.39	9.10E-05
GO:0051234	establishment of localization	658	21	9.4	9.30E-05
GO:0051179	localization	659	21	9.42	9.50E-05
GO:0009395	phospholipid catabolic process	4	2	0.06	0.0012
GO:0044242	cellular lipid catabolic process	8	2	0.11	0.0053
GO:0046434	organophosphate catabolic process	9	2	0.13	0.0067
GO:0016042	lipid catabolic process	13	2	0.19	0.0141
GO:0006979	response to oxidative stress	19	2	0.27	0.0293
GO:0006817	phosphate ion transport	3	1	0.04	0.0423
GO:0019566	arabinose metabolic process	3	1	0.04	0.0423
GO:0046373	L-arabinose metabolic process	3	1	0.04	0.0423

Figure 18: Gene ontology enrichment analysis of DE genes in *ΔZthog1*, *Δmyco5* and *Δmyco56*. GO terms enriched in the DE gene sets representative for each investigated mutant strain (denoted by the name of corresponding gene *ZtHOG1*, *MYCO5* and *MYCO56*) were analysed using TopGO package in R and the first 50 GO clusters were processed using web-based tool REVIGO. The redundancy of GO terms was removed and the biological process GO terms were clustered in TreeMap plots, where each rectangle represents a single cluster. Similar colors of the rectangles indicate semantic similarity. The size reflects the P-value obtained from TopGO analysis (the larger the size the smaller the P-value and the greater the enrichment factor for respective GO term). For each TreeMap the adjacent table provides only those GO clusters obtained from TopGO analysis, which were found to be significantly enriched according to classic Fisher analysis reflecting the P-value ≤ 0.05.

The most enriched categories were “metabolism”, “metabolic transformation” and “transport”, the latter containing 18.7% of DE genes, which is more than what we have observed for *MYCO5* and *MYCO56* regulons. Similarily, DE genes involved in oxidative stress response and signalling were found to be more represented in percentage terms in *ZtHOG1* regulon. As for the other strain-specific transcriptomes, most of the up-regulated genes were found to encode proteins with functions in metabolic processes, followed by those which are predicted to be involved in transport processes. At the same time, genes with significantly reduced transcript abundance were assigned to such GO-groups like “metabolism”, “metabolic transformation”, “transport” and “oxidative stress response”. This observation was also supported by the REVIGO clustering based on the preceding TopGO analysis (Figure 18). Among the enriched clusters were metabolism (GO:0008152), oxidative stress response (GO:0004601, GO:0006118) and transport-associated processes (GO:0006810), including numerous ABC- and MDR-transporters. Furthermore, clusters assigned to carbohydrate catabolic process (GO:0019321, GO:0046373, GO:0019321) and lipid metabolic/catabolic process (GO:0016042, GO:0044242, GO:0006644) were significantly enriched. Quite noticeable was the down-regulation of many genes encoding potential detoxification enzymes, including peroxidases, ABC transporters and UDP-glucosyl/glucuronyl transferases. For the other GO-groups, regarding the average expression data, no significant alteration compared to the wildtype strain IPO323 was evident.

Moreover, for each strain lacking the corresponding gene, we identified a set of genes harboring a very similar expression profile across all investigated strains as for the lacking gene in the respective mutant strain (Figure S11). For instance, for *MYCO56*, a set comprising 20 DE genes was identified, displaying a very similar expression (*MYCO56*-like expression) behaviour across all investigated strains. Genes exhibiting similar expression patterns as for *MYCO5*, *MYCO56* and *ZtHOG1* in the corresponding mutant strains suggest their potential transcriptional regulation dependency on the target genes or assignment to the same metabolic/signaling pathway.

3.5.1 Differences and similarities in transcriptional profiles across the investigated strains

Using Venn-diagram, we contrasted overlaps of the strain-specific transcriptomes, enabling us to perceive similarities and differences of significantly regulated genes under switch inducing condition between the mutant strains analysed and the wildtype. Several shared genes with differentially abundant transcript levels involved in the detoxification of reactive oxygen

species (ROS) were detected in the *MYCO56* and *ZtHOG1* regulons, exhibiting however opposed expression levels. One gene encoding chloroperoxidase with decreased level of expression was exclusively detected in case of the *ΔZthog1* mutant. Similarly, in case of *Δmyco5*, only one revealed a low transcript level compared to the wildtype strain. As far as *Z. tritici* conidia are subject to oxidative stress at least at the early stages of both compatible and incompatible interaction with the host plant, maintaining high levels of genes involved in ROS detoxification is crucial for successful colonization of plant tissue by lowering the negative effects of ROS exposure. The expression pattern of the peroxidases encoding genes in case of *Δmyco56* showed no alteration compared to wildtype. Furthermore, when observing the overlapping regulons of *MYCO5* and *ZtHOG1*, a set of 37 DE genes identified was apparent.

Figure 19: Strain-specific comparative analysis from RNA-Seq data obtained. Venn diagram provides gene expression overlaps of DE genes from RNA-Seq across the mutant strains *Δmyco5*, *Δmyco56* and *ΔZthog1* relative to wildtype strain IPO323. Numbers in each segment represent counts of genes, which correspond to the specific comparative category. Overall 352 out of 375 genes were found to be significantly regulated when compared to gene expression in wildtype.

Some of its representatives are genes encoding MFS peptide transporter (Protein ID: 104715) and ATPase P-Type transporter (Protein ID: 84460) showing in both mutants strains reduced transcript abundance compared to wildtype. When comparing DE genes of *Δmyco56* and *ΔZthog1* a total of 31 DE genes were found to be shared across these strains. Among them were those, which are predicted to encode G protein-coupled receptor and GTP-binding protein, indicating the involvement of signal transduction system, as well as one chitinase,

one secreted metalloprotease and verprolin, a protein previously shown to be involved in a cytoskeletal organization and cellular growth in yeast (Donnelly *et al.*, 1993). Interestingly, one gene predicted to encode a Myb-like DNA-binding protein was found in the common set of shared DE genes, showing homology to the known transcription factor FlbDp, previously found to be implicated in sporulation process in *Aspergillus nidulans*, *Fusarium oxysporum*, *Penicillium oxalicum* and *Magnaporthe oryzae* (Kwon *et al.*, 2010, Son *et al.*, 2011, 2013, Yao *et al.*, 2016, Matheis *et al.*, 2017). For both strains, a drastically reduced expression of this gene compared to wildtype was noticed. The overview of DE gene set overlaps is given in Figure 19 providing the counts as well as some of the representative genes for each gene set. For most of the DE genes shared across the strains, however, no functional annotation could be found, leading to the consequence that the potential function of corresponding gene products remains unknown.

3.5.2 Identification of genes unique for *Zymoseptoria tritici*

Searching exclusively for DE genes having no or few homologs in other fungal species could provide another important means to find genes implicated in the specific mechanisms of pathogenic development in *Z. tritici*. In order to identify genes, which are more likely appear to be unique for *Z. tritici*, we performed a comparison of the deduced amino acid sequences of significantly regulated genes obtained from RNA-Seq analysis against a fungi-database from NCBI by conducting BLASTp analysis (Figure 20). Overall, from 375 genes analyzed, we identified 280, which were found to have 20 or more orthologues across different fungal species.

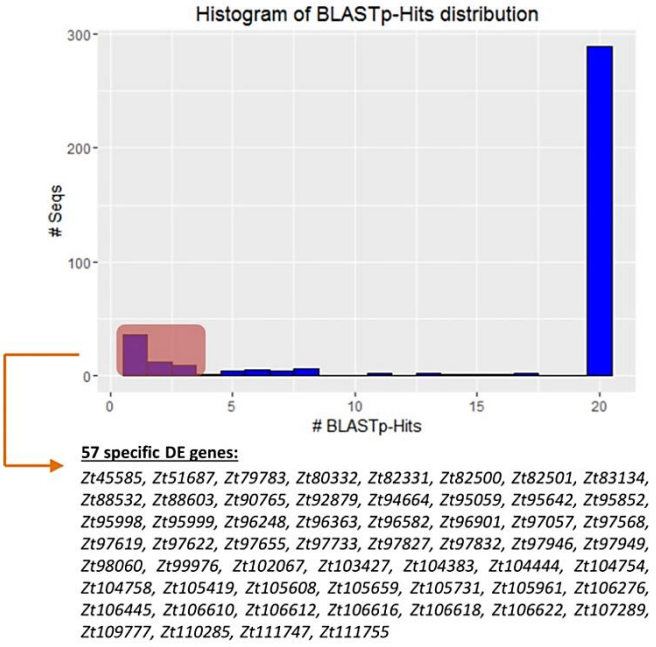

Figure 20: Histogram providing BLASTp-Hits distribution of DE genes.

The deduced protein sequences corresponding to DE genes obtained from RNA-Seq analysis were interrogated against NCBI "nr"-database in order to identify putative homologs. Protein sequences having only 1,2 or 3 orthologues in other fungal species were considered as unique or *Z. tritici* specific providing interesting candidates for further investigation.

A total of 37 genes we identified, appeared to have several orthologues in other fungal species, ranging from 4 to 19 representatives. At the same time, 57 were found to be potentially unique for *Z. tritici* or generally for *Zymoseptoria* phylum, having only one, two or three orthologues in other species (Figure 20). Expectedly, among these unique genes, the largest set with 95% was assigned to genes encoding hypothetical proteins, thus having no functional annotation. Only for three genes the functional information in the JGI database was found. The corresponding gene products are: a small threonine-rich protein (Protein ID: 105419), flocculin mucin-like precursor (Protein ID: 105608) and Ca^{2+}-modulated nonselective cation channel polycystin (Protein ID: 110285).

3.5.3 Comparison to publically available transcriptome data

Furthermore, we conducted a comparative analysis of RNA-Seq data obtained with data sets recently derived from transcriptome studies performed by other research groups (Yang *et al.*, 2013, Brunner *et al.*, 2013, Kellner *et al.*, 2014 and Rudd *et al.*, 2015). Most of these studies were particularly directed to the identification of DE genes following the complete infection cycle of wildtype in the host plant. Hence, by focusing primarily on genes commonly shared across these data sets, this approach may provide a list of potential candidate genes involved in the critical steps of pathogenic development of the fungus. Overall 274 DE genes were detected, which are present in common gene sets shared across DE gene set provided within this study and at least one further set of DE genes derived from previously published transcriptome data (Figure 21). A significant overlap comprising 260 DEG resulted from the comparison of DE genes provided in this study with the transcriptome data published by Rudd *et al.*, 2015. However, no differently expressed genes across all data sets regarded were found. Interestingly, none of the eleven target genes obtained from the

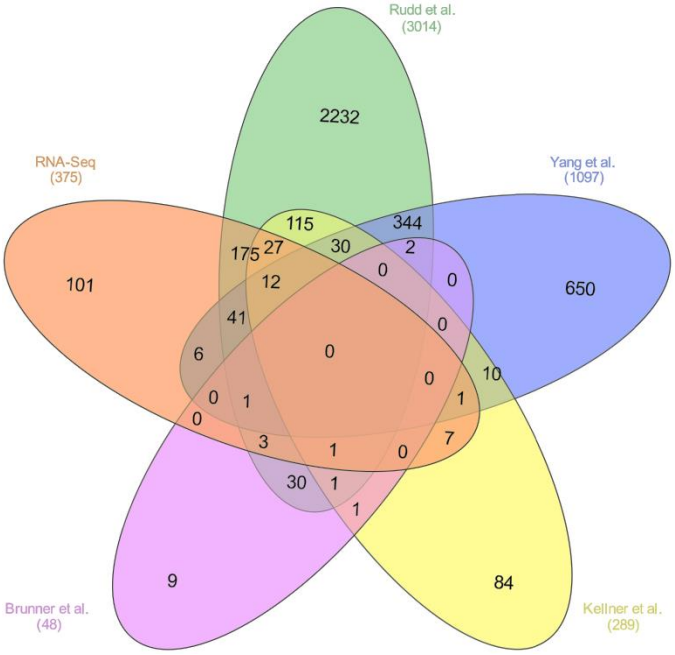

Figure 21: Comparative analysis with publically available RNA-Seq data. Venn diagram depicts the overlap of the DE genes obtained from RNA-Seq analysis with the publically available data sets provided by different studies. Total gene number of each condition is indicated.

random mutagenesis approach was found in any of the published data sets. The only exception is *ZtHOG1* being in a common set of DE genes according to RNA-Seq data published by Yang *et al.*, 2013. By exploiting combinatorial comparison of these data sets we present distinct lists of potential candidate genes putatively involved in the critical steps of pathogenic development of the fungus (Table S8). Furthermore, one gene with significantly changed transcript abundance across four data sets (Kellner *et al.*, Brunner *et al.*, Rudd *et al.* and this study) was noticeable, encoding a putative alpha-L-arabinofuranosidase AxhA-2p (Protein ID: 68922), a predicted homolog from *Colletotrichum higginsianum*. One further gene predicted to encode an alpha-L-arabinofuranosidase (Protein ID: 111130) was found across the data sets derived from Brunner *et al.*, Rudd *et al.* and this study. The importance of this gene stays in agreement with the proteome analysis provided by M'barek *et al.*, 2015, demonstrating the presence of the corresponding protein in the apoplastic fluids isolated from susceptible (Obelisk) wheat cultivar at 14 and 21 dpi after inoculation with *Z. tritici* strain IPO323.

3.5.4 Validation of the RNA-Seq data by qRT-PCR analysis

For the purpose of RNA-Seq data validation, gene expression analysis using qRT-PCR was applied, considering the same culture parameters as for the RNA-Seq experiment (incubation of the strains for 7 days at 18 °C). Overall 16 genes from the preceding RNA-Seq analysis were selected, showing different expression patterns across the investigated strains. Among them, six genes are suggested to be involved in oxidative stress response, five of which are predicted to encode chloroperoxidases (*Zt43487*, *Zt74298*, *Zt94368*, *Zt96677* and *Zt101235*) and one gene encoding a Cu/Zn superoxide dismutase (*Zt102956*). Three further DE genes, whose products might have functions in lipid metabolism, were chosen (Protein IDs: 105080, 109795, 81448 respectively), harbouring high transcript abundances in *Δmyco5* according to RNA-Seq data. In addition, two genes putatively encoding sugar transporters (*Zt68287*, *Zt74200*) and being down-regulated in *Δmyco5* were selected. For the other DE genes examined, diverse cellular processes including membrane vesicle trafficking, protein degradation and protein modification were suggested. Overall, the results obtained from the comparison of RNA-Seq and qRT-PCR profiles indicate a well-fitted correlation in regard to the expression of the examined genes (Figure 22). Although the magnitude of fold change values of some genes differed when comparing these two techniques, a similar trend concerning transcript abundance of the tested genes was apparent. Some differences

concerning transcriptional expression were observed for the genes *Zt74200*, *Zt74298* and *Zt109795*, when comparing RNA-Seq with qRT-PCR data.

		RNA-Seq (relative expression)			qRT-PCR (relative expression)		
	ProteinID	*Δmyco5*	*Δmyco56*	*ΔZthog1*	*Δmyco5*	*Δmyco56*	*ΔZthog1*
	Zt34453	-16.87	2.08	-2.31	-7.69	-1.08	1.03
	Zt38341	65.50	1.24	2.32	9.34	-1.04	1.87
	Zt43487	-1.42	-3.08	-10.16	-2.78	-1.05	-2.63
	Zt58641	12.78	-1.10	1.23	3.34	-1.56	1.32
	Zt59604	-11.82	2.18	1.12	-5.88	1.08	1.31
	Zt68287	-10.79	-1.01	1.55	-3.45	1.31	1.69
*	*Zt74200*	-14.22	-1.63	1.72	-4.76	-1.45	-9.09
*	*Zt74298*	-8.27	-17.43	-51.36	-2.44	1.36	1.80
	Zt81448	41.79	-2.22	-1.13	6.54	-1.23	1.32
	Zt84460	-10.88	1.57	2.80	-6.25	1.65	2.09
	Zt94368	-13.11	1.01	-2.23	-2.50	2.38	-2.04
	Zt96677	-1.71	14.04	-2.84	-2.56	2.54	-1.79
	Zt101235	5.75	1.39	-2.88	1.32	1.85	-2.70
	Zt102956	-1.64	11.47	7.00	-1.41	2.61	2.67
	Zt105080	50.03	-1.84	-1.09	4.16	-1.01	1.66
*	*Zt109795*	58.56	3.52	1.27	1.37	2.18	2.67

Figure 22: Validation of RNA-Seq data by qRT-PCR analysis. Heatmap illustrates a well-supported correlation of DE genes derived from RNA-seq and qRT-PCR experiments. Expression of 16 randomly selected genes in mutant strains relative to wildtype is examined. Three colored scheme (green, light green and white) was used to highlight differences in gene expression patters (relative fold changes) across the mutant strains investigated. Hence, genes exhibiting similar expression are depicted in the same color. Genes harbouring relative maximum values are highlighted in green. Genes exhibiting the intermediate values are depicted in light green and those with lowest fold changes in white. Red asterisks indicate genes harbouring pronounced differences in the expression patterns by comparing RNA-Seq and qRT-PCR outcomes with respect to mutant strains analysed.

Additionally, we examined the transcript levels of the genes upon nutrient-rich cultivation condition. Interestingly, there was no significant fluctuation in transcript abundances across the strains. Hence, a very similar expression pattern of the genes was noticed when incubating all strains on YEG (7d, 18 °C) (Figure 23B). This observation is in clear contrast to the considerably enhanced gene expression changes under N-starvation condition (Figure 23A), thus emphasizing their conditional regulation. Collectively, these results point to either a strain-specific or conditional expression manner of the genes inspected, suggesting their involvement in morphological and physiological aberrations of the corresponding strains.

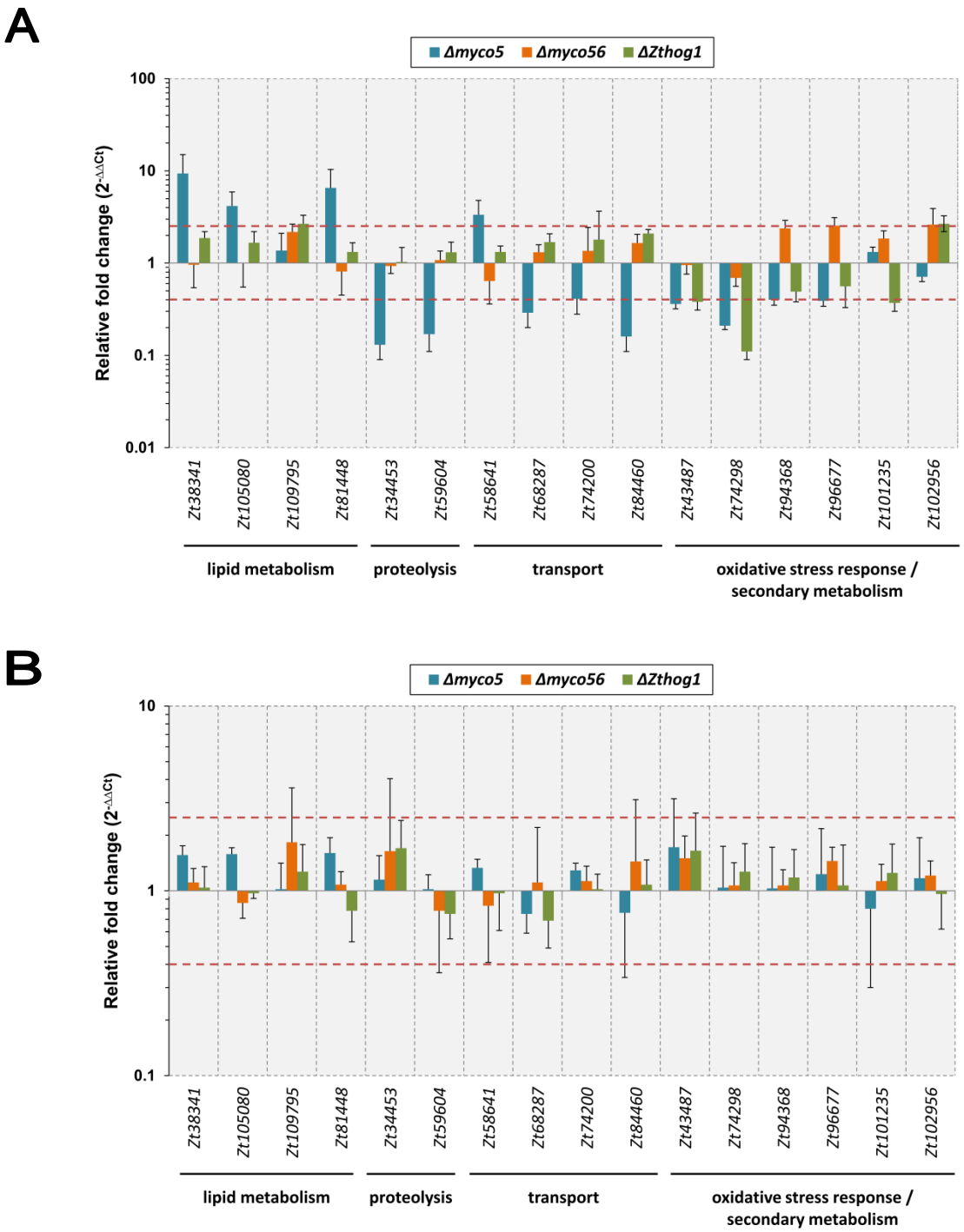

Figure 23: Conditional regulation of selected genes in the mutant strains *Δmyco5*, *Δmyco56* and *ΔZthog1* relative to the wildtype IPO323. In **(A)** expression pattern of selected candidate genes under N-deprivation condition is shown, representing a dimorphic switch inducing condition (7-days cultivation at 18 °C). **(B)** Transcription levels of the same genes as in (A) under nutrient-rich, non-filament-inducing cultivation condition (YEG solid medium, 7 days at 18 °C). Values are normalized to β-tubulin encoding gene as a constitutively expressed housekeeping control and calculated according to $2^{-\Delta\Delta Ct}$ method. Data presented are the mean including standard deviations of results from the 3 independent experiments with similar patterns. The dashed lines in red mark the upper and lower thresholds of 2.5 fold up-regulation or down-regulation of the genes.

3.6 Extended phenotypic analysis of the generated mutants

The observed transcriptional reprogramming associated with the adaptation response upon N-starvation condition unveiled a wealth of strain-specific genes, exhibiting differential expression pattern. Since these genes were assigned to different GO-terms reflecting their involvement into diverse pathways and metabolic networks, this might imply their influence on physiological properties of the corresponding mutant strains.

In order to validate the RNA-Seq results together with supported qRT-PCR data and to further investigate the different phenotypes of generated mutants, vegetative growth assays were performed. With these experiments, the intention was to gain more extensive information on the physiological features of the mutant strains and to assess particularly whether loss of gene function causes morphological aberrations. This experimental approach included incubation of the cultures on plates treated with different stress factors (providing osmotic stress, transient metals, cell wall stress and oxidative stress) and considering two different temperatures (18 °C and 28 °C).

3.6.1 *Δmyco1* is sensitive to osmotic stress

To test whether inactivation of the corresponding genes has an impact on the sensitivity to hyperosmolarity, the targeted mutant strains, as well as the reference strain IPO323, were grown on YEG and PDA agar media supplemented with different concentrations of sorbitol and NaCl. Preliminary experiment revealed that cultivation of IPO323 on PDA enables yeast-to-hyphal transition, whereas *ΔZthog1* lacks this ability. PDA was used as a "switch"-inducing medium for the *in vitro* growth assay, since the growth of strain cultures on N-deprivation medium supplemented with different stress factors was very sparse, making evaluation of the growth assay results more difficult. As expected, the growth of *ΔZthog1* was impaired compared to wildtype after 7-day incubation on YEG supplemented with 1 M sorbitol/NaCl or PDA with 1 M sorbitol/NaCl, resulting in reduced conidial density (Figure 24). A very similar phenotype to that of *ΔZthog1* was observed in the case of *Δmyco1*, which was accompanied by a drastic growth reduction on the agar media mentioned above.

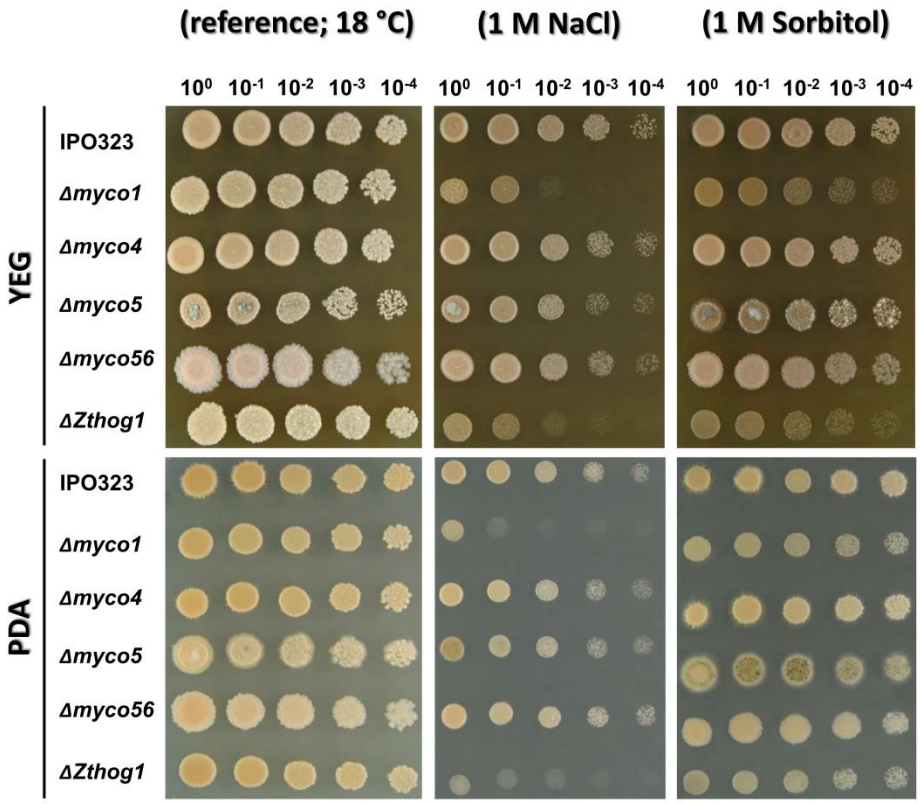

Figure 24: Influence of inactivation of target genes on growth under osmotic stress. Spores of the corresponding mutant strains shown were spotted on the indicated media in serial dilutions (1.5 µl; 10^8 spores/ml). The plates were incubated for 7 days at 18 °C. The phenotypes observed were verified by three independent experiments.

Furthermore, on PDA supplemented with 1 M sorbitol the anticipated sensitivity of *ΔZthog1* to osmotic stress could be confirmed as previously described by Mehrabi *et al.*, 2006. As expected, *Δmyco1* exhibited a *ΔZthog1*-like phenotype when incubating under the same condition, being considerably reduced in colony diameter (radial growth) and defective in dimorphic switch ability. Meanwhile, *Δmyco4* displayed a filamentous growth on both PDA and PDA supplemented with 1 M sorbitol. The vegetative growth was comparable to that observed for the wildtype strain IPO323, at the same time showing no sensitivity towards osmotic stress at defined concentrations. In the case of the *Δmyco5* mutant, the filamentous growth observed on PDA was pronounced to a much greater extent compared to wildtype. Furthermore, the mutant strain was found to be resistant to osmotic stress. For the mutant strain *Δmyco56*, neither dimorphic transition nor osmosensitivity or thermosensitivity was perceived when incubating the culture under the same cultivation condition.

3.6.2 *Δmyco56* displays an increased pigmentation upon propagation on nutrient poor medium and as submerged culture, while *Δmyco5* appears to be thermo-sensitive

Phenotypic analysis by cultivating the strains as submerged cultures revealed noticeable differences regarding the growth manner of the mutants. In the nutrient-rich YEG liquid medium, considering two different cultivation temperatures (18 °C and 28 °C), the vegetative growth of *Δmyco1*, *Δmyco4* and *ΔZthog1* is indistinguishable from that observed in case of the wildtype strain IPO323, showing exclusively yeast-like cell propagation. Meanwhile, *Δmyco5* was found to grow in YEG and PDA at 18 °C predominantly in filamentous form, producing yeast-like conidia as well, but at markedly low rate. Interestingly, the growth was drastically impaired when cultivation of the mutant strain was performed at 28 °C, both on solid medium (Figure 25A) and in liquid culture (Figure 25B), indicating an increased sensitivity to elevated temperatures. The growth in liquid culture is characterized by the formation of dense spheroid-like mycelial aggregates, suggesting a diminished total growth surface and as a consequence a reduced capacity for maintenance of sufficient nutrient uptake.

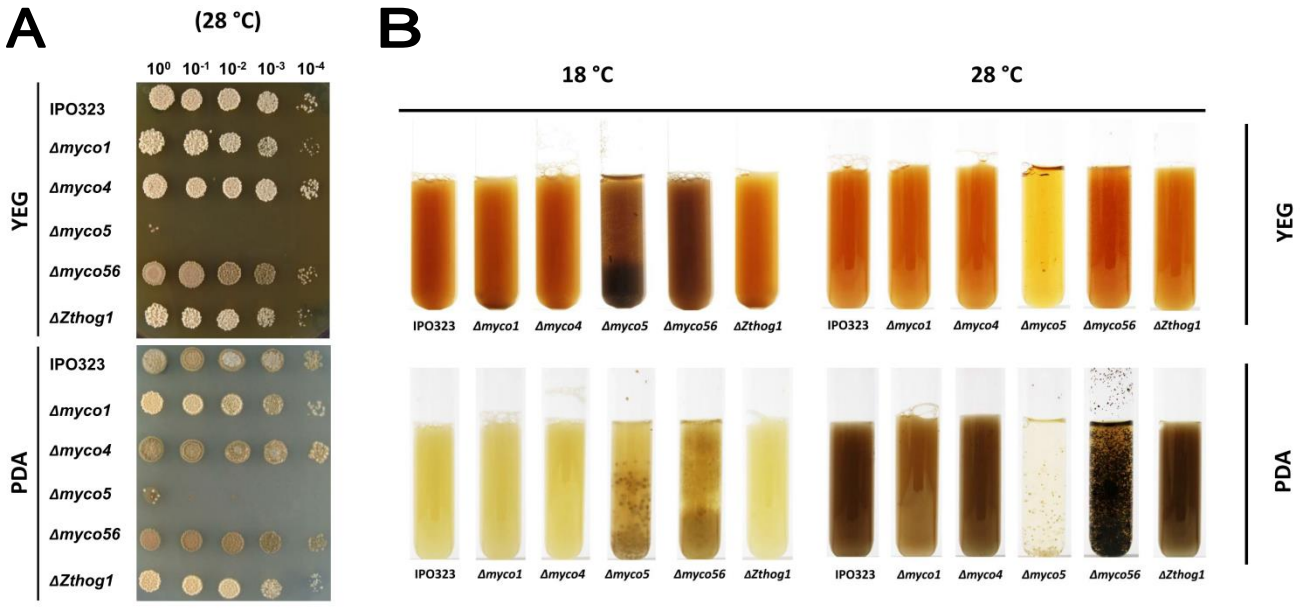

Figure 25: Growth of generated mutant strains at elevated temperature. (A) Axenic growth of *Zymoseptoria tritici* IPO323 and generated mutant strains at elevated temperature. The YEG cultures of the wildtype IPO323 and indicated mutant strains were spotted onto YEG/PDA plates from serial dilutions (1.5 µl; 5×10^7 spores/ml). Plates were imaged after 7 days of incubation at 28 °C. **(B)** Axenic growth of *Z. tritici* strains in liquid cultures under defined conditions**.** Notable are the cell aggregates and clumpy growth of *Δmyco5* in PDA or YEG and for *Δmyco56* in PDA compared to the homogeneous submers culture of IPO323. All cultures were shaken prior imaging. All cultures for each condition and strain were routinely incubated in 100 ml flasks without baffles for one week under shaking (120 rpm). Prior photographing they were transferred to glass-tubes. For *Δmyco5* a drastically impaired growth was apparent by incubation at elevated temperature. For the remaining strains *ΔZthog1*, *Δmyco1* and *Δmyco4* no alternations concerning the growth rate or sensitivity towards high incubation temperatures compared to wildtype were evident.

Expectedly, *Δmyco56* exhibits a pseudohyphal-like mode of growth in the submerged culture, similar to that, which was observed on the YEG solid medium. Both *Δmyco5* and *Δmyco56* grow in YEG at 18 °C as melanized cultures. Remarkable is, however, a highly increased degree of pigmentation in case of *Δmyco56* in contrast to wildtype, which was observed in both YEG and PDA liquid media, pointing to the increased activity of genes involved in 1,8-dihydroxynaphthalene (DHN)-melanin biosynthesis. Interestingly, the phenotype associated with an increased melanization of *Δmyco56* strain is not strictly limited to cultivation as submerged culture, but was also observed when incubating the strain on N-deprivation medium and water agar, however not on minimal medium. The pigmentation observed on water agar occurred though after a prolonged incubation of 21 days after inoculation (data not shown), suggesting at the same time that mobilization and utilization of internal nutrition sources may result in generation of precursors required for melanin production. Relying on the well-supported RNA-Seq data and the phenotypic difference between the wildtype and *Δmyco56*, this observation indicates that the increased pigmentation is not a result of exclusive triggering of the nutrient-deprivation environment, but may rather be coupled with *MYCO56* dependent regulation of melanin biosynthetic cluster genes.

3.6.3 Differences concerning cell wall composition in *Δmyco5* and *Δmyco56* compared to wildtype

It was interesting to observe that after centrifugation of the YEG submerged cultures of *Δmyco5* and *Δmyco56* mutants (incubated for 4 days at 18 °C), the resulting biomass pellets obtained were evidently viscous in their consistency compared to the solid pellets of other the strains analyzed (Figure 26A). To verify whether the corresponding genes influence the cell wall composition, the mutant strains *Δmyco5* and *Δmyco56* were tested towards hypersensitivity to cell wall-compromising agents such as Congo Red (CR) and Concanavalin A-FITC (ConA-FITC). This investigation reveals a significantly reduced staining of *Δmyco5* and *Δmyco56* cell walls by the lectin ConA (Figure 26C), which has a strong binding affinity for mannosyl residues (Baenziger and Fiete, 1979). Additionally, by application of low concentrations of the cell wall polymer intercalating agent Congo Red (250 µg/ml), which is thought to perturb cell wall synthesis by binding to the chitin component of the cell wall, no significant changes regarding the colony sizes in both mutants were detected compared to wildtype (data not shown). By applying a higher concentration of Congo Red (2 mg/ml), the colony growth of *Δmyco5* is drastically impaired, indicating an increased sensitivity towards this cell wall compromising agent (Figure 26B). The mutant strain *Δmyco56* also appears

sensitive against CR at this concentration, insofar as the colony density is significantly reduced compared to that of the wildtype, however not as radically as in the case of *Δmyco5*. Meanwhile, *Δmyco1* and *ΔZthog1* displayed the wildtype-like growth behaviour. Furthermore, the colony growth in the presence of sodium dodecyl sulfate (SDS) was examined, a detergent that compromises the integrity of the cell membrane. The basis for the sensitivity to SDS is not known, but it is suggested to be due to enhanced sensitivity of cell wall synthesis components or a general effect on the plasma membrane (Wang *et al.*, 2011). Thus, inspecting the growth of *Δmyco1*, *Δmyco5* and *ΔZthog1* on YEG treated with 0.01% SDS revealed a pronounced hypersensitivity of examined strains at a similar degree towards this cell wall perturbing agent (Figure 26B). Contrarily, IPO323 and *Δmyco4* display resistance towards SDS-treatment. The colony development of *Δmyco56* under the same growth condition is reduced, however indicating a slightly increased sensitivity towards SDS. As expected, for all mutants examined the genomic reintegration of the native copy of genes, for which the mutants were disrupted, could restore the wildtype phenotype, resulting in resistance of complementation strains against the cell wall compromising agents tested (data not shown). These findings indirectly support the deficiency in mannosylation and suggest an aberrant cell wall composition of these strains, at the same time highlighting a potential involvement of the corresponding genes in regulation processes of the cell wall integrity.

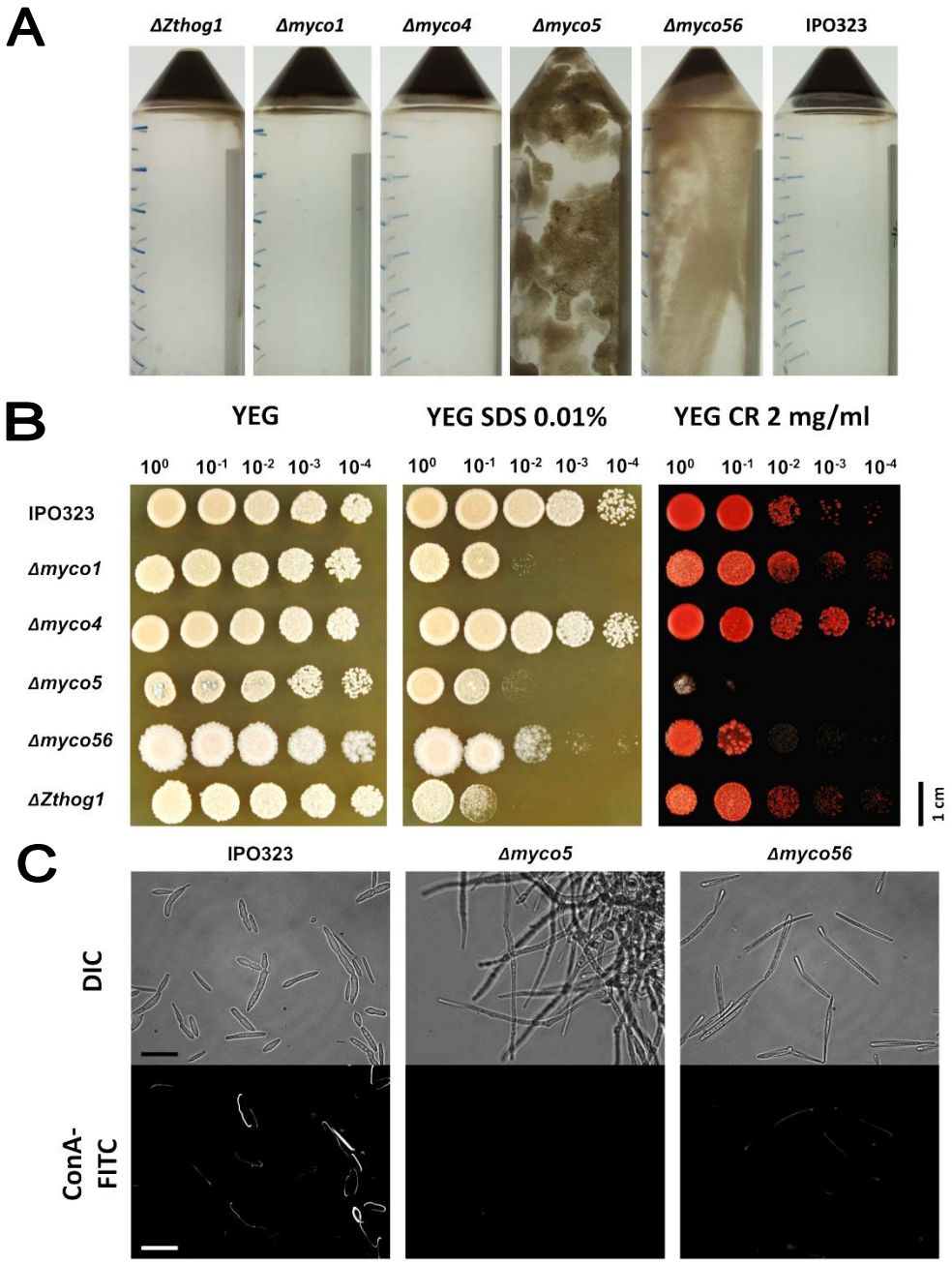

Figure 26: Involvement of the target genes *MYCO1*, *MYCO5* and *MYCO56* in maintaining the cell wall integrity. (A) Pellet stability analysis of the mutant strains. Prior centrifugation at 4,000 rpm the strains were cultured in YEG fluid medium for 4 days at 18 °C. After centrifugation, all resulted pellets were directly photographed. **(B) Sensitivity of mutant strains to cell wall perturbing agents.** The reference and mutant strains were grown on YEG medium, supplemented with 0.01% SDS or 2 mg/ml Congo Red (CR), for 7 days at 18 °C. Four times serial dilutions of the grown culture (1×10^8 spores/ml) were dropped on the plate. **(C) Examination of mutant strains towards binding affinity of the FITC-labelled alpha-D-mannose/alpha-D-glucose-specific lectin Concanavalin-A (ConA-FITC) using fluorescent microscopy.** Consistent differences between the mutant strains *Δmyco5*, *Δmyco56* mutants and wildtype conidia were apparent, concerning both the number of cells which bound ConA-FITC and the relative intensity of fluorescent signals detected. Scale bar corresponds to 20 μm.

Consistent with these results, the mutant conidia were further analyzed by testing their sensitivity to treatment with cell wall degrading enzymes. The enhanced sensitivity observed from the preceding tests would suggest that conidia from the mutant strains could be more sensitive to lysis due to the altered cell wall composition. The fungal cell wall is known to comprise α/β-(1,3)-glucan and chitin, representing the major structural constituents (Arana *et al.*, 2009, Fesel and Zuccaro, 2016, Erwig and Gow, 2016). Treatment with cell wall degrading enzymes from *Trichoderma harzianum*, containing β-glucanase with some cellulase, protease and chitinase activities, was conducted to investigate the strain-specific changes in cell wall composition. Consequently, conidia of all mutant strains except for *Δmyco4* form faster protoplasts than does the wildtype strain IPO323 (Figure 27). Furthermore, the results indicate that *Δmyco1* and *ΔZthog1* are more sensitive to enzyme treatment since more protoplasts are released upon incubation for 120 min, compared to wildtype strain IPO323. The mutant strains *Δmyco5* and *Δmyco56* display also sensitivity towards treatment with lysing enzymes, but to a lesser extent, exhibiting 60% and 40% of lysing rate percentage (protoplast release) respectively. Additionally, in contrast to other strains, many mycelial fragments and degraded hypha were noticed for the *Δmyco5* mutant.

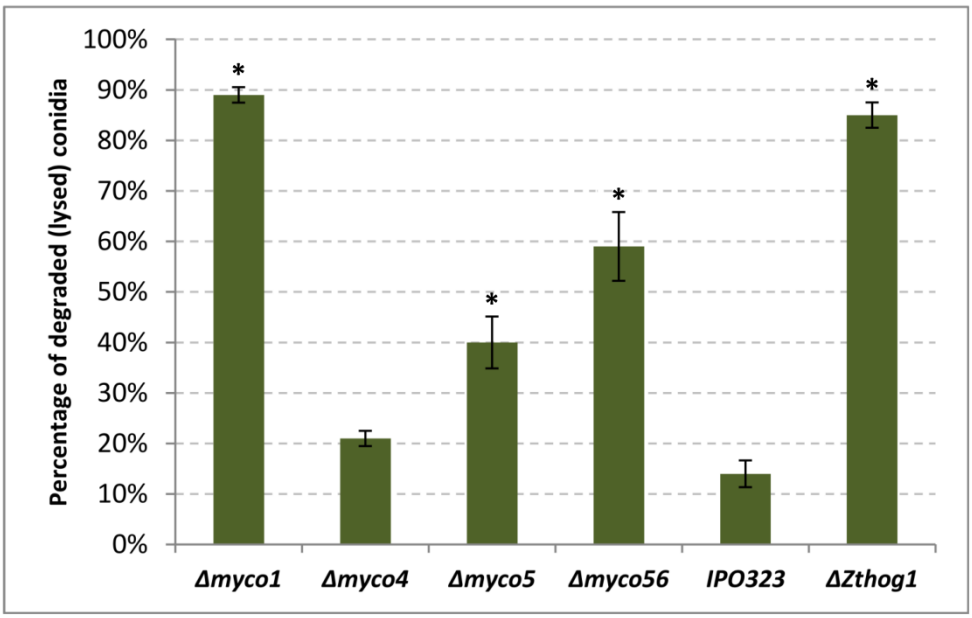

Figure 27: Lysis test to examine protoplast release of the wildtype IPO323 and generated mutant strains. Percentage of degraded conidia due to protoplast production of corresponding strains is shown. The mutant strains *Δmyco1*, *ΔZthog1*, *Δmyco5* and *Δmyco56* display an enhanced sensitivity towards treatment with cell wall degrading enzymes from *Trichoderma harzianum* compared to wildtype. Data presented are the mean (including standard deviations) of results from the 3 independent experiments. Asterisks indicate a significant difference between the mutant and wildtype strain at $P < 0.01$.

3.6.4 *MYCO1* and *MYCO5* are involved in oxidative stress response

As shown in Figure 28, a reduced growth for all strains was observed, when incubation was performed in the presence of 6 mM H_2O_2. They displayed, however, different degree of susceptibility towards oxidative stress. YEG complete medium was chosen as a basis medium, as it supported a conidial vitality of cultures upon exposure to oxidative stress mediating H_2O_2 and facilitated the evaluation of radial diameter of the strain cultures – a circumstance, which was not given in the case of N-deprivation medium. Exposure to low concentrations of H_2O_2 (2 mM) leads to visible inhibitory effects stated for *Δmyco1*, *ΔZthog1* and *Δmyco5* compared to wildtype strain, with more pronounced growth defects observed for *ΔZthog1* and *Δmyco1*. Thus, *ΔZthog1* and *Δmyco1* displayed already a significantly reduced growth when cultivating on YEG medium supplemented with 2 mM H_2O_2, and they were completely arrested in their growth by treatment with 4 mM H_2O_2. Meanwhile, strong inhibitory effects were exerted on the colony development of *Δmyco5* strain by exposure to 4-6 mM H_2O_2, which were however not detected to the same degree for the wildtype, *Δmyco4* and *Δmyco56* strains (Figure 28).

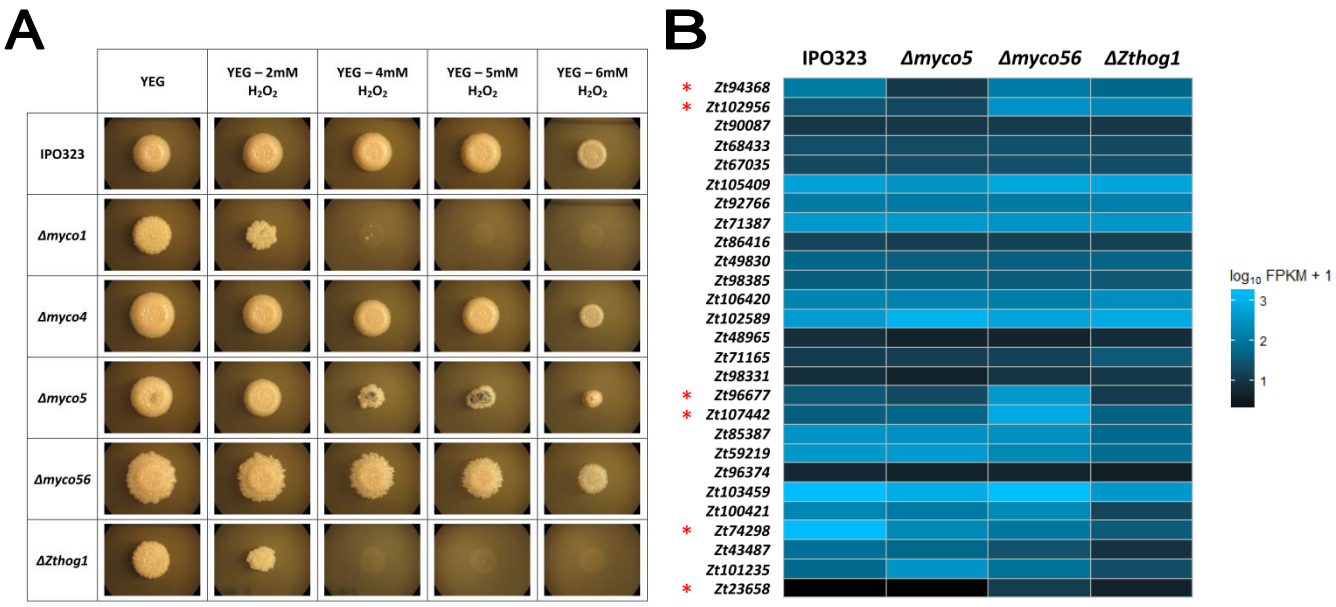

Figure 28: Examination of susceptibility of generated mutant strains to oxidative stress. A) Colony morphology of *Zymoseptoria tritici* IPO323 and generated mutants under oxidative stress growth conditions. The wildtype (WT) strain and indicated mutant strains of YEG cultures were spotted as dilution series (1.5 µl; 5×10^7 spores/ml) and incubated on YEG plates containing various concentrations of H_2O_2. Plates were imaged after 7 days of incubation at 18 °C. Strains lacking *MYCO1* or *ZtHOG1* are more susceptible to oxidative stress. For *Δmyco5* a slightly reduced growth was noticed. **B)** Expression of some annotated chloroperoxidases and superoxide dismutase encoding genes derived from RNA-Seq analysis. The remaining genes not shown in the figure exhibited similar expression among the investigated strains. The detected expression profiles of *Z. tritici* strains reveal on average a lower expression of peroxidase encoding genes in case of *Δmyco5* and *ΔZthog1*, meanwhile *Δmyco56* on the contrary the highest. Red asterisks indicate genes harbouring significant differences in their expression pattern across at least two compared strains.

Generally, the wildtype strain IPO323 along with *Δmyco4* and *Δmyco56* tolerated higher levels of oxidative stress than did *ΔZthog1*, *Δmyco1* and *Δmyco5* strains. Genomic complementation of the mutant strains restored the wildtype phenotype after reintroducing the corresponding wildtype alleles driven by native promoters. Expectedly, the strain-specific phenotypes observed coincide with expression profiles obtained from the foregoing RNA-Seq analysis. According to the transcriptome analysis, the mutant strains *ΔZthog1* and *Δmyco5* displayed on average lower expression levels of genes compared to wildtype, whose products might be involved in H_2O_2 detoxification, as they are predicted to encode chloroperoxidases and superoxide dismutases. When comparing the gene expression profile of the *Δmyco5* mutant with that of wildtype, four genes (*Zt94368*, *Zt102956*, *Zt96677*, *Zt74298*) were found to be down-regulated, whereas only one gene (*Zt101235*) displayed an increased expression in *Δmyco5* compared to the others strains. Contrarily, *Δmyco56* exhibited on average the highest expression of peroxidases encoding genes. Interestingly, most of these genes, such as *Zt94368*, *Zt102956*, *Zt96677*, *Zt107442* and *Zt23658* displayed significantly increased transcript abundance, not only in comparison to wildtype, but across all strains investigated. For the other genes examined, very similar transcriptional levels across the strains were detected.

3.6.5 Disruption of *MYCO1* results in fungicide resistance

The previous study by Mehrabi, 2006 provided evidence for an increased resistance of *ZtHOG1* disrupted mutant strains against phenylpyrrole fungicides, like fludioxonil and fenpiclonil, as well as dicarboximide fungicide iprodione. We examined the sensitivity of *Δmyco1* mutant against fludioxonil, to test whether inactivation of *MYCO1* gene encoding a regulator protein within *HOG1*-pathway would also result in increased resistance against this fungicide. As expected, the growth of *Δmyco1* on PDA supplemented with 30 µg/ml fludioxonil is in clear contrast to that of wildtype, as the mutant strain was highly resistant (Figure 29). The phenotype of *ΔZthog1* mutant is very similar to that of *Δmyco1*, displaying enhanced resistance as previously reported (Mehrabi, 2006), whereas the wildtype IPO323 and ectopic control strain exhibited a strongly pronounced sensitivity against fludioxonil. This observation also coincides with previously reported results with osmosensitive mutants of *Neurospora crassa*, *Colletotrichum lagenarium* and *Alternaria alternata* evidencing resistance to phenylpyrrole fungicides (Zhang *et al.*, 2002, Kojima *et al.*, 2004, Yu *et al.*, 2016).

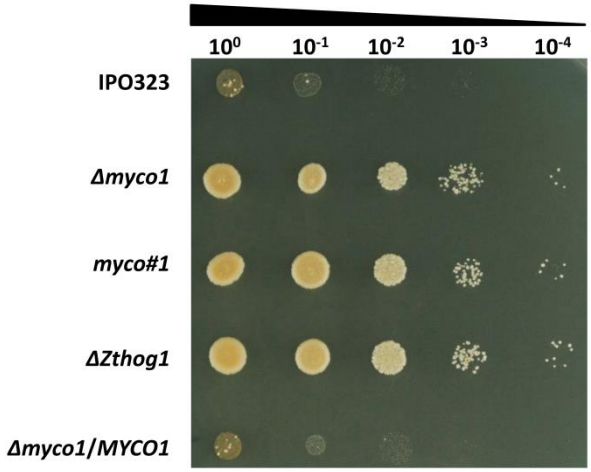

Figure 29: ***In vitro*** **fludioxonil fungicide sensitivity assay.** Prior to photographs the strains were incubated on PDA amended with fludioxonil (30 µg/ml, dissolved in EtOH) for 7 days at 18 °C. Four times serial dilutions of the YEG-grown culture (1×10^8 spores/ml) were dropped on the plate. The *Δmyco1*, *Δhog1* as well as random *myco#1* mutants confer resistance to the phenylpyrrole fungicide fludioxonil. Meanwhile, the wildtype strain IPO323 and the ectopic transformant exhibit abolished growth upon fludioxonil treatment.

3.6.6 *MYCO5* is involved in detoxification of transient metals

The preceding RNA-Seq analysis of *Δmyco5* mutant revealed a set of several DE genes predicted to encode ion transporters, suggesting their possible involvement in detoxification processes by lowering the intracellular concentration of different metal ions. Most of them were found to have reduced relative transcript abundance in the mutant strain. To verify the expected susceptibility towards metals toxicity, *Δmyco5* along with IPO323 and other strains were incubated on YEG medium amended with sublethal concentrations of transient metals, like $CuSO_4$ and $ZnSO_4$. Incubation of *Δmyco5* on YEG supplemented with 5 mM $CuSO_4$ resulted in impaired growth (Figure 30). At 10 mM $CuSO_4$ all of the investigated mutants were arrested in their growth. Similarly, incubation of all strains on YEG with 5 mM $ZnSO_4$ resulted in viable colonies displaying growth not significantly different from that observed on YEG reference medium, except for *Δmyco5* showing a retarded conidial propagation. Furthermore, the growth of *Δmyco5* was completely inhibited by applying of 10 mM $ZnSO_4$, whereas the wildtype IPO323 together with the other mutant strains tolerated the increased amount of $ZnSO_4$. The link between the *MYCO5* gene and the observed phenotype was confirmed by genetic complementation since the wildtype phenotype was restored when the native copy of the *MYCO5* gene with its endogenous promoter and terminator sequences was re-introduced into the genome of the mutant strain *Δmyco5* (data not shown).

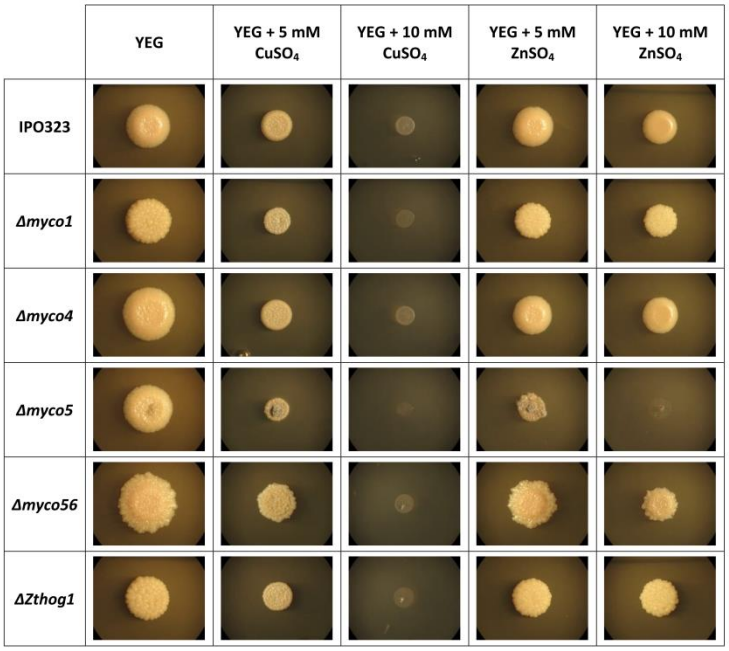

Figure 30: Colony morphology of *Zymoseptoria tritici* IPO323 and generated mutants under transient metal stress growth conditions. The mutant strain *Δmyco5* was found to be sensitive to elevated levels of metal ions in the medium. The wildtype (WT) strain and indicated mutant strains of YEG cultures were spotted from serial dilutions (1.5 µl; 5×10^7 spores/ml) onto YEG plates that were supplemented with transient metals $CuSO_4$ and $ZnSO_4$ each 5 mM and 10 mM. Plates were imaged after 7 days of incubation at 18 °C.

3.6.7 Mutant lacking *MYCO4* gene exhibits adenine auxotrophy

Proceeding from the previous BLASTp analysis with the *MYCO4* gene (see 3.4.1) revealed its involvement in *de novo* purine biosynthesis, insofar as significant functional orthologs previously characterized in other fungi were identified. Consistent with the putative role for *MYCO4* gene in the *de novo* purine biosynthesis, the incubation of *MYCO4* defective mutant on N-deprivation medium without adenine resulted in a drastically impaired growth (Figure 31A). As expected, *Δmyco4* also failed to grow on N-deprivation solid medium supplemented with 1 mM glutamine (Figure 31A), as well as glycine and aspartate (data not shown), which are normally required as precursors for *de novo* synthesis of purine nucleotides. Supplementation of N-deprivation medium with both, either adenine or hypoxanthine at 1 mM, restored the wildtype-like phenotype of the mutant completely, suggesting that the purine salvage pathway is operational in the mutant strain. The growth was also restored and was comparable to that of the wildtype strain when the native copy of the *MYCO4* gene was reintroduced in the loss-of-function mutant, indicating that the growth defect of *Δmyco4* was due to the lack of functional *MYCO4* allele. Interestingly, using lower concentrations of adenine added to N-deprivation medium the growth defect of *Δmyco4* mutant could be rescued and the colony development was similar to that observed for the wildtype strain IPO323. Furthermore, there was no difference in growth when *Δmyco4* was incubated on N-

starvation medium supplemented with higher concentration of adenine or hypoxanthine, suggesting a sufficient uptake of external purines from the medium. The same phenotype was observed by cultivating the *Δmyco4* mutant strain on N-starvation medium supplemented with reduced amount of hypoxanthine (Figure 31A). Furthermore, as previously mentioned, the yeast-to-hyphal transition of *Δmyco4* occurred after a lag period of approximately 14 days on N-deprivation medium and was completely abolished on water agar. With addition of external adenine, even at low concentration, the wildtype-like "dimorphic switch" ability of the mutant strain was restored (Figure 31B). Consequently, these observations indicate that *MYCO4* is involved in *de novo* purine biosynthesis in *Z. tritici*, since the loss-of-function allele causes auxotrophic requirement for adenine.

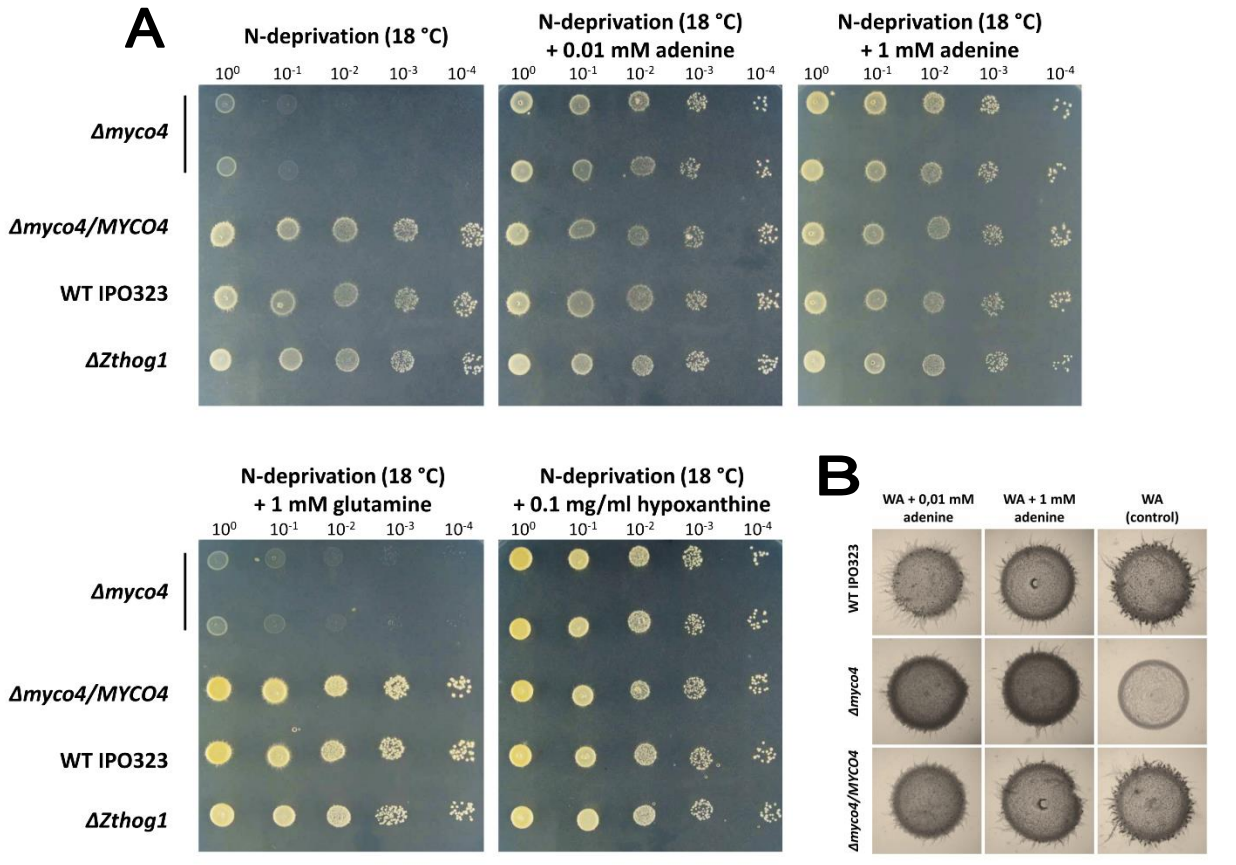

Figure 31: Growth of the *Δmyco4* mutant under purine auxotrophic conditions. (A) Inactivation of *MYCO4* gene results in the auxotrophic, purine requiring mutant. *MYCO4* deficient mutant is unable to grow on media, lacking the external source of adenine or hypoxanthine. Complementation of *Δmyco4* mutant with the full-length copy of *MYCO4* gene including its native promoter and terminator region or incubation of *Δmyco4* in the presence of 0.01/0.1 mM adenine or 0.1 mg/ml hypoxanthine restored the wildtype growth. The examination of colony growth and morphology was performed after 7 days incubation on respective media at 18 °C. The isolated spores were spotted as dilution series (1.5 µl; 10^8 spores/ml) **(B)** Yeast-to-hyphal transition restored for *Δmyco4* when incubating on water agar (WA) supplemented with 0.01 mM or 1 mM adenine for 7 days at 18 °C.

3.6.8 *MYCO5* is involved in maintaining the cellular lipid degradation status

Additionally, the RNA-Seq analysis delivered one further striking feature for *Δmyco5* mutant strain considering the expression of genes predicted to encode four different lipases/lysophospholipases and two triacylglycerol hydrolases (*Zt41969*, *Zt74078*, *Zt107391*, *Zt109795* and *Zt81448*, *Zt105080* respectively). In particular, the triacylglycerol hydrolase encoding genes (*Zt81448*, *Zt105080*) and one gene encoding a putative FabD lysophospholipase (*Zt109795*) exhibited highly abundant transcript levels in *Δmyco5* mutant compared to other strains including wildtype. The corresponding expression profiles are illustrated in CircosPlot (Figure 32A). To examine, whether the observed difference in the expression of relevant genes can shape the physiological properties of the mutant strain, a phenotypic investigation employing NileRed staining was conveyed. NileRed (9-diethylamino-5H-benzo[alpha]phenoxazine-5-one) is known as an excellent vital stain for the selective detection of intracellular neutral lipid droplets by fluorescence microscopy. Interestingly, a better selectivity for cytoplasmic lipid droplets was achieved when the cells were inspected for yellow-gold fluorescence (excitation, 450-500 nm; emission, greater than 528 nm) rather than red fluorescence (excitation, 515-560 nm; emission, greater than 590 nm), as previously described (Greenspan, 1985). Using this histochemical approach, the intracellular distribution of lipid droplets could be visualized. After three days incubation both in N-deprivation and YEG liquid media, an increased degradation of intracellular neutral lipid droplets in *Δmyco5* compared to the wildtype strain IPO323 (WT) was detected (Figure 32B). As expected the wildtype strain IPO323 was found to grow predominantly yeast-like under nutrient-rich condition (YEG) and numerous small intense yellow droplets in ungerminated conidia were clearly visible over a background of diffuse bright yellow fluorescence signal. Meanwhile, *Δmyco5* exhibited a strongly enhanced mycelium formation, though bearing only rarely yeast-like growing conidia. The hyphae fluoresced with a significantly weak diffuse yellow signal. Interestingly, the small portion of yeast-like conidia of *Δmyco5* was much more intensely fluorescent relative to predominant hyphae, and bright yellow vesicles were apparent, similar to that of the wildtype. Furthermore, the NileRed staining difference of fluorescence intensity was less pronounced when comparing WT and *Δmyco5* under dimorphic-switch inducing condition by incubating them on N-deprivation. Both exhibited dispersed yellow fluorescence signals decreased in intensity, indicating an enhanced degradation of neural lipids (data not shown). This observation leads to a presumption that the expression of the genes involved in lipid metabolism and the concomitant lipid degradation are rather more specific and coupled to the stage or growth modus.

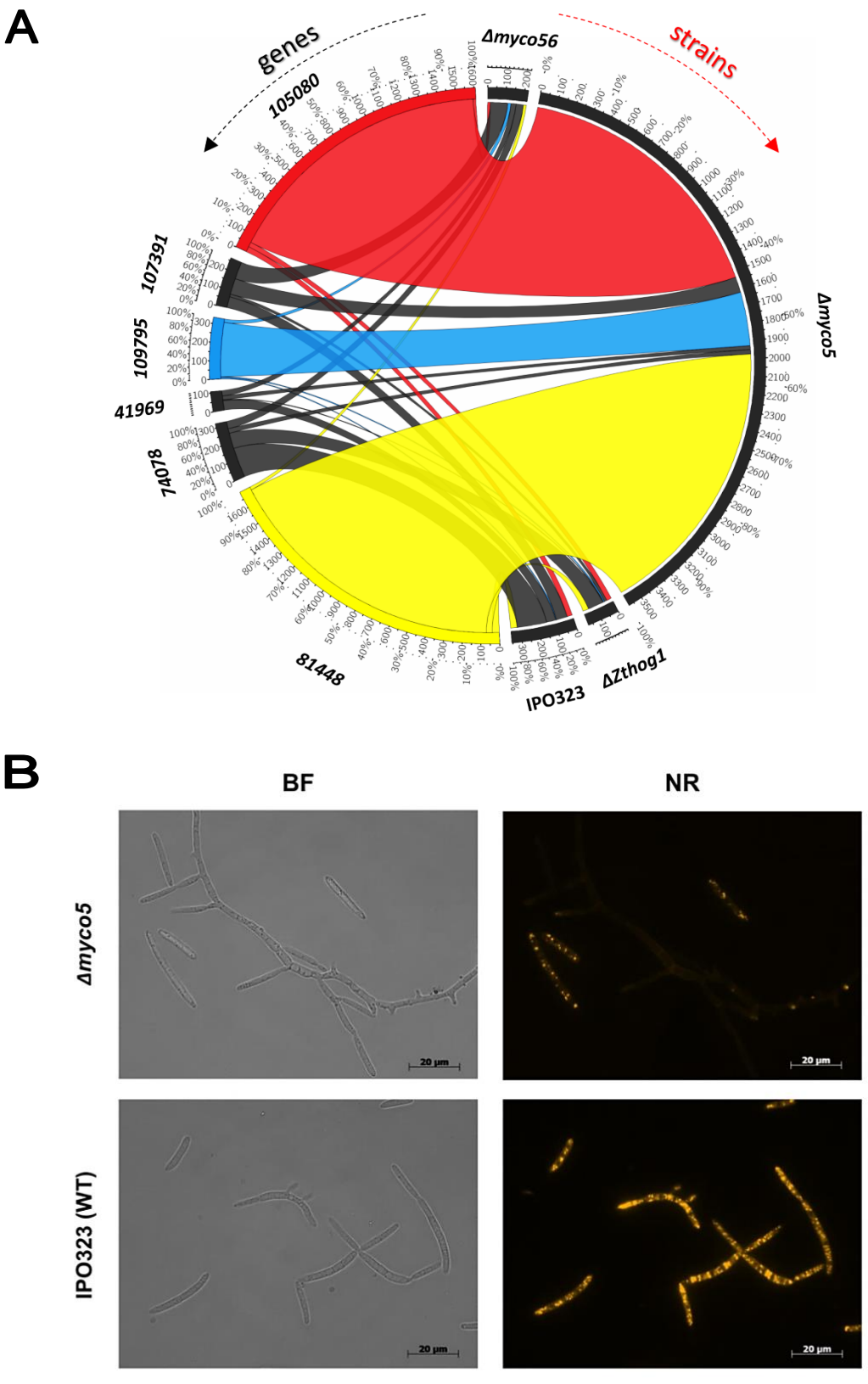

Figure 32: Alteration of lipid metabolism in the targeted mutant strain *Δmyco5*. (A) CircosPlot visualization of RNA-Seq expression data concerning phospholipase and esterase-encoding genes. The transcript abundance of genes with IDs: 105080, 109795 and 81448 were found to be strongly expressed in *Δmyco5* strain compared to wildtype and other strains. **(B) Semiquantitative analysis of cellular lipid content of *Δmyco5* mutant.** Intracellular localization of neutral lipids was visualized by Nile red staining of wildtype and *Δmyco5* mutant. BF: bright field microscopy; NR: Nile red staining.

3.6.9 *Δmyco5* exhibits reduced proteolytic activity

A set of DE genes encoding proteases was apparent from the preceding RNA-Seq analysis when comparing the regulon of *Δmyco5* with the transcriptome profile of IPO323. Interestingly, some of these genes predicted to encode secreted products (according to SignalP-analysis) showed decreased transcript levels in *Δmyco5* – an observation which may result in an altered proteolytic activity of the mutant (Figure 33B). To confirm this assumption, an *in vitro* growth assay was performed. In order to analyze the secretion of alkaline proteases and to examine the protease activity of *Δmyco5*, a comparison to the wildtype strain was performed by cultivating the strains on N-deprivation medium with pH 7.5 supplemented with skim milk (1%) as the sole nitrogen/protein source. The proteolytic activity was assessed qualitatively by inspecting the formation of halo zones around the colonies, pointing to the hydrolysis of protein components contained in the skimmed milk medium by extracellular proteases. Thus, the reference strains IPO323 and *ΔZthog1* exhibited large clearing zones (halos) (Figure 33A). Meanwhile, *Δmyco5* strain was found to be drastically reduced in its ability to degrade skimmed milk compared to control cultures. Contrarily, the complemented transformant *Δmyco5/MYCO5* can fully restore the defects, suggesting that normal expression level of Myco5p is necessary to maintain the wildtype levels of proteolytic activity in *Z. tritici*.

A

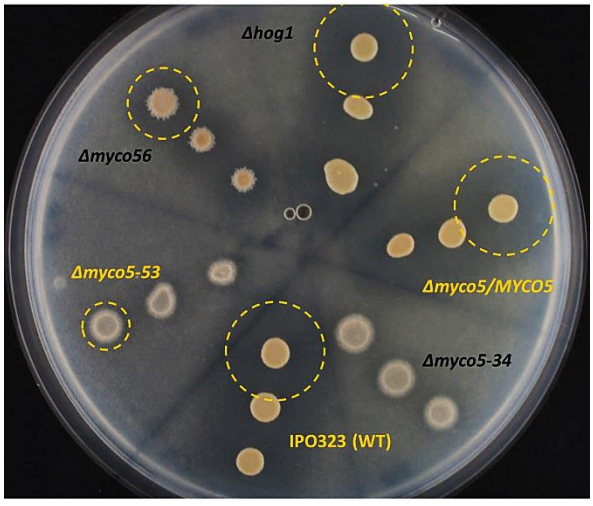

B

10 90

	IPO323	Δmyco5	Δmyco56	ΔZthog1
* Zt34453	103.14	6.11	214.05	44.70
Zt43961	19.99	141.52	46.94	27.44
Zt43998	2177.26	182.21	497.66	1070.55
* Zt59604	89.05	7.53	194.07	99.84
Zt71297	16.95	164.21	19.95	20.73
Zt72846	22.21	10.34	45.71	101.64
* Zt76021	27.82	16.52	91.56	183.82
Zt99102	9.37	122.61	12.66	2.89
Zt101415	14.15	43.23	87.97	11.01
* Zt108506	22.53	52.84	274.44	16.54

Figure 33: ***Δmyco5*** **exhibits reduced proteolytic activity. (A)** *In vitro* growth assay of mutant strains and IPO323 on N-deprivation medium containing skim milk (1%), to determine the proteolytic activities. The strains were inoculated over skim milk plates (1.5 µl; 5×10^7 spores/ml) and incubated for 7 days at 18 °C. The visible halos (clearing zones) surrounding the colonies indicate the extracellular protease activity. The relevant genotype of the strains is shown. Scale bar of the image corresponds to 20 µm. **(B)** Heatmap showing the transcript abundance (FPKM values) of DE genes predicted to encode proteases according to RNA-Seq data obtained. Red asterisks indicate DE genes predicted to encode secreted proteases.

3.6.10 *MYCO5* deficient mutant exhibits an attenuated glucose utilization

The RNA-Seq analysis revealed a set of differentially expressed genes being potentially involved in carbohydrate utilization, encoding either proteins involved in carbohydrate metabolism or transporter proteins mediating the uptake of external source of carbohydrates. Because most of these genes were found to have decreased transcript abundances in *Δmyco5* mutant compared to other strains investigated, it was of interest to verify the suggested *MYCO5*-dependent transcriptional regulation of predicted transporter encoding genes by *in vitro* growth assay. This was achieved by submerged cultivation of both *Δmyco5* and wildtype IPO323 in 300 ml YEG complete medium containing 1% glucose in baffled 1 L shake flasks at 18 °C and 28 °C and 120 rpm, followed by measuring of glucose content and pH-value throughout the complete cultivation period.

Figure 34A illustrates the strain-specific differences with respect to the utilization rates of glucose. In case of wildtype strain IPO323, the exogenous glucose was completely metabolized in YEG liquid medium after 5-days of incubation at 18 °C, whereas *Δmyco5* accomplished the complete glucose depletion after 7-days incubation under the same cultivation condition. This difference was even more pronounced when the wildtype strain and the *Δmyco5* mutant were incubated at elevated temperature (28 °C) in the YEG medium. Hence, fermentable glucose in the medium was completely consumed after 6 days in case of the wildtype strain IPO323. Contrarily, a prolonged incubation period of about 29 days was necessary for *Δmyco5* mutant to achieve a total depletion of external glucose in the medium (Figure 34A). This finding evidently approves the observation from the previous experiment, indicating that the growth of the mutant at elevated temperature is greatly reduced due to the increased thermosensitivity. In general, slower growth kinetics has been observed for *Δmyco5* mutants compared to the wildtype strain IPO323 (data not shown). For instance, a 3-day cultivation of the strains in YEG liquid medium showed a considerable difference in the sporulation rate. Hence, *Δmyco5* exhibits only 10% of the wildtype sporulation level (Figure 34B). Reintroduction of the native gene copy into the genome of the mutant rescued this defect and the complementation strain restored the wildtype level of sporulation when incubating under the same condition. Furthermore, the reduction of sporulation yield of *Δmyco5* was also reflected in the biomass obtained, as the dry weight of the *Δmyco5* strain culture determined was nearly two-fold lower compared to that of the wildtype and the complementation strain (Figure 35C).

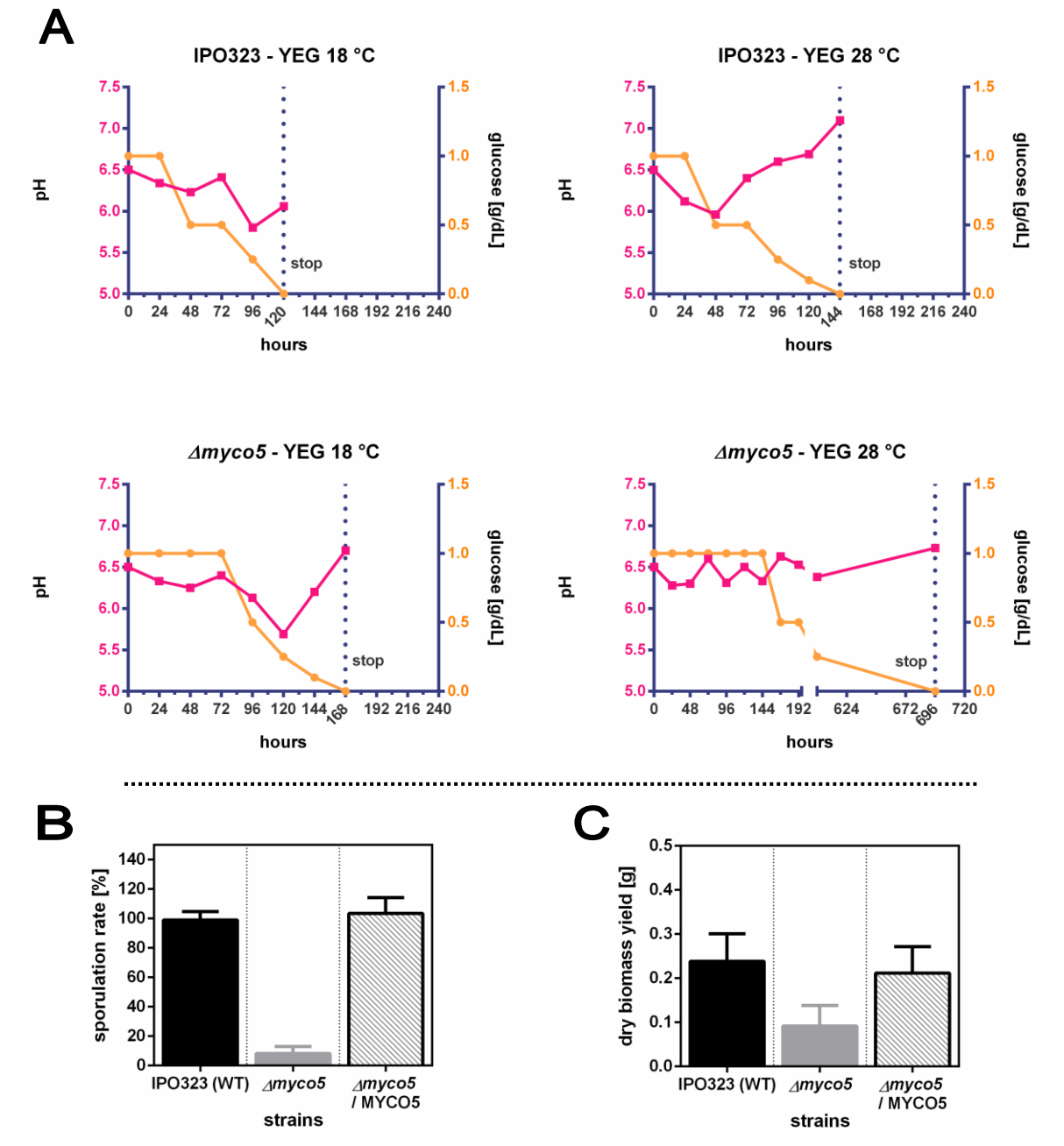

Figure 34: Temperature-dependent glucose utilization kinetics of *Δmyco5*. (A) The mutant strain *Δmyco5* along with the wildtype IPO323 were separately grown in 300 ml nutrient rich YEG medium. Cultivation parameters such as glucose content and pH were monitored. The doted lines mark time points, when the external glucose in the medium was completely depleted, followed by termination of fermentation process. **(B)** Investigation of sporulation rates of *Δmyco5*, IPO323 and complemented strain *Δmyco5*/*MYCO5*. **(C)** Measurement of dry biomass yields. Both, sporulation rate and dry biomass yield were quantified as described in 2.3.1/2.3.2 by culturing the strains in 50 ml YEG medium at 22 °C. Measurements were taken after 96 h when glucose was completely consumed in the strain cultures. The results were obtained from three independent experiments and expressed as mean values.

3.7 Localization studies using fluorescence microscopy

To determine the subcellular localization of the proteins encoded by investigated target genes, gene fusions to the green fluorescent protein (eGFP) encoding gene were performed. This was achieved by amplification of native promoter-gene fragments for the genes *MYCO4*, *MYCO5* and *MYCO56* and fusion of these to the *eGFP* gene followed by *NOS* terminator sequence in a translational *in-frame* manner, so that the protein products would be the proteins of interest fused at their C-termini to the eGFP (Figure 35A). The native promoter sequences for each construct, which had a length of approximately 1 kb, were examined by *in silico* analysis (using Promoter2.0 at CBS server) aiming to assess their functionality by the presence of predictive promoter elements. The resulting constructs were introduced by ATMT into the WT strain IPO323 and the generated transformants (indicated as *IPO323::myco4-eGFP*, *IPO323::myco5-eGFP* and *IPO323::myco56-eGFP*) containing single insertions along with a native copy of the corresponding gene were selected by Southern Blot analysis (data not shown). The genomic integration of the fusion constructs suggested an ectopic mode of recombination since they had no homologous flanks/regions at 3'-terminus suitable for the replacement of native gene by homologous recombination. Therefore, the resultant transformants were expected to express both versions of proteins, the protein derived from the expression of native gene copy, as well as eGFP-fused version. The protein localization studies were performed with at least five independent transformants for each mutant strain, in order to omit the potential negative side effect of random insertion by ectopic recombination, which may affect the expression of non-target genes (non-target effect). Those transformants, which displayed no significant aberration concerning the physiological characteristics compared to the wildtype strain IPO323, were analyzed as potential candidates. For each gene, corresponding mutants expressing eGFP-fused proteins under control of endogenous promoter were identified. Examining the cellular localization of eGFP fused proteins by fluorescent microscopy at pre-germination stadium indicated that Myco4p-eGFP fusion protein localizes to the cytosol since uniformly distributed fluorescence signals with an equal intensity over the entire conidial cells were detected (Figure 35B). Meanwhile, Myco5p-eGFP and Myco56-eGFP were found to be distributed throughout the conidial cells in a punctate manner, suggesting their location in the yet unknown cellular compartments (organelles). The corresponding fluorescence emission intensities detected for both proteins differed significantly, indicating different levels of protein expression. Thus, in contrast to Myco56p-eGFP, very faint fluorescence signals in case of Myco5p-eGFP were detected.

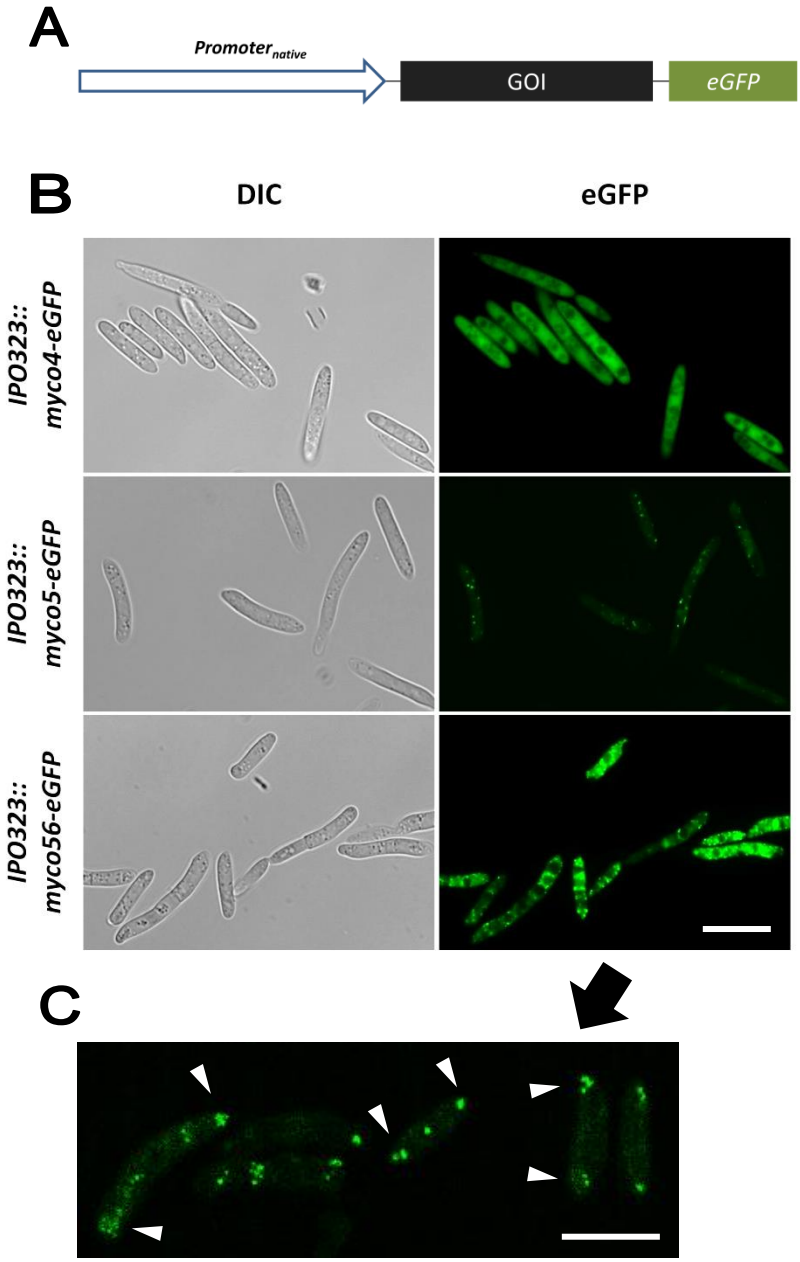

Figure 35: Localization studies of target eGFP-fused proteins by fluorescence microscopy.
(A) Schematic representation of the *eGFP*-fused gene constructs used for transformation of IPO323. The *eGFP* gene was inserted at the 3' end of each target gene, giving a functional *in-frame* fusion product. The expression of the *eGFP* fusion-gene is controlled by endogenous promoter of each of the target genes (*MYCO4*, *MYCO5* and *MYCO56*). GOI: gene of interest.
(B) Cellular localization of eGFP-fused proteins (Myco5p, Myco56p and Myco4p). The corresponding *Z. tritici* strains expressing the *eGFP*-fused gene products were cultivated in YEG for 4 days at 22 °C prior microscopic analysis. The images were acquired using Differential Interference Contrast microscopy (DIC) and fluorescence microscopy. Scale bar corresponds to 20 µm.
(C) Results of confocal microscopy showing protein expression of the target genes fused with green fluorescent protein encoding gene (*eGFP*). Myco56p-eGFP proteins tend to form aggregates at conidial apices at the pre-germination stadium of development (indicated by white arrow heads). Scale bar corresponds to 20 µm.

Interestingly, for Myco56p-eGFP a more detailed microscopic investigation revealed a biased accumulation at conidial apices, which was further supported by detailed examination using confocal laser scanning microscopy (Figure 35C). This observation leads to an assumption that Myco56p might be involved in conidiogenesis and germination, since both processes were affected by the loss of functionality of *MYCO56* gene. This finding attracted attention and awakened interest for a more profound analysis. Therefore, to get more insight into the spatiotemporal localization pattern of Myco56p-eGFP, a time-course analysis using fluorescent microscopy was performed, encompassing a period of 4 hours. Conidia expressing Myco56p-eGFP were incubated on the microscopic slides covered with water agar,

additionally supplemented with thiamine and biotin. In preliminary experiments these vitamins were found to induce germination of the spores when provided in high concentrations (data not shown). Following the time-course analysis, it was possible to observe the germination of conidia and analyze the cellular translocation of eGFP-fused proteins. Interestingly, monitoring the entire time course of germination, there was an onward increase in the fluorescence signal detectable in the areas in which the germ tube was formed (Figure 36; extension of germ tube begins at 150 min). Additionally, the protein localization studies were performed considering the late developmental stages of conidia coincident with the formation of mature vegetative hyphae upon "dimorphic switch"-inducing incubation, on microscopic slides covered with N-deprivation agar medium. Similarly to the situation in the pre-germinating conidium, a cytosolic localization for Myco4p-eGFP was found in the hyphal cells (Figure 37). The uniform distribution of the protein in cytosol goes along with the homogenous fluorescence signal detected in the hyphae formed. Together with functional *in silico* analysis of the gene, this finding approves the function of the protein in the *de novo* purine biosynthesis, as well as an essential requirement of the protein for primary metabolism, since a vigorous fluorescent signal coinciding with strong cytosolic protein expression was detected.

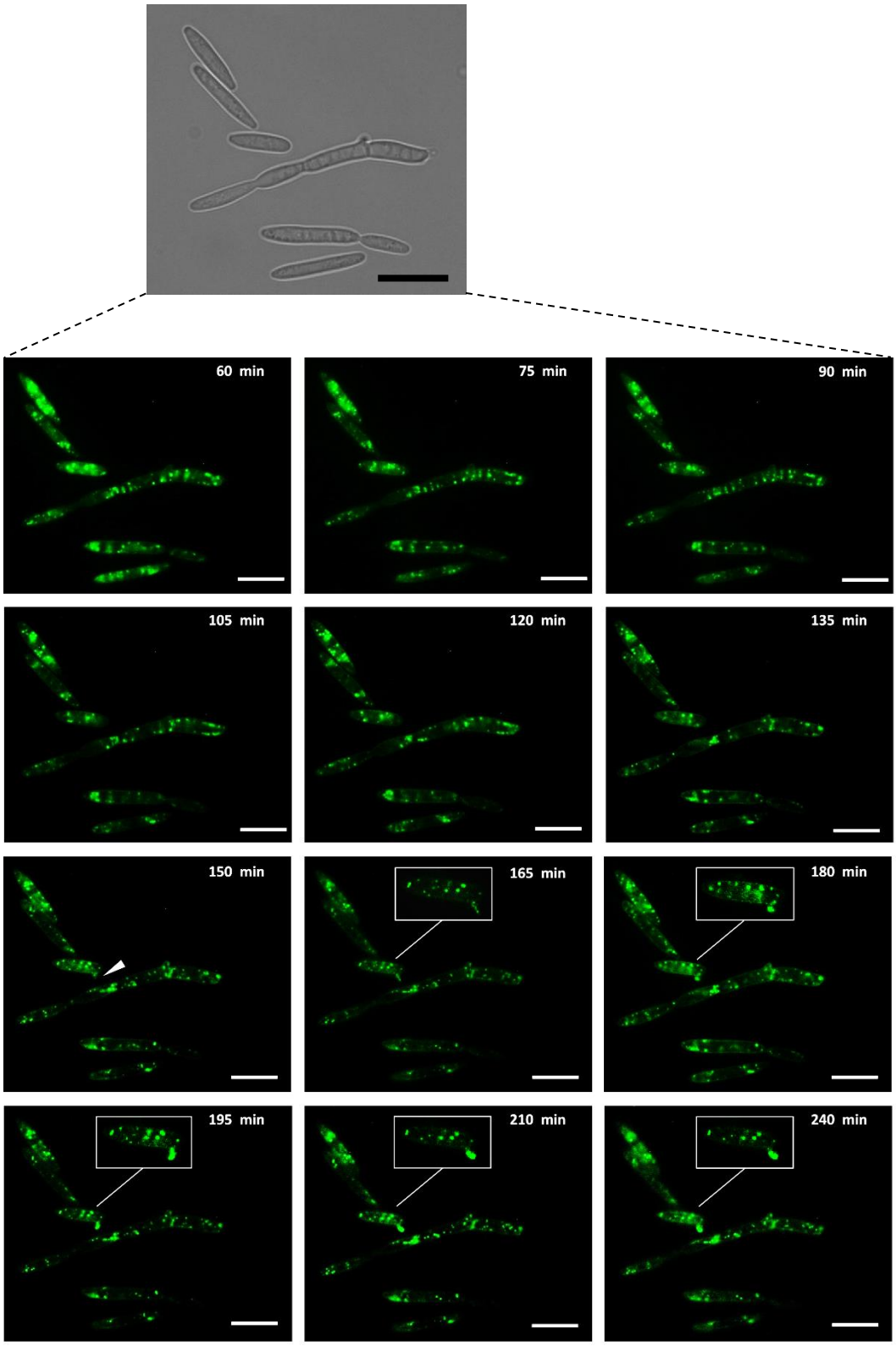

Figure 36: Time course analysis of the cellular localization and expression of Myco56p-eGFP fused protein in IPO323 during germination of pycnidiospores. The isolated spores of the strain *IPO323::myco56-eGFP* solved in water were dropped on object slide covered with a thin layer of water agar supplemented with 0.00025% (w/v) biotin and 0.001% (w/v) thiamine chlorid for the induction of germination. The incubation of spores was employed for 240 min. White arrow indicates the formation of hyphal extension (150 min), initiating the germination process. In white rectangles upscaled photographs of germinating spore are shown. Scale bar indicates 20 µm.

Moreover, in the late vegetative phase of development, which was accompanied by the formation of mature hyphae, the accumulation of Myco56p-eGFP at the apex of the growing hyphae retained (Figure 37). Together with the previous results from subcellular location analysis of Myco56p-eGFP at early stage of conidial development, this finding supports our hypothesis that Myco56p could also be important for germination-associated processes. However, a more profound microscopic time-course analysis is needed to get a more augmented insight into the dynamics of protein localization. Meanwhile, *IPO323::myco5-eGFP* exhibited a faint fluorescence signal throughout the formed hyphae in the punctate manner, pointing to a weak expression of the protein as previously observed for Myco5p-eGFP expressing yeast-like propagating conidia.

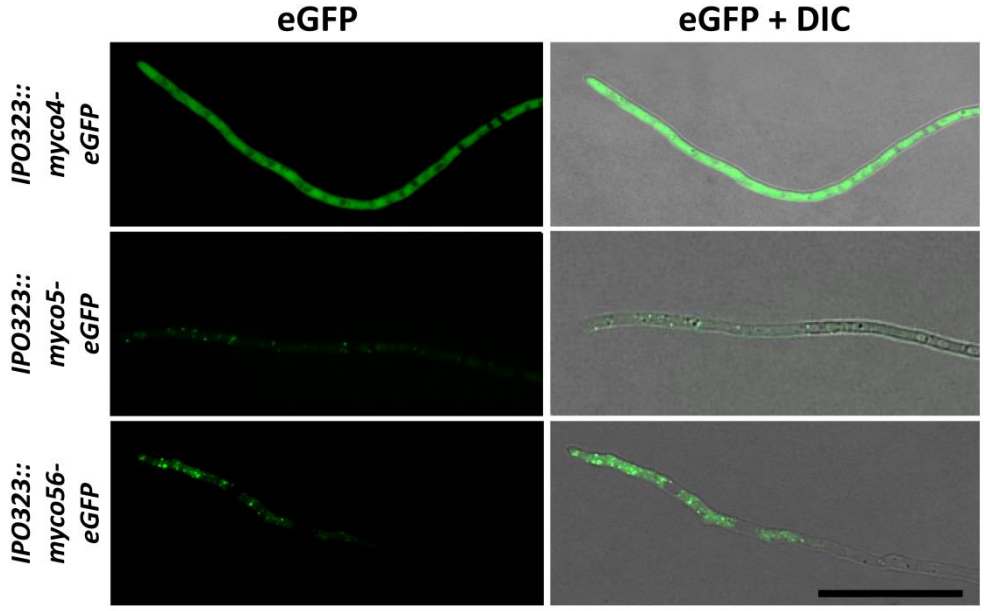

Figure 37: Fluorescent microscopic analysis of eGFP-fused proteins (Myco4p, Myco5p and Myco56p) expressed in wildtype strain IPO323 at the late developmental stage of the hyphal formation. Our results suggest that Myco5p, Myco56p and Myco4p are cytosolic proteins, however harboring different pattern of expression and localization. Myco4p-eGFP is characterized through the enhanced cytosolic expression consistent with a strong and evenly distributed, diffused fluorescence signal. Myco5p-eGFP is localized in a punctate manner throughout the hyphae, showing faint signals of fluorescence emission. Meanwhile, Myco56p-eGFP displays intense fluorescence signals indicating a biased apical accumulation at the hyphal tips. Scale bar of the images corresponds to 20 µm.

3.8 *In planta* gene expression analysis of the candidate genes

From the preceding bioinformatic analysis, the identified target genes (*MYCO1*, *MYCO5* and *MYCO56*) were predicted to encode regulators potentially affecting the gene regulation on a global transcriptional/translational scale. We hypothesized, furthermore, that they may be conditionally regulated and also function as responsive genetic determinants for the certain developmental stages within infection progression or interaction with host plant. Using qRT-PCR, this assumption was examined by monitoring the expression of the target genes following the whole asexual reproduction cycle of the fungus *in planta*, encompassing the developmental course between 1 and 28 dpi at distinct time points. In the first instance this interest was strengthened by the fact that among the 375 significantly regulated genes obtained from the RNA-Seq analysis, some orthologs previously characterized in other fungi, were found to be involved in pathogenicity relevant processes according to the PHI-database. On the other hand, according to comparative analysis of the generated RNA-Seq data with other transcriptome data published in the literature, we identified some common genes, which also appear to play a significant role in the pathogenic development of the fungus.

As indicated in Figure 38, the target genes exhibited different expression patterns during the time course of the infection process, encompassing both biotrophic and necrotrophic phases. The transcription profiles determined suggest a putative involvement of these genes in distinct developmental processes during *in planta* proliferation of the fungus. Thus, *MYCO5* exhibits significantly decreased transcript abundance at 4 and 14 dpi relative to 1 dpi used as reference condition. The transcript abundance of *MYCO4* during all phases of infection except for the last stage at 28 dpi was nearly unchanged. Interestingly, similar expression patterns were noticed for constituents of the same pathway, *MYCO1* and *ZtHOG1*. Both genes displayed decreased levels of transcripts at 4 and 14 dpi and were found to be significantly up-regulated at 28 dpi. Similar expression behaviour was observed for *MYCO56*, being significantly down-regulated at 4 and 14 dpi and displaying enhanced expression at 28 dpi. Noticeably, all genes showed the highest expression during necrotrophic growth at 28 dpi.

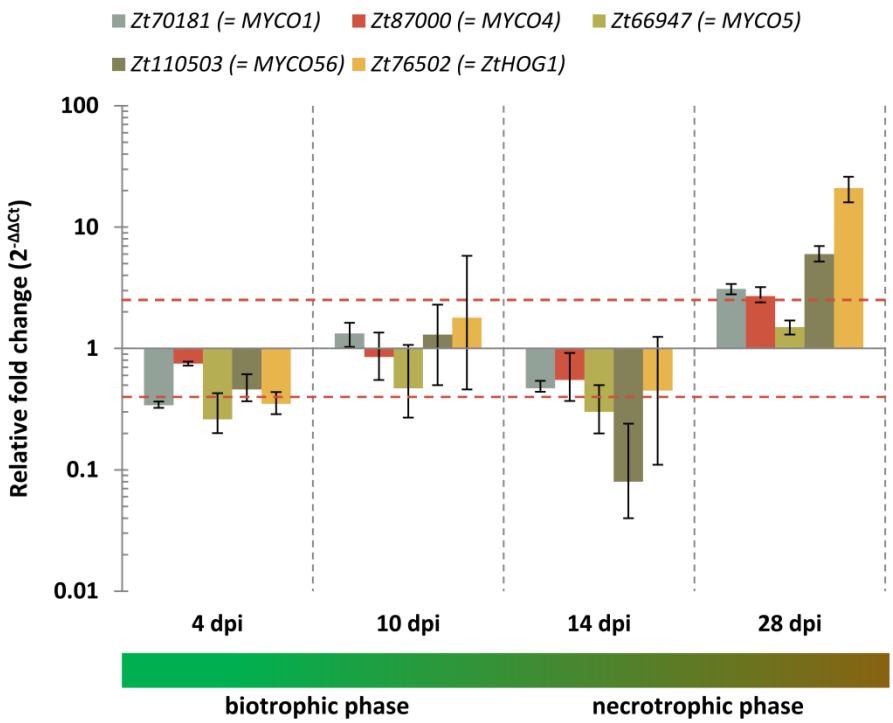

Figure 38: qRT-PCR quantification of transcription levels of examined genes *in planta* following the infection course of wildtype strain IPO323 ranging from 4 dpi to 28 dpi. Measurements of transcripts obtained by quantitative RT-PCR analysis were normalized to β-tubulin gene and expressed as relative values considering 1 dpi as a reference condition. Error bars represent standard error of the mean. The results are based on three technical repeats in two independent experiments. The dashed red lines indicate the upper and lower thresholds of 2.5 fold up-regulation or down-regulation of the genes.

3.9 *In planta* expression of chloroperoxidase-encoding genes derived from RNA-Seq

Several studies have previously elucidated the role of reactive oxygen species (ROS) in the *Zymoseptoria*-wheat pathosystem. Thus, Yang *et al.*, 2013 measured the accumulation of reactive oxygen species (ROS) in the plant during compatible and incompatible interaction with *Z. tritici*. Results of this study revealed an elevated accumulation of water peroxide in the early phase of infection within the incompatible interaction and an opposite behavior in the compatible reaction, underscoring the prominent role for ROS in the establishment of the disease. Scavenging enzymes produced by the pathogen can be therefore regarded as potential virulence determinants, enabling the fungus to overcome and suppress the host immune response or defense mechanisms. Among the 375 DE genes obtained from the RNA-Seq analysis several chloroperoxidase encoding genes were identified, underpinning the putative role of *MYCO1*, *MYCO5* and *MYCO56* in the transcriptional regulation of these genes. Suggesting potential involvement of the chloroperoxidase encoding genes in the antioxidant

response, irrespective of their preferential role in metabolic reactions, it was of interest to monitor their expression pattern during the compatible interaction with the susceptible host plant cultivar Riband. Thus, following the infection cycle, the infected plant leaves were sampled at distinct time points until 28 dpi and relative expression of the selected genes was monitored by qRT-PCR, considering 1 dpi as a reference condition. The gene *Zt74298* displayed a bimodal expression pattern, since decreased transcript levels were detected at 4, 10 and 14 dpi and there was a considerable increase in transcript abundance at 28 dpi resulting up to 50 fold change compared to the reference condition (Figure 39).

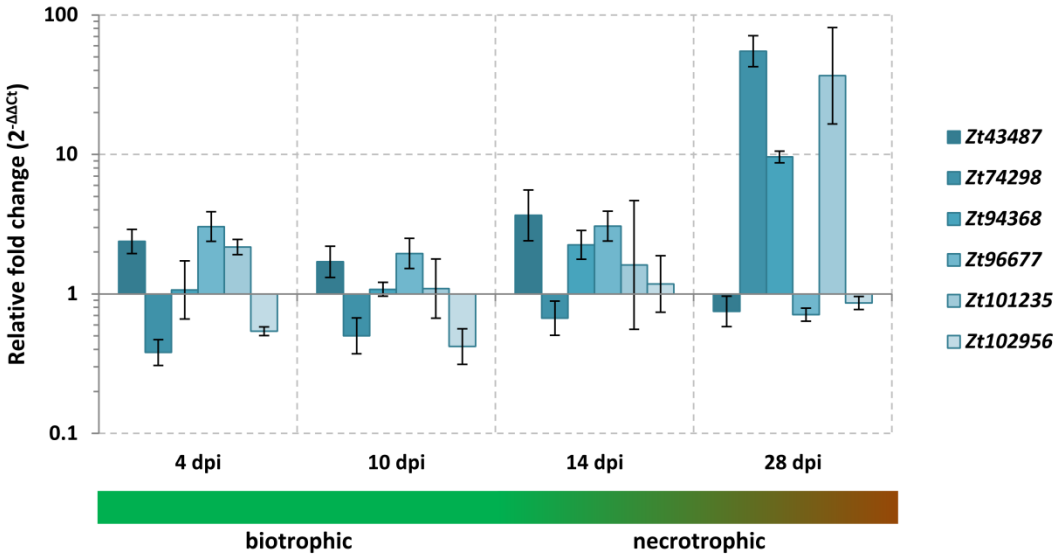

Figure 39: ***In planta*** **expression pattern of the** ***Zymoseptoria tritici*** **IPO323 chloroperoxidase encoding genes following the infection course.** Fold change represents a relative quantification of the expression levels of target genes at diverse stages of infection relative to the expression under nutrient rich condition (YEG); normalisation was conducted with the constitutively expressed β-tubulin gene. Infected leaves of wheat cultivar Riband were harvested 4, 10, 14 and 28 days post inoculation (dpi) with the wildtype strain IPO323. Error bars indicate the standard deviation of three technical replicates. The experiment was performed twice with similar results. The coloured bar represents the temporal transition from the biotrophic (green) to the necrotrophic (yellow, orange and red) phase.

The gene *Zt94368* was found to be induced at the beginning (14 dpi) and in the late necrotrophic phase (28 dpi), whereas no transcriptional changes were detected within the biotrophic development. Contrarily, transcription of the gene *Zt96677* was slightly induced in the biotrophic and beginning necrotrophic phases (ranging from 4 – 14 dpi), but showing decreased expression at late necrotrophic phase. Meanwhile, the gene *Zt101235* was found to be induced throughout the whole *in planta* development displaying the highest transcript level in the late necrotrophic phase (28 dpi). Conversely, we measured no significant transcriptional

activity for *Zt102956* in the necrotrophic phase, albeit decreased level of transcripts was detected in the biotrophic phase compared to the reference condition.

3.10 Identification of novel gene *ZtPTF1* encoding an essential transcription factor

Some genes predicted to encode transcription factors were identified in a set of DE genes obtained from RNA-Seq analysis. In order to get a more profound insight into the regulation network of dimorphic switch, we selected on the basis of RNA-Seq data one DE gene of this category to investigate its biological role by reverse genetics experiment (targeted inactivation followed by phenotypic analysis). The gene with the JGI Protein ID 109299 is predicted to encode a p53-like transcription factor with 695 amino acids in length (Figure 40C) and a predicted molecular mass of 75.137 kDa. We have designated the gene as *ZtPTF1* (relying on its similarity to **p**53-like **t**ranscription **f**actor). The structural analysis of the deduced protein sequence using InterProScan revealed a NDT80/phoG DNA-binding domain (PF05224) lying between amino acids 290–514. The presence of this domain is suggested to be characteristic for proteins, which might all be involved in sensing nutritional status and multiple aspects of meiosis and sporulation processes. Furthermore, using cNLS Mapper one potential monopartite nuclear localization signal (NLS) at position 460–469 (NNGKRRASQQ) was predicted with a score value 4, indicating that the predicted protein may localize to both the nucleus and the cytoplasm. Using BLASTp analysis of the deduced protein sequence, the predicted homologs were identified in *Z. brevis*, *M. oryzae*, *A. fumigatus*, *C. albicans* and *U.maydis* and others, sharing weighted score values (comprised of the E-value, pairwise identity and the coverage) of 99.2%, 51.0%, 43.8%, 19.3%, and 4.6%, respectively. The similarity between these putatively orthologous proteins is however largely confined to the region where the predicted DNA binding domain NDT80/phoG is located.

Interestingly, the predicted orthologs identified were constrained predominantly to fungi derived from the division *Ascomycetes*, suggesting that this protein might be regarded as specific among the fungal representatives of this phylum. Thus, only a weak similarity of Ndt80/PhoG domain was retrieved for the protein obtained from interrogation against the protein database of the phytopathogenic basidiomycete *U. maydis* (Figure 40B). Similar result was observed for the human p53 protein, which was used as outgroup for the phylogenetic tree construction (Figure 40A).

In order to evaluate the role of *ZtPTF1* in dimorphic transition of *Z. tritici*, we attempted to disrupt the gene by replacing the partial ORF with the hygromycin phosphotransferase

resistance cassette. The resultant hygromycin-resistant transformants were screened by genomic Screen-PCR. However, among the 200 transformants tested, none of the targeted gene inactivation mutants could be recovered, as only ectopic integrations of the construct were detected (data not shown).

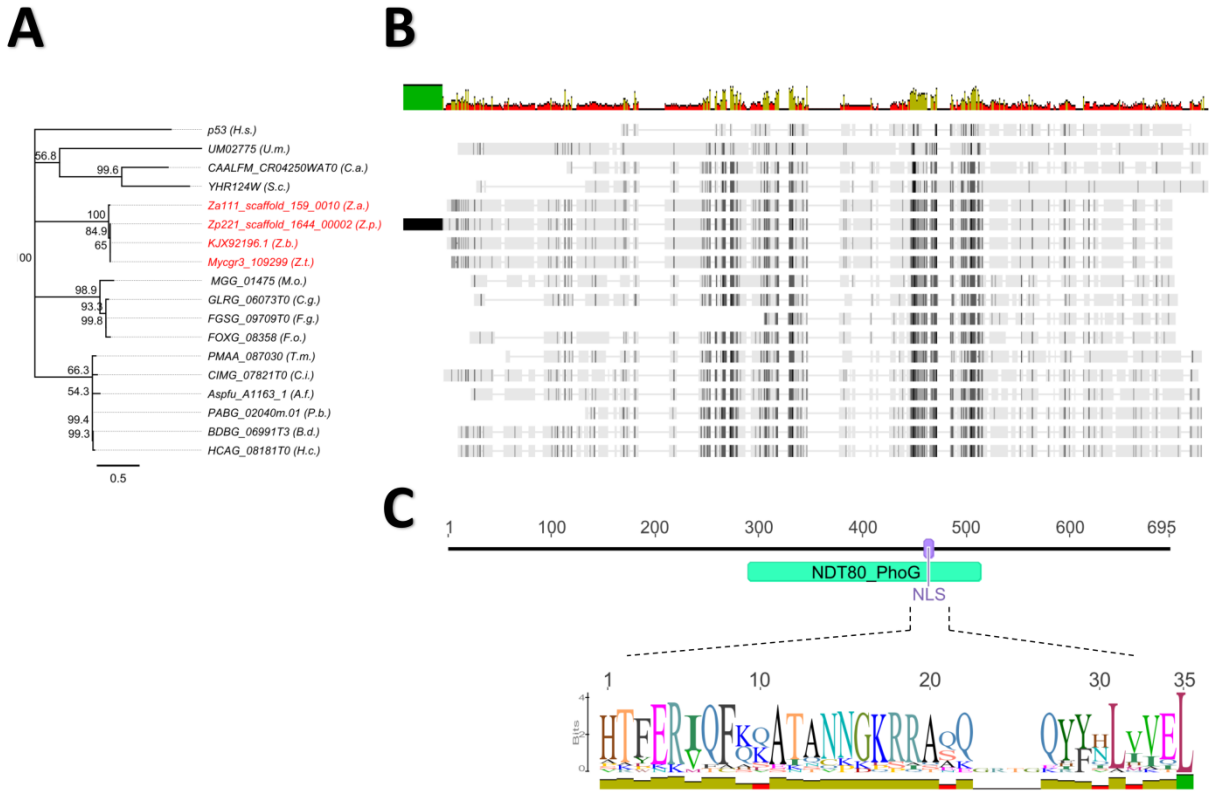

Figure 40: Phylogenetic analysis and domain structure of deduced ZtPtf1p. (A) Phylogenetic tree based on deduced ZtPtf1p sequence homologs of different fungi. The phylogenetic tree was constructed using neighbor-joining method implemented in Geneious program. The bootstrap values of the branches were obtained by testing the tree 100,000 times and are shown as percentage numbers. Branch lengths on the tree represent an average number of amino acid substitutions per site. The sequences are originating from *Aspergillus fumigatus* A1163 *(A.f.)*, *Blastomyces dermatitidis* SLH14081 *(B.d.)*, *Candida albicans* WO-1 (*C.a.*), *Coccidioides immitis* RS (*C.i.*), *Colletotrichum graminicola* M1.001 (*C.g.*), *Fusarium graminearum* PH-1 (*F.g.*), *Fusarium oxysporum* (*F.o.*), *Histoplasma capsulatum* NAm1 *(H.c.*), *Magnaporthe oryzae* 70-15 (*M.o.*), *Paracoccidioides brasiliensis* Pb03 (*P.b.*), *Saccharomyces cerevisiae* (*S.c.*), *Talaromyces marneffei* ATCC 18224 (*T.m.*), *Ustilago maydis* (*U.m.*), *Zymoseptoria ardabiliae* STIR04_1.1.1 *(Z.a.*), *Zymoseptoria brevis* ZBREZB163 *(Z.b.*), *Zymoseptoria pseudotritici* STIR04_2.2.1 (*Z.p.*), *Zymoseptoria tritici* IPO323 (*Z.t.*) and *Homo sapiens* (*H.s.*) as outgroup. **(B)** Schematic representation of the multiple sequence alignment underlying the phylogenetic analysis mentioned using MUSCLE within the Geneious program. Identical amino acids are highlighted in black, conserved amino acids in dark gray and similar amino acids in light gray. **(C)** Gene structure of *ZtPTF1* with conserved functional domain Ndt80_PhoG predicted by InterProScan. Sequence logo indicates the most conserved domain region, containing nuclear localization signal (NLS) predicted by cNLS Mapper.

This observation leads to the conclusion that the gene inactivation of *ZtPTF1* results presumably in the lethal phenotype. Interestingly, to date neither of the gene inactivations leading to a lethal phenotype of *Z. tritici* has been described in the literature, but such genes could be of great interest as potential fungicide targets.

As far as the target gene was predicted to encode a transcription factor, it was further of interest to verify whether the corresponding gene product harbors a nuclear localization which would be expected due to its putative role in transcriptional regulation of other genes. To this end an *eGFP*-fusion construct was generated, containing a complete ORF of the *ZtPTF1* gene with the strong constitutive promoter *EFA1* derived from *Magnaporthe oryzae* and fused c-terminally with *eGFP*. The generated construct was ectopically integrated into genome the recipient wildtype strain IPO323 in order to express ZtPtf1p-eGFP.

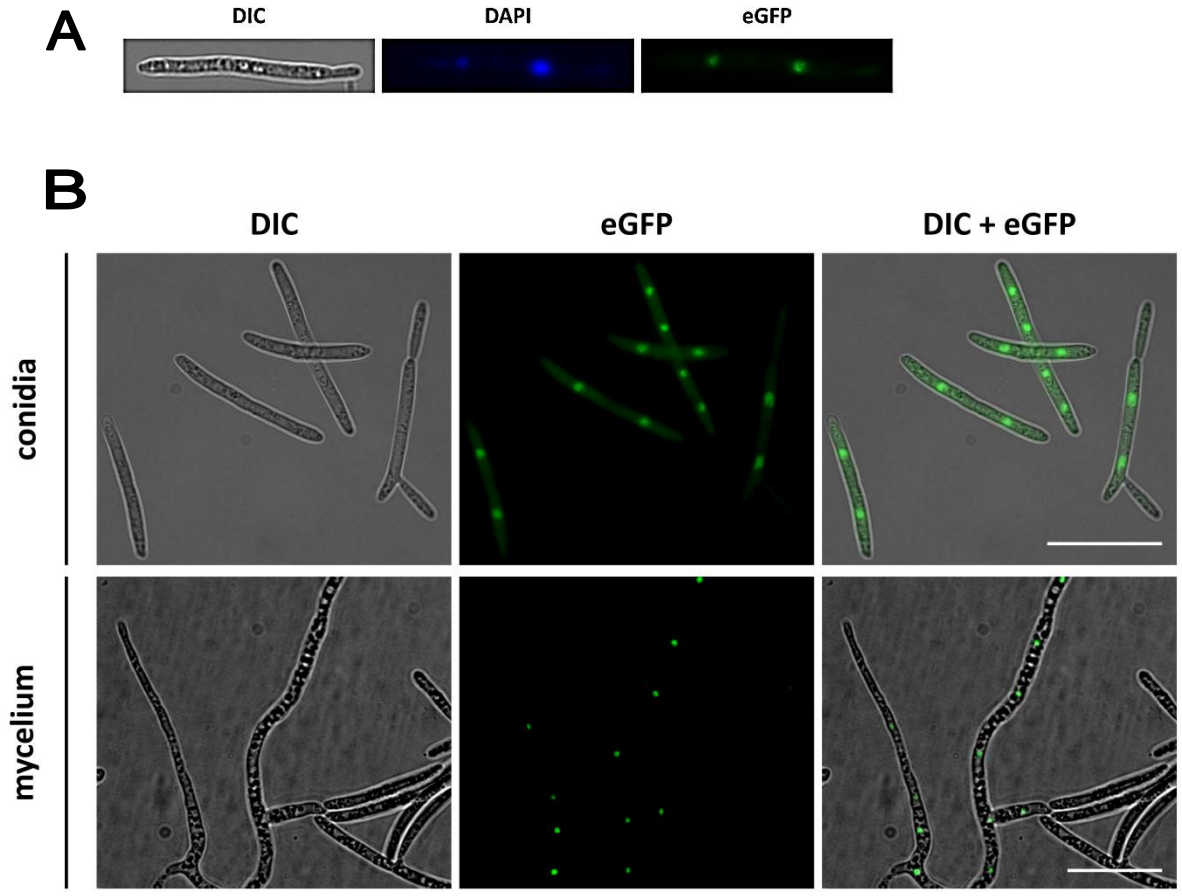

Figure 41: Nuclear localization of ZtPtf1p-eGFP. (A) *eGFP*-fused gene product was found to colocalize with the nuclear stain DAPI. **(B)** ZtPtf1p-eGFP is localized in the nucleus independent of cellular morphology. For examination of protein localization in yeast-like conidia, the strain expressing the ZtPtf1p-eGFP fusion protein driven by the constitutive *EFA1* promoter from *M. oryzae* was grown on YEG solid medium at 18 °C. For examination of expression and localization of ZtPtf1p-eGFP in mature hyphae, the incubation was performed on the N-deprivation medium covered with cellophane for 3 days at 18 °C prior imaging. DIC: differential interference contrast; eGFP: enhanced green fluorescent protein. Bars indicate 20 µm.

Transformants growing on YEG solid medium were examined using fluorescence microscopy, revealing that ZtPtf1p-eGFP expressed in the yeast-like pycnidiospores is localized to the nucleus, showing a clear and severe fluorescence signals in the conidial cell nuclei (Figure 41A,B). This result was further confirmed by an additional treatment with DAPI (Hoechst 33345), showing that the *eGFP*-fused gene product was found to colocalize with the nuclear stain (Figure 41A). Similarly, in the mature hyphae which were formed upon incubation of conidia on switch inducing medium the nuclear localization of ZtPtf1p-eGFP retained (Figure 41B).

3.11 *In silico* analysis of predictive binding sites of ZtPtf1p and deduction of potential function

Recently, several studies exploiting ChIP-on-chip technology have been used to investigate the biological role of Ndt80p in *C. albicans* and *S.* cereviseae. The *S. cerevisiae* Ndt80p has been described as global regulator of meiosis by acting as a transcription factor which selectively binds to a DNA consensus sequence known as the middle sporulation element (MSE). In doing so, Ndt80p activates expression of genes in the middle stages of meiosis (Lamoureux *et al.*, 2006). Previous statistical and mutational analyses revealed for the MSE a 9-bp consensus sequence corresponding to 5'-gNCRCAAAY-3' (where lowercase letters indicate semiconserved residues, R indicates a purine, N indicates any nucleotide, and Y indicates either a thymine or a cytosine) (Lamoureux *et al.*, 2006, Sellam *et al.*, 2009) (Figure 42B). Using this information, a *de novo* prediction of putative Ndt80p-bound promoters based on *in silico* motif analysis was performed to evaluate potential functions of ZtPtf1p in regulation of cellular biological processes. To assess the occurrence of the core MSE consensus in all Ndt80p targets, we interrogated the whole-genome sequence of *Z. tritici* provided by JGI and found 1400 potential binding sites containing Ndt80p binding consensus motif sequence (Figure 42A). From these, 81 predicted motifs were found to be located within the predicted promoters (1500 bp upstream of the predicted ATG-codon) of JGI annotated genes (Figure 42C) spread predominantly across the core chromosomes, with most of them localizing on chromosome 1. Subsequent enrichment analysis exploiting REVIGO revealed sets of significantly enriched genes implicated among others in such biological processes like amino acids metabolism, cellular response to glucose starvation and signal transduction pathways (Figure 42D).

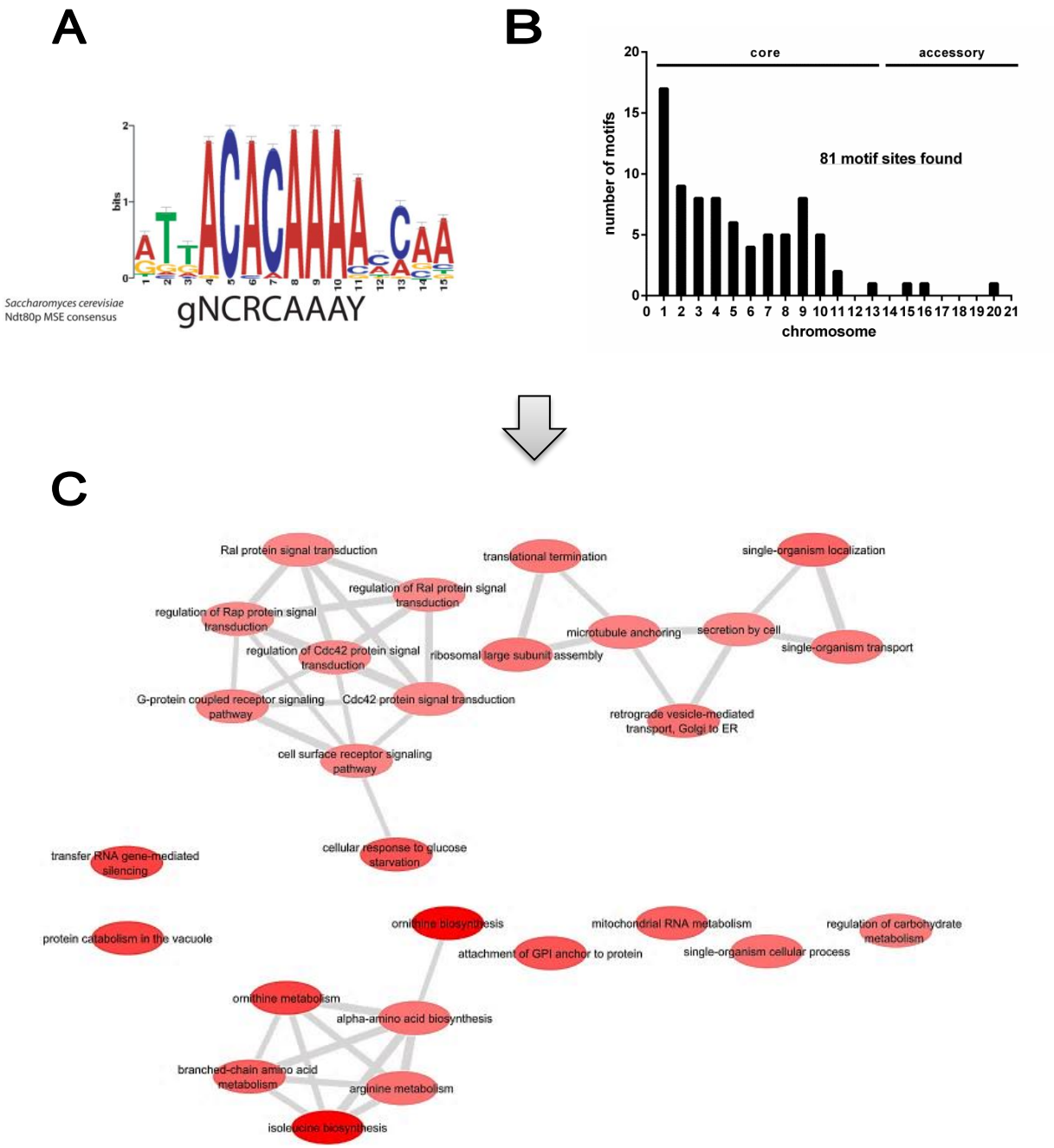

Figure 42: ***In silico*** **analysis of binding sites and enrichment analysis of genes potentially regulated by ZtPtf1p. A)** MSE consensus binding site previously determined for *S. cerevisiae* and *Candida albicans* (adapted from Sellam *et al.*, 2009). Lowercase letters indicate semiconserved residues, R indicates a purine, N indicates any nucleotide, and Y indicates either a thymine or a cytosine.**B)** Chromosomal mapping of MSE consensus binding sites (Ndt80p binding consensus motif) against entire JGI genome sequence from *Z. tritici*. Identification of Ndt80p binding consensus motifs was performed under constraint of their location within the predicted promoters (1500 bp upstream of the predicted ATG-codon) of JGI annotated genes. **C)** Interactive graph of biological process predicted for putative *ZtPTF1*-regulated genes. The interactive network was generated by REVIGO (http://revigo.irb.hr) and visualized using Cytoscape platform v3.5 (Shannon *et al.*, 2003). The size and red colour density and intensity of the circles are directly proportional to the number of genes associated with the specific GO terms.

In particular, one gene encoding a predicted Cdc42 activating protein (*Zt73435*) was apparent, suggesting to interact with *KSS1* and other signalling pathways that modulate diverse cellular functions in *S. cerevisiae* and *C. albicans*, including yeast cell polarization and filamentous (invasive) growth (Brand *et al.*, 2014, Bardwell *et al.*, 1998). Furthermore, among the genes with potential implication in morphogenesis were genes encoding gamma-tubulin (*Zt107760*), exocyst complex component (*Zt85776*), lysophospholipase (*Zt110012*) and endoglucanase (*Zt46444*). Additionally, the presence of genes encoding G-protein alpha subunit and one predicted protein kinase provides a further link for *ZtPTF1* to signaling and regulative cellular mechanisms by influencing transcription of diverse signaling components. Moreover, several genes encoding MFS transporters have been enriched, suggesting that *ZtPTF1*, along with its involvement in nutrient status maintenance, could also be involved in cellular detoxification reactions.

4. Discussion

The ascomycete *Zymoseptoria tritici* is a causal agent of wheat blotch disease, representing one of the most economically damaging and devastating diseases on wheat plants. Understanding molecular mechanisms that regulate pathogenicity related processes of the fungus and govern the plant-pathogen interactions is of primary importance to combat STB (*Septoria* blotch disease). In order to elucidate gene networks and to decipher molecular processes that determine the pathogenic development of the fungus, it is crucial to identify genes that control the disease-causing ability (Mehrabi *et al.*, 2006, Kramer *et al.*, 2009). By uncovering the molecular determinants and thus understanding which pathways, proteins and genes are involved in the pathogenesis, we can finally unveil the potential targets in the fungus for chemical control (fungicides or antifungal drugs) or use genetically modified host plant genotypes by modifying of targets in the host plant, thereby reducing its susceptibility to the pathogen (Baldwin *et al.*, 2006). In this thesis, a high-throughput forward genetic screen based on *Agrobacterium tumefaciens*-mediated transformation (ATMT)-mediated insertional mutagenesis was developed, with the aim to identify mutant strains of *Z. tritici* that are blocked in the dimorphic transition. For *Z. tritici*, dimorphic switch is an essential prerequisite for initiation of its pathogenic development. Hence, the crucial role of dimorphism in the establishment of the disease has been already suggested and validated for *Z. tritici*, considering e.g. the switch-deficient mutants *ΔZthog1* and *ΔZtAlg2* previously characterized (Mehrabi *et al.*, 2006, Motteram *et al.*, 2011). Being locked in the yeast-like nonpathogenic stadium and thus preventing the fungus to penetrate the host plant via natural openings like stomata with the subsequent colonization of plant tissue, could give us an alternative direction for the screening and development of novel protective fungicides on the non-fungitoxic basis. Thus, preventing the fungus from switching between two growth phases could be one of the successful strategies to meet the high demand for protective and fungistatic approaches to combat the STB (Mehrabi *et al.*, 2006, Nadal *et al.*, 2008).

4.1 Forward genetics using ATMT reveals a plethora of dimorphic switch deficient mutants confirming its suitability for investigation of this process

The main goal in the creation of the insertion strain library was to identify dimorphic switch mutants that have not been previously identified by means of reverse genetics approach, which in turn aims to inactivate the targeted genes first and then screen for the resulting phenotypes of the generated mutants. In this regard, the forward genetics approach bypasses

the bottleneck of reverse genetics, allowing precisely in a high-through-put manner to screen for the desired phenotype of the generated mutants. The forward genetic screen (random mutagenesis) has proven a very useful and efficient method, especially considering the ATMT approach, allowing in a relatively short time to generate a substantial library of random insertional mutants (Michielse *et al.*, 2005). ATMT-based approaches such as random insertional mutagenesis within forward genetics and targeted gene inactivation/disruption methods representing a reverse genetics approach have become important tools in post-genomic era of fungal biology and are widely used for gene functional analysis in terms of investigation of the plant-pathogen interactions and pathogenicity relevant processes (Weld *et al.*, 2006). Previously published reports clearly demonstrate that this approach is advantageous over conventional transformation methods like $CaCl_2$/PEG-mediated protoplast transformation or lithium acetate-mediated transformation regarding labor to generate strains. This also concerns the versatility in choosing which starting material to transform, higher transformation efficiencies, as well as the nature of the insertion patterns (Flowers and Vaillancourt, 2005, Betts *et al.*, 2007, Bhadauria *et al.*, 2009, Islam *et al.*, 2012). Generally, the ultimate objective of T-DNA insertional mutagenesis is to isolate the sequence flanking T-DNA and to explain the relationship between the insertional locus and observed mutation phenotype. The creation of random mutagenesis library by means of ATMT was already performed in different studies and was applied to various fungal species, like *Fusarium graminearum*, *Magnaporthe oryzae*, *Botrytis cinerea*, *Aspergillus nidulans*, *Nectria haematococca*, as well as *Zymoseptoria tritici*. In the current study, we presented a random mutagenesis approach applied to *Z. tritici* as an initial core procedure within the described screening pipeline aiming to identify strains defective in dimorphic switch ability. Conform to studies provided by other research groups, we found ATMT to be a very robust and amenable transformation method concerning its suitability for insertional random mutagenesis program, offering a high rate of transformation. This suitability is primarily linked to the observed insertion patterns of generated ATMT mutants, which resulted in mostly single insertions. The varied banding pattern (hybridization signal pattern) of T-DNA insertions and their associated flanking DNA in Southern Blot analysis suggests a random mode of genomic integration. However to validate the suggestion concerning the statistical significance of the observed pattern, a more precise and extensive study of the integration distribution should be undertaken, considering a larger population of generated random mutants. Previous studies aiming to examine conditional factors with impact on fungal transformation revealed, that the efficiency of ATMT increases with longer co-cultivation times (*A. tumefaciens* cells and

fungal conidia), but can at the same time result in the increased tendency for the T-DNA to integrate in multiple sites in the genome concurrently (Abuodeh *et al.*, 2000, Mullins *et al.*, 2001, Rho *et al.*, 2001). According to our results, the cocultivation of *Z. tritici* conidia with *A.t.*-cells at 28 °C for 48 hours resulted in a quite acceptable transformation rate, and the indicated percentage of multiple integrations makes the experimental setup described here an efficient approach within the random mutagenesis program. Following the Southern Blot assessment revealed that nearly 70% of the obtained transformants contained a single T-DNA insertion copy, which is consistent with the results that have been observed in *F. oxysporum, B. bassiana* and *Leptosphaeria maculans* (Blaise *et al.*, 2007, Leclerque *et al.*, 2004, Mullins *et al.*, 2001).

Both via the *in vivo* high throughput screening program based on the cultivation of the random mutants on switch inducing N-deprivation medium to investigate their dimorphic switch ability, and infection assays on whole plants, we have identified 11 random mutant strains out of 10000 generated transformants with impaired switch-ability. At the same time, it allowed us to validate the hypothesis, that the sustained ability to perform the dimorphic switch is essential for the establishment of full pathogenicity for *Z. tritici*, since the random mutants obtained failed to infect the host plants.

4.2 Identification of T-DNA disrupted gene loci and approvement using reverse genetics for the selected random mutants

Using genome walking approach, as previously described by Zhang and Gurr, 2000, the disrupted gene loci could be identified by means of alignment sequence analysis between the genomic sequence obtained and the known T-DNA sequence. Recovery of sequences flanking T-DNA insertions from 11 mutant strains revealed potential new genes according to JGI annotation and BLAST analysis (Table 4, p.75), suggested to be important for dimorphic transition. All of these random mutant strains were affected not only in the ability to perform the morphogenetic switch, but were also drastically impaired in virulence (data not shown), indicating that the screening pipeline established was also suitable in effectively identifying of pathogenicity mutants. As already mentioned earlier, this is not surprising, since the ability to complete the yeast-to-hyphal conversion is *a priori* essential for the formation of the invasive hyphae and as a consequence for the penetration through the stomata openings, followed by colonization of the plant tissue. Despite the observation that some of the random mutants obtained harbored multiple sites of T-DNA insertion (3 out of 11), the gene loci recovered by genome walking could be assigned to functionally annotated genes by exploiting the BLASTp

analysis. Interestingly, some of them are predicted to encode proteins belonging to protein families previously shown to be implicated in pathogenicity related processes in other fungal organisms. Multiple scenarios and possible outcomes regarding the potential roles of the identified genes for dimorphic switch are discussed below:

For instance, in random mutant *myco#3*, the T-DNA integration occurred in ORF of the gene predicted to encode protein of *LETM1* family. *LETM1* domain (leucine–zipper–EF hand-containing transmembrane region) containing proteins represent mitochondrial proteins conserved in all lower eukaryotes, animals, and plants (Nowikovsky *et al.*, 2004). The role of homologs belonging to this family has been previously investigated. For instance, *Saccharomyces cerevisiae* encodes two *LETM1* orthologues, YOL027c and YPR125w, both of which were previously shown to be implicated in in the formation of an active K^+/H^+ exchanger (KHE) system. Defects in this system are responsible for the increased matrix K^+ content and induce autophagic decay of the organelles (Waldherr *et al.*, 1993, Dimmer *et al.*, 2002, Frazier *et al.*, 2006). Intriguing in this context remains the link to dimorphism, when considering the corresponding phenotype of *myco#3* mutant. One possible scenario would be a potential modulation through the Rim101 pathway, previously shown to have novel functional roles for membrane potential maintenance, intracellular pH and potassium homeostasis in *S. cerevisiae* (Mira *et al.*, 2009). Rim101p in turn was shown to be activated by proteolytic cleavage in response to alkaline stress or high extracellular concentrations of KCl (Bahn *et al.*, 2013). Moreover, the involvement of Rim101 system in regulating dimorphic transition in *C. albicans* was previously evidenced, since mutants defective in components of this system were unable to perform dimorphic switch upon synthetic inducing conditions (Nobile *et al.*, 2008).

Identification of T-DNA insertion in *myco#26* mutant revealed two potential genes affected, both of which are suggested to be responsible for the observed phenotype of the mutant, since the integration site is located within promoter regions of both genes. For the first gene, no functionally characterized homologs from other organisms were found when performing the BLASTp analysis. However, the second one was found to encode a protein belonging to RING zinc finger protein family, indicating its role as a transcription factor. Generally, zinc finger proteins can bind to DNA, RNA, other proteins, or lipids as a modular domain in combination with other conserved structures (Ravasi *et al.*, 2003). Due to diversity in interaction possibilities, different members of this protein family may influence diverse cellular processes, including transcriptional activation, translational control, regulation of protein turn-over and mRNA-stabilization and processing (Ravasi *et al.*, 2003). For instance,

RING-14 proteins (Really Interesting New Genes) were shown to play various roles in signal transduction and cellular development processes. They bind to the β subunit of the G-protein in *S. cerevisiae* and inhibit the *FUS3* mediated pheromone signal transduction pathway (Secco *et al.*, 2012). The Fus3 mitogen-activated protein kinase (MAPK) cascade in turn was previously shown to modulate the activity of the transcription factor Ste12p, whose implication in mating and filamentous growth has been elucidated in different fungi including *B. cinerea*, *N. crassa* and *Zymoseptoria tritici* (Schamber *et al.*, 2010, Bobrowicz *et al.*, 2005, Kramer *et al.*, 2009). Therefore, it is likely to conclude that similar mechanisms may exist in *Z. tritici* providing a putative explanation or being causative for the phenotype of *myco#26*.

Meanwhile, in random mutant *myco#76*, the T-DNA insertion was identified in the promoter region of the gene encoding a hypothetical protein harbouring *DUF* domain. We conclude therefore, that this gene might be implicated in the dimorphic switch related processes. Since no functional homologs were found in other organisms, it is tempting to functionally characterize this gene by reverse genetics approach (targeted inactivation).

One further dimorphic switch deficient mutant assigned *myco#77* was found to be disrupted either in gene with no functional annotation or gene predicted to encode copper (Cu) homeostasis protein CutC. Besides the predicted implication in maintenance of copper homeostasis, the function of the homologous proteins in fungal organisms has not been elucidated. Generally, roles of copper for pathogenesis and development in fungal organisms are poorly characterized. However, in spite of its biological significance for general physiology as an essential cofactor for various proteins participating in diverse metabolic pathways, copper could have functions related, among others, to dimorphic switch relevant processes. For instance, the activities of such proteins like superoxide dismutase and cytochrome c oxidase depend on Cu availability. In addition, copper plays a crucial role for melanin biogenesis and iron uptake through Cu-dependent ferroxidase activity (Ding *et al.*, 2011, Hordyjewska *et al.*, 2014, Sun *et al.*, 2014).

In case of *myco#100*, a Patatin/Phospholipase A2-related protein encoding gene was affected by T-DNA disruption. The T-DNA insertion was located in the ORF of the gene. Generally, phospholipases A2 (PLA2s) belongs to a superfamily of enzymes catalyzing the hydrolysis of the sn-2 fatty acids of membrane phospholipids. These enzymes are suggested to exert multiple functions in maintaining the membrane phospholipid homeostasis and for production of a variety of lipid mediators, which in turn act as second-messenger in diverse cellular signalling events. Comparison with publicly available data from other fungal species revealed a potential role for this gene in morphogenesis as well as in pathogenicity associated

processes. For instance, in *Sporothrix shenkii* a link between G-protein mediated signalling and PLA2 has been evidenced. The heterotrimeric G-proteins seem to interact with the cytosolic phospholipase A2 (cPLA2), participating in the control of dimorphic switch (Valentin-Berrios *et al.*, 2009). Hence, using cPLA2 inhibitors, this enzyme was shown to affect stimulation of yeast-to-hyphal transition in *S. schenckii* by blocking re-entry into the yeast cell cycle.

Finally, in the random mutant *myco#5552* the integration site of T-DNA occurred in chromosome 2 between the annotated genes potentially encoding Δ12-fatty acid desaturase (FAD) and methionine synthase respectively. Whether the observed inability of the mutant strain to undergo dimorphic switch is due to inactivation of the first gene or the second one, or rather the result of additive inactivation effect, remains speculative and requires further analysis. Nevertheless, the role of the homologous or related genes in several pathogenic fungi has been elucidated, suggesting that both of them can be involved in morphological processes associated with the hyphal formation. For instance, in the opportunistic pathogen *Candida parapsilosis* the role of Ole1 fatty acid desaturase (stearoyl-CoA desaturase), which synthesizes oleic acid, has been previously examined. Mutants disrupted in the gene exhibited diverse physiological aberrations including severely impaired pseudohyphal formation, drastically reduced virulence and hypersensitivity to macrophages and various stress-inducing factors, such as salts, SDS, and H_2O_2 (Nguyen *et al.*, 2011). Similarly, a partial repression of *OLE1* in *C. albicans* prevented hyphal development in aerobic conditions and blocked the formation of chlamydospores (Krishnamurthy *et al.*, 2004). Methionine biosynthesis also appears crucial for dimorphism. For instance, methionine was previously shown to be implicated in promoting the dimorphic transition as it was observed that the presence of methionine induced the filamentous growth in *C. albicans* (Maidan *et al.*, 2005). Likewise, in *Pichia fermentans*, methionine has been demonstrated, probably after its conversion to methanol, to enable the shift from yeast-like to pseudohyphal morphology *in vitro* (Sanna *et al.*, 2012).

For *myco#20* the genomic T-DNA location was found on two different chromosomes, thus indicating an ectopic mode of integration. However, in both cases a relatively large distance to the nearest neighbor genes was apparent, casting doubt on their contribution to the resulting phenotype. It is also conceivable that multiple T-DNA insertions could have occurred, which were not detected by genome walking and Southern Blot analyses performed. Nevertheless, it is also known that eukaryotic promoters can span a wide range of DNA sequences, having several regulatory elements such as enhancers several kilo bases away from the transcription

start site (Cooper, 2000). Therefore, the impact of both genes, predicted to encode hypothetical proteins, on the resulting phenotype should be investigated. Additionally, the presence of further possible (ectopic) integrations of the *HPT* cassette would have to be determined in subsequent experiments, for example by using Southern Blot.

The putative role of the remaining four genes assigned as *MYCO1*, *MYCO4*, *MYCO5* and *MYCO56* is described below, as they were selected as target genes for a further detailed investigation, exploiting reverse genetics experiments. The choice of these target genes was dictated primarily by predicted single T-DNA insertions within the promoter or ORF of the corresponding JGI annotated genes. Furthermore, it was important to consider the relative proximity to neighbor genes, which shouldn't be affected by T-DNA insertion. Consequently, the four genes selected were successfully inactivated through replacement of ORF-portion of corresponding genes with *HPT* cassette conferring hygromycin resistance. All of the generated mutants exhibited the phenotype of corresponding random mutants. Genetic complementation by re-introduction of wildtype allele of the native gene into the corresponding gene disruption mutant recovers the phenotypic and physiological characteristics of the wildtype strain IPO323, thus validating the link between phenotypes observed and the genetic basis. Our further findings obtained from phylogenetic analysis and homology comparison indicate that the identified genes are common in diverse fungal groups as far as orthologues were found in fungal species harboring different infection strategies. Performing BLASTp analysis with deduced protein sequences indicated for *MYCO1*, *MYCO4* and *MYCO56* orthologues previously characterized in closely and distantly related fungal organisms, whereas in the case of *MYCO5* no functionally characterized orthologues were found. Below, results of the studies presented here are discussed, including phenotypes of the targeted disruption strains as well as possible functions of the four genes influencing virulence and dimorphic switch of *Z. tritici*. Finally, future objectives and perspectives are considered.

In summary, these results indicate that all genes obtained from random mutagenesis may represent potential virulence factors for *Z. tritici* and therefore attractive drug targets for disease prevention. All of these mutant strains were affected in their dimorphic switch ability and were found to be drastically impaired in virulence (data not shown). This is not surprising since the ability to complete the yeast-to-hyphal conversion is *a priori* essential for the formation of the invasive hyphae and as a consequence for the penetration through the stomata openings, followed by colonization of the plant tissue. Thus, these potential pathogenicity genes are expected to be validated for their functions by further reverse genetics experiments and phenotypic *in vitro* assays of generated mutant strain. Although, our initial

T-DNA insertion analysis has not identified some of the already characterized pathogenicity genes in *Z. tritici*, we attribute that to the small subset of mutants analyzed.

4.3 *MYCO1* encodes a component of *HOG1* signaling pathway, regulating morphological transition and physiological processes

As already mentioned, one of the target genes obtained from the genome walking analysis was designated *MYCO1*. Relying on BLASTp analysis the gene was found to encode Ssk1p, a previously characterized component of the *HOG1* pathway in several fungi, but not yet described in *Z. tritici*. Generally HOG1 pathway (for high-osmolarity glycerol) is a well-conserved signaling system in fungi, mediating a canonical cellular response upon osmotic stress, having at the same time numerous functions for the fungal physiology as was previously shown in diverse studies, indicating that the *HOG1* encoded MAPK may function in more than one pathway (Biswas *et al.*, 2007). Generally, mitogen-activated protein kinase (MAPK) Hog1p is responsible for the regulation of glycerol accumulation to maintain cellular turgor in response to external hyperosmotic condition. In *Saccharomyces cerevisiae*, external high osmolarity activates via two-component sensing system the downstream transcription factor Hog1p, which controls various aspects of osmoadaptation. Ssk1p in turn represents a homolog of bacterial two-component response regulators and a core component of the multistep phosphorelay mechanism (Sln1p-Ypd1p-Ssk1p) which activates in the unphosphorylated (active) form the downstream Ssk2 MAPK kinase kinase (Horie *et al.*, 2008). Within the kinase cascade, the MAP3Ks Ssk2 phosphorylates the MAP2K Pbs2, which in turn phosphorylates the MAP kinase Hog1p. Following this signal modulation concept, when Hog1p is activated (phosphorylated), it moves from the cytoplasm to the nucleus where it activates several transcription factors that regulate genetic and diverse metabolic programs, protecting the fungus from osmotic, oxidative, thermal, and ultraviolet stresses (Dexter *et al.*, 2015). Previously the *ZtHOG1* gene was functionally characterized in *Z. tritici* (Mehrabi, 2006). However, neither upstream nor downstream components of this pathway in *Z. tritici* have been yet elucidated, albeit the orthologues genes (for *S. cerevisiae SSK2*, *PBS2*, *YPD1* and *SLN1*) exist in the genome (data not shown). In this work the role of *Z. tritici* Ssk1p homolog with respect to dimorphism has been investigated.

Reverse genetics experiment performed in this thesis revealed that *MYCO1* (= *ZtSSK1*) deficient mutants exhibit a dramatic defect in filamentous growth on switch inducing media at 18 °C and fail to initiate the formation of germ tubes. As a consequence, the mutant strains lacking the *MYCO1* gene are non-pathogenic, consonant with a general view that a proper

yeast-to-hyphal transition is an essential prerequisite for plant invasion and tissue colonization. Furthermore, they display irregularly shaped and swollen conidia, resembling the phenotype of *ΔZthog1* mutants previously described by Mehrabi (2006). Hence, consonant with results previously demonstrated by Mehrabi *et al.*, we demonstrate and validate the central role of *ZtHOG1* pathway for dimorphic switch in *Z. tritici*. These findings emphasize conserved role of the HOG1 pathway in regulation of morphogenetic transition that has also been defined, among others, for such fungal organism as *A. fumigatus* and *C. albicans* (Du *et al.*, 2006, Xue *et al.*, 2004, Monge *et al.*, 2006). For most of these fungi mentioned, HOG1 pathway has also been demonstrated to be critical for pathogenicity. However, participation of HOG1 pathway in pathogenicity related process is not unambiguous and cannot be generalized to fungal species harboring different life styles and exhibiting different modes of infection strategies. While *HOG1* promotes dimorphic proliferation in *Z. tritici* and other fungi mentioned above, at the same time highlighting its role as virulence factor, it doesn't match for phytopathogenic fungi like *Magnaporthe oryzae*, *Colletotrichum lagenarium* or *Bipolaris oryzae*, which exhibit an appressorial mode of infection. Indeed, in these fungi, Hog1p is not considered as pathogenicity related factor, since the corresponding loss-of-function mutant strains are still pathogenic (Dixon *et al.*, 1999, Kojima *et al.*, 2004, Moriwaki *et al.*, 2006). This observation emphasizes, therefore, a unique function of Hog1p for fungi harboring dimorphic life-style and highlights its role as a genetic determinant for pathogenic development. Because SSK1p represents a core regulator of HOG1 pathway, we expected for *MYCO1* (in the following designated *ZtSSK1*) deficient mutant strains *ΔZthog1*-like phenotypic signatures. In fact, within all experiments conducted we noticed similar behaviour and phenotype resembling that of *ΔZthog1*. Interestingly, as for *ZtHOG1* deficient mutant, the *Z. tritici Δssk1* is able to perform dimorphic switch upon incubation at elevated temperature, indicating that other sensory mechanisms and signaling networks promoting transcription of dimorphic switch related genes are induced by this stress condition. However, the role and impact of temperature-induced genes for dimorphic switch in *Z. tritici* remains to be elucidated. Therefore, further deep studies employing, for instance, complementing transcriptome and proteome analyses would be crucial to examine the putative link between the temperature-induced stress response and morphogenetic transition. Other similarities concerning the phenotype of the mutants are coupled with the lack of melanization and increased susceptibility upon cell wall stress. The *ΔZtssk1* mutant strains displayed sensitivity to SDS treatment but not to the cell wall stress mediated by Congo Red application. Moreover, the mutant strains were found to be frequently lysed when treated with lysing

enzymes from *Trichoderma harzianum*. Hence, neither *ΔZtssk1* nor *ΔZthog1* were able to generate any viable protoplasts and formed numerous broken cell fragments indicative of cell autolysis. This observation is in agreement with results recently obtained from the study with the systemic dimorphic fungus *Taloromyces marneffei* (Boyce *et al.*, 2016). As for *Z. tritici ZtSSK1* disruptants, the *T. marneffei* mutant strains failed to maintain a wildtype growth on medium amended with SDS. The authors concluded a remodeled/altered cell wall and membrane composition of the mutant strain compared to wildtype (Boyce *et al.*, 2016), which could also explain the situation with *ΔZtssk1* and *ΔZthog1* mutant strains. This observation is also consistent with the role of HOG1 pathway in regulation of cell wall biosynthesis and integrity previously reported for *Candida albicans*. Thus, mutant strain lacking *CaHOG1* is highly susceptible to treatment of β-1,3-glucanases and is prevented to form chlamydospores (Eisman et *al.*, 2006). These findings indicate, therefore, that *ZtHOG1* and *ZtSSK1* may have a relationship with cell wall biogenesis in *Z. tritici*.

Furthermore, consistent with the conservation of HOG1-signaling pathway among diverse fungal groups we also confirmed the canonical involvement of *SSK1* in osmotic stress response. As expected the *Z. tritici ΔZtssk1* mutant is sensitive to osmotic stress/salt stress mediated by Sorbitol or NaCl, indicating that *ZtSSK1* is required for adaptation to high external osmolarity and a proper osmotic stress response. Previously, it was shown that genetic disruptions of the orthologues genes in *Aspergillus nidulans, Cryptococcus neoformans, Cochliobolus heterostrophus, Taloromyces marneffei* and *Candida albicans* result in sensitivity to osmotic stress (Bahn *et al.*, 2006, Izumitsu *et al.*, 2007, Hagiwara *et al.*, 2009, Boyce *et al.*, 2016, Chauhan *et al.*, 2003), albeit the sensitivity for *C. albicans* was less pronounced (Nagahashi *et al.*, 1998, Calera *et al.*, 2000). For *C. albicans*, the role of HOG1 pathway is primarily linked to regulation of processes related to adaptation to oxidative stress (Chauhan *et al.*, 2003). In fact, it was previously shown that inactivation of *CaSSK1* prevented the activation of CaHog1p in response to oxidative stress. At the same time, the wild-type levels of phosphorylated Hog1p could be restored in *ΔCassk1* after osmotic stress (Chauhan *et al.*, 2003). This stays in contrast to the observation in *S. cerevisiae* where inactivation of Sln1p-osmosensing branch (but also Sho1p-branch) disables signal transduction to Hog1p, suggesting molecular rewiring mechanisms implemented in *C. albicans* (Cheetham *et al.*, 2007). The implication of HOG1 pathway in oxidative stress response could be also confirmed for *Z. tritici*, since both mutant strains *ΔZtssk1* and *ΔZthog1* were impaired in growth when treated with H_2O_2 (4 mM). In addition, we assessed whether inactivation of *ZtSSK1* confers resistance to the dicarboximide and phenylpyrrole classes of

antifungals, such as fludioxonil and iprodione, as was previously stated for other fungi. The fungicidal activity of the phenylpyrrole fludioxonil is achieved by constitutive activation of the HOG1 MAPK pathway inducing the glycerol accumulation under hypoosmotic condition, which leads inevitably to cell death, although a detailed mechanism of this activation is still unknown. As expected, our results revealed that inactivation of the *Z. tritici* genes *SSK1* as well as *ZtHOG1*, as previously described by Mehrabi *et al.*, confers fludioxonil resistance.

Taken together, these findings point on the one hand to the conserved role of HOG1 pathway for versatile stress response among representatives of different fungal genera. We postulate that the core mechanisms of phosphorelay system may follow the accepted scheme of signal transduction as for other fungi. On the other hand, the outcome of RNA-Seq analysis of *ΔZthog1* mutant upon dimorphic switch condition conducted in this thesis provides a plethora of metabolic pathways and proteins participating in signaling, such as transcription factors, suggesting a complex cross-talk to other signaling pathways. The observed phenotypic signatures of the HOG1 signalling pathway-deficient mutants especially considering the differences and similarities stated, compared to published phenotypes, lead to the conclusion that some mechanisms of regulation are conserved, but some may have been diverged in the course of the evolutionary processes. In particular, it would be interesting to identify dimorphic switch related downstream factors modulated by ZtHog1p activity. Certainly, the implication of *HOG1* in regulation of common metabolic pathways required for normal viability of different fungi is anticipated. In fact, a common set of genes implicated in general stress response has been already validated by transcriptome studies from other fungi. In these terms, *HOG1* is postulated to be induced in response to different stress condition (known as environmental stress response, ESR), and modulate expression of core stress responsive genes previously described in *S. cerevisiae* and *Candida* sp. (Gasch, 2007, Roetzer *et al.*, 2008). On the other hand, the involvement of *HOG1* in morphological transition, albeit not in all fungi, implies a functional divergence of the MAPK as result of evolutionary adaptation and suggests, therefore, participation in the regulation of downstream regulators governing the yeast-to-hyphal transition, most of them yet unknown. Therefore identification and characterization of downstream factors of *ZtHOG1* pathway would extend our understanding of its impact on dimorphic switch related processes in *Z. tritici*. In this context, especially a genetic link to *SKN7* (the homologous gene was identified in *Z. tritici* genome) is intriguing and awaits detailed characterization, since in some dimorphic fungi the encoded transcription factor has already been shown to modulate a morphogenetic response upon different environmental triggers.

4.4 *MYCO4* encodes phosphoribosylglycinamide synthetase responsible for *de novo* purine biosynthesis with impact on dimorphic transition

An interesting phenotype was observed in case of the *myco#4* random mutant. The gene in which the corresponding mutant was disrupted was found to encode a bifunctional phosphoribosylglycinamide synthetase (glycinamide ribotide synthase/aminoimidazole ribotide synthase; indicated as GART*), which is known for the second and fifth catalyzing step of *de novo* purine biosynthesis in *Schizosaccharomyces pombe* (McKenzie *et al.*, 1987). *De novo* purine biosynthesis has been extensively studied in different organisms, including fungi, bacteria, plants and animals, particularly in much detail in baker's yeast *S. cerevisiae* and *Drosophila melanogaster* and has been reported to be highly conserved in evolution, even between prokaryotes and eukaryotes. This conservation relies in the first instance on the central role of purine biosynthesis for biogenesis of essential molecules being critical for proper cellular metabolism. For instance, these molecules include essential coenzymes NAD, NADP, FAD and CoA, the ubiquitous energy source ATP, the signaling molecule cAMP and finally AMP and GMP representing DNA/RNA precursors (Roberts *et al.*, 2003). Generally, in eukaryotic organisms, the *de novo* purine synthesis pathway requires 10 enzymatic reactions to synthesize the common purine precursor inosine monophosphate (IMP). IMP represents a branch point to produce either adenosine monophosphate (AMP) or guanosine monophosphate (GMP) (O'Donnell *et al.*, 2000).

Since our preliminary BLAST analysis indicated a high degree of conservation of purine biosynthetic enzymes in *Z. tritici* with those of distantly related *Schizosaccharomyces pombe* as well as closely related filamentous fungi such as *Neurospora crassa*, *Magnaporthe oryzae*, *Aspergillus nidulans* and *Fusarium graminearum*, it is highly conceivable that a similar pathway is present in *Z. tritici*.

Interestingly, the structural analysis of the deduced protein sequences revealed a diverged structure (and function) of the corresponding protein orthologs. The evidence for this is provided by comparison of deduced Myco4p with bifunctional homologs of other fungi including *S. cerevisiae* and the trifunctional mammalian homolog. Hence, InterProScan analysis revealed for *Z. tritici* and closely related fungi from *Mycosphaerellaceae* family only GARS domains responsible for conversion of 5-phospho-β-D-ribosylamine (PRA) to 5-phosphoribosylglycinamide (GAR), in contrast to other fungal representatives harbouring an additional AIRS domain (Figure S2). Meanwhile, the *Homo sapiens* homolog combines the functions of Ade5,7p, catalyzing the second and fifth steps of the *de novo* purine biosynthesis in analogy to fungal representatives, but owns additional domain responsible for the

conversion of 5-phosphoribosylglycinamide (GAR) to 5-phosphoribosyl-N-formylglycinamide (FGAR). This finding is intriguing since the monofunctional members are only common for bacteria and plants. Hence, the three steps mentioned are catalyzed by three enzymes in bacteria and plants, but two in fungi (Figure 43).

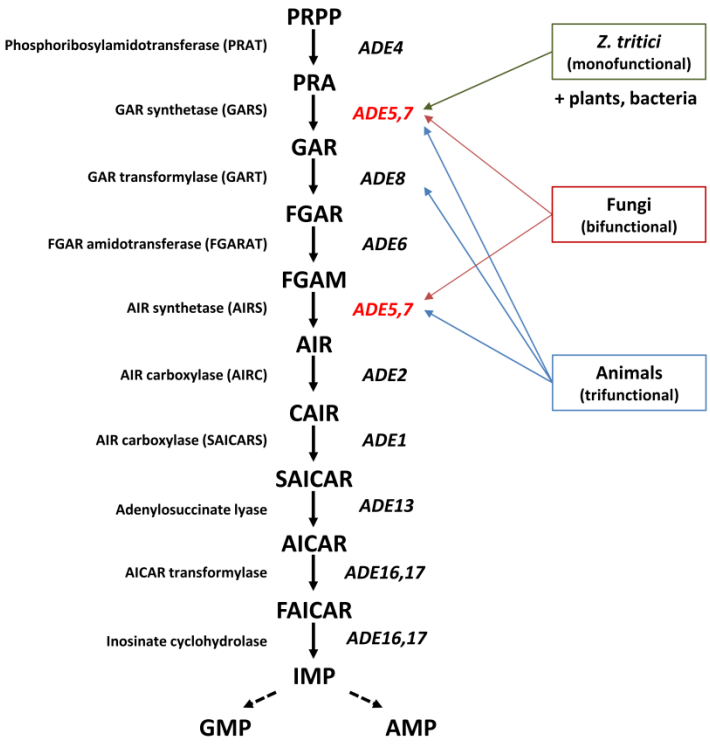

Figure 43: Schematic representation of the *de novo* purine biosynthesis in the yeast *Saccharomyces cerevisiae*. Abbreviations: PRPP: 5-phospho-ribosyl-1α-pyrophosphate, PRA: 5-phospho-β-D-ribosylamine, GAR: 5-phosphoribosylglycinamide, FGAR: 5'-phosphoribosyl-N-formyl glycinamide, FGAM: 5'-phosphoribosyl-N-formylglycinamidine, AIR: 5'-phosphoribosyl-5-aminoimidazole, CAIR: 5'-phosphoribosyl-5-aminoimidazole-4-carboxylate, SAICAR: 5'-phosphoribosyl-4-(N-succinocarboxamide)-5-aminoimidazole, AICAR: 5'-phosphoribosyl-4-carboxamide-5-aminoimidazole, FAICAR: 5'-phosphoribosyl-4-carboxamide-5-formamidoimidazole, IMP: inosine monophosphate, AMP: adenosine monophosphate, GMP: guanosine monophosphate. The *S. cerevisiae* gene *ADE5,7* (depicted in red) is homologous to *Z. tritici MYCO4*. In contrast to bifunctional yeast counterpart, the *Z. tritici* has only GARS activity (monofunctional). The animal counterpart is predicted to encode a bifunctional enzyme complex, exhibiting GARS, AIRS and FGAR activities. The trifunctional human GART* is highlighted by blue box.

The reason for the predominant monofunctional variant of the GART* protein in *Zymoseptoria* clade is currently unknown and the biological role for this phenomenon remains to be elucidated. However, this structural/functional difference observed may result in differentially coordinated regulation of the three enzymatic activities (assigned to three

different enzymes in *Z. tritici*) with global impact on metabolic processes. The remaining two genes encoding AIRS (Protein ID: 74864) and GART (Protein ID: 73624) were found in *Z. tritici* genome.

The striking difference in conformational structure suggested between mammalian and fungal orthologs implies that Myco4p may be regarded as a potential therapeutic target for the development of novel antifungal drugs. In fact, because the human GART requires 10-formyl-tetrahydrofolate (THF) as a cofactor, the corresponding part of the trifunctional enzyme has been addressed as an anticancer target for THF analogues by inhibiting its activity (Kaye, 1998). This difference emphasizes the phylogenetic divergence of the fungal GART*s and their human counterparts. In light of the assumed structural difference, but at the same time retained functional conservation of the enzyme, the question remains, however, whether it is possible to identify inhibitors that are specific to the fungal GART*s.

Within this thesis, the *MYCO4* gene was functionally characterized and its essential role in biological processes has been validated. As expected, targeted gene inactivation and subsequent reintegration of the native intact gene copy demonstrated that disruption of *MYCO4* is responsible for the purine auxotrophy of the mutant strain. Interestingly, no obvious alterations regarding the morphological characteristics of the *Δmyco4* mutant colonies could be observed when compared to the wildtype, except for the drastically delayed (sparse) growth behavior on water agar and N-deprivation media, but at the same time the mutant strain exhibited a normal vegetative growth, biomass accumulation and conidiation rate on nutrient-rich medium. The morphology of conidia did not differ from that of the wildtype strain. Expectedly, a wildtype-like growth rate could be restored when incubating the *MYCO4* deficient mutants on MM, N-deprivation, as well as water agar media supplemented with adenine or hypoxanthine, even at minimal concentrations, indicating that the uptake and purine salvage pathway are operational in the mutant. Furthermore, the impaired purine biosynthesis of the *Δmyco4* mutant was found to result in evidently reduced virulence, a phenotype which is similar to the adenine auxotrophs of other phytopathogenic fungi, such as *Fusarium oxysporum* f. sp. *melonis* (Denisov, 2005) and *Magnaporthe oryzae* (Fernandez, 2013). Hence, in contrast to the wildtype, the mutant strain *Δmyco4* was found on average to be drastically attenuated in virulence against the host wheat plant cv. Riband and caused in worst-case scenario only small necrotic lesions at 21 dpi, but no further disease symptoms developed. This observation is consistent with the general view that adenine auxotrophs are expected to exhibit a short phenotypic or physiological lag due to the immediate requirement of adenine/guanine during DNA synthesis, which may result in reduced disease symptoms

(Korn *et al.*, 2015). Since purine *de novo* biosynthesis is important for a wide spectrum of biological processes, it is conceivable that defect in this pathway affects different cellular functions, resulting in pleiotropic effects including pathogenicity (as a secondary effect). Consistent with this view, the conducted germination assay indicated a decreased tendency for *Δmyco4* mutants to form germination tubes upon nutrient deprivation mimicked by incubation on water agar. In fact, only 22% of exposed spores of the mutant were able to proceed germination under dimorphic switch inducing conditions, whereas in the case of wildtype 80% of germinating spores under the same condition were observed (Figure S7). Furthermore, we speculate that the attenuated virulence of the *Δmyco4* mutant could be related to the metabolic constraints encountered in the host, which reduces its fitness. In the previous study, purine biosynthesis in the rice pathogenic fungus *Magnaporthe oryzae* was investigated, demonstrating an absolute dependency and essential role of fungal purine metabolism on rice blast disease establishment and progression (Fernandez *et al.*, 2013). Thus, deletion of the gene *MoADE1*, encoding SAICAR synthetase, resulted in the abolished biotrophic *in planta* growth of the fungus. Interestingly the pre-penetration, as well as early-penetration phase, were unaffected in the deletion mutant since *de novo* purine biosynthesis was shown to be not required for appressorium formation or rice cuticle penetration. However further *in planta* growth upon morphogenetic conversion to bulbous invasive hyphae was aborted, indicating that purine metabolism is essential for establishing biotrophic growth in rice cells (Fernandez *et al.*, 2013). Whether the mentioned pathogenic development and hyphal branching *in planta*, as for *M. oryzae*, is affected by Myco4p inactivation in *Z. tritici* remains unclear and should be addressed in further experiments by cytological and histological investigations.

Collectively, our observations lead to the conclusion that the impaired purine (adenine) biosynthesis in *MYCO4* deficient mutant strain affects cellular functions associated with growth and development, and appears to be causative for abolished pathogenicity. Previously, the role of *de novo* purine biosynthesis has also been addressed in dimorphic systemic fungi like *C. albicans* and *C. neoformans*, showing that disruption of genes involved in this pathway results in attenuated or complete loss of virulence in mammalian models and general growth defects (Jiang *et al.*, 2010, Morrow *et al.*, 2012). Consequently, this implies that Myco4p represents a virulence factor necessary for disease establishment. Questionable is, however, the ability of mutant strain to use the exogenous purine nucleotides *in planta*, since our results indicate that growth of the mutant strain is restored by supplementing the synthetic media with exogenous adenine/hypoxanthine sources even at lower concentrations compared to those that are present in the plant apoplast. Therefore, further investigations should be

carried out in order to analyze the ability/inability for the exogenous purine uptake *in planta*. The approach for this investigation could include qRT-PCR analysis of genes *in planta*, encoding orthologous nucleotide/purine transporters previously examined in *M. oryzae*.

Additionally, the attributed traits concerning the auxotrophy of the mutant strain open up a number of further approaches which could be advantageous for the utilization within biotechnological and molecular biological applications. Complementation of the *MYCO4*-disruption strain with the intact copies of *MYCO4* suggests that there could be a potential use of this gene as new selectable auxotrophic marker for genetic transformation as previously shown for *Giberella* zeae (*Fusarium graminearum*) (Kim *et al.*, 2007). In general, genes responsible for adenine or arginine auxotrophic phenotype in other fungi have been broadly used as selection markers for transformation systems in *Pichia pastoris, Aspergillus oryzae* and *Saccharomyces cerevisiae* (Jin *et al.*, 2004, Cereghino *et al.*, 2001). The usage of *MYCO4* in a similar way would undoubtedly extend the arsenal of selection markers used today for transformation and functional genomics of *Z. tritici*. Hence, the generated *Δmyco4* strain, which appears isogenic to the wildtype strain IPO323 apart from inactivated *MYCO4* gene, could be used as a recipient strain for a new fungal transformation system using *MYCO4* as a selection marker. Moreover, relying on the idea to exploit *MYCO4* as a potential selection marker, there would be at least one more beneficial feature over the conventional use of fungicide resistance based markers. Apart from the cost efficiency, the purine deprivation may result in enhanced transformation frequency. Thus, previous studies revealed that purine synthesis inhibitors cause supersensitivity to *A. tumefaciens* transformation in three plant species (Roberts *et al.*, 2003). Additionally, adenine auxotrophs of yeast were found to be supersensitive to *A. tumefaciens*-mediated transformation and the more severe effect was achieved when yeast cells were deprived of adenine during cocultivation with *Agrobacterium* cells (Roberts *et al.*, 2003). These findings emphasize the purine biosynthesis as a key determinant of transformation efficiency. Therefore, it will be of particular interest to determine whether purine biosynthesis deficient mutant as recipient strain, along with the usage of purine synthesis inhibitors enhance the production of stable transformants, especially considering manipulation of genes being recalcitrant to efficient transformation of fungus. With this approach we could circumvent the limitations inherent in using genetic manipulations of the wildtype with the aim to improve transformation efficiency and to the utility of *A. tumefaciens* in genetic engineering applications.

4.5 *MYCO5* encodes a novel virulence factor involved in regulation of dimorphism and diverse physiological processes

In case of the random mutant *myco#5*, the single T-DNA insertion occurred in the promoter region of predicted ORF of the annotated gene *Zt66947*, which encodes a protein with no significant homology to any functionally characterized proteins in other fungal species. Targeted gene inactivation, as well as subsequent genetic complementation, confirmed the link between the phenotype observed with the single genetic locus predicted. The hypothetical homologs of the deduced protein were found in closely related species like *Z. brevis* and *Z. arabidae* as well as in distantly related phytopathogenic filamentous fungi harboring appressorial and non-appressorial modes of infection. However, the similarity observed was restricted to the protein region comprising *mod_r* functional domain. The presence of predicted *mod_r* domain (E-value 1.28e-08) in Myco5p, also observed in the previously characterized yeast protein Vps37p, suggests its function in the assembly of ESCRT-I complex, as a putative constituent of the Endosomal Sorting Complexes Required for Transport machinery. Moreover, this suggestion is also supported by results obtained from 3D modeling analysis of Myco5p using Phyre2, by delivering Vps37p as one of the best-matched results, showing a significant confidence for structural similarity. However, when considering the sequence of the yeast protein Vps37p in alignment analysis, no common features with the query protein sequence of Myco5p were apparent, resulting in 17% of pairwise similarity (data not shown).

In order to investigate the potential function of Myco5p in cellular processes, we performed a functional characterization of the gene by targeted deletion. Phenotypic characterization of the generated mutant strain *Δmyco5* revealed pleiotropic effects caused by the gene inactivation. In contrast to other target genes involved in dimorphism, the inactivation of *MYCO5* resulted in mutants exhibiting a pronounced hyperfilamentation phenotype even when cultivation of the mutants was performed under nutrient rich condition, which normally supports a prevalent yeast-like growth of the wildtype. The increased formation of hyphal cells independent of growth conditions or stress suggests that Myco5p negatively regulates the mycelium formation. Furthermore, the effects caused by gene inactivation included an attenuated glucose utilization (uptake) in submers culture, an increased sensitivity to elevated temperatures, a susceptibility to cell wall perturbing agents, increased sensitivity to transient metals like copper and zinc and completely abolished pathogenicity. Most of these mutant-specific attributes were supported by RNA-Seq performed within this thesis. Hence, transcriptome analysis of *Δmyco5* upon nitrogen deprivation revealed several glucose

transporters encoding genes with drastically decreased transcript abundance compared to wildtype, providing a convincing explanation for attenuated glucose uptake of the mutant strain. However, a more detailed observation revealed, that fluctuations in yeast/mycelium ratio of growing *Δmyco5* cultures significantly determined the resulting metabolization velocity of external glucose in the medium. Thus, at low temperature (18 °C) the mutant strain was found to grow as a mixed culture, accumulating a significant percentage of yeast-like conidia, albeit still forming an enhanced and prevailing amount of mycelium in comparison to wildtype strain IPO323. Under this condition, the glucose metabolization was found to occur at a similar rate as for the wildtype. However, with gradually raised temperature (28 °C) promoting increased hyphal growth of the *Δmyco5* culture, the situation changed towards drastically reduced glucose consumption of the mutant strain compared to wildtype. Relying on these results it is likely to conclude that the reduced utilization of exogenous glucose observed is likely linked to either physiological or morphological features of the *MYCO5* loss-of-function mutant coinciding with its filamentous growth mode and enhanced thermosensitivity observed, rather than exerted at the level of uptake catalyzed by diverse transporter mechanisms. Nevertheless, at this point it is important to emphasize that these findings do not invalidate the concept of reduced glucose uptake in *Δmyco5* mutant strain, giving an explanation for its attenuated growth. Hence, the data do not exclude the possibility that the predicted transporters might be regulated conditionally or their expression might be coupled with physiological/morphological status of conidia, enabling glucose transport under specific condition. However to validate this hypothesis further investigations should be carried out by exploiting, for instance, gene expression experiments using qRT-PCR, considering different temperatures and time points of cultivation. A more direct approach to measuring cellular metabolic activity and glucose transport could include glucose uptake experiments exploiting, for instance, glucose analoga in a colorimetric assay.

Moreover, gene expression analysis by qRT-PCR revealed that *MYCO5* is differentially expressed *in planta*, displaying at 4 dpi and 14 dpi decreased transcript abundance. This observation emphasizes its role in the early biotrophic phase (4 dpi) and early necrotrophic phase (14 dpi). The underlying symptomless biotrophic phase is known to be associated with the hyphal growth of the fungus, which begins with the morphological yeast-to-hyphal transition on the plant leaf followed by penetration and subsequent colonization process *in planta* (Mehrabi 2006, Orton *et al.*, 2011). Referring to the pathogenicity relevant morphology and the described phenotype of *MYCO5* defective mutant, we can therefore draw the hypothesis that *MYCO5* may encode a negative regulator of dimorphic transition

displaying differential expression *in planta*, also suggesting its requirement for plant penetration. Additionally, consonant with its role as a negative regulator of mycelium formation, *MYCO5* expression measured by qRT-PCR was found to be greater in conidia exhibiting yeast morphology (on YEG medium) and is decreased during hyphal cell induction (induced by N-deprivation) (data not shown).

In light of the predominantly filamentous growth form of the mutant, at least one question arises in this context: what are the factors blocking the pathogenic development of this mutant strain considering its ability to grow almost filamentously and to produce a high amount of mycelium representing an important prerequisite for successful penetration of the host plant. The answer to this question may be probably spread at the level of plant-pathogen-interaction and awaits a detailed histological *in planta* characterization of the mutant. Generally, mutant strains with reduced virulence are expected either to lack functions directly required for plant penetration or *in planta* growth or to be defective in suppressing host defense mechanisms (Korn *et al.*, 2015). The evidence for the first instance may be primarily linked to impaired polarization growth and prevented *in planta* branching in analogy to a characterized role of ZtFus3 MAP kinase (Mehrabi *et al.*, 2006). The explanation for the second instance may be referred to an insufficient ability of the *MYCO5* disruption mutant to evade host defense mechanisms (primarily associated with a hypersensitive reaction of plants which plays a prevailing role in *Zymoseptoria* pathosystem). The evidence for this is delivered by phenotypic assay indicating an increased susceptibility of the *Δmyco5* mutant to hydrogen peroxide on synthetic media. This suggestion is also supported by findings obtained from RNA-Seq analysis, assuming a potentially reduced ability of the mutant to withstand the plant defense mechanisms by detoxification of plant-born antimicrobial compounds such as glycosylated triterpenoids (saponins), steroids or steroidal alkaloids, as far as a vast majority of genes encoding MFS and MDR transporters previously shown to play a critical role in detoxification reaction displayed reduced expression level. The role of such transporters in plant-pathogen interaction has been reported in other fungi. For instance, the previous characterization of *ABC1* encoding an ATP-driven efflux pump in the rice blast fungus *M. oryzae* indicates that this protein could constitute an important part of the mechanism by which *M. oryzae* detoxifies plant defense compounds such as rice phytoalexins (Urban *et al.*, 1999). Furthermore, a set of genes encoding predicted chloroperoxidases and Cu/Zn-dismutases were found to be down-regulated in *Δmyco5* suggesting an increased susceptibility of the mutant towards oxidative stress found in the host plant environment. In fact, *Δmyco5* displayed an abolished growth on artificial media supplemented with H_2O_2 compared to

wildtype. The potential implication of these chloroperoxidase encoding genes in scavenging of hydrogen peroxide produced by host plant is supported by qRT-PCR analysis, since most of them were differentially expressed in the wildtype strain IPO323 throughout the course of infection (see Figure 39, page 125). Most of them were also found in DE gene sets obtained from transcriptome profiling studies of *Z. tritici* infection cycle, provided by other research groups (Kellner *et al.*, 2014, Rudd *et al.*, 2015), indicating their role for the pathogenic development of the fungus. However to strengthen this hypothesis further experiments considering qRT-PCR analysis of *Δmyco5* mutant strain *in planta* should be conducted to provide a more substantial basis for this suggestion. To evaluate the interaction between *Δmyco5* and the susceptible host plant, further investigation exploiting *in vivo* histological characterization is required.

Further effects associated with *MYCO5* inactivation included a strongly reduced proteolytic activity of the mutant strain as well as enhanced lipid degradation of internal lipid stores (lipid droplets), as was shown by *in vitro* assays performed. Both findings were additionally supported by RNA-Seq analysis, since sets of DE genes with roles in proteolysis and lipid metabolism were apparent. However, which pathway of lipid degradation has a dominated role for mutant physiology remains speculative. Both the role for energy providing via mitochondrial/peroxisomal β-oxidation of released fatty acids and implication into membrane remodeling and cell signaling are possible, since lysophospholipases, esterases, epoxide hydrolases and glycosyltransferases were among products of genes having significantly increased transcript abundances. Interestingly, the staining assay by NileRed to investigate the lipid storage usage revealed only slight differences between wildtype IPO323 and the mutant strain when incubating both under dimorphic switch condition, induced by N-deprivation (data not shown). This leads to suggestion that the lipid degrading enzymes mentioned are probably not directly regulated by *MYCO5* gene product, but rather coupled to filamentous growth mode mediated by the activity of certain signaling pathways (as a secondary effect), supporting at the same time the hypothesis that lipids may represent an energy source for the initiation of hyphal formation and vegetative growth of the mycelium (Rudd *et al.*, 2015). Nevertheless, it requires a more detailed analysis of lipid droplets degradation kinetics, which should include both the histochemical investigation and qPCR experiments, to analyze the expression of lipid metabolism related genes within a time course experiment under dimorphic switch inducing condition and *in planta*. Additionally, consistent with this view, the gene encoding Acyl-CoA dehydrogenase (Protein ID: 38075) catalyzing the first step of β-oxidation was found to be 10 fold up-regulated in *Δmyco5* strain compared to wildtype or

other mutant strains investigated. Meanwhile, genes involved in fatty acid biosynthesis exhibited in *Δmyco5* mutant a relatively decreased transcript level (data not shown).

4.6 Myco5p may represent a putative component of ESCRT-I system

Relying on these data, it seems clear that the putative Myco5p represents a very intriguing novel key determinant of dimorphic switch, with broad impact on diverse cellular metabolic processes. The presence of *mod_r* domain suggests an involvement of this protein in endosomal trafficking. However, the lack of significant similarity to proteins belonging to ESCRT-I system indicates a unique or maybe evolutionarily diverged function, making this protein a potentially valuable therapeutic target. Due to the evident divergence concerning the protein structure, it is likely to conclude that the protein domain has evolved or may have gained additional functions aside to the conserved function in the endocytic transport system. The morphological examination of conidial cells lacking the *MYCO5* gene, combined with a global analysis of transcriptomes (based on RNA-Seq data) between the *Δmyco5* and wildtype strain, indicates that Myco5p acts to repress hyphal cell formation by regulating of dimorphism-related genes. Evidence for that is further provided by genes predicted to encode several transcription factors, like *ZtPTF1* characterized in this study and *ZtTEC1*. In *S. cerevisiae*, the TEA/ATTS transcription factor Tec1p is known to play a crucial role for dimorphic transition (Gavrias *et al.*, 1996). Similarly, the YlTec1p homolog from *Yarrowia lipolytica* and *C. albicans* CaTec1p were both shown to control the yeast-to-hypha transition, albeit in case of *C. albicans* to a lesser extent (Zhao *et al.*, 2013, Schweizer *et al.*, 2000). Generally, these results indicate the presence of a complex regulatory network involving distinct, yet interrelated, pathways that may function in the regulation of mycelial growth in *Z. tritici*. Indeed, the plenty of observed attributes of the mutant and the diversity of the metabolic pathways affected point to a putative role of Myco5p in global posttranslational regulation processes through its potential participation in ESCRT system. This presumption is also supported by observed up-regulation of gene encoding ubiquitin protein ligase (E3) (Protein ID: 95327), being significantly (>50 fold) up-regulated in *Δmyco5* compared to other targeted mutant strains including wildtype. This may emphasize the link between ubiquitination and endocytic system in *Z. tritici*, consistent with the established role of ESCRT complex in protein turn-over as well as protein degradation previously described in yeast (Schmidt and Teis, 2012).

Generally, the role of ESCRT (endosomal sorting complex required for transport) system has been extensively described in different organisms, and shown to have impact on diverse

cellular processes, including sorting of vacuolar proteins, cytokinesis, autophagy, viral budding, multivesicular body (MVB) biogenesis and other pathways (Hurley, 2010). Being part of the endocytic system, ESCRT is known to play a central role in endosomal trafficking and sorting of different proteins in the cell. The endocytic system consists of several compartments, and activates processing mechanisms after receiving cargo from the plasma membrane, either by the turnover of the membrane proteins followed by recycling mechanisms or by delegating them to vacuolar (fungal counterpart of the mammalian lysosome) degradation. The ESCRT complex is composed of heterogeneous core polyprotein complexes ESCRT-0, ESCRT-I (Mvb12p, Vps23p, Vps37p, and Vps28p), ESCRT-II and ESCRT-III, which function in a sequential manner being recruited to the endosomal membrane (Katzmann *et al.*, 2003, Wolf *et al.*, 2010). The first evidence for a crucial role of endocytic pathway for morphogenesis-related processes was previously shown in *Ustilago maydis*. After that, numerous studies in filamentous fungi shed light on the relevance of the endocytic pathways for hyphal growth and pathogenicity (Steinberg, 2014). Hence, nearly all components of ESCRT complex in *Aspergillus nidulans* appear to be essential for growth (Calcagno-Pizarelli *et al.*, 2011). In *Candida albicans*, ESCRT activity is required for pathogenesis and colonisation (Alfred and Vaccari, 2016).

Therefore, assuming participation of Myco5p in assembly and proper functioning of ESCRT-I complex, the pleiotropic physiological effects, including cell wall perturbation observed in the *Z. tritici* mutant strain, may be a logical result of *MYCO5* inactivation. However further experiments should be carried out to elucidate the role of *Z. tritici* Myco5p in postulated pathways in more depth. They could include protein interaction studies like yeast-2-hyprid analysis, Co-immunoprecipitation, Bimolecular fluorescence complementation (BIFC) with the aim to unveil a potential interaction between Myco5p and other homologs from *S. cerevisiae* previously characterized, including such components like Vps23p or Vps37p as core constituents of ESCRT-I system. In addition, functional complementation analysis should be performed to verify whether the protein of *Z. tritici* would complement the homologous protein of *S. cerevisiae* functionally. Recently, several tools were established for monitoring the endosomal trafficking in *Z. tritici* by using such molecular and biochemical cytological markers as neutral red, FM4-64 and recently characterized proteins fused with eGFP. These proteins include the determinants of early and late endosomes, Rab5p, Rab7p, and actin-bindind protein Fim1p, contributing to the endocytic uptake at the cell surface (Kilaru *et al.*, 2015). These tools would provide useful markers for histochemical

investigation in combination with time course analysis by monitoring the GFP-fused Myco5p in conidial cells or hyphae.

Collectively, these results lead to the suggestion that Myco5p could represent a novel factor, which may either be involved in endosomal sorting mechanisms provided by the endocytic system or have strongly diverged function in the course of evolution emphasizing its role in diverged regulation processes. This suggestion is also supported by BLASTp analysis conducted to identify the ESCRT homologs in *Z. tritici* based on deduced protein sequences. Hence, the yeast Vps37p seems to have no direct sequence homologs in *Z. tritici*, whereas for the remaining ESCRT components the sequence homologs with different degree of conservation were identified (data not shown). Therefore, relying on this observation, it is conceivable to consider this protein as a potential target for biological control.

4.7 *MYCO56* encodes RNA-binding protein required for a proper morphology, cell branching, dimorphic switch and coordinated melanin biosynthesis

Meanwhile, *MYCO56* was found to encode a predicted homolog of Cip2p from fission yeast *Schizosaccharomyces pombe*. The homology was supported by both, the Phyre2 modeling approach as well as BLASTp analysis, albeit showing only a weak conservation covering only 25.7% of its 743 aa deduced protein primary sequence. This *S. pombe* protein homolog was previously functionally characterized and shown to interact with Csx1p, which in turn controls global gene expression during oxidative stress in *S. pombe* by regulating the turnover rate of *ATF1* transcripts. The RNA binding protein Csx1p harbors three RNA recognition motifs (*RRM*s) and acts to stabilize the *ATF1*-mRNA. *ATF1*, in turn, encodes a *b-ZIP* transcription factor, which is thought to directly induce transcription of genes with essential functions in oxidative stress response (Rodriguez-Gabriel *et al.*, 2003, Madrid *et al.*, 2004). Cip1p and Cip2p (Csx1p Interacting Protein 1 and 2) are suggested to counteract the function of Csx1p in *S. pombe*, since inactivation of any of them rescued the elevated sensitivity of *Δcsx1* to oxidative stress and re-established expression of Csx1p regulated genes (Martin *et al.*, 2006).

The presence of the predicted *RRP*-domain in Myco56p is very intriguing, as far as this is a common feature of RNA-binding proteins, which directly implies the involvement of these proteins in post-transcriptional processes either by stabilizing the mRNA-transcripts and regulating the alternative splicing or functioning in both cleavage and/or polyadenylation processes (Martin *et al.*, 2006). For instance, a fascinating example is given by *RPB35*, which was functionally characterized in *Magnaporthe oryzae*. From gene inactivation experiments,

the corresponding protein was shown to be involved in preprocessing of mRNAs associated with developmental and virulence-related processes, however being at the same time not essential for viability of the fungus (Franceschetti *et al.*, 2011). The *RPB35* defective mutants in *M. oryzae* are non-pathogenic and were found to be highly sensitive to oxidative and osmotic stress. These findings indicate that focusing on novel RNA-binding proteins implicated in global regulation of mRNA-stability and affecting the translation of proteins in a global manner could provide insights into post-transcriptional networks and cellular processes, which in turn could aid to unveil pathogenicity-associated determinants.

By means of reverse genetics, the effect of *MYCO56* gene inactivation was examined concerning the impact on physiological and morphological properties of the generated mutant strains. Thus, the targeted gene disruption of *MYCO56* appears to have pleiotropic effects on *Z. tritici*. This is primarily reflected in a distinctive morphology of conidia displaying prolonged shape in the mutant strain and strongly resembling pseudohyphal mode of growth in contrast to the wildtype strain IPO323. The morphological property of asexual spores is accompanied by a remarkably reduced ability of lateral conidial branching. These effects stated were previously not described in the *CIP2* deficient *S. pombe* strains, thus emphasizing a particular and specific role of this protein in the physiology and morphology related processes in *Z. tritici*. Furthermore, the mutant strain was abolished in dimorphic transition and failed to infect the susceptible wheat cultivar Riband. In addition, a functional discrepancy of Myco56p and *S. pombe* Cip2p is linked to a different growth behavior of corresponding "loss-of-function" mutants upon oxidative stress treatment. While *S. pombe CIP2* mutant strains displayed an enhanced ability to tolerate higher concentrations of hydrogen peroxide mediating oxidative stress compared to wildtype (Martin *et al.*, 2006), no of such pronounced effects were observed for *Δmyco56* strains, which retained a wildtype-like level of oxidative stress susceptibility.

Furthermore, disruption of the *MYCO56*-gene was found to positively influence the colony pigmentation of *Z. tritici* mutant strain. When incubated on N-deprivation medium, mature colonies of *Δmyco56* strain turned dark, whereas the colonies of the wildtype strain IPO323 exhibited no or very reduced degree of pigmentation. This phenotypic analysis is consistent with the results obtained from RNA-Seq, indicating that several genes encoding enzymes with functions in DHN-melanin biosynthesis maintained increased level of transcripts in the mutant strain compared to wildtype. Generally, melanin has been reported as an important virulence factor for numerous pathogenic fungi, including phytopathogenic fungi like *Magnaporthe oryzae* and *Verticillium dahlia* (Vidal-Cros, 1994, Chumley and Valent, 1990,

Fan *et al.*, 2017) and in several human pathogenic fungi like *Paracoccidioides brasiliensis* and *Histoplasma capsulatum* (Taborda *et al.*, 2008). For instance, previous studies have demonstrated the melanin requirement of *M. oryzae* for the formation of functional appressoria crucial for successful plant infection (Howard and Ferrari, 1989). Mutants lacking the melanin biosynthesis ability in *M. oryzae* were found to be non-pathogenic. However, the function of melanin in *Z. tritici* remains hypothetical, suggesting its role in protection against a broad range of toxic insults but on the other hand reinforcing the doubt on the association with the virulence due to the non-appressorial mode of penetration. Consequently, this finding points to a unique function of Myco56p in *Z. tritici*, since no correlation between the expression of the gene *CIP2* and melanin biosynthesis was reported in the previous studies with *S. pombe*. Furthermore, this observation opens up a broader hypothesis margin for this gene and illustrates its involvement in global regulatory processes, affecting both the physiology and genetic signaling processes on a large scale.

Finally, subcellular localization and time-course expression analysis of eGFP-fused Myco56p revealed an unexpected and intriguing participation of the protein in the conidial formation and germination. Monitoring the protein expression and translocation within 4 hours, highlighting the early developmental process of the conidia, revealed an enhanced accumulation of protein in apical and subapical regions of conidia. In particular, zones of enhanced protein accumulation were detected in regions where the subsequent branching/budding of conidia occurred, indicating implication of Myco56p in cell division and conidial biogenesis. Furthermore, by monitoring the protein localization in the late phases of development, a preferentially increased location in subapical regions of mature hyphae was noticed, indicating participation in polar growth. This finding may point to a diverged role of Cip2p homolog in *Z. tritici* compared to effects described in the case of *S. pombe* and awaits a more detailed investigation considering its involvement in processes associated with conidial proliferation.

Collectively, the precise function of Myco56p and its implication in signaling networks in *Z. tritici* remains unknown and requires further in-depth functional analysis. For instance, a functional complementation of yeast mutant phenotypes by *MYCO56* would provide valuable information concerning function conservation of the protein, and contribute to answering the question whether *Z. tritici* homolog can replace the yeast gene functionally. Exploiting yeast-two-hybrid system, or similar techniques such as bimolecular fluorescence complementation (BIFC), focusing on homologs previously characterized in *S. pombe*, like Csx1p or Cip1p, would also provide a substantial evidence on interaction of these proteins previously

demonstrated in fission yeast. Because it remains still unclear when and how specific Myco56p may bind to gene transcripts in the cytosol, additional studies will have to clarify the mechanistic details of these events by conducting e.g. protein-RNA-binding studies using ChIP-Seq. However, the relatively weak conservation of the deduced *Z. tritici* and *S. pombe* protein sequences as well as specific traits observed exclusively for *MYCO56* deficient mutant and previously not described for *S. pombe* lead to conclusion that this protein may exert common and diverged function in *Z. tritici* with an evidenced role in dimorphism. Intriguing remains in this context a putative connection of *MYCO56* to other signaling pathways governing dimorphism related processes. Evidence for such hypothetical interaction is provided by the previous study in *S. pombe*. Hence, exploiting coimmunoprecipitation and colocalization experiments, Duncan *et al.*, 2014 demonstrated a cotranslational interaction between the Sty1 MAP kinase, a Hog1p homolog of *S. pombe,* and the *CIP2* mRNA. Whether a similar association between ZtHog1p and *MYCO56* mRNA (either on transcript or protein level) holds true for *Z. tritici* remains to be elucidated and should be addressed in ongoing studies.

4.8 Transcriptome analysis provides crucial insights into regulatory processes of dimorphic switch

In order to understand the gene regulatory network required for dimorphic switch and to obtain a global view of the genes potentially regulated by Myco5p, Myco56p and ZtHog1p during the yeast-to-hyphal transition, we generated and compared the transcriptional profiles of the mentioned mutant strains by RNA-Seq analysis. Having different phenotypes of the selected mutants concerning their growth behavior under switch inducing condition, it was of interest to dissect their gene expression profiles to identify genes, which are more likely associated with their phenotypes under investigated condition. With this approach, we expected that this would allow us at the same time to make suggestions about a potential involvement of significantly regulated genes in the dimorphic switch related processes. The early development of hyphae from yeast cells (yeast-to-mycelium transition) must require, in addition to regulation of genes encoding transcription factors, the coordinated expression of many genes. Among them genes are expected encoding proteins with functions in signal transduction pathways, cell cycle regulation and the cell elongation process, or genes, which are implicated in synthesis and organization of the cell wall. In fact, surveying the transcriptomes of the targeted strains *Δmyco5*, *Δmyco56*, *ΔZthog1* and IPO323 associated with dimorphic transition indicated a profound global transcriptional reprogramming related to

such biological processes like metabolism, cell wall biogenesis, cell signaling and transport-associated processes. This observation was common to all investigated strains, though the expression of significantly regulated genes related to these processes was different in each case. In addition, according to our results, each strain displayed a specific transcriptional regulation pattern upon switch inducing condition. In each instance, we determined strain-specific gene sets, suggesting their transcriptional dependence on the target genes for which the targeted mutant strains have been disrupted. At this point it is important to reiterate that the RNA-Seq analysis was employed without sample duplication. Certainly, this may result in potentially biased interpretation of the transcriptome data. Nevertheless, the results obtained were in agreement with that of the qRT-PCR analysis used to validate expression of several selected genes, indicating that data obtained is reliable for further exploration. In addition, when examining the RNA-Seq profiles of targeted mutants, the disruption (inactivation) of the respective target genes could be confirmed, since no transcripts were detected in the corresponding gene loci (Figure 13).

The substantial amount of transcripts obtained revealed DE genes involved transport- and metabolism associated processes. Moreover, most of the genes involved in cell wall remodelling, morphology regulation, signaling as well as tolerance and response to environmental stress were found in the obtained *MYCO5*-, *MYCO56*- and *HOG1*-regulons. Furthermore, within this thesis different bioinformatics approaches were applied to extract the maximal information from the RNA-Seq data generated. Explorative analysis by comparison of strain-specific transcriptomes using Venn-diagrams revealed sets of DE genes, being shared across all investigated strains. By exploiting the PHI-Base, we investigated the data sets obtained for the presence of genes previously characterized in other fungal organisms as potential pathogenicity factors. Some of these genes were previously shown to have a morpho-pathogenic significance in different fungi, including dimorphic fungi. Among them are for instance a deduced homolog of Gel2p encoding gene from *Aspergillus fumigatus* (Mouyna *et al.*, 2005), *PLB1* from *Candida albicans* (Leidlich *et al.*, 1998), *MEP1* from *Coccidioides posadasii* (Hung *et al.*, 2005) and *LIG4* from *Candida albicans* (Andaluz *et al.*, 2001), whose expression was previously shown to be coupled to the yeast-to-mycelium transition. *LIG4* was earlier characterized in *Candida albicans* as a gene encoding a structural and functional homolog of the yeast ligase IV, exhibiting significant rise in mRNA levels during the morphological transition. Moreover, null mutants, lacking both alleles, exhibited a dramatic effect on mycelium formation (Andaluz *et al.*, 2001). Hence, the suggested positive role of *LIG4* in morphogenesis may stay in agreement with *MYCO5*-dependent regulon

obtained, revealing a significant up-regulation of the homologous gene during the dimorphic switch. Moreover, the obtained *Δmyco56* and *ΔZthog1* transcriptome profiles during the dimorphic switch revealed significant increase in transcript level of *FLBD* homolog, known to play a crucial role in conidiation and conidiophore development, as was previously shown for several fungi including *M. oryzae* (Matheis *et al.*, 2017). Interestingly, when comparing the strain-specific transcriptomes *Δmyco56* and *ΔZthog1*, a pronounced similarity in gene expression patterns was evident, an observation which is also reflected in PCA analysis (see Figure S13). Thus, both mutants shared DE genes that may play crucial roles in cell signaling, cell wall remodeling and (oxidative) stress response. This stays in agreement with data previously obtained for *C. albicans*, wherein approximately 25% of genes with altered expression levels in the *Δssk1* mutant are related to stress adaptation functions and cell wall remodelling, including the two-component histidine kinase encoding gene *CHK1* and flocculation gene *FLO1* (Chauhan *et al.*, 2003, Zhao *et al.*, 2007).

Meanwhile, *MYCO5* dependent regulon indicated the onset of some more genes, including for instance *TEC1* and *CNAA*, whose role in dimorphism was previously shown in several fungi exhibiting dimorphic growth modes. In *A. fumigatus*, the role of calcineurin, a Ca^{2+}/calmodulin (CaM)-dependent protein phosphatase, has been previously investigated. Thus, calcineurin catalytic subunit CnaAp mutants showed dramatic hyphal defects, including decreased apical extension and polarized growth (Steinbach *et al.*, 2006, Pasricha *et al.*, 2013). Meanwhile, *TEC1* was found to encode a TEA/ATTS transcription factor playing an important role in the dimorphic transition, since inactivation of *TEC1* prevented a haploid invasive growth and diploid pseudohyphal growth in *S. cerevisiae* (Gavrias *et al.*, 1996, Zhao *et al.*, 2013). Additionally, examining the *MYCO5* regulon, a significantly increased expression level of the gene predicted to encode a t-SNARE protein (*Zt58641*) was apparent, consistent with its implication in cell polarity, exocytosis and apical growth (Brennwald and Rossi., 2007). Moreover, it is not surprising, that a group of DE genes was apparent, which are predicted to encode products having potential functions in cell wall biogenesis and remodeling. This cluster includes for instance DE genes encoding chitinase, 1,3-β glucanase, several glycosyl transferases and one hydrolase. It is well known that cell wall of fungi plays an essential role in survival and growth of the cell, maintaining not only the structural shape of corresponding growth form (yeast-like, pseudohyphal or filamentous), but also representing an interface between organism and surrounding environment. Consistent with this view was the observation that in the case of *Δmyco5* several genes related to lipid metabolism were differentially expressed. According to previous reports, lipids are thought to

play important roles in the regulation of dimorphism and virulence in several pathogenic fungi. For instance, among different phospholipases already mentioned, the phospholipase D from *C. albicans* was previously shown to be required for yeast-to-hyphae transition (McLain and Dolan, 1997). Similarly, the secreted phospholipase B (PLB) is also known to be a virulence factor in *C. albicans*, being involved in the dimorphic switch (Leidlich *et al.*, 1998). Both genes encoding products homologous to PLB were found to be down-regulated in Δ*Zthog1*, suggesting their involvement in regulation of the dimorphic transition in *Z. tritici*.

Furthermore, using advanced BLAST analysis we identified an exceptional list of 57 *Z. tritici* unique genes, being differentially expressed during the dimorphic switch and having no homologues or having only one, two or three orthologues in other fungal genomes listed in public databases. Some of these genes display a drastically altered strain-specific expression profile, indicating their implication in dimorphism related mechanisms. Furthermore, it is likely to conclude that they may represent promising candidates for finding novel fungicide targets for plant protection.

Finally, the RNA-seq results obtained were compared to publically available data sets from studies aimed at examining expression profiles *in planta*. With this approach we attempted to find DE genes, whose products may be important for pathogenicity or may exert their functions in plant-pathogen interaction. These studies encompass the previously published RNA-Seq analysis by Yang *et al.*, Brunner *et al.*, Kellner *et al.* and Rudd *et al.*, as mentioned earlier, which were particularly directed to the identification of DE genes following the complete infection cycle (at distinct time points) of *Z. tritici* in susceptible host plants. Hence, by focusing primarily on DE genes commonly shared across these data sets, we provide a list of potential candidates putatively involved in the critical steps of pathogenic development of the fungus (Table S8).

Taking résumé from the obtained RNA-Seq data, we can therefore conclude that the observed families of genes involved in metabolism, cell wall biogenesis and organization, as well as genes related to transporter activity and encoding components of signal transduction pathways, are crucial for the cell differentiation and proliferation associated with the dimorphic transition. Overall, the gene expression profiles described highlight key similarities and also differences in the investigated strains representing yeast-like or filamentous growth forms. By providing a list with potential candidate genes (see Table S7), we emphasized some dimorphism related processes which should receive a broader attention for further investigation. Undoubtedly, these data provide a solid basis for accelerating research on this economically important phytopathogenic fungus *Z. tritici* and generally on the process

underlying the dimorphic transition, which also has a huge impact on pathogenic development of systemic dimorphic fungi presenting a serious global health threat for humans.

4.9 Regulation of target genes *MYCO1*, *MYCO4*, *MYCO5* and *MYCO56 in planta*

In light of their dimorphism related role, the target genes were further examined regarding their potential involvement in the pathogenic development of the fungus *in planta*. To this end, expression profiles of the target genes in the wildtype strain IPO323 during the invasive fungal growth on susceptible wheat cultivar Riband were examined. Our analysis revealed that all genes displayed a similar pattern of expression during the time course of the infection process, encompassing both biotrophic and necrotrophic phases. The transcription profiles determined suggest a putative involvement of these genes in distinct developmental processes during *in planta* proliferation of the fungus.

Thus, *MYCO5* exhibits significantly decreased transcript abundance at 4 and 14 dpi relative to 1 dpi used as reference condition. Both genes, *MYCO1* (= *ZtSSK1*) and *ZtHOG1*, displayed decreased levels of transcripts at 4 and 14 dpi and were found to be significantly up-regulated at 28 dpi. This observation indicates the early induction of HOG1 signalling pathway genes during the penetrative phase, being potentially required for regulation of dimorphism related genes, whereas the early *in planta* development events (4 dpi) require activation of *MYCO5* suggested to encode a negative regulator of filamentation. Similar expression behaviour was observed for *MYCO56*, being significantly down-regulated at 4 and 14 dpi and displaying enhanced expression at 28 dpi. Interestingly, all of the target genes examined were found to be upregulated in the late necrotrophic phase (28 dpi). This phase is characterized by development of necrotic lesions bearing pycnidia (Steinberg, 2015), hence, indicating a particular role of these genes for the metabolic reprogramming in the late phase of the infection cycle and formation of pycnidia. However, we noticed a discrepancy of expression profiles, when comparing these findings with data previously published (relying on RNA-Seq data from Yang *et al.*, Rudd *et al.*, Kellner *et al.*). Except for *ZtHOG1*, which exhibits increased transcript abundance in the late biotrophic phase according to Rudd *et al.*, 2015, all other genes appear to have a basal expression following the time course of infection.

We postulate that this difference may be due to different wheat cultivars used. It is conceivable that susceptible wheat cultivars used in earlier studies (cv. Sevin or cv. Obelisk) and susceptible cultivar used in our investigation (cv. Riband) may have different response dynamics to *Z. tritici* infection. This could in turn have a significant impact on the differential expression of fungal genes required for distinct phases of infection cycle and *in planta*

development. Therefore, caution should be exercised in the interpretation of the data, since different susceptible cultivars may result in ambiguous output of transcriptome or proteome data. Optimal further studies should be, therefore, standardized and consider only one cultivar in order to compare different experimental outcomes. Reliable in this context is also the application of different sequencing platforms as well as software programs used for analyzing and processing the NGS data. Nevertheless, the qRT-PCR data obtained fits very well the requirement of the target genes in the early development stages of plant infection of *Z. tritici* in view of their requirement for dimorphic switch.

4.10 Identification of novel gene *ZtPTF1* encoding an essential transcription factor in *Zymoseptoria tritici*

Based on the results of generated RNA-Seq data we examined the role of one DE gene, designated *ZtPTF1*, encoding a predicted p53-like transcription factor, which belongs to a Ndt80 protein family. The assignment of the protein to this family was due to the presence of *NDT80/PhogG* domain, identified by InterProScan analysis. Interestingly we found only two genes encoding proteins of this family, *Zt109299* (this study) and *Zt84654*, according to JGI annotation.

Generally, the number of *NDT80*-like genes appears highly variable among different fungi and until now their role has been examined only in a limited number of fungal species (Katz and Cooper, 2015). The complete analysis of all *NDT80*-like genes has been restricted only to three fungi, the haploid ascomycetes *Saccharomyces cerevisiae*, *Aspergillus nidulans* and *Neurospora crassa*, which have one, two, and three representatives, respectively (Katz and Cooper, 2015). For instance, the *S. cerevisiae* Ndt80 protein comprising the *NDT80/PhoG*-like DNA-binding domain was previously characterized as the founding member of a class of p53-like transcription factors functioning as a meiosis-specific transcription factor required for the transition into meiosis (Xu *et al.*, 1995, Kupiec *et al.*, 1997) by inducing transcription of genes during the middle phase (Chu *et al.*, 1998, Katz and Cooper, 2015).

Another member of the family contains *VIB-1*, previously characterized as a regulator of conidiation in *Neurospora crassa*. It was shown to be required for expression of genes involved in heterokaryon-incompatibility programmed cell death and appears to function as a positive regulator of extracellular protease production (Dementhon *et al.*, 2006, Hutchison and Glass 2010, Xiang and Glass 2004). Furthermore, the role of p53-like proteins has been addressed in the opportunistic pathogen, *Candida albicans* and in the phytopathogenic fungus *Aspergillus nidulans*. The CaNdt80p was found to be required for hyphal growth, biofilm

formation and virulence (Nobile *et al.*, 2012, Sellam *et al.*, 2010). Furthermore, it was found to be involved in antifungal drug resistance by activating *CDR1* (Chen *et al.*, 2006). In the filamentous fungus, *A. nidulans*, the function of one Ndt80-like protein (XprGp) has been elucidated, demonstrating that it may represent transcriptional activator involved in response to nutrient limitation by influencing the autolysis/autophagy processes (Cheetham *et al.*, 2000, Katz *et al.*, 2013). Furthermore, a link to secondary metabolism was established, since mycotoxin and penicillin production were suggested to be regulated by XprGp (Katz *et al.*, 2006, 2013). The second *A. nidulans* Ndt80-like protein (NdtAp) exhibits a stronger sequence similarity to Ndt80p and when deleted results in loss of sexual development (Katz *et al.*, 2013).

These examples highlight diverse functions of p53-like proteins, indicating a connection to different signaling pathways, regulating biologically important and vital cellular processes. Relying on RNA-Seq data obtained within this work, the *ZtPTF1* gene was found to be transcriptionally up-regulated in *Δmyco5* and *Δmyco56* mutant compared to IPO323 and *ΔZthog1* reference strains. Considering the aberrant conidial morphology of both strains, the pseudohyphal growth form in case of *Δmyco56* and filamentous form in case of *Δmyco5*, it is likely to suggest that *ZtPTF1* might be involved in processes linked to cytokinesis and spore morphogenesis. We decided, therefore, to functionally characterize the gene by means of reverse genetics approach using targeted gene disruption by ATMT. However, our attempts to inactive the gene yielded no vital mutants, since among the 200 transformants tested no targeted mutants generated by homologous recombination event were detected. The outcome of the experiment leads to the conclusion that inactivation of the gene results presumably in lethal phenotype. Interestingly, this is the first report on the essential role of the *NDT80*-family protein for the vitality of fungus, since genetic inactivation of homologs in other fungal species reported so far were not associated with lethality of generated mutants.

4.11 ZtPtf1p localizes to nucleus and may regulate transcriptional programs similar to other fungal organisms previously described

To verify the presumptive role of ZtPtf1p as a DNA-binding protein and transcriptional factor, we analyzed the subcellular localization of the ZtPtf1 protein in *Z. tritici* by fusing eGFP to the C-terminus of ZtPtf1p under the control of the constitutive promote *EFA1* from *Magnaporthe oryzae*. Preliminary attempt to use the native promoter of *ZtPTF1* was not successful, since no fluorescence signals were detectable. This observation suggests either a limited length of promoter sequence used for *eGFP*-fused construct generation

(approximately 1.5 kb), being not sufficient for proper gene expression, or low levels of basal expression of the gene under investigated condition, potentially emphasizing its conditional regulation. To determine whether the nuclear localization of ZtPtf1p-eGFP was affected by cell growth forms or incubating conditions, we examined the subcellular localization of fused eGFP gene product under nutrient rich condition which promotes the yeast-like growth, as well as under dimorphic switch inducing condition, wherein conidia consist of a mixture of yeast and filaments. Hence, upon both conditions the fluorescence signals were observed in the nuclei of both, the yeast-like and hyphal cells, indicating that ZtPtf1p-eGFP is localized in the nucleus independent of cellular morphology. This observation supports and validates therefore the predicted function of ZtPtf1p in transcriptional regulation.

As mentioned in preceding section, previous studies revealed that transcription factors of *NDT80* family participate in biological processes associated with conidial proliferation, morphogenesis (hyphal growth) and metabolism related processes. Ndt80p is a known meiosis-specific transcription factor in *S. cerevisiae* that controls the expression of meiotic middle genes (Winter, 2012). Based on previous electrophoretic mobility shift assay (EMSA) and Chip-on-Chip studies, Ndt80p was shown to bind to the middle sporulation element (MSE), assigned as "gNCRCAAAW", which is found in almost all promoters of the meiotic middle genes. Similar results were achieved with *C. albicans* exploiting ChIP-chip technology to investigate the roles of Ndt80p by examining its promoter binding pattern (Sellam *et al.*, 2009, 2010). Relying on these data published, we performed *in silico* analysis followed by clustering by gene enrichment analysis focusing primarily on genes which may underlie the regulation by ZtPtf1p. Therefore we used this information to explore a putative regulon of Ndt80p. To this end, a subset of genes having binding consensus sequence in the promoter regions was taken into consideration. Most of the genes with adjacent biological processes were found to coincide with data previously obtained from other studies. Using this bioinformatics approach, a total of approximately 2200 binding sites in the genome of *Z. tritici* were identified, distributed across 21 chromosomes. To eliminate false positives, the pattern search was restricted to 5'-regions of genes (promoter regions) containing the consensus MSE motif ranging from 50 to 1500 from ATG codon (upstream of the translation initiation site) of annotated genes, whereby 81 candidate genes were identified as putative targets of Ndt80p. Following the gene ontology analysis of these Ndt80p targets revealed significant enrichment of genes predicted to be involved in different aspects of physiological processes like carbohydrate metabolism, hyphal development, stress responses, cell wall biogenesis, multidrug transport and the cell cycle (Sellam *et al.*, 2009). The implication of

Ndt80p in hyphal development in other fungi has also been reported. For instance, in *C. albicans*, Ndt80p was found to bind promoters of hyphal growth regulators, such as transcription factors Cph2p, Efg1p, Ume6p and Flo8p, which activate filamentation-specific genes when the fungus undergoes morphological switching (Sellam *et al.*, 2009). Based on this observation, Ndt80p was suggested to be important for regulation of morphogenesis. In fact, mutants lacking the *NDT80* gene failed to form hyphae under different filamentation-inducing conditions (Sellam *et al.*, 2010), albeit the precise mechanisms involving Ndt80p in hyphal growth are elusive and need to be clarified.

In particular, a *CDC42* activating protein was among potential *Z. tritici* targets, evidencing an implication of ZtPtf1p in signal transduction systems. A cell division control protein 42 (Cdc42p) in its turn is a small GTPase of the Rho family, which is known to regulate signaling pathways that control diverse cellular functions and and certain cellular processes in a variety of organisms (Park and Bi, 2007, Simon *et al.*, 1995). It was originally identified in *S. cerevisiae* and found to be involved in regulation of the cell-cycle and associated with biological processes including cell morphology, cell migration and endocytosis (Bender and Pringle, 1989, Adams *et al.*, 1990, Cullen *et al.*, 2012).

In conclusion, we postulate that ZtPtf1p represents a global regulator in *Z. tritici* having impact on diverse cellular processes similar to those described in other fungi, including hyphal development. The predicted genes which may underlie the control of ZtPtf1p appear interesting candidates for future experimental validation. Using more restrictive criteria (considering published data from other organisms or using positional constraints and evolutionarily conservation data), this approach can be used to make better predictions of the ZtPtf1p regulatory target genes. However, it should be complemented by genomic approaches that determine the regulatory targets. For instance, it will be of future interest to experimentally identify and validate the binding motif of ZtPtf1p by Chromatin-Immunoprecipitation experiments combined with next generation sequencing techniques (e.g. ChIP-Seq or SELEX) and by electrophoretic mobility shift assays.

The essential role of ZtPtf1p for cell viability as well as its role as transcription factor verified through *in silico* analysis together with the outcome of localization assay give rise to a possibility of establishing a screening system based on this protein as a biosensor. This can be applied for instance using a nuclear translocation assay, in a manner as was previously described for cytosolic hormone receptors in other biological systems (Figure 44). For instance using the same eGFP-fused product as demonstrated in this thesis, we can detect and monitor the translocation of the protein to the nucleus. Another approach for this purpose

could be realized by utilizing a fragment complementation to identify this translocation event. The ZtPtf1p would be expressed as a fusion protein with a portion of β-galactosidase. A complementary portion of β-galactosidase is constitutively expressed in the nucleus. Upon translocation to nucleus the two portions of β-galactosidase form a functional enzyme capable of metabolizing a substrate and producing light signals. The emitted light produced in the reaction can be quantified in order to extrapolate the amount of ZtPtf1p in the nucleus. This experimental setup opens up a possibility to use such systems in high-throughput-manner for screening new compounds that interact with ZtPtf1p. Hence, this assay can be designed to search for general inhibitors of ZtPtf1p shuttling by monitoring the translocation of the ZtPtf1-eGFP fusion protein from the cytoplasm to the nucleus.

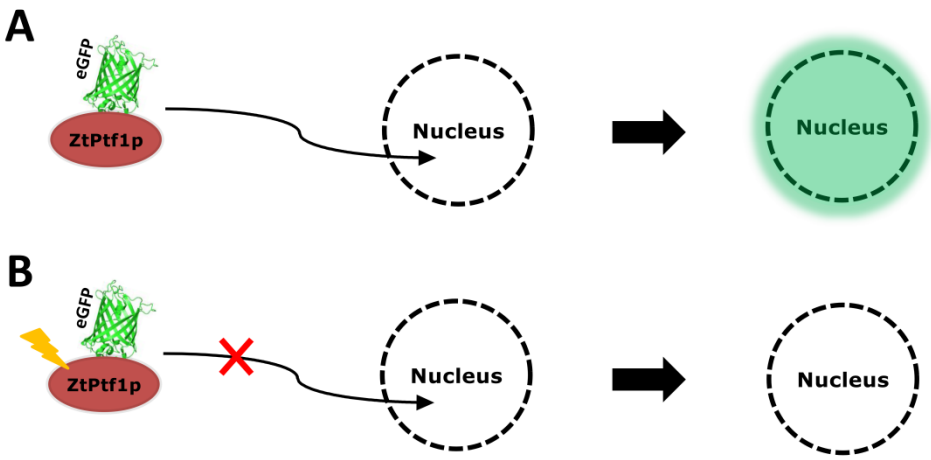

Figure 44: Schematic representation of a fluorescence-based translocation assay with ZtPtf1p-eGFP. An antagonist test is shown. **A)** Without the addition of the bioactive substance, the transcription factor fused with the eGFP as a biosensor is translocated to the nucleus, whereby a fluorescence signal can be detected in the cell nucleus. **B)** With the addition of a potential inhibitor, the fluorescence signal is no longer detectable in the nucleus. (Adapted from Laufer (master thesis, 2015))

5. Conclusion and Outlook

In this thesis, the genetic mechanisms underlying dimorphic switch in *Z. tritici* have been addressed by employing a forward genetics approach complemented by reverse genetics and RNA-Seq transcriptome analysis. The main goal was to establish a screening system in order to obtain dimorphic switch deficient mutant strains and to unveil novel determinants of dimorphic transition in *Z. tritici*. This was possible due to morphologically uncoupled and distinguishable growth forms of *Z. tritici* triggered *in vitro*. In summary, the screening program resulted in identification of the eleven interesting mutant strains affected in dimorphic switch capability. Making use of genome walking approach, we identified the disrupted gene loci and validated the usability of the established screening system by targeted gene inactivation of four of these candidate genes.

The four target genes designated *MYCO1*, *MYCO4*, *MYCO5* and *MYCO56* were functionally characterized by employing reverse genetics approach. Phenotypic characterization of the generated mutant strains revealed many intriguing pleiotropic effects caused by respective gene inactivation, showing a well-fitted compatibility with RNA-Seq data obtained. The outcome of this characterization allows us to draw some hypothesis on how these factors may contribute to regulation of dimorphic switch *Z. tritici*. Thus, examining transcriptomes of the selected mutants under nutrient deprivation condition (N-deprivation), we gained the first insight in the dimorphism associated processes in *Zymoseptoria tritici*. Among the DE genes obtained from RNA-Seq analysis were those, whose role in the pathomorphogenic processes was previously established in other fungal pathogens, including both dimorphic and filamentous fungi. Moreover, making use of bioinformatic analysis, we also identified sets of unique DE genes previously not described in the literature. In conclusion, these genes may provide a wealth of candidates potentially implicated in unique or specific pathways regulating dimorphic switch related process in *Z. tritici*. Therefore, these genes should be addressed in future reverse genetics experiments to examine their biological roles.

However, a more sophisticated study of dimorphism-related processes requires primarily an integrative approach considering the complementary use of proteome analysis, at least for the reason that the transcriptome and the proteome abundances not always display an anticipated correlation. Additionally, an advanced RNA-Seq incorporating more time points should be a subject of further investigations, to gain insight into early activation dynamics of the key signaling mediators governing dimorphic transition. Moreover, transcriptional profiling of the wildtype strain under nutrient-rich and nutrient-deprivation conditions would provide insights into the complexity of regulation network of dimorphic switch. By surveying the mutant

strain-specific transcriptomes under nitrogen-deprivation condition, one further DE gene designated *ZtPTF1* was identified, homologous to NDT80p encoding genes previously characterized in some fungi including the yeast *S. cerevisiae*. The *in silico* analysis performed in this work revealed a plenty of biological processes, which may be influenced by this transcription factor. The results obtained appear consistent with previous findings published, indicating a similar function in *Z. tritici*. Since it was not possible to inactivate this gene, another approach by exploiting e.g. RNA interference (RNAi) could provide more insights into its biological role for *Z. tritici*.

In summary, further experiments are required to establish connection among the factors identified in this work, to understand the tightly regulating mechanisms controlling dimorphic switch in *Z. tritici*. Thus, the proposed experimental directions, scenarios and ideas discussed (provided in the Discussion section) should be addressed in ongoing experiments to integrate the identified candidate genes within gene regulatory network governing dimorphic transition. Further detailed characterization regarding the physiological and morphological features of the generated mutant strains should be carried out.

There is no doubt that integration of data obtained from this thesis, as well as ongoing experiments together with published findings will provide a powerful tool to understand mechanisms underlying dimorphic transition. Preventing the dimorphic switch, that is the critical step of the infection cycle of *Z. tritici*, could be one of the successful strategies to combat the disease caused by this plant pathogen. The findings presented here demonstrate that integration of forward genetics approach and functional analyses accompanied by RNA-Seq transcriptome investigation provide a strong framework for the identification of new pathogenicity-related factors. The outcome from our results provides an excellent basis for further extended investigations to deepen our understanding of molecular mechanisms associated with dimorphism.

6. References

Abuodeh, R. O., Orbach, M. J., Mandel, M. A., Das, A., & Galgiani, J. N. (2000). Genetic transformation of *Coccidioides immitis* facilitated by *Agrobacterium tumefaciens*. *Journal of Infectious Diseases*, *181*(6), 2106-2110.

Adams, A. E., Johnson, D. I., Longnecker, R. M., Sloat, B. F., & Pringle, J. R. (1990). CDC42 and CDC43, two additional genes involved in budding and the establishment of cell polarity in the yeast *Saccharomyces cerevisiae*. *J. Cell Biol*, *111*(1), 131-42.

Alexa A and Rahnenfuhrer J (2016). topGO: Enrichment Analysis for Gene Ontology. R package version 2.26.0.

Alfred, V., & Vaccari, T. (2016). When membranes need an ESCRT: endosomal sorting and membrane remodelling in health and disease. *Swiss Med Wkly*, *146*, w14347.

Andaluz, E., Calderone, R., Reyes, G., & Larriba, G. (2001). Phenotypic analysis and virulence of *Candida albicans* LIG4 mutants. *Infection and immunity*, *69*(1), 137-147.

Arana, D. M., Prieto, D., Román, E., Nombela, C., Alonso-Monge, R., & Pla, J. (2009). The role of the cell wall in fungal pathogenesis. *Microbial biotechnology*, *2*(3), 308-320.

Arraiano, L. S., Worland, A. J., Ellerbrook, C., & Brown, J. K. M. (2001). Chromosomal location of a gene for resistance to *Septoria tritici* blotch (*Mycosphaerella graminicola*) in the hexaploid wheat'Synthetic 6x'. *Theoretical and Applied Genetics*, *103*(5), 758-764.

Arraiano, L. S., Balaam, N., Fenwick, P. M., Chapman, C., Feuerhelm, D., Howell, P., ... & Brown, J. K. M. (2009). Contributions of disease resistance and escape to the control of *Septoria tritici* blotch of wheat. *Plant Pathology*, *58*(5), 910-922.

Atkinson, N. J., & Urwin, P. E. (2012). The interaction of plant biotic and abiotic stresses: from genes to the field. *Journal of experimental botany*, *63*(10), 3523-3543.

Bache, K. G., Slagsvold, T., Cabezas, A., Rosendal, K. R., Raiborg, C., & Stenmark, H. (2004). The growth-regulatory protein HCRP1/hVps37A is a subunit of mammalian ESCRT-I and mediates receptor down-regulation. *Molecular biology of the cell*, *15*(9), 4337-4346.

Baenziger, J. U., & Fiete, D. (1979). Structural determinants of concanavalin A specificity for oligosaccharides. *Journal of Biological Chemistry*, *254*(7), 2400-2407.

Bahn, Y. S., Kojima, K., Cox, G. M., & Heitman, J. (2006). A unique fungal two-component system regulates stress responses, drug sensitivity, sexual development, and virulence of *Cryptococcus neoformans*. *Molecular biology of the cell*, *17*(7), 3122-3135.

Bahn, Y. S., & Jung, K. W. (2013). Stress signaling pathways for the pathogenicity of *Cryptococcus*. *Eukaryotic cell*, *12*(12), 1564-1577.

Baldwin, I. T., Halitschke, R., Paschold, A., Von Dahl, C. C., & Preston, C. A. (2006). Volatile signaling in plant-plant interactions: "talking trees" in the genomics era. *Science*, *311*(5762), 812-815.

Bardwell, L., Cook, J. G., Voora, D., Baggott, D. M., Martinez, A. R., & Thorner, J. (1998). Repression of yeast Ste12 transcription factor by direct binding of unphosphorylated Kss1 MAPK and its regulation by the Ste7 MEK. *Genes & development*, *12*(18), 2887-2898.

Bayles, R. A. (1991). Research note: varietal resistance as a factor contributing to the increased importance of *Septoria tritici* Rob. and Desm. in the UK wheat crop. *Plant Varieties & Seeds*, *4*(3), 177-183.

Bazan, N. G. (2009). Cellular and molecular events mediated by docosahexaenoic acid-derived neuroprotectin D1 signaling in photoreceptor cell survival and brain protection. *Prostaglandins, Leukotrienes and Essential Fatty Acids*, *81*(2), 205-211.

Bender, A., & Pringle, J. R. (1989). Multicopy suppression of the cdc24 budding defect in yeast by CDC42 and three newly identified genes including the ras-related gene RSR1. *Proceedings of the National Academy of Sciences*, *86*(24), 9976-9980.

Berraies, S., Ammar, K., Salah Gharbi, M., Yahyaoui, A., & Rezgui, S. (2014). Quantitative inheritance of resistance to *Septoria tritici* blotch in durum wheat in Tunisia. *Chilean journal of agricultural research*, *74*(1), 35-40.

Betts, M. F., Tucker, S. L., Galadima, N., Meng, Y., Patel, G., Li, L., ... & Mandel, M. A. (2007). Development of a high throughput transformation system for insertional mutagenesis in *Magnaporthe oryzae*. *Fungal Genetics and Biology*, *44*(10), 1035-1049.

Bhadauria, V., Banniza, S., Wei, Y., & Peng, Y. L. (2009). Reverse genetics for functional genomics of phytopathogenic fungi and oomycetes. *Comparative and functional genomics*, 2009.

Biswas, S., Van Dijck, P., & Datta, A. (2007). Environmental sensing and signal transduction pathways regulating morphopathogenic determinants of *Candida albicans*. *Microbiology and Molecular Biology Reviews*, *71*(2), 348-376.

Blaise, F., Rémy, E., Meyer, M., Zhou, L., Narcy, J. P., Roux, J., ... & Rouxel, T. (2007). A critical assessment of *Agrobacterium tumefaciens*-mediated transformation as a tool for pathogenicity gene discovery in the phytopathogenic fungus *Leptosphaeria maculans*. *Fungal Genetics and Biology*, *44*(2), 123-138.

Bowler, J., Scott, E., Tailor, R., Scalliet, G., Ray, J., & Csukai, M. (2010). New capabilities for *Mycosphaerella graminicola* research. *Molecular plant pathology*, *11*(5), 691-704.

Boyce, K. J., & Andrianopoulos, A. (2015). Fungal dimorphism: the switch from hyphae to yeast is a specialized morphogenetic adaptation allowing colonization of a host. *FEMS microbiology reviews*, fuv035.

Boyce, K. J., Cao, C., & Andrianopoulos, A. (2016). Two-Component Signaling Regulates Osmotic Stress Adaptation via SskA and the High-Osmolarity Glycerol MAPK Pathway in the Human Pathogen *Talaromyces marneffei*. *mSphere*, *1*(1), e00086-15.

Brand, A. C., Morrison, E., Milne, S., Gonia, S., Gale, C. A., & Gow, N. A. (2014). Cdc42 GTPase dynamics control directional growth responses. *Proceedings of the National Academy of Sciences*, *111*(2), 811-816.

Brennwald, P., & Rossi, G. (2007). Spatial regulation of exocytosis and cell polarity: yeast as a model for animal cells. *FEBS letters*, *581*(11), 2119-2124.

Brunner, P. C., Torriani, S. F., Croll, D., Stukenbrock, E. H., & McDonald, B. A. (2013). Coevolution and life cycle specialization of plant cell wall degrading enzymes in a hemibiotrophic pathogen. *Molecular biology and evolution*, mst041.

Buffo, J., Herman, M. A., & Soll, D. R. (1984). A characterization of pH-regulated dimorphism in *Candida albicans*. *Mycopathologia*, *85*(1-2), 21-30.

Calcagno-Pizarelli, A. M., Hervás-Aguilar, A., Galindo, A., Abenza, J. F., Peñalva, M. A., & Arst, H. N. (2011). Rescue of *Aspergillus nidulans* severely debilitating null mutations in ESCRT-0, I, II and III genes by inactivation of a salt-tolerance pathway allows examination of ESCRT gene roles in pH signalling. *J Cell Sci*, *124*(23), 4064-4076.

Calera, J. A., Herman, D., & Calderone, R. (2000). Identification of YPD1, a gene of *Candida albicans* which encodes a two-component phosphohistidine intermediate protein. *Yeast*, *16*(11), 1053-1059.

Carillo, P., Annunziata, M. G., Pontecorvo, G., Fuggi, A., & Woodrow, P. (2011). Salinity stress and salt tolerance. *Abiotic Stress Plants-Mech. Adapt.*

Carroll, A. M., Sweigard, J. A., & Valent, B. (1994). Improved vectors for selecting resistance to hygromycin. *Fungal Genetics Reports*, *41*(1), 22.

Carswell, G. (1997). Agricultural intensification and rural sustainable livelihoods: a 'think piece'.

Cereghino, G. P. L., Cereghino, J. L., Sunga, A. J., Johnson, M. A., Lim, M., Gleeson, M. A., & Cregg, J. M. (2001). New selectable marker/auxotrophic host strain combinations for molecular genetic manipulation of *Pichia pastoris*. *Gene*, *263*(1), 159-169.

Chauhan, N., Inglis, D., Roman, E., Pla, J., Li, D., Calera, J. A., & Calderone, R. (2003). *Candida albicans* response regulator gene SSK1 regulates a subset of genes whose functions are associated with cell wall biosynthesis and adaptation to oxidative stress. *Eukaryotic cell*, *2*(5), 1018-1024.

Cheetham, B. F., & Katz, M. E. (2000). Analysis of two *Aspergillus nidulans* genes encoding extracellular proteases. *Fungal Genetics and Biology*, *29*(3), 201-210.

Cheetham, J., Smith, D. A., da Silva Dantas, A., Doris, K. S., Patterson, M. J., Bruce, C. R., & Quinn, J. (2007). A single MAPKKK regulates the Hog1 MAPK pathway in the pathogenic fungus *Candida albicans*. *Molecular biology of the cell*, *18*(11), 4603-4614.

Chen, C. G., Yang, Y. L., Shih, H. I., Su, C. L., & Lo, H. J. (2004). CaNdt80 is involved in drug resistance in *Candida albicans* by regulating CDR1. *Antimicrobial agents and chemotherapy*, *48*(12), 4505-4512.

Choi, Y. E., & Goodwin, S. B. (2011). Gene encoding a c-type cyclin in *Mycosphaerella graminicola* is involved in aerial mycelium formation, filamentous growth, hyphal swelling, melanin biosynthesis, stress response, and pathogenicity. *Molecular plant-microbe interactions*, *24*(4), 469-477.

Choi, Y. E., & Goodwin, S. B. (2011). MVE1, encoding the velvet gene product homolog in *Mycosphaerella graminicola*, is associated with aerial mycelium formation, melanin biosynthesis, hyphal swelling, and light signaling. *Applied and environmental microbiology*, *77*(3), 942-953.

Chumley, F. G., & Valent, B. (1990). Genetic analysis of melanin-deficient, nonpathogenic mutants of *Magnaporthe grisea*. *Mol. Plant-Microbe Interact*, *3*(3), 135-143.

Chungu, C., Gilbert, J., & Townley-Smith, F. (2001). *Septoria tritici* blotch development as affected by temperature, duration of leaf wetness, inoculum concentration, and host. *Plant disease*, *85*(4), 430-435.

Cohen, L., & Eyal, Z. (1993). The histology of processes associated with the infection of resistant and susceptible wheat cultivars with *Septoria tritici*. *Plant Pathology*, *42*(5), 737-743.

Conesa, A., & Götz, S. (2008). Blast2GO: A comprehensive suite for functional analysis in plant genomics. *International journal of plant genomics*, 2008.

Cools, H. J., & Fraaije, B. A. (2008). Are azole fungicides losing ground against *Septoria* wheat disease? Resistance mechanisms in *Mycosphaerella graminicola*. *Pest management science*, *64*(7), 681-684.

Cooper, G. M. (2000). Regulation of transcription in eukaryotes. *The Cell: A Molecular Approach. 2nd Edition*,(Sinauer Associates).

Cousin, A., Mehrabi, R., Guilleroux, M., Dufresne, M., Van der Lee, T., Waalwijk, C., ... & Kema, G. H. (2006). The MAP kinase-encoding gene MgFus3 of the non-appressorium phytopathogen *Mycosphaerella graminicol*a is required for penetration and *in vitro* pycnidia formation. *Molecular plant pathology*, *7*(4), 269-278.

Cullen, P. J., & Sprague, G. F. (2012). The regulation of filamentous growth in yeast. *Genetics*, *190*(1), 23-49.

Darling, A. C., Mau, B., Blattner, F. R., & Perna, N. T. (2004). Mauve: multiple alignment of conserved genomic sequence with rearrangements. *Genome research*, *14*(7), 1394-1403.

De Groot, M. J., Bundock, P., Hooykaas, P. J., & Beijersbergen, A. G. (1998). *Agrobacterium tumefaciens*-mediated transformation of filamentous fungi. *Nature biotechnology*, 16.

Dean, R., Van Kan, J. A., Pretorius, Z. A., Hammond-Kosack, K. E., Di Pietro, A., Spanu, P. D., ... & Foster, G. D. (2012). The Top 10 fungal pathogens in molecular plant pathology. *Molecular plant pathology*, *13*(4), 414-430.

Deller, S., Hammond-Kosack, K. E., & Rudd, J. J. (2011). The complex interactions between host immunity and non-biotrophic fungal pathogens of wheat leaves. *Journal of plant physiology*, *168*(1), 63-71.

Denisov, Y., Yarden, O., & Freeman, S. (2005). Impaired purine biosynthesis affects pathogenicity of *Fusarium oxysporum* f. sp. *melonis*. *European journal of plant pathology*, *112*(3), 293-297.

Dexter, J. P., Xu, P., Gunawardena, J., & McClean, M. N. (2015). Robust network structure of the Sln1-Ypd1-Ssk1 three-component phospho-relay prevents unintended activation of the HOG MAPK pathway in *Saccharomyces cerevisiae*. *BMC systems biology*, *9*(1), 17.

DeZwaan, T. M., Carroll, A. M., Valent, B., & Sweigard, J. A. (1999). *Magnaporthe grisea* pth11p is a novel plasma membrane protein that mediates appressorium differentiation in response to inductive substrate cues. *The Plant Cell*, *11*(10), 2013-2030.

Ding, C., Yin, J., Tovar, E. M. M., Fitzpatrick, D. A., Higgins, D. G., & Thiele, D. J. (2011). The copper regulon of the human fungal pathogen *Cryptococcus neoformans* H99. *Molecular microbiology*, *81*(6), 1560-1576.

Dimmer, K. S., Fritz, S., Fuchs, F., Messerschmitt, M., Weinbach, N., Neupert, W., & Westermann, B. (2002). Genetic Basis of Mitochondrial Function and Morphology in *Saccharomyces cerevisiae*. *Molecular biology of the cell*, *13*(3), 847-853.

Dixon, K. P., Xu, J. R., Smirnoff, N., & Talbot, N. J. (1999). Independent signaling pathways regulate cellular turgor during hyperosmotic stress and appressorium-mediated plant infection by *Magnaporthe grisea*. *The Plant Cell*, *11*(10), 2045-2058.

do Amaral, A. M., Antoniw, J., Rudd, J. J., & Hammond-Kosack, K. E. (2012). Defining the predicted protein secretome of the fungal wheat leaf pathogen *Mycosphaerella graminicola*. *PLoS One*, *7*(12), e49904.

Donnelly, S. F., Pocklington, M. J., Pallotta, D., & Orr, E. (1993). A proline-rich protein, verprolin, involved in cytoskeletal organization and cellular growth in the yeast *Saccharomyces cerevisiae*. *Molecular microbiology*, *10*(3), 585-596.

Du, C., Sarfati, J., Latge, J. P., & Calderone, R. (2006). The role of the sakA (Hog1) and tcsB (sln1) genes in the oxidant adaptation of *Aspergillus fumigatus*. *Medical mycology*, *44*(3), 211-218.

Duncan, K. E., & Howard, R. J. (2000). Cytological analysis of wheat infection by the leaf blotch pathogen *Mycosphaerella graminicola*. *Mycological research*, *104*(09), 1074-1082.

Duncan, C. D., & Mata, J. (2014). Cotranslational protein-RNA associations predict protein-protein interactions. *BMC genomics*, *15*(1), 298.

Edgar, R., Domrachev, M., & Lash, A. E. (2002). Gene Expression Omnibus: NCBI gene expression and hybridization array data repository. *Nucleic acids research*, *30*(1), 207-210.

Edgar, Robert C. (2004). MUSCLE: multiple sequence alignment with high accuracy and high throughput, *Nucleic Acids Research*, *32*(5), 1792-97.

Eisman, B., Alonso-Monge, R., Roman, E., Arana, D., Nombela, C., & Pla, J. (2006). The Cek1 and Hog1 mitogen-activated protein kinases play complementary roles in cell wall biogenesis and chlamydospore formation in the fungal pathogen *Candida albicans*. *Eukaryotic Cell*, *5*(2), 347-358.

Erwig, L. P., & Gow, N. A. (2016). Interactions of fungal pathogens with phagocytes. *Nature Reviews Microbiology*, *14*(3), 163-176.

Estep, L. K., Zala, M., Anderson, N. P., Sackett, K. E., Flowers, M., McDonald, B. A., & Mundt, C. C. (2015). First report of resistance to QoI fungicides in North American populations of *Zymoseptoria tritici*, causal agent of *Septoria tritici* blotch of wheat. *Advances in Applied Microbiology*, *29*, 92.

Eyal, Z. (1987). The *Septoria* diseases of wheat: concepts and methods of disease management. *Cimmyt.*

Fan, R., Klosterman, S. J., Wang, C., Subbarao, K. V., Xu, X., Shang, W., & Hu, X. (2017). Vayg1 is required for microsclerotium formation and melanin production in *Verticillium dahliae*. *Fungal Genetics and Biology*, *98*, 1-11.

Fayed, T. B., El-Sarag, E. I., Hassanein, M. K., & Magdy, A. (2015). Evaluation and prediction of some wheat cultivars productivity in relation to different sowing dates under North Sinai region conditions. *Annals of Agricultural Sciences*, *60*(1), 11-20.

Fesel, P. H., & Zuccaro, A. (2016). β-glucan: crucial component of the fungal cell wall and elusive MAMP in plants. *Fungal Genetics and Biology*, *90*, 53-60.

Fernandez, J., Yang, K. T., Cornwell, K. M., Wright, J. D., & Wilson, R. A. (2013). Growth in rice cells requires de novo purine biosynthesis by the blast fungus *Magnaporthe oryzae*. *Scientific reports*, *3*, 2398.

Floros, J. D., Newsome, R., Fisher, W., Barbosa-Cánovas, G. V., Chen, H., Dunne, C. P., ... & Knabel, S. J. (2010). Feeding the world today and tomorrow: the importance of food science and technology. *Comprehensive Reviews in Food Science and Food Safety*, *9*(5), 572-599.

Flowers, J. L., & Vaillancourt, L. J. (2005). Parameters affecting the efficiency of *Agrobacterium tumefaciens*-mediated transformation of *Colletotrichum graminicola*. *Current genetics*, *48*(6), 380-388.

Fones, H., & Gurr, S. (2015). The impact of *Septoria tritici* Blotch disease on wheat: an EU perspective. *Fungal Genetics and Biology*, *79*, 3-7.

Fonzi, W. A. (2002). Role of pH response in *Candida albicans* virulence. *Mycoses*, *45*(S1), 16-21.

Fraaije, B. A., Cools, H. J., Fountaine, J., Lovell, D. J., Motteram, J., West, J. S., & Lucas, J. A. (2005). Role of ascospores in further spread of QoI-resistant cytochrome b alleles (G143A) in field populations of *Mycosphaerella graminicola*. *Phytopathology*, *95*(8), 933-941.

Franceschetti, M., Bueno, E., Wilson, R. A., Tucker, S. L., Gómez-Mena, C., Calder, G., & Sesma, A. (2011). Fungal virulence and development is regulated by alternative pre-mRNA 3′ end processing in *Magnaporthe oryzae*. *PLoS Pathog*, *7*(12), e1002441.

Frazier, A. E., Taylor, R. D., Mick, D. U., Warscheid, B., Stoepel, N., Meyer, H. E., ... & Rehling, P. (2006). Mdm38 interacts with ribosomes and is a component of the mitochondrial protein export machinery. *J Cell Biol*, *172*(4), 553-564.

Gasch, A. P. (2007). Comparative genomics of the environmental stress response in ascomycete fungi. *Yeast*, *24*(11), 961-976.

Gauthier, G., & Klein, B. S. (2008). Insights into Fungal Morphogenesis and Immune Evasion: Fungal conidia, when situated in mammalian lungs, may switch from mold to pathogenic yeasts or spore-forming spherules. *Microbe* (Washington, DC), *3*(9), 416.

Gauthier, G. M. (2015). Dimorphism in fungal pathogens of mammals, plants, and insects. *PLoS Pathog*, *11*(2), e1004608.

Gavrias, V., Andrianopoulos, A., Gimeno, C. J., & Timberlake, W. E. (1996). *Saccharomyces cerevisiae* TEC1 is required for pseudohyphal growth. *Molecular microbiology*, *19*(6), 1255-1263.

Gibson, D. G., Young, L., Chuang, R. Y., Venter, J. C., Hutchison, C. A., & Smith, H. O. (2009). Enzymatic assembly of DNA molecules up to several hundred kilobases. *Nature methods*, *6*(5), 343-345.

Gill, S. S. (2013). Crop improvement under adverse conditions. N. Tuteja (Ed.). *New York*: Springer.

Gold, S., Duncan, G., Barrett, K., & Kronstad, J. (1994). cAMP regulates morphogenesis in the fungal pathogen *Ustilago maydis*. *Genes & Development*, *8*(23), 2805-2816.

Goodwin, S. B., M'barek, S. B., Dhillon, B., Wittenberg, A. H., Crane, C. F., Hane, J. K., ... & Antoniw, J. (2011). Finished genome of the fungal wheat pathogen *Mycosphaerella graminicola* reveals dispensome structure, chromosome plasticity, and stealth pathogenesis. *PLoS Genet*, *7*(6), e1002070.

Greenspan, P., Mayer, E. P., & Fowler, S. D. (1985). Nile red: a selective fluorescent stain for intracellular lipid droplets. *The Journal of cell biology*, *100*(3), 965-973.

Grishin, N. V. (1998). The R3H motif: a domain that binds single-stranded nucleic acids. *Trends in biochemical sciences*, *23*(9), 329-330.

Hagiwara, D., Asano, Y., Marui, J., Yoshimi, A., Mizuno, T., & Abe, K. (2009). Transcriptional profiling for *Aspergillus nidulans* HogA MAPK signaling pathway in response to fludioxonil and osmotic stress. *Fungal Genetics and Biology*, *46*(11), 868-878.

Hamel, L. P., Nicole, M. C., Duplessis, S., & Ellis, B. E. (2012). Mitogen-activated protein kinase signaling in plant-interacting fungi: distinct messages from conserved messengers. *The Plant Cell*, *24*(4), 1327-1351.

Hamer, J. E., & Talbot, N. J. (1998). Infection-related development in the rice blast fungus *Magnaporthe grisea*. *Current opinion in microbiology*, *1*(6), 693-697.

Hammond-Kosack, K., & Jones, J. D. (2000). Responses to plant pathogens. Biochemistry and molecular biology of plants, 1, 1102-1156.

Hammond-Kosack, K. E., & Rudd, J. J. (2008). Plant resistance signalling hijacked by a necrotrophic fungal pathogen. *Plant signaling & behavior*, *3*(11), 993-995.

Hardwick, N. V., Jones, D. R., & Slough, J. E. (2001). Factors affecting diseases of winter wheat in England and Wales, 1989–98. *Plant Pathology*,*50*(4), 453-462.

Herms, D. A., & Mattson, W. J. (1992). The dilemma of plants: to grow or defend. *The quarterly review of biology*, *67*(3), 283-335.

Höglund, A., Dönnes, P., Blum, T., Adolph, H. W., & Kohlbacher, O. (2006). MultiLoc: prediction of protein subcellular localization using N-terminal targeting sequences, sequence motifs and amino acid composition.

Hordyjewska, A., Popiołek, Ł., & Kocot, J. (2014). The many "faces" of copper in medicine and treatment. *Biometals*, *27*(4), 611-621.

Horie, T., Tatebayashi, K., Yamada, R., & Saito, H. (2008). Phosphorylated Ssk1 prevents unphosphorylated Ssk1 from activating the Ssk2 mitogen-activated protein kinase kinase kinase in the yeast high-osmolarity glycerol osmoregulatory pathway. *Molecular and cellular biology*, *28*(17), 5172-5183.

Howard, R. J., & Ferrari, M. A. (1989). Role of melanin in appressorium function. *Experimental Mycology*, *13*(4), 403-418.

Hilu, H. M., & BEVEE, W. (1957). Inoculation, oversummering, and susceptpathogen relationship of *Septoria tritici* on *Triticum* species. *Phytopathology*, *47*(8), 474-480.

Hung, C. Y., Seshan, K. R., Yu, J. J., Schaller, R., Xue, J., Basrur, V., ... & Cole, G. T. (2005). A metalloproteinase of *Coccidioides posadasii* contributes to evasion of host detection. *Infection and immunity*, *73*(10), 6689-6703.

Hunter, T., Coker, R. R., & Royle, D. J. (1999). The teleomorph stage, *Mycosphaerella graminicola*, in epidemics of *Septoria tritici* blotch on winter wheat in the UK. *Plant Pathology*, *48*(1), 51-57.

Hurley, J. H., & Hanson, P. I. (2010). Membrane budding and scission by the ESCRT machinery: it's all in the neck. *Nature reviews Molecular cell biology*, *11*(8), 556-566.

Hutchison, E. A., & Glass, N. L. (2010). Meiotic regulators Ndt80 and ime2 have different roles in *Saccharomyces* and *Neurospora*. *Genetics*, *185*(4), 1271-1282.

Islam, M. N., Nizam, S., & Verma, P. K. (2012). A highly efficient *Agrobacterium* mediated transformation system for chickpea wilt pathogen *Fusarium oxysporum* f. sp. *ciceri* using DsRed-Express to follow root colonisation. *Microbiological research*, *167*(6), 332-338.

Izumitsu, K., Yoshimi, A., & Tanaka, C. (2007). Two-component response regulators Ssk1p and Skn7p additively regulate high-osmolarity adaptation and fungicide sensitivity in *Cochliobolus heterostrophus*. *Eukaryotic cell*, *6*(2), 171-181.

Jacob, S., Foster, A. J., Yemelin, A., & Thines, E. (2015). High osmolarity glycerol (HOG) signalling in *Magnaporthe oryzae*: Identification of MoYPD1 and its role in osmoregulation, fungicide action, and pathogenicity. *Fungal biology*, *119*(7), 580-594.

Jezewski, S., von der Heide, M., Poltermann, S., Härtl, A., Künkel, W., Zipfel, P. F., & Eck, R. (2007). Role of the Vps34p-interacting protein Ade5, 7p in hyphal growth and virulence of *Candida albicans*. *Microbiology*, *153*(7), 2351-2362.

Jiang, L., Zhao, J., Guo, R., Li, J., Yu, L., & Xu, D. (2010). Functional characterization and virulence study of ADE8 and GUA1 genes involved in the de novo purine biosynthesis in *Candida albicans*. *FEMS yeast research*, *10*(2), 199-208.

Jezewski, S., von der Heide, M., Poltermann, S., Härtl, A., Künkel, W., Zipfel, P. F., & Eck, R. (2007). Role of the Vps34p-interacting protein Ade5, 7p in hyphal growth and virulence of *Candida albicans*. *Microbiology*, *153*(7), 2351-2362.

Jin, F. J., Maruyama, J. I., Juvvadi, P. R., Arioka, M., & Kitamoto, K. (2004). Development of a novel quadruple auxotrophic host transformation system by argB gene disruption using adeA gene and exploiting adenine auxotrophy in *Aspergillus oryzae*. *FEMS microbiology letters*, *239*(1), 79-85.

Jones, E. W., & Fink, G. R. (1982). Regulation of amino acid and nucleotide biosynthesis in yeast. *Cold Spring Harbor Monograph Archive*, *11*, 181-299.

Jørgensen, L. N., Secher, B. J., & Hossy, H. (1999). Decision support systems featuring *Septoria* management. *Septoria* on Cereals: a Study of Pathosystems. JA Lucas, P. Bowyer, and HM Anderson (eds.). CABI Publishing, Wallingford, UK, 251-262.

Jørgensen, L. N., Hovmøller, M. S., Hansen, J. G., Lassen, P., Clark, B., Bayles, R., ... & Czembor, J. J. (2014). IPM Strategies and Their Dilemmas Including an Introduction to www. eurowheat. org. *Journal of Integrative Agriculture*, *13*(2), 265-281.

Kahmann, R., Basse, C., & Feldbrügge, M. (1999). Fungal–plant signalling in the *Ustilago maydis*–maize pathosystem. *Current opinion in microbiology*, *2*(6), 647-650.

Katz, M. E., Gray, K. A., & Cheetham, B. F. (2006). The *Aspergillus nidulans* xprG (phoG) gene encodes a putative transcriptional activator involved in the response to nutrient limitation. *Fungal Genetics and Biology*, *43*(3), 190-199.

Katz, M. E., Braunberger, K., Yi, G., Cooper, S., Nonhebel, H. M., & Gondro, C. (2013). A p53-like transcription factor similar to Ndt80 controls the response to nutrient stress in the filamentous fungus, *Aspergillus nidulans*. *F1000Research*, 2.

Katz, M. E., & Cooper, S. (2015). Extreme diversity in the regulation of Ndt80-like transcription factors in fungi. *G3: Genes| Genomes| Genetics*, *5*(12), 2783-2792.

Katzmann, D. J., Stefan, C. J., Babst, M., & Emr, S. D. (2003). Vps27 recruits ESCRT machinery to endosomes during MVB sorting. *J Cell Biol*, *162*(3), 413-423.

Kaye, S. B. (1998). New antimetabolites in cancer chemotherapy and their clinical impact. *British journal of cancer*, *78*(Suppl 3), 1.

Kearse, M., Moir, R., Wilson, A., Stones-Havas, S., Cheung, M., Sturrock, S., ... & Thierer, T. (2012). Geneious Basic: an integrated and extendable desktop software platform for the organization and analysis of sequence data. *Bioinformatics*, *28*(12), 1647-1649.

Kelley, L. A., Mezulis, S., Yates, C. M., Wass, M. N., & Sternberg, M. J. (2015). The Phyre2 web portal for protein modeling, prediction and analysis. *Nature protocols*, *10*(6), 845-858.

Kellner, R., Bhattacharyya, A., Poppe, S., Hsu, T. Y., Brem, R. B., & Stukenbrock, E. H. (2014). Expression profiling of the wheat pathogen *Zymoseptoria tritici* reveals genomic patterns of transcription and host-specific regulatory programs. *Genome biology and evolution*, *6*(6), 1353-1365.

Kema, G. H., Yu, D., Rijkenberg, F. H., Shaw, M. W., & Baayen, R. P. (1996). Histology of the pathogenesis of *Mycosphaerella graminicola* in wheat. *Phytopathology*, *86*(7), 777-786.

Kilaru, S., Schuster, M., Latz, M., Guo, M., & Steinberg, G. (2015). Fluorescent markers of the endocytic pathway in *Zymoseptoria tritici*. *Fungal Genetics and Biology*, *79*, 150-157.

Kilaru, S., & Steinberg, G. (2015). Yeast recombination-based cloning as an efficient way of constructing vectors for *Zymoseptoria tritici*. *Fungal Genetics and Biology*, *79*, 76-83.

Kim, J. E., Myong, K., Shim, W. B., Yun, S. H., & Lee, Y. W. (2007). Functional characterization of acetylglutamate synthase and phosphoribosylamine-glycine ligase genes in *Gibberella zeae*. *Current genetics*, *51*(2), 99-108.

Klein, B. S., & Tebbets, B. (2007). Dimorphism and virulence in fungi. *Current opinion in microbiology*, *10*(4), 314-319.

Kleinboelting, N., Huep, G., Appelhagen, I., Viehoever, P., Li, Y., & Weisshaar, B. (2015). The structural features of thousands of T-DNA insertion sites are consistent with a double-strand break repair-based insertion mechanism. *Molecular plant*, *8*(11), 1651-1664.

Klengel, T., Liang, W. J., Chaloupka, J., Ruoff, C., Schröppel, K., Naglik, J. R., ... & Levin, L. R. (2005). Fungal adenylyl cyclase integrates CO 2 sensing with cAMP signaling and virulence. Current Biology, 15(22), 2021-2026.

Kojima, K., Takano, Y., Yoshimi, A., Tanaka, C., Kikuchi, T., & Okuno, T. (2004). Fungicide activity through activation of a fungal signalling pathway. *Molecular microbiology*, *53*(6), 1785-1796.

Korn, M., Schmidpeter, J., Dahl, M., Müller, S., Voll, L. M., & Koch, C. (2015). A genetic screen for pathogenicity genes in the hemibiotrophic fungus *Colletotrichum higginsianum* identifies the plasma membrane proton pump Pma2 required for host penetration. *PloS one*, *10*(5), e0125960.

Kosugi S., Hasebe M., Tomita M., and Yanagawa H. (2009). Systematic identification of yeast cell cycle-dependent nucleocytoplasmic shuttling proteins by prediction of composite motifs. *Proc. Natl. Acad. Sci. USA 106*, 10171-10176.

Kramer, B., Thines, E., & Foster, A. J. (2009). MAP kinase signalling pathway components and targets conserved between the distantly related plant pathogenic fungi *Mycosphaerella graminicola* and *Magnaporthe grisea*. *Fungal Genetics and Biology*, *46*(9), 667-681.

Krishnamurthy, S., Plaine, A., Albert, J., Prasad, T., Prasad, R., & Ernst, J. F. (2004). Dosage-dependent functions of fatty acid desaturase Ole1p in growth and morphogenesis of *Candida albicans*. *Microbiology*, *150*(6), 1991-2003.

Krüger, J., Loubradou, G., Regenfelder, E., Hartmann, A., & Kahmann, R. (1998). Crosstalk between cAMP and pheromone signalling pathways in *Ustilago maydis*. *Molecular and General Genetics MGG*, *260*(2), 193-198.

Kubo, Y., Takano, Y., Endo, N., Yasuda, N., Tajima, S., & Furusawa, I. (1996). Cloning and structural analysis of the melanin biosynthesis gene SCD1 encoding scytalone dehydratase in *Colletotrichum lagenarium*. *Applied and environmental microbiology*, *62*(12), 4340-4344.

Kupiec, M., Byers, B., Esposito, R. E., & Mitchell, A. P. (1997). 11 Meiosis and Sporulation in *Saccharomyces cerevisiae*. *Cold Spring Harbor Monograph Archive*, *21*, 889-1036.

Kwon, N. J., Garzia, A., Espeso, E. A., Ugalde, U., & Yu, J. H. (2010). FlbC is a putative nuclear C2H2 transcription factor regulating development in *Aspergillus nidulans*. *Molecular microbiology*, *77*(5), 1203-1219.

Lamoureux, J. S., & Glover, J. M. (2006). Principles of protein-DNA recognition revealed in the structural analysis of Ndt80-MSE DNA complexes. *Structure*, *14*(3), 555-565.

Larkin, M. A., Blackshields, G., Brown, N. P., Chenna, R., McGettigan, P. A., McWilliam, H., ... & Thompson, J. D. (2007). Clustal W and Clustal X version 2.0. *bioinformatics*, *23*(21), 2947-2948.

Laufer Julian (2015). „Untersuchungen zum Dimorphismus und Identifizierung von Pathogenitätsfaktoren in *Zymoseptoria tritici*“. (Master thesis)

Leberer, E., Harcus, D., Dignard, D., Johnson, L., Ushinsky, S., Thomas, D. Y., & Schröppel, K. (2001). Ras links cellular morphogenesis to virulence by regulation of the MAP kinase and cAMP signalling pathways in the pathogenic fungus *Candida albicans*. *Molecular microbiology*, *42*(3), 673-687.

Leclerque, A., Wan, H., Abschütz, A., Chen, S., Mitina, G. V., Zimmermann, G., & Schairer, H. U. (2004). *Agrobacterium*-mediated insertional mutagenesis (AIM) of the entomopathogenic fungus *Beauveria bassiana*. *Current genetics*, *45*(2), 111-119.

Lee, W. S., Rudd, J. J., & Kanyuka, K. (2015). Virus induced gene silencing (VIGS) for functional analysis of wheat genes involved in *Zymoseptoria tritici* susceptibility and resistance. *Fungal Genetics and Biology*, 79, 84-88.

Leidich, S. D., Ibrahim, A. S., Fu, Y., Koul, A., Jessup, C., Vitullo, J., ... & Ghannoum, M. A. (1998). Cloning and disruption of caPLB1, a phospholipase B gene involved in the pathogenicity of *Candida albicans*. *Journal of Biological Chemistry*, *273*(40), 26078-26086.

Leroux, P., & Walker, A. S. (2011). Multiple mechanisms account for resistance to sterol 14α-demethylation inhibitors in field isolates of *Mycosphaerella graminicola*. *Pest management science*, *67*(1), 44-59.

Li, D., Bobrowicz, P., Wilkinson, H. H., & Ebbole, D. J. (2005). A mitogen-activated protein kinase pathway essential for mating and contributing to vegetative growth in *Neurospora crassa*. *Genetics*, *170*(3), 1091-1104.

Livak, K. J., & Schmittgen, T. D. (2001). Analysis of relative gene expression data using real-time quantitative PCR and the $2^{-\Delta\Delta CT}$ method. *methods*, *25*(4), 402-408.

Lovell, D. J., Parker, S. R., Hunter, T., Royle, D. J., & Coker, R. R. (1997). Influence of crop growth and structure on the risk of epidemics by *Mycosphaerella graminicola* (*Septoria tritici*) in winter wheat. *Plant Pathology*, *46*(1), 126-138.

Lu, Q., Hope, L. W., Brasch, M., Reinhard, C., & Cohen, S. N. (2003). TSG101 interaction with HRS mediates endosomal trafficking and receptor down-regulation. *Proceedings of the National Academy of Sciences*, *100*(13), 7626-7631.

Madhani, H. D., & Fink, G. R. (1998). The control of filamentous differentiation and virulence in fungi. *Trends in cell biology*, *8*(9), 348-353.

Madrid, M., Soto, T., Franco, A., Paredes, V., Vicente, J., Hidalgo, E., ... & Cansado, J. (2004). A cooperative role for Atf1 and Pap1 in the detoxification of the oxidative stress induced by glucose deprivation in *Schizosaccharomyces pombe*. *Journal of Biological Chemistry*, *279*(40), 41594-41602.

Maidan, M. M., De Rop, L., Serneels, J., Exler, S., Rupp, S., Tournu, H., ... & Van Dijck, P. (2005). The G protein-coupled receptor Gpr1 and the Gα protein Gpa2 act through the cAMP-protein kinase A pathway to induce morphogenesis in *Candida albicans*. *Molecular biology of the cell*, *16*(4), 1971-1986.

Maloy, O. C. (2005). Plant disease management. *The plant health instructor*, *10*.

Maresca, B., & Kobayashi, G. S. (1989). Dimorphism in *Histoplasma capsulatum*: a model for the study of cell differentiation in pathogenic fungi. *Microbiological reviews*, *53*(2), 186-209.

Marshall, R., Kombrink, A., Motteram, J., Loza-Reyes, E., Lucas, J., Hammond-Kosack, K. E., ... & Rudd, J. J. (2011). Analysis of two in planta expressed LysM effector homologs from the fungus *Mycosphaerella graminicola* reveals novel functional properties and varying contributions to virulence on wheat. *Plant physiology*, *156*(2), 756-769.

Martín, V., Rodríguez-Gabriel, M. A., McDonald, W. H., Watt, S., Yates, J. R., Bähler, J., & Russell, P. (2006). Cip1 and Cip2 are novel RNA-recognition-motif proteins that counteract Csx1 function during oxidative stress. *Molecular biology of the cell*, *17*(3), 1176-1183.

Matheis, S., Yemelin, A., Scheps, D., Andresen, K., Jacob, S., Thines, E., & Foster, A. J. (2017). Functions of the *Magnaporthe oryzae* Flb3p and Flb4p transcription factors in the regulation of conidiation. *Microbiological Research*.

Mayorga, M. E., & Gold, S. E. (1999). A MAP kinase encoded by the ubc3 gene of *Ustilago maydis* is required for filamentous growth and full virulence. *Molecular microbiology*, *34*(3), 485-497.

M'Barek, S. B., Cordewener, J. H., van der Lee, T. A., America, A. H., Gohari, A. M., Mehrabi, R., ... & Kema, G. H. (2015). Proteome catalog of *Zymoseptoria tritici* captured during pathogenesis in wheat. *Fungal Genetics and Biology*, *79*, 42-53.

McDonald, M. C., McDonald, B. A., & Solomon, P. S. (2015). Recent advances in the *Zymoseptoria tritici*–wheat interaction: insights from pathogenomics. *Frontiers in plant science*, *6*, 102.

McGranahan, G., & Tacoli, C. (2006). Rural-urban migration in China: policy options for economic growth, environmental sustainability and equity (Vol. 12). IIED.

McKenzie, R., Schuchert, P., & Kilbey, B. (1987). Sequence of the bifunctional ade1 gene in the purine biosynthetic pathway of the fission yeast *Schizosaccharomyces pombe*. *Current genetics*, *12*(8), 591-597.

McLain, N., & Dolan, J. W. (1997). Phospholipase D activity is required for dimorphic transition in *Candida albicans*. *Microbiology*, *143*(11), 3521-3526.

Mehrabi, R., Zwiers, L. H., de Waard, M. A., & Kema, G. H. (2006). MgHog1 regulates dimorphism and pathogenicity in the fungal wheat pathogen *Mycosphaerella graminicola*. *Molecular Plant-Microbe Interactions*, *19*(11), 1262-1269.

Mehrabi, R., van der Lee, T., Waalwijk, C., & Kema, G. H. (2006). MgSlt2, a cellular integrity MAP kinase gene of the fungal wheat pathogen *Mycosphaerella graminicola*, is dispensable for penetration but essential for invasive growth. *Molecular Plant-Microbe Interactions*, *19*(4), 389-398.

Mehrabi, R., M'Barek, S. B., van der Lee, T. A., Waalwijk, C., de Wit, P. J., & Kema, G. H. (2009). Gα and Gβ proteins regulate the cyclic AMP pathway that is required for development and pathogenicity of the phytopathogen *Mycosphaerella graminicola*. *Eukaryotic cell*, *8*(7), 1001-1013.

Meng, Y., Patel, G., Heist, M., Betts, M. F., Tucker, S. L., Galadima, N., ... & Xu, J. R. (2007). A systematic analysis of T-DNA insertion events in *Magnaporthe oryzae*. *Fungal Genetics and Biology*, *44*(10), 1050-1064.

Michielse, C. B., Hooykaas, P. J., van den Hondel, C. A., & Ram, A. F. (2005). *Agrobacterium*-mediated transformation as a tool for functional genomics in fungi. *Current genetics*, *48*(1), 1-17.

Michielse, C. B., Hooykaas, P. J., Van Den Hondel, C. A., & Ram, A. F. (2008). *Agrobacterium*-mediated transformation of the filamentous fungus *Aspergillus awamori*. *Nature protocols*, *3*(10), 1671-1678.

Mira, N. P., Lourenço, A. B., Fernandes, A. R., Becker, J. D., & Sá-Correia, I. (2009). The RIM101 pathway has a role in *Saccharomyces cerevisiae* adaptive response and resistance to propionic acid and other weak acids. *FEMS yeast research*, *9*(2), 202-216.

Mirzadi Gohari, A., Mehrabi, R., Robert, O., Ince, I. A., Boeren, S., Schuster, M., ... & Kema, G. H. (2014). Molecular characterization and functional analyses of ZtWor1, a transcriptional regulator of the fungal wheat pathogen *Zymoseptoria tritici*. *Molecular plant pathology*, *15*(4), 394-405.

Monge, R. A., Roman, E., Nombela, C., & Pla, J. (2006). The MAP kinase signal transduction network in *Candida albicans*. *Microbiology*, *152*(4), 905-912.

Morais, D., Laval, V., Sache, I., & Suffert, F. (2015). Comparative pathogenicity of sexual and asexual spores of *Zymoseptoria tritici* (*Septoria tritici* blotch) on wheat leaves. *Plant Pathology*.

Moriwaki, A., Kubo, E., Arase, S., & Kihara, J. (2006). Disruption of SRM1, a mitogen-activated protein kinase gene, affects sensitivity to osmotic and ultraviolet stressors in the phytopathogenic fungus *Bipolaris oryzae*. *FEMS microbiology letters*, *257*(2), 253-261.

Morrow, C. A., Valkov, E., Stamp, A., Chow, E. W., Lee, I. R., Wronski, A., ... & Kobe, B. (2012). De novo GTP biosynthesis is critical for virulence of the fungal pathogen *Cryptococcus neoformans*. *PLoS Pathog*, *8*(10), e1002957.

Motteram, J., Lovegrove, A., Pirie, E., Marsh, J., Devonshire, J., van de Meene, A., ... & Rudd, J. J. (2011). Aberrant protein N-glycosylation impacts upon infection-related growth transitions of the haploid plant-pathogenic fungus *Mycosphaerella graminicola*. *Molecular microbiology*, *81*(2), 415-433.

Mouyna, I., Morelle, W., Vai, M., Monod, M., Léchenne, B., Fontaine, T., ... & Latgé, J. P. (2005). Deletion of GEL2 encoding for a β (1–3) glucanosyltransferase affects morphogenesis and virulence in *Aspergillus fumigatus*. *Molecular microbiology*, *56*(6), 1675-1688.

Muench, S., Ludwig, N., Floss, D. S., Sugui, J. A., Koszucka, A. M., Voll, L. M., ... & Deising, H. B. (2011). Identification of virulence genes in the corn pathogen *Colletotrichum graminicola* by *Agrobacterium tumefaciens*-mediated transformation. *Molecular plant pathology*, *12*(1), 43-55.

Mullins, E. D., Chen, X., Romaine, P., Raina, R., Geiser, D. M., & Kang, S. (2001). *Agrobacterium*-mediated transformation of *Fusarium oxysporum*: an efficient tool for insertional mutagenesis and gene transfer. *Phytopathology*, *91*(2), 173-180.

Nadal, M., García-Pedrajas, M. D., & Gold, S. E. (2008). Dimorphism in fungal plant pathogens. *FEMS Microbiology Letters*, *284*(2), 127-134.

Nagahashi, S., Mio, T., Ono, N., Yamada-Okabe, T., Arisawa, M., Bussey, H., & Yamada-Okabe, H. (1998). Isolation of CaSLN1 and CaNIK1, the genes for osmosensing histidine kinase homologues, from the pathogenic fungus *Candida albicans*. *Microbiology*, *144*(2), 425-432.

Nemecek, J. C., Wüthrich, M., & Klein, B. S. (2006). Global control of dimorphism and virulence in fungi. *Science*, *312*(5773), 583-588.

Nguyen, L. N., & Nosanchuk, J. D. (2011). Lipid droplet formation protects against gluco/lipotoxicity in *Candida parapsilosis*: an essential role of fatty acid desaturase Ole1. *Cell cycle*, *10*(18), 3159-3167.

Nobile, C. J., Solis, N., Myers, C. L., Fay, A. J., Deneault, J. S., Nantel, A., ... & Filler, S. G. (2008). *Candida albicans* transcription factor Rim101 mediates pathogenic interactions through cell wall functions. *Cellular microbiology*, *10*(11), 2180-2196.

Nobile, C. J., Fox, E. P., Nett, J. E., Sorrells, T. R., Mitrovich, Q. M., Hernday, A. D., ... & Johnson, A. D. (2012). A recently evolved transcriptional network controls biofilm development in *Candida albicans*. *Cell*, *148*(1), 126-138.

Nowikovsky, K., Froschauer, E. M., Zsurka, G., Samaj, J., Reipert, S., Kolisek, M., ... & Schweyen, R. J. (2004). The LETM1/YOL027 gene family encodes a factor of the mitochondrial K+ homeostasis with a potential role in the Wolf-Hirschhorn syndrome. *Journal of Biological Chemistry*, *279*(29), 30307-30315.

O'Donnell, A. F., Tiong, S., Nash, D., & Clark, D. V. (2000). The *Drosophila melanogaster* ade5 gene encodes a bifunctional enzyme for two steps in the de novo purine synthesis pathway. *Genetics*, *154*(3), 1239-1253.

O'Driscoll, A., Doohan, F., & Mullins, E. (2015). Exploring the utility of *Brachypodium distachyon* as a model pathosystem for the wheat pathogen *Zymoseptoria tritici*. *BMC research notes*, *8*(1), 132.

Orlowski, M. (1991). *Mucor* dimorphism. *Microbiological reviews*, *55*(2), 234-258.

Orton, E. S., Deller, S., & Brown, J. K. (2011). *Mycosphaerella graminicola*: from genomics to disease control. *Molecular plant pathology*, *12*(5), 413-424.

Palmer, C. L., & Skinner, W. (2002). *Mycosphaerella graminicola*: latent infection, crop devastation and genomics. *Molecular Plant Pathology*, *3*(2), 63-70.

Papai, G., Weil, P. A., & Schultz, P. (2011). New insights into the function of transcription factor TFIID from recent structural studies. *Current opinion in genetics & development*, *21*(2), 219-224.

Park, H. O., & Bi, E. (2007). Central roles of small GTPases in the development of cell polarity in yeast and beyond. *Microbiology and Molecular Biology Reviews*, *71*(1), 48-96.

Pasricha, S., Payne, M., Canovas, D., Pase, L., Ngaosuwankul, N., Beard, S., ... & Andrianopoulos, A. (2013). Cell-Type–Specific Transcriptional Profiles of the Dimorphic Pathogen *Penicillium marneffei* Reflect Distinct Reproductive, Morphological, and Environmental Demands. *G3: Genes| Genomes| Genetics*, *3*(11), 1997-2014.

Paveley, N. D. (1999). Integrating *Septoria* risk variables. *Septoria* on cereals. *A study of pathosystems*, 230-250.

Perez-Nadales, E., Nogueira, M. F. A., Baldin, C., Castanheira, S., El Ghalid, M., Grund, E., ... & Naik, V. (2014). Fungal model systems and the elucidation of pathogenicity determinants. *Fungal Genetics and Biology*, *70*, 42-67.

Perpetua, N. S., Kubo, Y., Yasuda, N., Takano, Y., & Furusawa, I. (1996). Cloning and characterization of a melanin biosynthetic THR1 reductase gene essential for appressorial penetration of *Colletotrichum lagenarium*. *Molecular plant-microbe interactions: MPMI*, *9*(5), 323-329.

Pfaffl, M. W. (2001). A new mathematical model for relative quantification in real-time RT–PCR. *Nucleic acids research*, *29*(9), e45-e45.

Ponomarenko, A., Goodwin, S. B., & Kema, G. H. (2011). *Septoria tritici* blotch (STB) of wheat. *Plant Health Instructor*.

Poppe, S., Dorsheimer, L., Happel, P., & Stukenbrock, E. H. (2015). Rapidly evolving genes are key players in host specialization and virulence of the fungal wheat pathogen *Zymoseptoria tritici* (*Mycosphaerella graminicola*). *PLoS Pathog*, *11*(7), e1005055.

Ravasi, T., Huber, T., Zavolan, M., Forrest, A., Gaasterland, T., Grimmond, S., ... & Riken GER Group. (2003). Systematic characterization of the zinc-finger-containing proteins in the mouse transcriptome. *Genome research*, *13*(6b), 1430-1442.

Rho, H. S., Kang, S., & Lee, Y. H. (2001). *Agrobacterium tumefaciens*-mediated transformation of the plant pathogenic fungus, *Magnaporthe grisea*. *Molecules and cells*, *12*(3), 407-411.

Rice, P., Longden, I., & Bleasby, A. (2000). EMBOSS: the European molecular biology open software suite.

Roberts, R. L., Metz, M., Monks, D. E., Mullaney, M. L., Hall, T., & Nester, E. W. (2003). Purine synthesis and increased *Agrobacterium tumefaciens* transformation of yeast and plants. *Proceedings of the National Academy of Sciences*, *100*(11), 6634-6639.

Robinson, J. T., Thorvaldsdóttir, H., Winckler, W., Guttman, M., Lander, E. S., Getz, G., & Mesirov, J. P. (2011). Integrative genomics viewer. *Nature biotechnology*, *29*(1), 24-26.

Rodríguez-Gabriel, M. A., Burns, G., McDonald, W. H., Martín, V., Yates, J. R., Bähler, J., & Russell, P. (2003). RNA-binding protein Csx1 mediates global control of gene expression in response to oxidative stress. *The EMBO journal*, *22*(23), 6256-6266.

Roetzer, A., Gregori, C., Jennings, A. M., Quintin, J., Ferrandon, D., Butler, G., ... & Schüller, C. (2008). *Candida glabrata* environmental stress response involves *Saccharomyces cerevisiae* Msn2/4 orthologous transcription factors. *Molecular microbiology*, *69*(3), 603-620.

Romano A (1966) Dimorphism. *The Fungi*, Vol. 2 (Ainsworth GC & Sussman AS, eds), pp. 181–209. Academic Press, New York.

Rudd, J. J. (2015). Previous bottlenecks and future solutions to dissecting the *Zymoseptoria tritici*–wheat host-pathogen interaction. *Fungal Genetics and Biology*, *79*, 24-28.

Rudd, J. J., Kanyuka, K., Hassani-Pak, K., Derbyshire, M., Andongabo, A., Devonshire, J., ... & Hooper, J. (2015). Transcriptome and metabolite profiling of the infection cycle of *Zymoseptoria tritici* on wheat reveals a biphasic interaction with plant immunity involving differential pathogen chromosomal contributions and a variation on the hemibiotrophic lifestyle definition. *Plant physiology*, *167*(3), 1158-1185.

Saito, H., & Tatebayashi, K. (2004). Regulation of the osmoregulatory HOG MAPK cascade in yeast. *The Journal of Biochemistry*, *136*(3), 267-272.

Sambrook, J. Russell DW (2001). Molecular cloning: a laboratory manual. *Cold Spring laboratory Press*, new York.

Sánchez-Martínez, C., & Pérez-Martín, J. (2001). Dimorphism in fungal pathogens: *Candida albicans* and *Ustilago maydis* – similar inputs, different outputs. *Current opinion in microbiology*, *4*(2), 214-221.

Sánchez-Vallet, A., McDonald, M. C., Solomon, P. S., & McDonald, B. A. (2015). Is *Zymoseptoria tritici* a hemibiotroph?. *Fungal Genetics and Biology*, *79*, 29-32.

Sanna, M. L., Zara, S., Zara, G., Migheli, Q., Budroni, M., & Mannazzu, I. (2012). *Pichia fermentans* dimorphic changes depend on the nitrogen source. *Fungal biology*, *116*(7), 769-777.

Schamber, A., Leroch, M., Diwo, J., Mendgen, K., & Hahn, M. (2010). The role of mitogen activated protein (MAP) kinase signalling components and the Ste12 transcription factor in germination and pathogenicity of *Botrytis cinerea*. *Molecular plant pathology*, *11*(1), 105-119.

Schmidt, O., & Teis, D. (2012). The ESCRT machinery. *Current Biology*, *22*(4), R116-R120.

Schuster, M., Kilaru, S., Latz, M., & Steinberg, G. (2015). Fluorescent markers of the microtubule cytoskeleton in *Zymoseptoria tritici*. *Fungal Genetics and Biology*, *79*, 141-149.

Schweizer, A., Rupp, S., Taylor, B. N., Röllinghoff, M., & Schröppel, K. (2000). The TEA/ATTS transcription factor CaTec1p regulates hyphal development and virulence in *Candida albicans*. *Molecular microbiology*, *38*(3), 435-445.

Secco, D., Wang, C., Arpat, B. A., Wang, Z., Poirier, Y., Tyerman, S. D., ... & Whelan, J. (2012). The emerging importance of the SPX domain containing proteins in phosphate homeostasis. *New Phytologist*, *193*(4), 842-851.

Sellam, A., Tebbji, F., & Nantel, A. (2009). Role of Ndt80p in sterol metabolism regulation and azole resistance in *Candida albicans*. *Eukaryotic cell*, *8*(8), 1174-1183.

Sellam, A., Askew, C., Epp, E., Tebbji, F., Mullick, A., Whiteway, M., & Nantel, A. (2010). Role of transcription factor CaNdt80p in cell separation, hyphal growth, and virulence in *Candida albicans*. *Eukaryotic cell*, *9*(4), 634-644.

Shannon, P., Markiel, A., Ozier, O., Baliga, N. S., Wang, J. T., Ramage, D., ... & Ideker, T. (2003). Cytoscape: a software environment for integrated models of biomolecular interaction networks. *Genome research*, *13*(11), 2498-2504.

Shaw, M. W., & Royle, D. J. (1989). Airborne inoculum as a major source of *Septoria tritici* (*Mycosphaerella graminicola*) infections in winter wheat crops in the UK. Plant Pathology, *38*(1), 35-43.

Shaw, M. W., & Royle, D. J. (1989). Estimation and validation of a function describing the rate at which *Mycosphaerella graminicola* causes yield loss in winter wheat. *Annals of applied Biology*, *115*(3), 425-442.

Shaw, M. W. (1991). Interacting effects of interrupted humid periods and light on infection of wheat leaves by *Mycosphaerella graminicola* (*Septoria tritici*). *Plant Pathology*, *40*(4), 595-607.

Shaw, M. W., & Royle, D. J. (1993). Factors determining the severity of epidemics of *Mycosphaerella graminicola* (*Septoria tritici*) on winter wheat in the UK. *Plant Pathology*, *42*(6), 882-899.

Shetty, N. P., Kristensen, B. K., Newman, M. A., Møller, K., Gregersen, P. L., & Jørgensen, H. L. (2003). Association of hydrogen peroxide with restriction of *Septoria tritici* in resistant wheat. *Physiological and Molecular Plant Pathology*, *62*(6), 333-346.

Shipton, W. A., Boyd, W. R. J., Rosielle, A. A., & Shearer, B. I. (1971). The common *Septoria* diseases of wheat. The *Botanical Review*, *37*(2), 231-262.

Shrivastava, P., & Kumar, R. (2015). Soil salinity: A serious environmental issue and plant growth promoting bacteria as one of the tools for its alleviation. *Saudi journal of biological sciences*, *22*(2), 123-131.

Sidhu, Y. S., Cairns, T. C., Chaudhari, Y. K., Usher, J., Talbot, N. J., Studholme, D. J., ... & Haynes, K. (2015). Exploitation of sulfonylurea resistance marker and non-homologous end joining mutants for functional analysis in *Zymoseptoria tritici*. *Fungal Genetics and Biology*, *79*, 102-109.

Simon, M. N., De Virgilio, C., Souza, B., & Pringle, J. R. (1995). Role for the Rho-family GTPase Cdc42 in yeast mating-pheromone signal pathway. *Nature*, *376*(6542), 702.

Soković, M. D., Glamočlija, J. M., & Ćirić, A. D. (2013). Natural Products from plants and Fungi as Fungicides. *Fungicides-Showcases of Integrated Plant Disease Management from Around the World*, *In Tech*, 185-232.

Son H, Seo Y-S, Min K, Park AR, Lee J, *et al.* (2011). A phenome-based functional analysis of transcription factors in the cereal head blight fungus, *Fusarium graminearum*. *PLoS Pathog*, *7*(10), e1002310.

Son, H., Kim, M. G., Min, K., Seo, Y. S., Lim, J. Y., Choi, G. J., ... & Lee, Y. W. (2013). AbaA regulates conidiogenesis in the ascomycete fungus *Fusarium graminearum*. *PLoS one*, *8*(9), e72915.

Southern, E. M. (1975). Detection of specific sequences among DNA fragments separated by gel electrophoresis. *Journal of molecular biology*, *98*(3), 503IN3509-508IN5517.

Spain, B. H., Koo, D., Ramakrishnan, M., Dzudzor, B., & Colicelli, J. (1995). Truncated forms of a novel yeast protein suppress the lethality of a G protein α subunit deficiency by interacting with the β subunit. *Journal of Biological Chemistry*, *270*(43), 25435-25444.

Stammler, G., & Semar, M. (2011). Sensitivity of *Mycosphaerella graminicola* (anamorph: *Septoria tritici*) to DMI fungicides across Europe and impact on field performance. *EPPO Bulletin*, *41*(2), 149-155.

Steinbach, W. J., Cramer, R. A., Perfect, B. Z., Asfaw, Y. G., Sauer, T. C., Najvar, L. K., ... & Perfect, J. R. (2006). Calcineurin controls growth, morphology, and pathogenicity in *Aspergillus fumigatus*. *Eukaryotic cell*, *5*(7), 1091-1103.

Steinberg, G. (2014). Endocytosis and early endosome motility in filamentous fungi. *Current opinion in microbiology*, *20*, 10-18.

Steinberg, G. (2015). *Septoria tritici* blotch disease of wheat: Tools and techniques to study the pathogen *Zymoseptoria tritici*. *Fungal Genetics and Biology*, *79*, 1-196 (June 2015), Edited by Gero Steinberg

Steinberg, G. (2015). Cell biology of *Zymoseptoria tritici*: Pathogen cell organization and wheat infection. *Fungal Genetics and Biology*, *79*, 17-23.

Stergiopoulos, I., Zwiers, L. H., & De Waard, M. A. (2003). The ABC transporter MgAtr4 is a virulence factor of *Mycosphaerella graminicola* that affects colonization of substomatal cavities in wheat leaves. *Molecular plant-microbe interactions*, *16*(8), 689-698.

Stuchell, M. D., Garrus, J. E., Müller, B., Stray, K. M., Ghaffarian, S., McKinnon, R., ... & Sundquist, W. I. (2004). The human endosomal sorting complex required for transport (ESCRT-I) and its role in HIV-1 budding. *Journal of Biological Chemistry*, *279*(34), 36059-36071.

Stukenbrock, E. H., Bataillon, T., Dutheil, J. Y., Hansen, T. T., Li, R., Zala, M., ... & Schierup, M. H. (2011). The making of a new pathogen: insights from comparative population genomics of the domesticated wheat pathogen *Mycosphaerella graminicola* and its wild sister species. *Genome research*, *21*(12), 2157-2166.

Suffert, F., Sache, I., & Lannou, C. (2013). Assessment of quantitative traits of aggressiveness in *Mycosphaerella graminicola* on adult wheat plants. *Plant Pathology*, *62*(6), 1330-1341.

Sun, T. S., Ju, X., Gao, H. L., Wang, T., Thiele, D. J., Li, J. Y., ... & Ding, C. (2014). Reciprocal functions of *Cryptococcus neoformans* copper homeostasis machinery during pulmonary infection and meningoencephalitis. *Nature communications*, 5.

Supek, F., Bošnjak, M., Škunca, N., & Šmuc, T. (2011). REVIGO summarizes and visualizes long lists of gene ontology terms. *PloS one*, *6*(7), e21800.

Sweigard, J. A., Chumley, F., Carroll, A., Farrall, L., & Valent, B. (1997). A series of vectors for fungal transformation. *Fungal Genetics Newsletter*, 52-53.

Taborda, C. P., Da Silva, M. B., Nosanchuk, J. D., & Travassos, L. R. (2008). Melanin as a virulence factor of *Paracoccidioides brasiliensis* and other dimorphic pathogenic fungi: a minireview. *Mycopathologia*, *165*(4), 331-339.

Takahara, H., Tsuji, G., Kubo, Y., Yamamoto, M., Toyoda, K., Inagaki, Y., ... & Shiraishi, T. (2004). *Agrobacterium tumefaciens*-mediated transformation as a tool for random mutagenesis of *Colletotrichum trifolii*. *Journal of General Plant Pathology*, *70*(2), 93-96.

Takano, Y., Kubo, Y., Shimizu, K., Mise, K., Okuno, T., & Furusawa, I. (1995). Structural analysis of PKS1, a polyketide synthase gene involved in melanin biosynthesis in *Colletotrichum lagenarium*. *Molecular and General Genetics MGG 249*(2), 162-167.

Tendulkar, S. R., Gupta, A., & Chattoo, B. B. (2003). A simple protocol for isolation of fungal DNA. *Biotechnology letters*, *25*(22), 1941-1944.

Thorvaldsdóttir, H., Robinson, J. T., & Mesirov, J. P. (2013). Integrative Genomics Viewer (IGV): high-performance genomics data visualization and exploration. *Briefings in bioinformatics*, *14*(2), 178-192.

Torriani, S. F., Brunner, P. C., McDonald, B. A., & Sierotzki, H. (2009). QoI resistance emerged independently at least 4 times in European populations of *Mycosphaerella graminicola*. *Pest management science*, *65(2)*, 155-162.

Trapnell, C., Pachter, L., & Salzberg, S. L. (2009). TopHat: discovering splice junctions with RNA-Seq. *Bioinformatics*, *25*(9), 1105-1111.

Tsuji, G., Kenmochi, Y., Takano, Y., Sweigard, J., Farrall, L., Furusawa, I., ... & Kubo, Y. (2000). Novel fungal transcriptional activators, Cmr1p of *Colletotrichum lagenarium* and Pig1p of *Magnaporthe grisea*, contain Cys2His2 zinc finger and Zn (II) 2Cys6 binuclear cluster DNA-binding motifs and regulate transcription of melanin biosynthesis genes in a developmentally specific manner. *Molecular microbiology*, *38*(5), 940-954.

Tsuji, G., Sugahara, T., Fujii, I., Mori, Y., Ebizuka, Y., Shiraishi, T., & Kubo, Y. (2003). Evidence for involvement of two naphthol reductases in the first reduction step of melanin biosynthesis pathway of *Colletotrichum lagenarium*. *Mycological research*, *107*(7), 854-860.

Turgeon, B. G., & Yoder, O. C. (2000). Proposed nomenclature for mating type genes of filamentous ascomycetes.

Urban, M., Bhargava, T., & Hamer, J. E. (1999). An ATP driven efflux pump is a novel pathogenicity factor in rice blast disease. *The EMBO Journal*, *18*(3), 512-521.

Urban, M., Pant, R., Raghunath, A., Irvine, A. G., Pedro, H., & Hammond-Kosack, K. E. (2014). The Pathogen-Host Interactions database (PHI-base): additions and future developments. *Nucleic acids research*, gku1165.

Valentín-Berríos, S., González-Velázquez, W., Pérez-Sánchez, L., González-Méndez, R., & Rodríguez-del Valle, N. (2009). Cytosolic phospholipase A2: a member of the signalling pathway of a new G protein α subunit in *Sporothrix schenckii*. *BMC microbiology*, *9*(1), 100.

van den Berg, F., van den Bosch, F., & Paveley, N. D. (2013). Optimal fungicide application timings for disease control are also an effective anti-resistance strategy: a case study for *Zymoseptoria tritici* (*Mycosphaerella graminicola*) on wheat. *Phytopathology*, *103*(12), 1209-1219.

Veettil, M. V., Kumar, B., Ansari, M. A., Dutta, D., Iqbal, J., Gjyshi, O., ... & Chandran, B. (2016). ESCRT-0 component Hrs promotes macropinocytosis of Kaposi's sarcoma-associated herpesvirus in human dermal microvascular endothelial cells. *Journal of virology*, *90*(8), 3860-3872.

VIDAL-CROS, A., Viviani, F., Labesse, G., Boccara, M., & Gaudry, M. (1994). Polyhydroxynaphthalene reductase involved in melanin biosynthesis in *Magnaporthe grisea*. *The FEBS Journal*, *219*(3), 985-992.

Waldherr, M., Ragnini, A., Jank, B., Teply, R., Wiesenberger, G., & Schweyen, R. J. (1993). A multitude of suppressors of group II intron-splicing defects in yeast. *Current genetics*, *24*(4), 301-306.

Wang, W., Vinocur, B., & Altman, A. (2003). Plant responses to drought, salinity and extreme temperatures: towards genetic engineering for stress tolerance. *Planta*, *218*(1), 1-14.

Wang, H. X., Douglas, L. M., Aimanianda, V., Latgé, J. P., & Konopka, J. B. (2011). The *Candida albicans* Sur7 protein is needed for proper synthesis of the fibrillar component of the cell wall that confers strength. *Eukaryotic cell*, *10*(1), 72-80.

Weld, R. J., Plummer, K. M., Carpenter, M. A., & Ridgway, H. J. (2006). Approaches to functional genomics in filamentous fungi. *Cell research*, *16*(1), 31-44.

Winter, E. (2012). The Sum1/Ndt80 transcriptional switch and commitment to meiosis in *Saccharomyces cerevisiae*. *Microbiology and Molecular Biology Reviews*, *76*(1), 1-15.

Wolf, J. M., Johnson, D. J., Chmielewski, D., & Davis, D. A. (2010). The *Candida albicans* ESCRT pathway makes Rim101-dependent and-independent contributions to pathogenesis. *Eukaryotic cell*, *9*(8), 1203-1215.

Xiang, Q., & Glass, N. L. (2004). The control of mating type heterokaryon incompatibility by vib-1, a locus involved in het-c heterokaryon incompatibility in *Neurospora crassa*. *Fungal Genetics and Biology*, *41*(12), 1063-1076.

Xu, L., Ajimura, M., Padmore, R., Klein, C., & Kleckner, N. (1995). NDT80, a meiosis-specific gene required for exit from pachytene in *Saccharomyces cerevisiae*. *Molecular and Cellular Biology*, *15*(12), 6572-6581.

Xu, J. R. (2000). MAP kinases in fungal pathogens. *Fungal Genetics and Biology*, *31*(3), 137-152.

Xue, T., Nguyen, C. K., Romans, A., & May, G. S. (2004). A mitogen-activated protein kinase that senses nitrogen regulates conidial germination and growth in *Aspergillus fumigatus*. *Eukaryotic cell*, *3*(2), 557-560.

Yang, F., Li, W., & Jørgensen, H. J. (2013). Transcriptional reprogramming of wheat and the hemibiotrophic pathogen *Septoria tritici* during two phases of the compatible interaction. *PLoS One*, *8*(11), e81606.

Yao, G., Li, Z., Wu, R., Qin, Y., Liu, G., & Qu, Y. (2016). *Penicillium oxalicum* PoFlbC regulates fungal asexual development and is important for cellulase gene expression. *Fungal Genetics and Biology*, *86*, 91-102.

Yu, P. L., Chen, L. H., & Chung, K. R. (2016). How the pathogenic fungus *Alternaria alternata* copes with stress via the response regulators SSK1 and SHO1. *PLOS one*, *11*(2), e0149153.

Zhang, Z., & Gurr, S. J. (2000). Walking into the unknown: a 'step down'PCR-based technique leading to the direct sequence analysis of flanking genomic DNA. *Gene*, *253*(2), 145-150.

Zhang, Y., Lamm, R., Pillonel, C., Lam, S., & Xu, J. R. (2002). Osmoregulation and fungicide resistance: the *Neurospora crassa* os-2 gene encodes a HOG1 mitogen-activated protein kinase homologue. *Applied and Environmental Microbiology*, *68*(2), 532-538.

Zhao, X., & Xu, J. R. (2007). A highly conserved MAPK-docking site in Mst7 is essential for Pmk1 activation in *Magnaporthe grisea*. *Molecular microbiology*, *63*(3), 881-894.

Zhao, X. F., Li, M., Li, Y. Q., Chen, X. D., & Gao, X. D. (2013). The TEA/ATTS transcription factor YlTec1p represses the yeast-to-hypha transition in the dimorphic yeast *Yarrowia lipolytica*. *FEMS yeast research*, *13*(1), 50-61.

Zwiers, L. H., & De Waard, M. A. (2001). Efficient *Agrobacterium tumefaciens*-mediated gene disruption in the phytopathogen *Mycosphaerella graminicola*. *Current Genetics*, *39*(5-6), 388-393.

7. Supplementary materials

7.1 Summary of primers used in this work

Table S1: Primers used for generation of gene inactivation constructs. Lower case sequences represent the tails of the primers used for overlapping of fragments within Gibson assembly reaction.

Primer name	Direction	Sequence (5‘ to 3‘)
myco1-fr.1-for	sense	gaattaattcctaggccaccatgttgggccTGACGAAATGATTGCCAGTTATATTTTTC
myco1-fr.1-rev	antisense	ttcaatatcatcttcGGAGAACTCGGATCAAGGCAAG
myco1-fr.2-for	sense	tgatccgagttctccGAAGATGATATTGAAGGAGCATTTTTG
myco1-fr.2-rev	antisense	tctcctccagctcgcTCTTGTTCGGTCGGCATCTAC
myco1-fr.3-for	sense	gccgaccgaacaagaGCGAGCTGGAGGAGAAGCAG
myco1-fr.3-rev	antisense	acgtggtggtggtggtggctagcgttaacaGGACAGCAGAGAGGTCCTTCTC
myco4-5‘-for	sense	CCATTCGATGCGACGCTGGC
myco4-5‘-rev	antisense	TTGCCGACGAGGAGGATGCG
myco4-3‘-for	sense	CTTCTCATACCTGGCCCGGAAGC
myco4-3‘-rev	antisense	AGGATTGAGTCTCCGGGTCGCC
myco5-fr.1-for	sense	ggcccggcgcgccgaattcccggggatccgTTGGCTTCTTTAGCTGCGGC
myco5-fr.1-rev	antisense	ttcaatatcatcttcGATAAGACGAAGACCAATCTGACG
myco5-fr.2-for	sense	ggtcttcgtcttatcGAAGATGATATTGAAGGAGCATTTTTG
myco5-fr.2-rev	antisense	ggtaggggatggatcTCTTGTTCGGTCGGCATCTA
myco5-fr.3-for	sense	gccgaccgaacaagaGATCCATCCCCTACCGCACTT
myco5-fr.3-rev	antisense	gtcagatctaccatggtggactcctcttaaACTGTCGATGCAGCGACGAT
myco56-for	sense	CTCGATGCTTGCGCCGGTCT
myco56-rev	antisense	TCCGGACGAGTGGCGATGGT
PTF1-fr.1-for	sense	ggcccggcgcgccgaattcccggggatccgGTCGTTGCTGTTTGTCCGGC
PTF1-fr.1-rev	antisense	caaaaaatgctccttcaaAAGGATGGGTCCTGCACGAG
PTF1-fr.2-for	sense	gcaggacccatccttTTGAAGGAGCATTTTTTGGG
PTF1-fr.2-rev	antisense	gtcgatcccgtcctgTCGACGTTAACTGGTTCCCG
PTF1-fr.3-for	sense	accagttaacgtcgaCAGGACGGGATCGACTGGAT
PTF1-fr.3-rev	antisense	gtcagatctaccatggtggactcctcttaaGCACTCCGGTTGAAGTGAAG

Table S2: Primers used for genome walking analysis

Primer name	Direction	Sequence (5‘ to 3‘)
gspAa	antisense	TCGCGGTGAGTTCAGGCTTTTTCATGATCG
gspA	antisense	CGCACAAGTTATCGTGCACCAAGCAGCAGA
gspBa	sense	TCAGAGCTTGGTTGACGGCAATTTCGATGA
gspB	sense	ATGGCTGTGTAGAAGTACTCGCCGATAGTG

PPR1	-	**PO_4**-CTAGGGCCACCACG-**NH_2**
Pad1	-	GTAATACGACTCACTATAGGGCACGCTGGTGGCC
PP1	-	GTAATACGACTCACTATAGGGC
PPR2	-	**PO_4**-CCGGTGCCACCACG-**NH_2**
Pad2	-	GTAATACGACTCACTATAGGGCACGCGTGGTGGCA
PP2	-	ACTATAGGGCACGCGTGGT

Table S3: Primers used for complementation constructs

Primer name	Direction	Sequence (5‘ → 3‘)
myco1-Comp-for	sense	AAGCCGCCGGTCCCTTAGGT
myco1-Comp-rev	antisense	GCTCGAAGGCGAGTGGCAGG
myco4-Comp-for	sense	CGCTCATTGCGAACAGCAGGC
myco4-Comp-rev	antisense	TCGGCGACCACTTCGGTGTC
myco5-Comp-for	sense	GCCTTTTCCTTGGCCTCCTTCAA
myco5-Comp-rev	antisense	CCGACTGATTGCCCACGGGA
myco56-Comp-for	sense	GCGAGAGGCCGAGCAAGTGT
myco56-Comp-rev	antisense	TGCGGCGGCATCGATACGTG

Table S4: Primers used for probe generation (for Southern Blot analysis)

Primer name	Direction	Sequence (5‘ → 3‘)
myco1-probe-for	sense	TCGTGAGGCATGGATGAAGT
myco1-probe-rev	antisense	CTAACGAACCAAGCGAGCAG
myco4-probe-for	sense	ACGGCACAACATCCCGACTGC
myco4-probe-rev	antisense	GCTACTGGTGCCGGTGCGTA
myco5-probe-for	sense	CTGAAGGTACTGCGCTGTCT
myco5-probe-rev	antisense	CAGGGCTCTAGAGATGCCTC
myco56-probe-for	sense	GCCGTCCGCATCGCAAAAGG
myco56-probe-rev	antisense	AACGCAGGATTCGCCGGTGG
PTF1-probe -for	sense	CAGCAACGATCGATACTCTCAC
PTF1-probe -rev	antisense	CTCCTTCTCATGCTGACTTGGT
HPT-probe-for	sense	CGAAGAATCTCGTGCTTTCAGC
HPT-probe-rev	antisense	CCAGAAGAAGATGTTGGCGAC

Table S5: Primers used for Screen PCR

Primer name	Direction	Sequence (5‘ to 3‘)
myco1-Comp-for	sense	AAGCCGCCGGTCCCTTAGGT
myco1-Comp-rev	antisense	GCTCGAAGGCGAGTGGCAGG

myco4-5‘-for	sense	CCATTCGATGCGACGCTGGC
myco4-3‘-rev	antisense	AGGATTGAGTCTCCGGGTCGCC
myco5-fr.1-for	sense	ggcccggcgcgccgaattcccggggatccgTTGGCTTCTTTAGCTGCGGC
myco5-fr.3-rev	antisense	gtcagatctaccatggtggactcctcttaaACTGTCGATGCAGCGACGAT
myco56-for	sense	CTCGATGCTTGCGCCGGTCT
myco56-rev	antisense	TCCGGACGAGTGGCGATGGT
BAR-for	sense	TACATCGAGACAAGCACGGT
BAR-rev	antisense	GAAGTCCAGCTGCCAGAAAC

Table S6: Primers used for qRT-PCR

Primer name	Direction	Sequence (5‘ to 3‘)
myco-b-tub-for	sense	CTTCCGCCCAGACAACTTCGT
myco-b-tub-rev	antisense	TCTGGAAACCCTGGAGGCAGT
hog1-qPCR-for	sense	ATCTCCACCGCCTCCTCAC
hog1-qPCR-rev	antisense	GCAGTTCTCGTTCACCAGGA
myco1-qPCR-for	sense	GGAGCATCGCCCGAAATATG
myco1-qPCR-rev	antisense	TTGGCATGGACGCTTTCAGA
myco4-qPCR-for	sense	ACCTCTAGTCAAAGGCATCGC
myco4-qPCR-rev	antisense	GAATCGAGCAGTCGGGATGT
myco5-qPCR-for	sense	CTCAGCAACCTCGGATCTCA
myco5-qPCR-rev	antisense	TATGGACGGGTGAGCTGTTG
myco56-qPCR-for	sense	CTACACTTTGGCTTGGCGTC
myco56-qPCR-rev	antisense	GCGGTTGGCGTTATTGTCA
Zt34453- qPCR-for	sense	CATTTCCCACCGTCAGAAGG
Zt34453- qPCR-rev	antisense	TCCAGGGTAGAAGGTCTTGC
Zt38341- qPCR-for	sense	GACCCGCAAATGACCAACTT
Zt38341- qPCR-rev	antisense	GAGAAGTTCGAGCATACCGG
Zt58641- qPCR-for	sense	CAATGCCATCCTCAACGACT
Zt58641- qPCR-rev	antisense	ATGATGTCTGCAGAGAGGGAG
Zt59604- qPCR-for	sense	CTCCGTTCCTGGCAGTGAT
Zt59604- qPCR-rev	antisense	GGAGCGATCCAGACTGTCTT
Zt68287- qPCR-for	sense	CGTGCCATCTCTCTTGCAG
Zt68287- qPCR-rev	antisense	GCGTGGTACTTCGTGAGGAT
Zt74200- qPCR-for	sense	GCTGGGGAATCATCATCGGA
Zt74200- qPCR-rev	antisense	TCGGTGATCAGGAGAGGAGA
Zt81448- qPCR-for	sense	GTCAGCGAACATCACTGGAA
Zt81448- qPCR-rev	antisense	TCGCATCGATGTCTCCTGAG
Zt84460- qPCR-for	sense	ATCCGACCGAGACTGCTATC
Zt84460- qPCR-rev	antisense	TGTTCTCCATTATCACGGACATC
Zt105080- qPCR-for	sense	AACATTGCTGCTTTCGGAGG

Zt105080- qPCR-rev	antisense	GGTGCGAGCAAAGTTTGACT
Zt109795- qPCR-for	sense	ATTCGGAAAAGGCAGGGAGA
Zt109795- qPCR-rev	antisense	ACTTCTCCCACTCCCAGATC
Zt43487-qPCR-for	sense	CGCTCTTTTCGAGGCCATTC
Zt43487-qPCR-rev	antisense	AGCCATTTCGGGGTAAGAGG
Zt74298-qPCR-for	sense	TGGACAACTCCATGCTCTCC
Zt74298-qPCR-rev	antisense	TCCACCTTTTCTGGCGTTGT
Zt94368-qPCR-for	sense	CGATCTTCGAGGCCGTTCAA
Zt94368-qPCR-rev	antisense	GCTGCCCTCTGAAATGTCGAT
Zt96677-qPCR-for	sense	GACAAGGAGGCGCAGTACAT
Zt96677-qPCR-rev	antisense	CTGCTGGATGGTGGCGTAT
Zt101235-qPCR-for	sense	CCGCAGCAAACCACAACTTC
Zt101235-qPCR-rev	antisense	TGACTAGATCGCCATCGGTG
Zt102956-qPCR-for	sense	AGAATGCGCTCGGAGTCAC
Zt102956-qPCR-rev	antisense	GAGCAGTTGCCGTTGGTGA

7.2 Plasmid construction for targeted inactivation and complementation of the target genes in *Zymoseptoria tritici*

MYCO1 (JGI Protein ID: 70181):

The construction of transformation vector used for inactivation of *MYCO1* gene was employed using the Gibson Assembly® approach (2.2.4.4). To this end, three required fragments were amplified by PCR using the primer pairs containing the overhangs overlapping with the neighboring fragments. The primer pairs myco1-fr.1-for and myco1-fr.1-rev as well as myco1-fr.3-for and myco1-fr.3-rev were used to amplify fragments representing the ORF sequence regions of the *MYCO1* gene suitable for homologous recombination using genomic DNA as template. For the amplification of *HPT* cassette from the pCB1636 the primers myco1-fr.2-for and myco1-neu-fr.2-rev were used. Thereby it was possible to generate the desired final gene inactivation vector pCAMB-myco1-HPT-Final within a single assembly reaction. The generated transformation plasmid was verified by restriction analysis and could be directly used for ATMT.

For complementation of the *MYCO1*-inactivated mutant the construct pCAMB-myco1-Comp-BAR was generated by amplification of the WT gene locus from strain IPO323 using the primers myco1-Comp-for and myco1-Comp-rev. The amplified PCR product was ligated to pGEM-T easy to give pGEM-myco1-Comp. Subsequently the insert excised using *Not*I was cloned into the vector pCAMB-BAR (7747 bp) restricted with *Psp*OMI. The generated final

vector pCAMB-myco1-Comp-BAR was verified by restriction analysis and could be directly used for transformation of hygromycin resistant mutants.

MYCO4 (JGI Protein ID: 87000):

For inactivation of *MYCO4* gene the primers myco4-5'-for, myco4-5'-rev and myco4-3'-for, myco4-3'-rev were used to generate two PCR products, representing the gene flank regions with 616 bp and 700 bp respectively. The 5'-flank was subsequently subcloned into the vector pJet to generate pJet-myco4-5'-correct (3590 bp). The 3'-fragment (700 bp) was ligated into pGEM-T easy giving the resulting vector pGEM-myco4-3' (3717 bp).

pGEM-myco4-3' was restricted with the enzyme combination *EcoRI*+*Spe*I and a 700 bp fragment was cloned into *EcoRI*+*Avr*II restricted pCAMB-HPT(*Sal*I) giving the resulting vector pCAMB-myco4-3'-HPT. Finally the *Bgl*II+*Xba*I restricted fragment of pJet-myco4-5'-correct was cloned into *Bgl*II+*Spe*I resctricted vector pCAMB-myco4-3'-HPT to give the completed gene inactivation vector pCAMB-myco4-HPT-Final. The generated transformation plasmid was verified by restriction analysis and could be directly used for ATMT.

For complementation of the *MYCO4*-inactivated mutant the construct pCAMB-myco4-Comp-BAR was generated by amplification of the WT gene locus from strain IPO323 using the primers myco4-Comp-for and myco4-Comp-rev. The amplified PCR product was ligated to pGEM-T easy. The resulting pGEM-myco4-Comp vector was restricted by using *Not*I and a 4394 bp fragment was cloned into pCAMB-BAR (7747 bp) restricted with *Psp*OMI. The generated final vector was verified by restriction analysis and could be directly used for transformation of hygromycin resistant mutants.

MYCO5 (JGI Protein ID: 66947):

For deletion of *MYCO5* gene the generation of the gene deletion construct was conducted using the Gibson Assembly® approach (2.2.4.4). Therefore three required fragments were amplified by PCR using the primer pairs containing the overhangs overlapping with the neighboring fragments. The primer pairs myco5-neu-fr.1-for and myco5-neu-fr.1-rev as well as myco5-neu-fr.3-for and myco5-neu-fr.3-rev were used to amplify the fragments representing the flanking regions of the myco5 gene using genomic DNA as template. For the amplification of *HPT* cassette from the pCB1636 the primers myco5-neu-fr.2-for and myco5-neu-fr.2-rev were used. Thereby it was possible to generate the desired final deletion vector pCAMB-myco5-HPT-Final within a single assembly reaction. The generated transformation plasmid was verified by restriction analysis and could be directly used for ATMT.

For complementation of the *MYCO5*-deleted mutant the construct pCAMB-myco5-Comp-BAR was generated by amplification of the WT gene locus from strain IPO323 using the primers myco5-Comp-for and myco5-Comp-rev. The amplified PCR product was ligated to pGEM-T easy and then the insert excised using *Not*I and cloned into the vector pCAMB-BAR (7747 bp) restricted with *Psp*OMI. The generated final vector was verified by restriction analysis and could be directly used for transformation of hygromycin resistant mutants.

MYCO56 (JGI Protein ID: 110503):

For inactivation of *MYCO56* gene a 3657 bp PCR product was amplified using the primers myco56-for and myco56-for from genomic DNA of *Z.tritici* IPO323 and cloned into pJet (Promega, Mannheim; Germany) giving the resulting vector pJet-myco56KO. In the next step this vector was cleaved by *Sal*I and a 1962 bp fragment of the coding sequence was replaced by a *HPT* cassette from the *Sal*I restricted pCAMB-HPT(*Sal*I) to give pJET-myco56-HPT. Finally the *Xba*I+*Not*I restricted fragment of pJET-myco56-HPT was cloned into *Spe*I+*Psp*OMI resctricted pCAMB0380 to give the completed gene inactivation vector pCAMB-myco56-HPT-Final. The generated transformation plasmid was verified by restriction analysis and could be directly used for ATMT.

For complementation of the *MYCO56*-disrupted mutant the construct pCAMB-myco56-Comp-BAR was generated by amplification of the WT gene locus from strain IPO323 using the primers myco56-Comp-for and myco56-Comp-rev. The amplified PCR product was ligated to pGEM-T easy to give pGEM-myco56-Comp. Subsequently the insert excised using *Not*I was cloned into the vector pCAMB-BAR (7747 bp) restricted with *Psp*OMI. The generated final vector pCAMB-myco56-Comp-BAR was verified by restriction analysis and could be directly used for transformation of hygromycin resistant mutants.

ZtPTF1 (JGI Protein ID: 109299):

The inactivation vector for disruption of *ZtPTF1* was generated by Julian Laufer within his master thesis (2015), employing Gibson assembly method (2.2.4.4). Flanking regions of *ZtPTF1* coding sequence were amplified by PCR, using the primer pairs PTF1-fr.1-for, PTF1-fr.1-rev and PTF1-fr.3-for, PTF1-fr.3-rev, and *Z. tritici* IPO323 gDNA as a template. The *HPT* cassette sequence was amplified from pCB1636 using the primers PTF1-fr.2-for and PTF1-fr.2-rev. The amplified fragments were then ligated into pCAMB0380 linearized with *Sal*I and *Hind*III restriction, giving the final inactivation vector pCAMB-PTF1-HPT. The

generated transformation plasmid was verified by restriction analysis and could be directly used for ATMT.

7.3 Construction of *eGFP*-gene fused vectors for localization studies

All *eGFP* fusion vectors used for protein localization studies were generated following the same principle according to Gibson assembly® method (2.2.4.4). The *Apa*I + *Eco*RI restricted vector pCAMB-HPT(*Sal*I) was used as a vector backbone. The sequence of the gene of interest (*MYCO4*, *MYCO5*, *MYCO56* or *ZtPTF1*), including upstream promoter region, was amplified from *Z. tritici* IPO 323 genomic DNA employing PCR with defined primers. Only for generation of *ZtPTF1-eGFP* construct a constitutive *EFA1* promoter derived from *Magnaporthe oryzae* 70-15 was used, hence gDNA from *M. oryzae* was used within PCR. The *eGFP* sequence used for Gibson assembly was obtained from the vector pAJF-EFA1-GFP (see 2.1.7) by PCR with appropriate primers. The generated transformation vectors were verified by restriction analysis and could be directly used for ATMT.

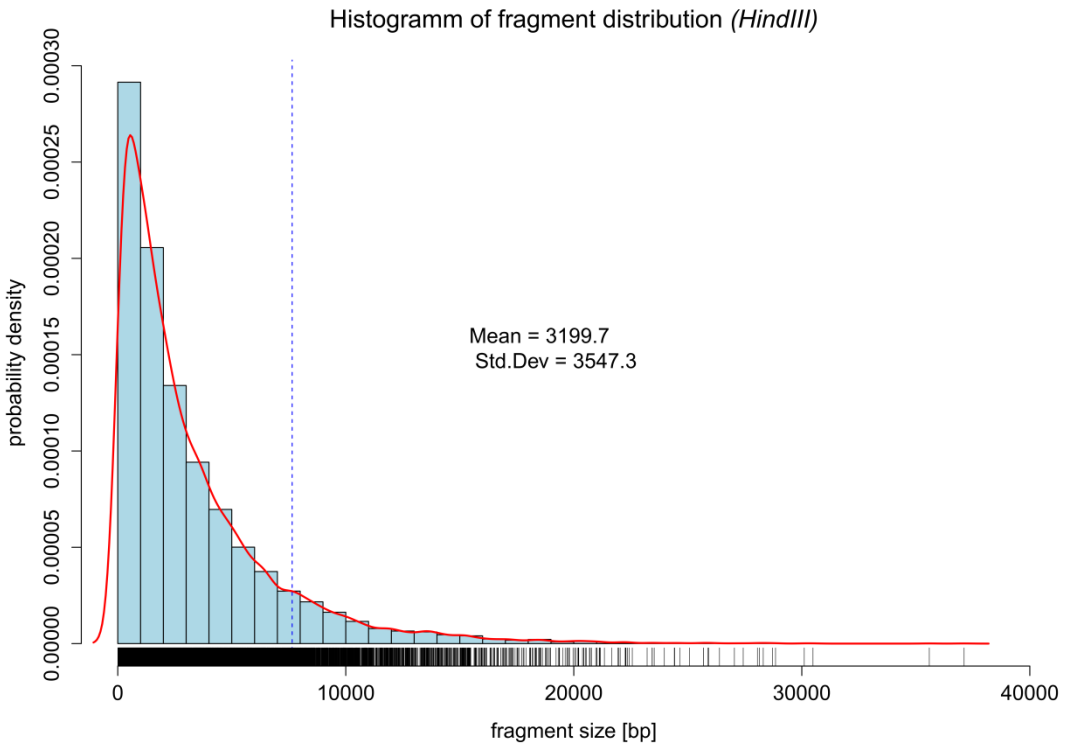

Figure S1: Theoretical fragment distribution of *Hind*III restricted genome of IPO323. Examining the current genome version of wildtype strain IPO323 retrieved from EnsemblGenomes (*Zymoseptoria tritici*, Assembly: MG2), 12403 restriction enzyme recognition sites of *Hind*III were identified across 21 chromosomes. Distribution of restriction site distances (theoretical "fragment lengths") is visualized as histogram using a generic function *hist()* in R. The bins are equidistant, with difference between breaks = 1000 bp. The sum of the probability densities adds up to 1. Mean and standard deviation of distances are calculated. The pointed line at ca. 7 kbp marks the interval of integration giving 0.9 probability density, meaning for 90% of all generated restriction fragments a length distribution between 1 and 7 kbp.

Figure S2: Protein sequence analysis of deduced Myco4p homologs. Multiple sequence alignment analysis of deduced protein sequences was performed by MUSCLE with default parameters. Identical amino acids are shaded in black, conserved amino acids in dark gray and similar amino acids in light gray. Protein sequences derived from the *Mycosphaerellaceae* family are clustered in one clade since they harbour only *GARS* functional domain (comprised of *GARS_N*, *GARS_A* and *GARS_C*) predicted by InterProScan. All other fungal representatives including yeast possess bifunctional proteins, indicated by the presence of two additional functional domains *AIRS* and *AIRS_C* (depicted in blue). Red arrows indicate Myco4p (*Zt87000*) and one predicted protein (*Zt74864*) with *AIRS* domain. Both appear monofunctional, but may together reconstitute the bifunctionality of yeast counterpart The human ortholog is trifunctional due to the presence of *Formyl_trans_N* domain (highlighted in red), additionally conferring the GART activity.

7.4 Screen-PCR and Southern Blot analysis

MYCO1 – Strategy used for generation of the *Δmyco1* using targeted gene inactivation and Southern Blot providing evidence of gene replacement

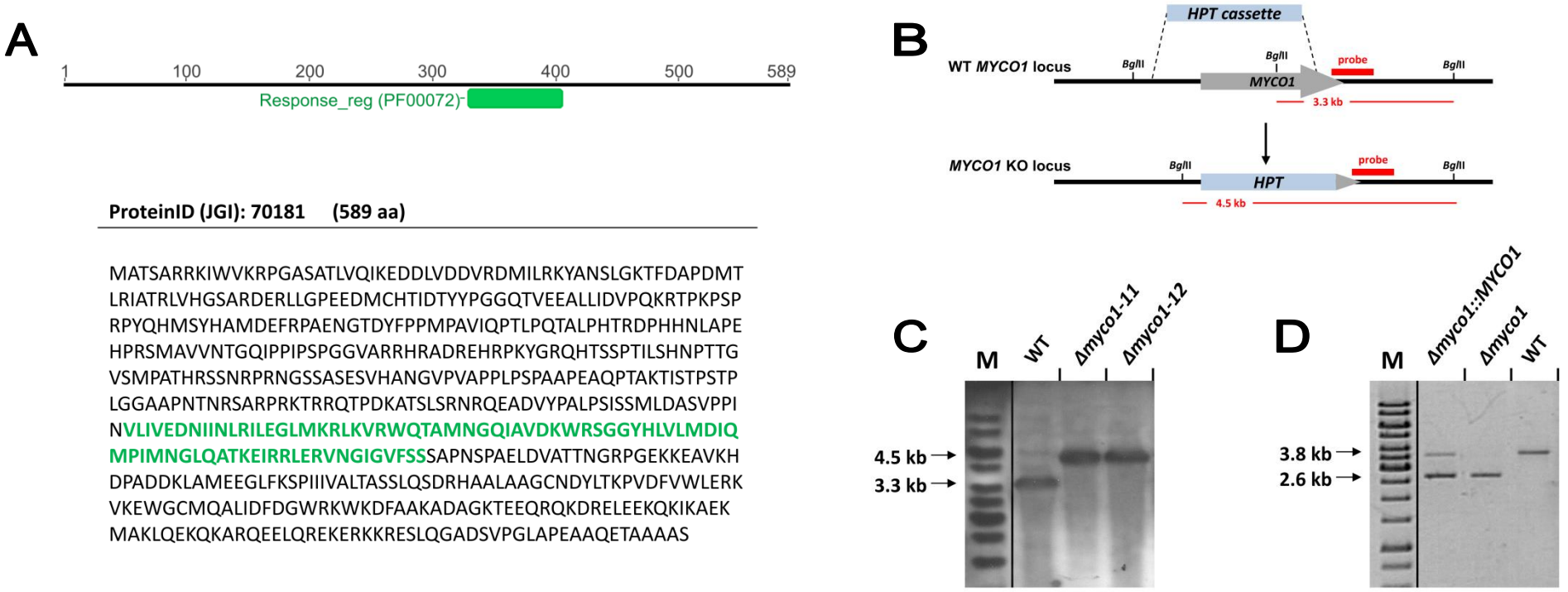

Figure S3: Targeted gene inactiation of *MYCO1*. **(A)** Gene structure of *MYCO1* with functional domain predicted by InterProScan as well as adjacent protein sequence deduced are shown. Sequence region matching the predicted domain is highlighted in green. **(B)** Construction of the gene inactivation construct and targeted gene disruption by replacing a significant portion of ORF of the gene with *HPT* cassette. Location of genomic sequence for probe hybridization and restriction sites used for Southern Blot are indicated. **(C)** Southern Blot analysis. Genomic DNA derived from wildtype strain IPO323 and potential *Δmyco1* mutants was restricted with *Bgl*II and then probed with a 300 bp fragment amplified with the primers . **(D)** Screen-PCR was employed to confirm the loss of functional copy of *MYCO1* gene in the *Δmyco1* mutant and the presence of additional gene copy in the complementation strain *Δmyco1*/*MYCO1*, using the primers myco1-fr.1-for and myco1-fr.3-rev.

MYCO4 – Strategy used for generation of the *Δmyco4* using targeted gene inactivation and Southern Blot providing evidence of gene replacement

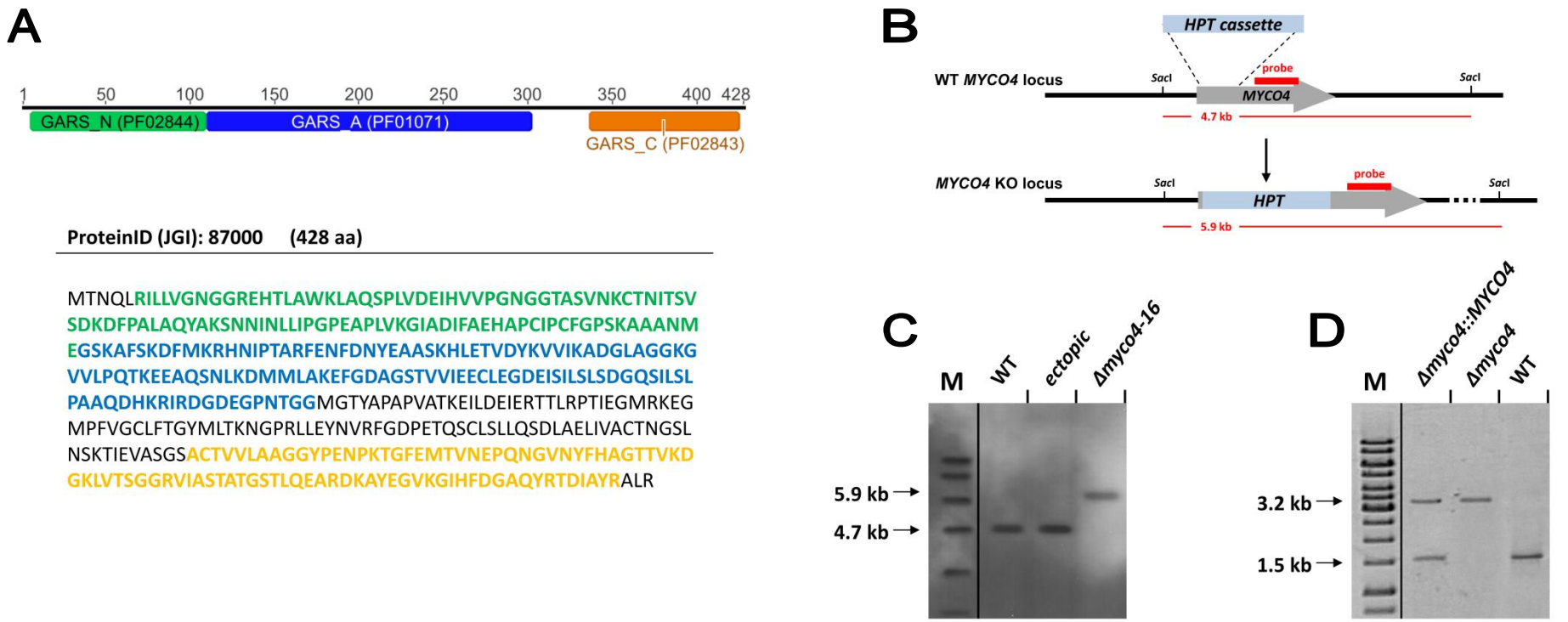

Figure S4: Targeted gene inactiation of *MYCO4*. (A) Gene structure of *MYCO4* with functional domain predicted by InterProScan as well as adjacent protein sequence deduced are shown. Sequence regions matching the predicted domains are highlighted in respective colours. **(B)** Schematic representation of targeted gene disruption by replacing a significant portion of ORF of the gene with *HPT* cassette. Location of genomic sequence for probe hybridization and restriction sites used for Southern Blot are indicated. **(C)** Southern Blot analysis. Genomic DNA derived from wildtype strain IPO323 and potential *Δmyco4* mutants was restricted with *Sac*I and then probed with a 378 bp fragment amplified with the primers myco4-probe-for and myco4-probe-rev. **(D)** Screen-PCR was employed to confirm the loss of functional copy of *MYCO4* gene in the *Δmyco4* mutant and the presence of additional gene copy in the complementation strain *Δmyco4*/*MYCO4*, using the primers myco4-5‘-for and myco4-3‘-rev.

MYCO5 – Strategy used for generation of the *Δmyco5* using targeted gene inactivation and Southern Blot providing evidence of gene replacement

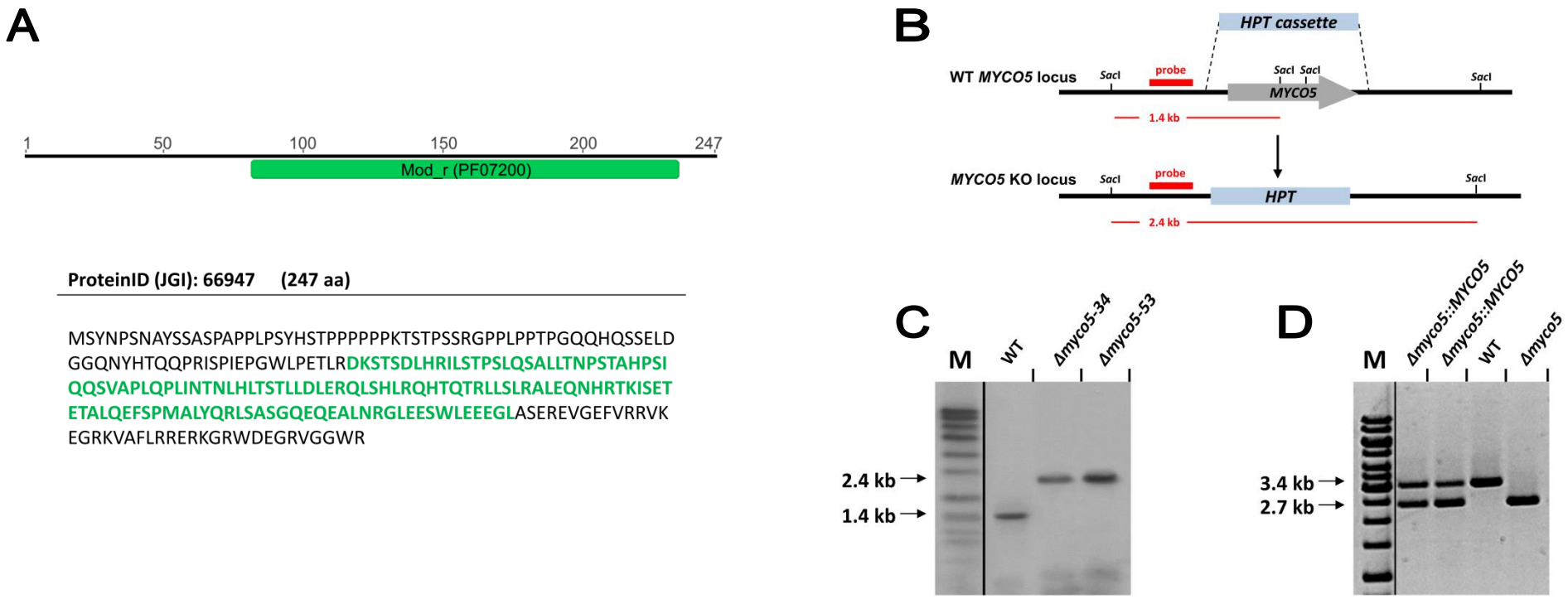

Figure S5: Targeted gene inactivation of *MYCO5*. (A) Gene structure of *MYCO5* with functional domain predicted by InterProScan as well as adjacent protein sequence deduced are shown. Sequence region matching the predicted domain is highlighted in green. **(B)** Schematic representation of targeted gene disruption by replacing a significant portion of ORF of the gene with *HPT* cassette. Location of genomic sequence for probe hybridization and restriction sites used for Southern Blot are indicated. **(C)** Southern Blot analysis. Genomic DNA derived from wildtype strain IPO323 and potential *Δmyco5* mutants was restricted with *Sac*I and then probed with a 334 bp fragment amplified with the primers myco5-probe-for and myco5-probe-rev. **(D)**. Screen-PCR was employed to confirm the loss of functional copy of *MYCO5* gene from the *Δmyco5* mutant and the presence of additional gene copy in the complementation strain *Δmyco5*/*MYCO5*, using the primers myco5-fr.1-for and myco5-fr.3-rev.

MYCO56 – Strategy used for generation of the *Δmyco56* using targeted gene inactivation and Southern Blot providing evidence of gene replacement

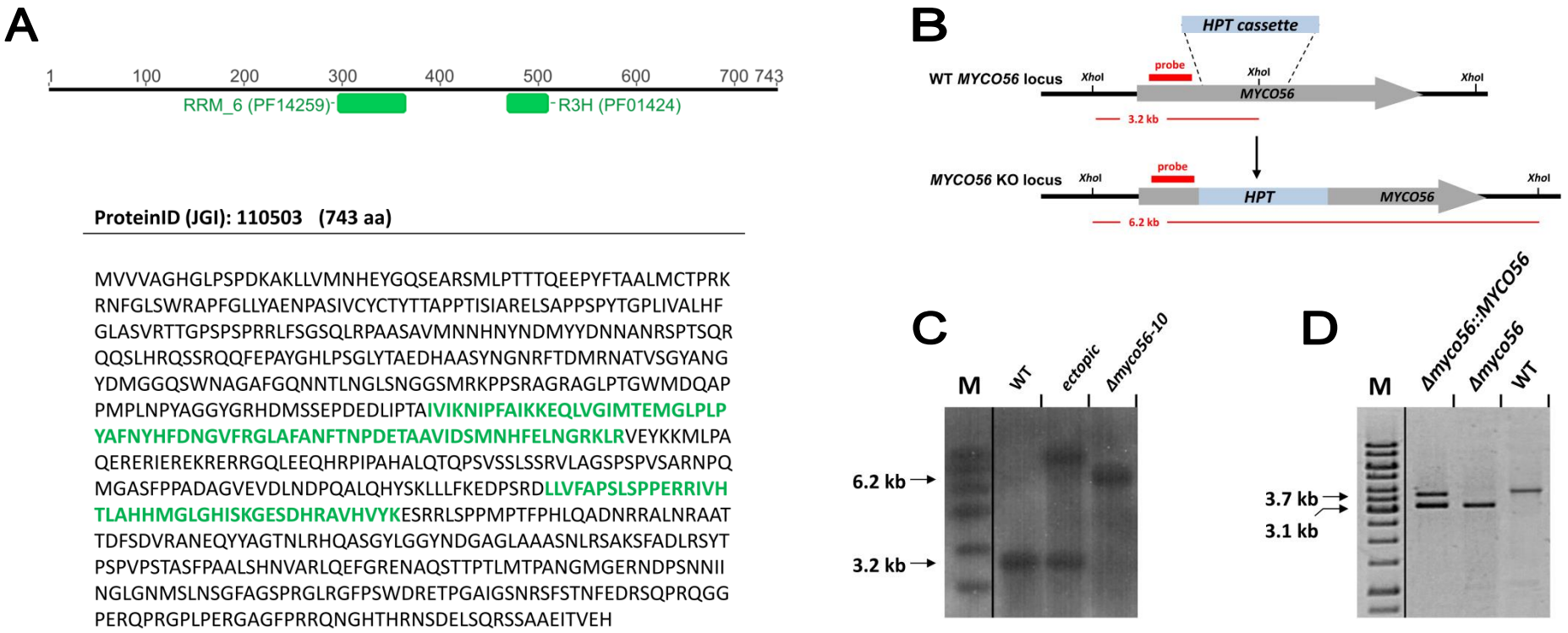

Figure S6: Targeted gene disruption of *MYCO56*. (A) Gene structure of *MYCO56* with functional domain predicted by InterProScan as well as adjacent protein sequence deduced are shown. Sequence regions matching the predicted domains are highlighted in green. **(B)** Schematic representation of targeted gene disruption by replacing a significant portion of ORF of the gene with *HPT* cassette. Location of genomic sequence for probe hybridization and restriction sites used for Southern Blot are indicated. **(C)** Southern Blot analysis. Genomic DNA derived from wildtype strain IPO323 and potential *Δmyco56* mutants was restricted with *Xho*I and then probed with a 335 bp fragment amplified with the primers myco56-probe-for and myco56-probe-rev. **(D)**. Screen-PCR was employed to confirm the loss of functional copy of *MYCO56* gene from the *Δmyco56* mutant and the presence of additional gene copy in the complementation strain *Δmyco56*/*MYCO56*, using the primers myco56-for and myco56-rev.

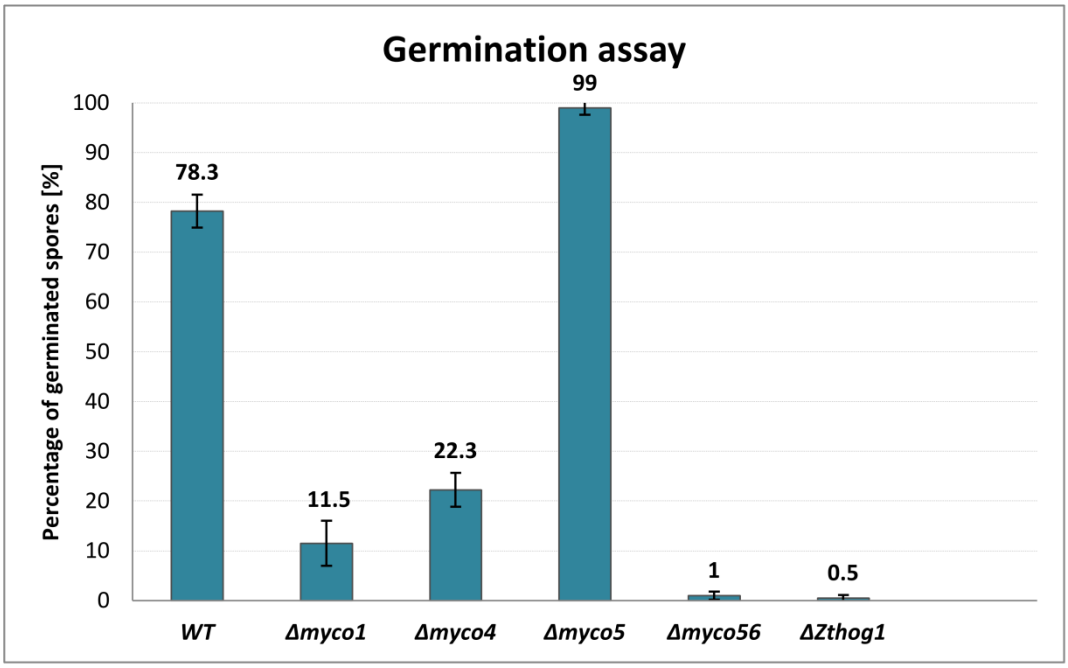

Figure S7: ***In vitro*** **germination assay of wildtype strain IPO323 (WT) and targeted mutant strains.** For each strain 100 µl of spore suspension at final concentration of 10^6/ml were spotted on microscopic slide covered with a thin layer of H_2O agar and incubated in the dark chamber with nearly full-saturated humidity at 18 °C. The ratio of germination was calculated as the mean percentage of conidia germinated after 60 h. For each strain three biological replicates were analyzed.

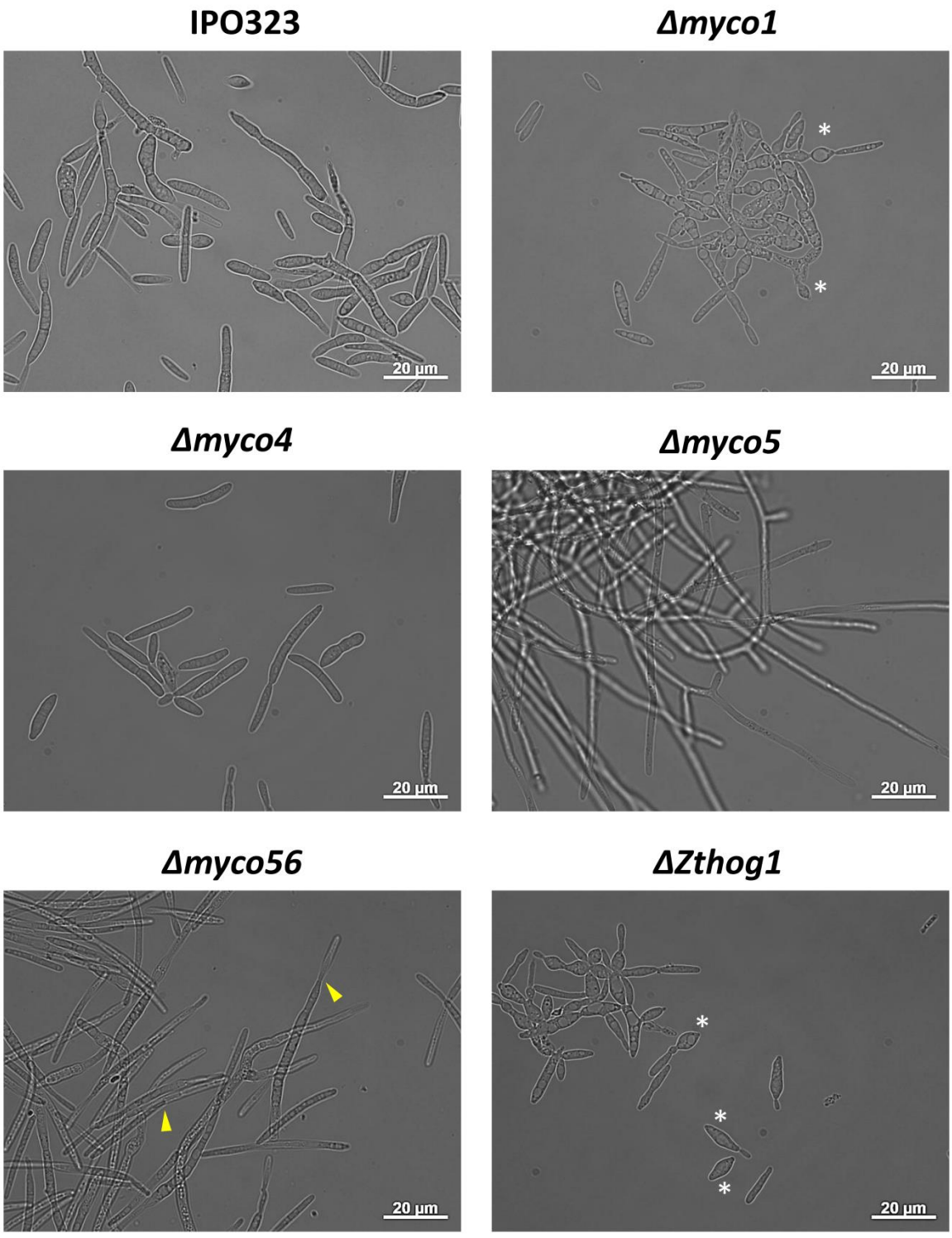

Figure S8: Comparative phenotyping of *Zymoseptoria tritici* mutants on microscopic scale. The strains were previously icubated in YEG at 18 °C under daylight settings for 3 days. The *Δmyco56* disruptants produced significantly longer spores in YEG compared to WT. *Δmyco5* mutant shows predominantly mycelial growth, however the yeast like cells are also present but to a lesser extent. Yellow arrows indicate the point of branching, however the conidia remain adjacent giving the mutant strain *Δmyco56* a pseudohyphal appearance. White asterisks depict irregular shaped, ovoid conidia in case of *ΔZthog1* and *Δmyco1*, consistent with phenotypes previously reported for homologous mutant strains in other fungi.

Global statistics and quality control

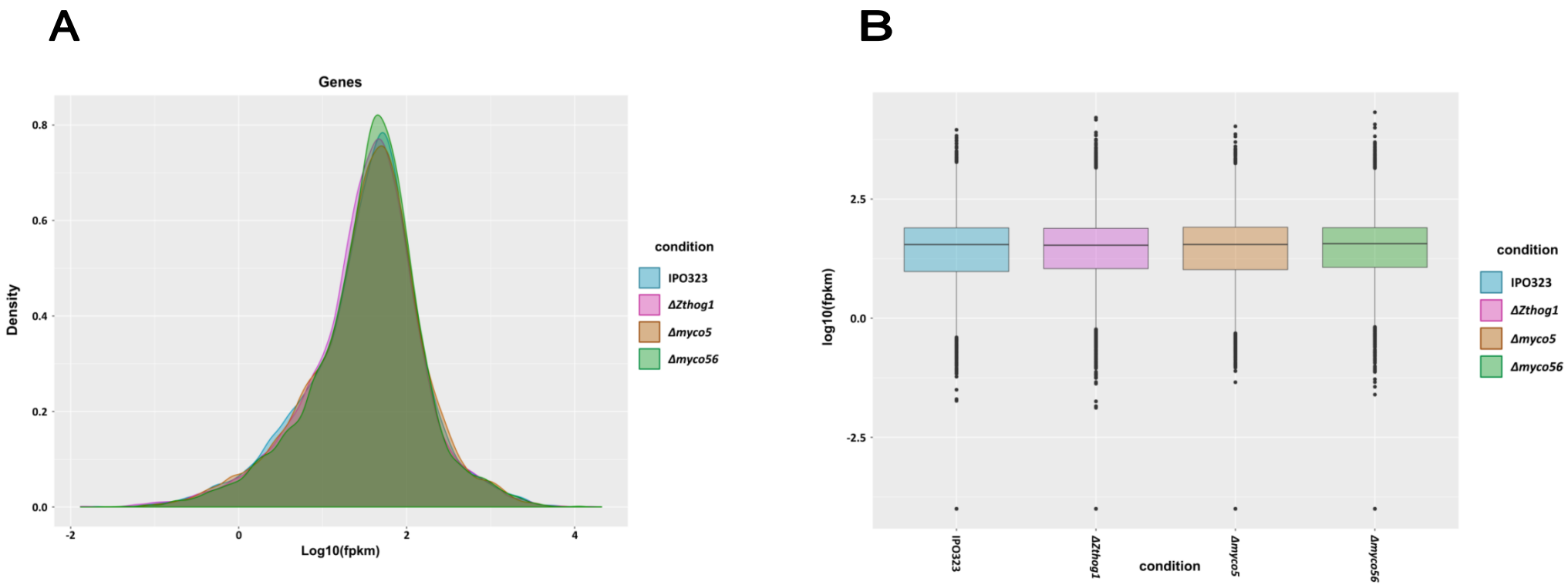

Figure S9: Global statistics and quality control of RNA-Seq data obtained. (A) Density plot displaying the probability densities of expression levels of genes transcribed in each of the corresponding strains. **(B)** Boxplots displaying the gene distribution at each mean FPKM values across the investigated strains. The data confirmed that there was no reduction of values (reads) across investigated strains, indicating that the sequencing depth and coverage were sufficient.

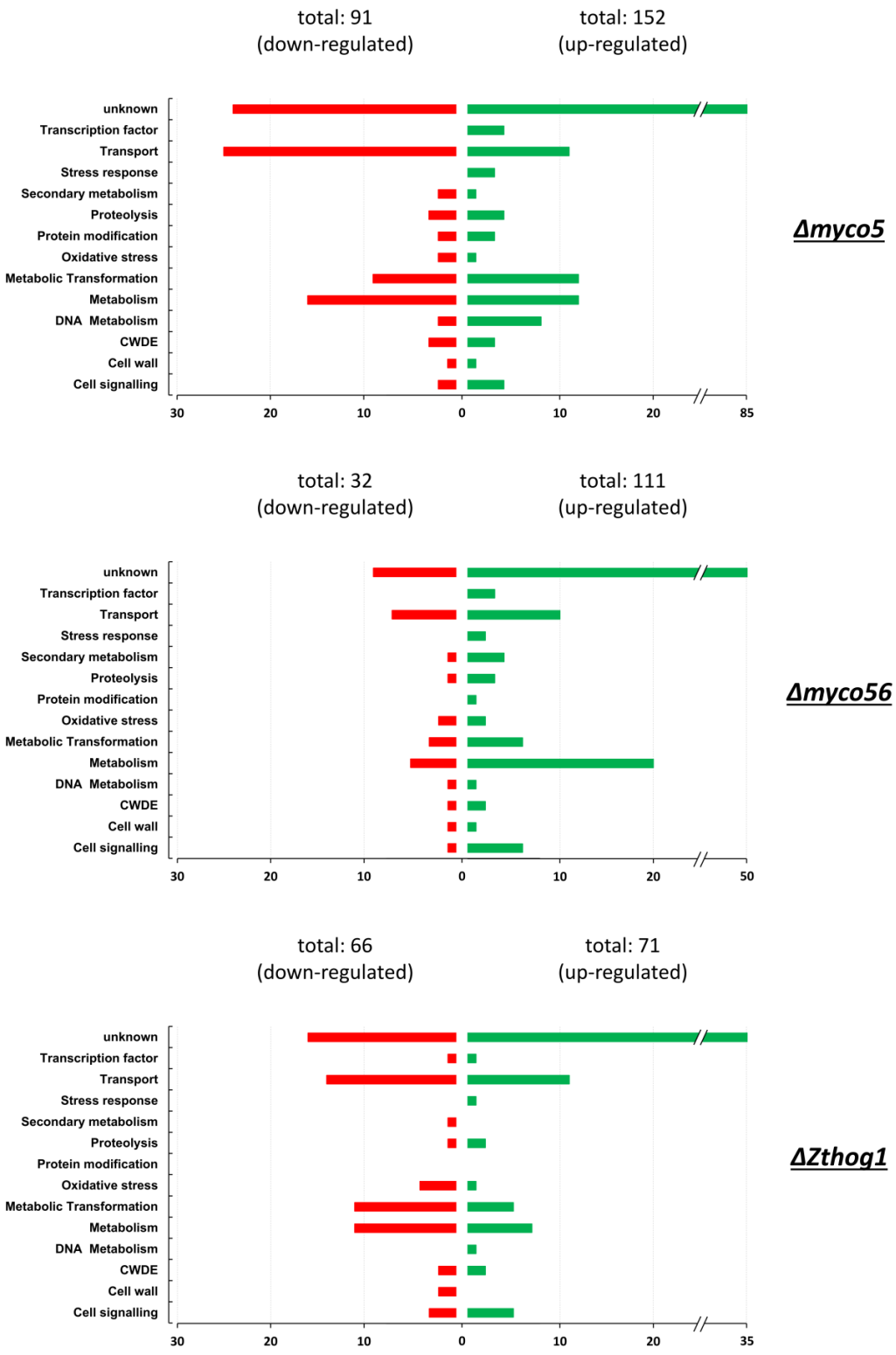

Figure S10: Functional classification of the products of DE genes obtained from RNA-Seq, complementing the Figure 17. Bar charts represent an augmented functional classification of products of the differentially regulated genes for each strain-specific regulon, considering the absolute number of down- and up-regulated genes for each Biological Process (BP) investigated. The products of the DE genes according to RNA-Seq analysis were manually annotated by assigning a function based on the presence of conserved functional domains, GO annotation and/or the best meaningful match to the predicted protein. Only the top fourteen enriched function-related terms are represented in the respective bar chart. Red bars represent significant functional categories for products of the down-regulated genes. Green bars indicate those for up-regulated genes.

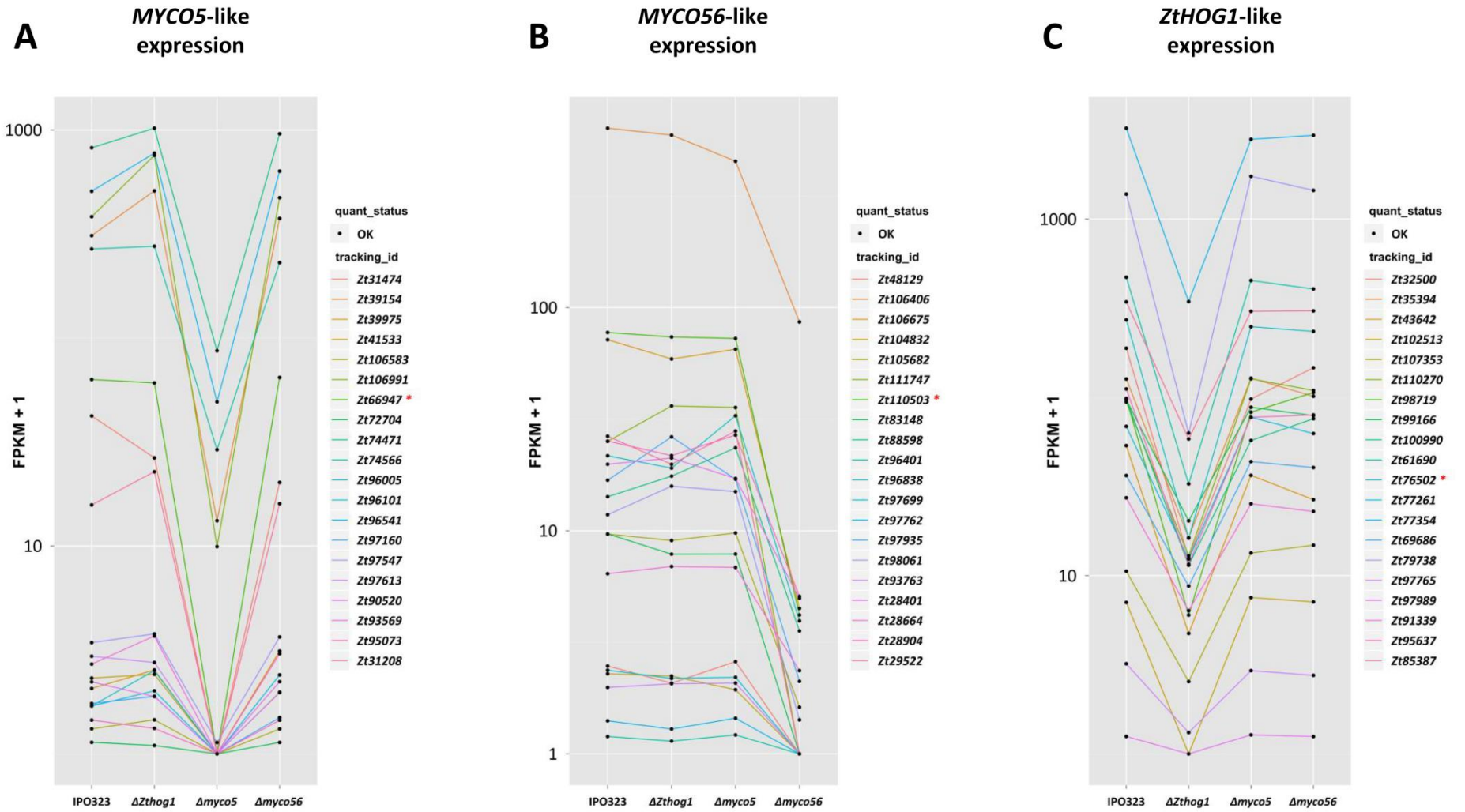

Figure S11: Identification of the most similar genes to a given target gene. Analysis was performed using *findsimilar()*-function implemented in CummeRbund package in R. The similarty is determined by Jensen-Shannon distance between the probability distributions of each gene across the investigated mutants. Top 20 most similar genes to a provided expression profile by **(A)** *MYCO5*-gene (*Zt66947*), **(B)** *MYCO56*-gene (*Zt110503*) and **(C)** *ZtHOG1*-gene (*Zt76502*) across investigated mutants are shown. The target genes are indicated by red asterisks.

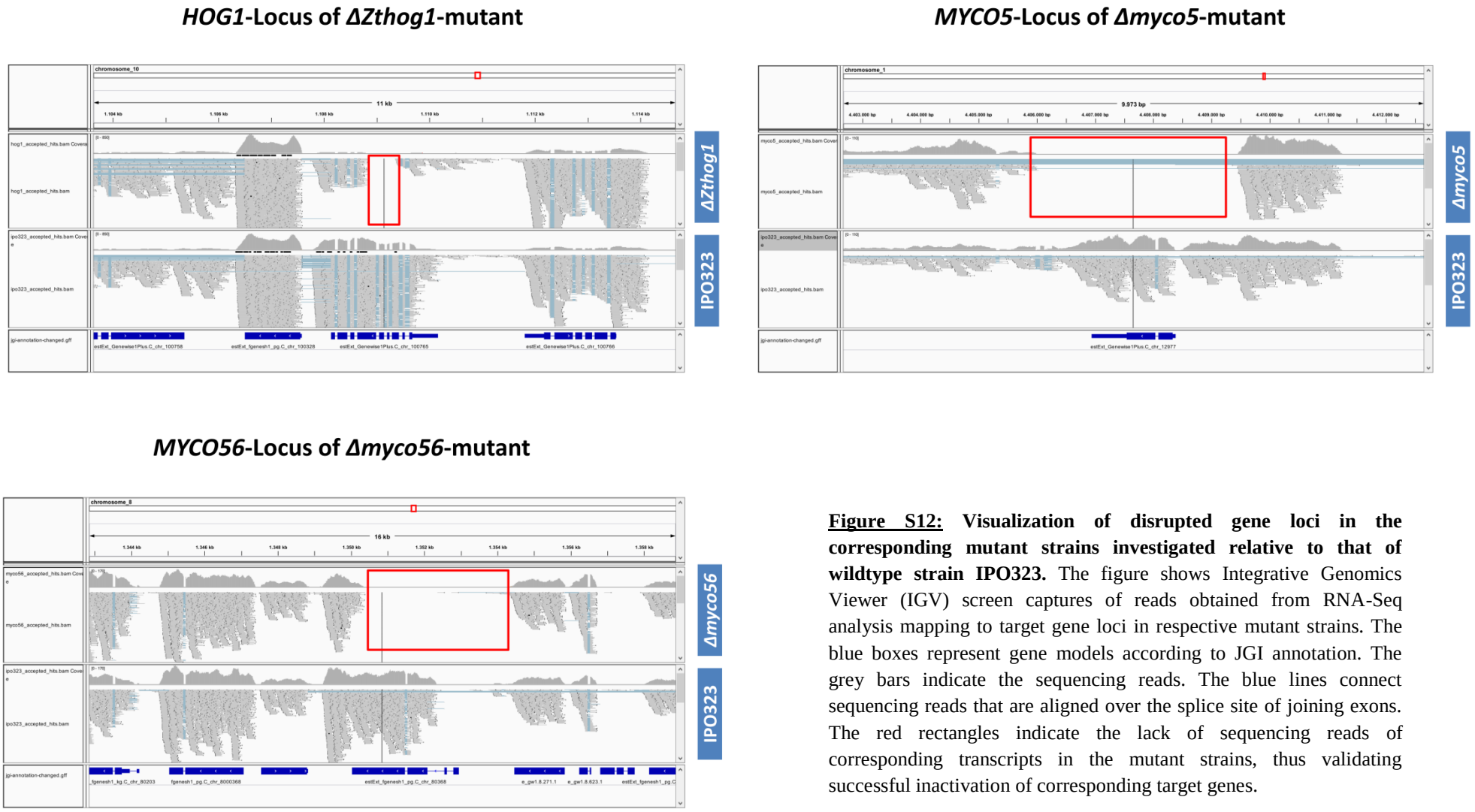

Figure S12: Visualization of disrupted gene loci in the corresponding mutant strains investigated relative to that of wildtype strain IPO323. The figure shows Integrative Genomics Viewer (IGV) screen captures of reads obtained from RNA-Seq analysis mapping to target gene loci in respective mutant strains. The blue boxes represent gene models according to JGI annotation. The grey bars indicate the sequencing reads. The blue lines connect sequencing reads that are aligned over the splice site of joining exons. The red rectangles indicate the lack of sequencing reads of corresponding transcripts in the mutant strains, thus validating successful inactivation of corresponding target genes.

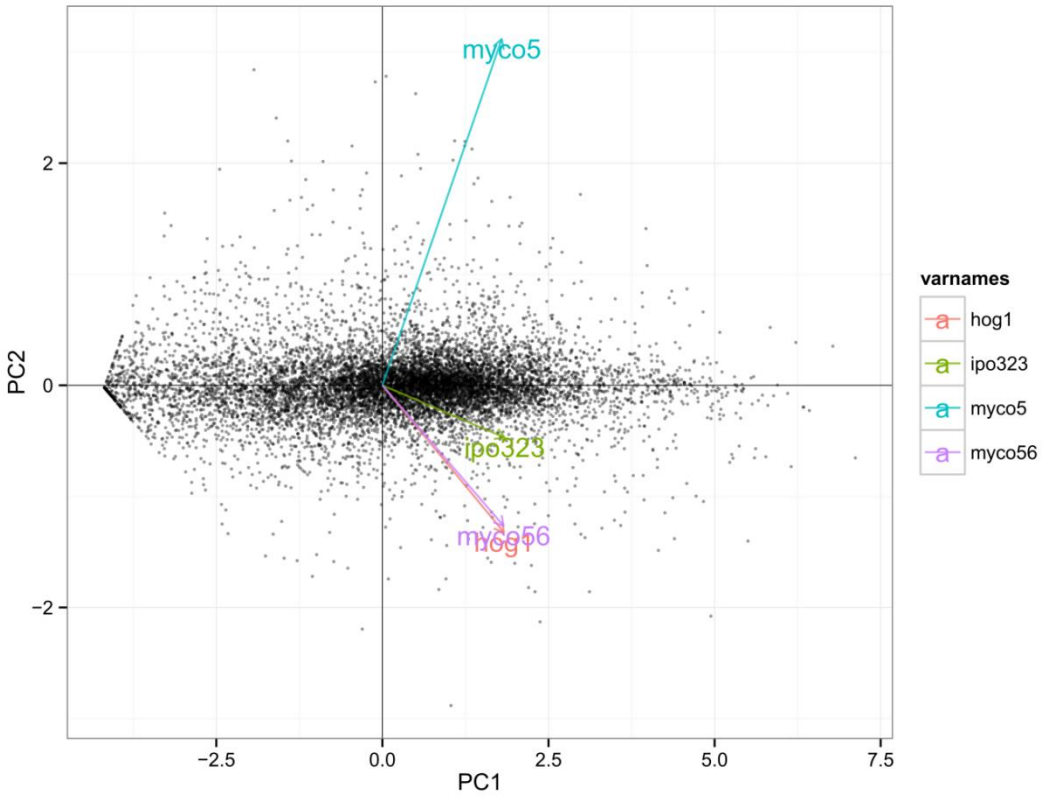

Figure S13: Principal components analysis (PCA) of provided gene expression profiles of investigated mutants obtained from RNA-Seq analysis. PCA reduces the dimensionality of RNA-Seq data by using linear combinations of the gene expression values to define a new set of unrelated variables (principal components). Thus, it allows clustering and visualizing the relationship between the gene profiles by their variance and description of data sets with a reduced number of variables. These new variables are orthogonal to each other, avoiding redundant information. According to this analysis *ΔZthog1*, *Δmyco56* and IPO323 form one cluster, indicating a similarity concerning their gene expression profiles and are distinguishable from that of *Δmyco5*. ("varnames" used: ipo323 for the reference strain IPO323, hog1 for the mutant strain *ΔZthog1*, myco5 for *Δmyco5* and myco56 for *Δmyco56*).

Table S7: RNA-Seq analysis with the target mutant strains *Δmyco5*, *Δmyco56*, *ΔZthog1* and wildtype IPO323 upon nitrogen deprivation (after 7 days incubation). Indicated are the Protein IDs according to JGI, the FPKM values resulted from CuffDiff analysis, the best match to known proteins (BLASTp, NCBI), the predicted fuction after Blast2GO analysis designated as customized category, SignalP 4.1 prediction results and PHI-Base interrogation results. PHI-Base Pathogen Host Interactions database, contains expertly curated molecular and biological information on genes proven to affect the outcome of pathogen-host interactions (accessible at: http://www.phi-base.org/). The following color scheme for PHI-base terms was used: red color indicates "Loss of pathogenicity", orange "reduced virulence" and green "increased virulence or unaffected pathogenicity".

Protein ID (JGI)	IPO323 (FPKM)	*Δmyco5* (FPKM)	*Δmyco56* (FPKM)	*ΔZthog1* (FPKM)	Description (best hit according to BLASTp analysis against "nr" database)	E-value	category (customized)	SignalP 4.1 (secreted?)	PHI-Base (4.0) terms (best hit according to BLASTp analysis; threshold E-value: 1E-30)
110285	14.13	3.53859	3.3637	51.5345	hypothetical protein	no	unknown	0.553	
107442	38.6197	50.7448	890.46	44.6045	hypothetical protein	no	unknown	-	
105608	186.764	110.137	1576.14	1519.55	hypothetical protein	no	unknown	-	
105419	7.54079	11.3583	108.244	8.1349	small threonine-rich protein - specific [*Zymoseptoria tritici* IPO323]	2.00E-21	unknown	0.831	
66947	62.1437	0	63.5835	59.8027	hypothetical protein	no	unknown	-	
61630	68.1566	1021.26	22.2648	13.258	CipC protein [*Beauveria bassiana* ARSEF 2860]	2.00E-41	unknown	-	
104715	845.237	108.557	2089.7	2193.37	MFS peptide transporter [*Aspergillus kawachii* IFO 4308]	0	Transport	-	Ptr2_Phaeosphaeria_nodorum_(related:_Stagonospora_nodorum)
84460	124.746	11.4651	196.466	349.651	ATPase P-type Cu/Zn/Na/Ca/H-transporter [*Macrophomina phaseolina* MS6]	0	Transport	-	Calcium-transporting_ATPase_3_Magnaporthe_oryzae
74200	4588.28	322.777	2809.64	7910.01	Sugar/inositol transporter [*Macrophomina phaseolina* MS6]	0	Transport	-	
70129	82.0347	2.74879	1.81625	1.90241	amino acid transporter [*Colletotrichum gloeosporioides* Nara gc5]	7.00E-95	Transport	0.807	
69117	41.8675	15.8516	7.20771	2.59371	MFS transporter, SP family, sugar:H+ symporter [*Fusarium oxysporum*]	0	Transport	-	Srt1_Ustilago_maydis
68287	512.114	47.4414	508.786	794.444	sugar transporter [*Magnaporthe oryzae* 70-15]	0	Transport	-	
58641	117.76	1505.49	106.742	145.399	t-SNARE [*Sphaerulina musiva* SO2202]	3.00E-147	Transport	-	GzSYN1_Fusarium_graminearum_Reduced_virulence
109299	4.23654	28.9577	74.5928	7.20884	p53-like transcription factor [*Sphaerulina musiva* SO2202]	0	Transcription factor	-	
92404	3.27423	102.173	3.72659	3.02928	Tec1-like protein [*Zymoseptoria tritici* IPO323]	0	Transcription factor	-	TEC1_Candida albicans_Reduced_virulence
87993	5.74934	4.26903	42.8276	5.69164	transcription factor Cmr1 [*Pyrenophora tritici-repentis* Pt-1C-BFP]	0	Transcription factor	-	Amr1_Alternaria_brassicicola_Increased_virulence_(Hypervirulence)
96592	2.57465	3.88954	96.5995	3.47836	polyketide synthase [*Zymoseptoria tritici* IPO323]	0	Secondary metabolism	-	PKSP_Aspergillus_fumigatus_Reduced_virulence
87994	25.3668	34.4917	684.721	28.7174	ESC reductase [*Sphaerulina musiva* SO2202]	7.00E-160	Secondary metabolism	-	BUF1_Magnaporthe_oryzae_Loss_of_pathogenicity
68710	9.2054	9.91022	390.619	20.7514	1,3,6,8-tetra-HN reductase [*Sphaerulina musiva* SO2202]	1.00E-165	Secondary metabolism	-	BUF1_Magnaporthe_oryzae_Loss_of_pathogenicity
18775	31.0067	35.6135	1076.36	50.75	Scytalone dehydratase [*Zymoseptoria tritici* IPO323]	3.00E-115	Secondary metabolism	-	SCD1_Colletotrichum_lagenarium_Reduced_virulence
108506	22.5321	52.8377	274.438	16.5446	serine carboxypeptidase [*Zymoseptoria tritici* IPO323]	0	Proteolysis	0.635	
101415	14.1513	43.2293	87.9658	11.0058	SAP peptidase [*Pseudocercospora fijiensis* CIRAD86]	1.00E-172	Proteolysis	-	ACP_Candida_tropicalis_Reduced_virulence
99102	9.37118	122.611	12.6645	2.88595	aspartic endopeptidase Pep1 [*Aspergillus fumigatus* A1163]	3.00E-111	Proteolysis	-	
76021	27.8192	16.5219	91.5561	183.818	metalloprotease [*Sphaerulina musiva* SO2202]	5.00E-102	Proteolysis	0.843	MEP1_Coccidioides_posadasii_Reduced_virulence
72846	22.2136	10.34	45.7149	101.637	metalloprotease [*Sphaerulina musiva* SO2202]	9.00E-57	Proteolysis	-	MEP1_Coccidioides_posadasii_Reduced_virulence
71297	16.9508	164.21	19.9526	20.7343	proteinase [*Aspergillus niger* CBS 513.88]	4.00E-139	Proteolysis	-	
59604	89.0479	7.5346	194.068	99.8351	zinc carboxypeptidase A [*Sphaerulina musiva* SO2202]	0	Proteolysis	0.703	
43998	2177.26	182.211	497.657	1070.55	metalloprotease [*Sphaerulina musiva* SO2202]	2.00E-100	Proteolysis	-	MEP1_Coccidioides_posadasii_Reduced_virulence
43961	19.985	141.523	46.9411	27.4362	cysteine proteinase [*Aspergillus ruber* CBS 135680]	9.00E-152	Proteolysis	-	
34453	103.138	6.11321	214.051	44.7001	subtilase [*Zymoseptoria tritici* IPO323]	0	Proteolysis	0.734	SPM1_Magnaporthe_oryzae_Reduced_virulence
95327	16.3381	862.511	15.2086	16.3595	E3 ubiquitin protein ligase TOM1-like protein [*Chaetomium thermophilum* var. thermophilum DSM	4.00E-37	Protein modification	-	
51025	168.892	15.2231	392.347	370.879	beta-1,3 glucanosyltransferase [*Zymoseptoria tritici* IPO323]	0	Protein modification	0.661	GEL2_Aspergillus_fumigatus_Reduced_virulence
23658	0.585179	0.644726	11.6091	3.86588	catalase-like protein [*Ceraceosorus bombacis*]	3.00E-152	Oxidative stress	-	
102956	29.49	17.9949	338.343	206.462	Cu,Zn superoxide dismutase-like protein, partial [*Sphaerulina musiva* SO2202]	4.00E-41	Oxidative stress	0.820	
101235	62.2268	357.975	86.3628	21.6137	Cloroperoxidase [*Sphaerulina musiva* SO2202]	3.00E-174	Oxidative stress	0.822	
96677	31.9909	18.6919	449.089	11.2813	Cloroperoxidase [*Sphaerulina musiva* SO2202]	0	Oxidative stress	-	
94368	123.594	9.42399	125.002	55.308	Cloroperoxidase [*Sphaerulina musiva* SO2202]	3.00E-143	Oxidative stress	0.500	
74298	1804.84	218.149	103.523	35.1417	Cloroperoxidase [*Sphaerulina musiva* SO2202]	2.00E-163	Oxidative stress	0.775	
43487	77.5169	54.7066	25.1927	7.62675	Cloroperoxidase [*Sphaerulina musiva* SO2202]	3.00E-166	Oxidative stress	0.671	
109795	5.21449	305.356	18.3531	6.60444	FabD/lysophospholipase-like protein [*Sphaerulina musiva* SO2202]	0	Metabolism	-	
107391	62.5889	89.111	98.2086	15.4688	lysophospholipase Plb2 [*Sphaerulina musiva* SO2202]	0	Metabolism	0.487	PLB1_Candida_albicans_Reduced_virulence

(continued)

105080	30.6726	1534.7	16.6611	28.1385	triacylglycerol hydrolase [*Zymoseptoria tritici* IPO323]	9.00E-170	Metabolism	-	
81448	38.3712	1603.69	17.3133	34.1054	triacylglycerol hydrolase [*Zymoseptoria tritici* IPO323]	4.00E-58	Metabolism	0.693	
74078	168.347	25.5995	42.9741	88.7807	esterase/lipase [*Cladophialophora yegresii* CBS 114405]	0	Metabolism	0.700	
68922	127.918	13.6616	20.9847	19.4836	alpha-L-arabinofuranosidase axhA-2 [*Colletotrichum higginsianum*]	5.00E-149	Metabolism	0.706	
66294	53.5423	189.204	15.3187	36.8484	d-arabinitol 2-dehydrogenase [*Ophiostoma piceae* UAMH 11346]	2.00E-103	Metabolism	-	Mdh1_Phaeosphaeria_nodorum_(related:_Stagonospora_nodorum)
41969	52.0178	23.9762	29.9129	4.08442	lysophospholipase [*Marssonina brunnea* f. sp. 'multigermtubi' MB_m1]	1.00E-96	Metabolism	0.897	PLB1_Candida_albicans_Reduced_virulence
29873	167.298	26.6351	500.668	110.963	sterol esterase carbohydrate esterase family CE10 [*Colletotrichum higginsianum*]	1.00E-134	Metabolism	-	LIP1_Botrytis_cinerea_Unaffected_pathogenicity
109100	26.7912	71.1037	264.663	24.6167	cytochrome P450 [*Sphaerulina musiva* SO2202]	0	Metabolic Transformation	-	Related_to_O-methylsterigmatocystin_oxidoreductase_Gibberella_zeae
72602	259.806	908.742	136.567	74.7064	Alkylglycerol monooxygenase [*Fusarium oxysporum* f. sp. cubense race 1]	3.00E-161	Metabolic Transformation	-	
49735	56.2009	190.06	104.977	12.0264	cytochrome P450 [Sphaerulina musiva SO2202]	0	Metabolic Transformation	0.516	
38341	5.97507	391.372	7.41006	13.8854	UDP-glucuronosyl/UDP-glucosyltransferase [*Zymoseptoria tritici* IPO323]	0	Metabolic Transformation	-	CHIP6_Colletotrichum_gloeosporioides_Reduced_virulence
68344	17.8786	87.7367	16.9889	22.0173	DNA ligase 4 [*Coccidioides immitis* RS]	0	DNA Metabolism	-	LIG4_Candida_albicans_reduced virulence
110503	76.3459	71.7002	3.19077	72.839	RNA-binding protein Cip2 [*Marssonina brunnea* f. sp. 'multigermtubi' MB_m1]	9.00E-124	DNA Metabolism	-	
111130	461.574	39.7913	217.738	133.473	alpha-L-arabinofuranosidase [*Colletotrichum higginsianum*]	0	CWDE	0.790	
106779	25.0507	10.1316	83.5794	7.08085	glucan 1,3-beta-glucosidase precursor [*Pyrenophora tritici-repentis* Pt-1C-BFP]	6.00E-171	CWDE	0.672	
99379	3.82299	8.9125	43.5275	51.5959	chitinase [*Aspergillus fumigatus*]	6.00E-68	CWDE	0.713	
111657	166.127	297.019	363.317	14.1029	CFEM domain-containing protein [*Colletotrichum orbiculare* MAFF 240422]	3.00E-78	Cell Wall	0.672	PTH11_Magnaporthe_oryzae_Reduced_virulence
77055	461.555	15.9829	137.944	127.749	hydrophobic surface binding protein B [*Aspergillus oryzae*]	1.00E-30	Cell wall	0.828	
106573	179.744	266.555	526.678	4.08667	family A G protein-coupled receptor-like protein [*Sphaerulina musiva SO2202*]	1.00E-157	Cell signalling	-	
102785	10.9167	26.4409	128.226	67.6919	verprolin [*Pyrenophora tritici-repentis* Pt-1C-BFP]	3.00E-104	Cell signalling	-	
102068	135.675	316.4	1707.29	714.145	GTP-binding protein EsdC [*Colletotrichum higginsianum*]	5.00E-48	Cell signalling	-	
76502	271.281	248.051	233.365	15.2237	MAP kinase Hog1p [*Zymoseptoria tritici* IPO323]	0	Cell signalling	-	Hog1_Cochliobolus_heterostrophus_Reduced_virulence
62856	54.5492	37.3717	611.434	214.025	Myb-like DNA-binding protein [*Pyronema omphalodes* CBS 100304]	4.00E-53	Cell signalling	-	GzFlbD_Gibberella_zeae_(related:_Fusarium_graminearum)
36575	417.234	33.7421	20.8306	24.8928	protein kinase domain protein [*Aspergillus clavatus* NRRL 1]	2.00E-59	Cell signalling	-	

Table S8: Comparative analysis of RNA-Seq data obtained from this study with publically available data obtained from previous studies derived from Yang *et al.*, 2013, Brunner *et al.*, 2013, Kellner *et al.*, 2014 and Rudd *et al.*, 2015. The most significantly up-regulated genes across the investigated strains are depicted in green, the down-regulated in red.

Protein ID (JGI)	Description (best hit according to BLASTp analysis against "nr" database)	IPO323 (FPKM)	Δmyco5 (FPKM)	Δ myco56 (FPKM)	ΔZthog1 (FPKM)
39898	aquaporin [*Sphaerulina musiva* SO2202]	549.536	216.701	198.042	3.22396
40311	monooxygenase [*Marssonina brunnea* f. sp. 'multigermtubi' MB_m1]	13.1775	32.607	4.32617	4.83675
49735	cytochrome P450 [*Sphaerulina musiva* SO2202]	56.2009	190.06	104.977	12.0264
54115	hypothetical protein	68.1847	59.0519	189.132	22.6154
59219	gamma-carboxymuconolactone decarboxylase [*Acidiphilium cryptum*]	391.239	448.25	225.279	66.8631
61630	CipC protein [*Beauveria bassiana* ARSEF 2860]	68.1566	1021.26	22.2648	13.258
61690	methyltransferase domain-containing protein [*Aspergillus kawachii* IFO 4308]	470.407	451.253	404.321	31.6863
63646	Similar to Heat shock protein hsp9; acc. no. P50519 [*Pyronema omphalodes* CBS 100304]	67.4331	106.629	398.668	51.0766
72883	alcohol oxidase [*Passalora fulva*]	4.957	7.8624	53.2553	7.01333
76071	phosphate-repressible phosphate permease [*Verticillium dahliae* VdLs.17]	60.6567	16.0432	41.638	193.768
78442	hypothetical protein	680.94	3980.14	1335.71	508.501
78859	hypothetical protein	121.504	1293.69	104.831	149.988
79738	hypothetical protein	1379.95	1737.26	1447.88	62.0477
82331	hypothetical protein	53.1536	42.1277	285.565	83.4238
89280	hypothetical protein	439.694	1283.34	930.465	20.451
97057	hypothetical protein	7.59355	6.15755	90.6693	4.71592
97372	hypothetical protein	82.2995	571.656	82.4657	89.6057
102108	hypothetical protein	29.8917	26.0472	132.817	172.507
102341	beta-glucanosyltransferase [*Zymoseptoria tritici* IPO323]	163.597	986.234	90.7826	97.7283
102657	hypothetical protein	211.404	332.848	283.528	32.3409
103427	hypothetical protein	2.40576	121.674	11.8477	2.59686
103460	Ferritin/ribonucleotide reductase-like protein [*Macrophomina phaseolina* MS6]	764.607	160.182	3210.32	2332.38
103760	D-arabinitol 2-dehydrogenase [*Pyrenophora tritici-repentis* Pt-1C-BFP]	54.7537	205.572	88.7439	26.7973
104299	tyrosinase [*Zymoseptoria tritici* IPO323]	39.7574	79.0825	355.99	180.37
104444	hypothetical protein	84.018	30.0313	61.617	330.321
104758	hypothetical protein	60.5515	23.8547	172.282	57.4455
105182	hypothetical protein	1101.96	304.016	735.894	82.6818
105661	hypothetical protein	366.478	305.017	655.649	25.9987
105791	aldehyde dehydrogenase [*Sphaerulina musiva* SO2202]	8998.19	3590.62	11698.4	16205.3
106037	hypothetical protein	5.55365	1338.33	9.70826	4.7686
106329	hypothetical protein	312.722	12.601	1078.76	233.282
106335	hypothetical protein	2763.41	82.3477	9924.33	2345.6
106452	related to cell wall glycoprotein [*Claviceps purpurea* 20.1]	8.14558	78.4578	62.6951	7.83113
106843	hypothetical protein	477.853	326.467	550.206	9.1945
107781	hypothetical protein	24.5588	63.5981	155.646	75.7964
108499	von Willebrand and RING finger domain containing protein [*Pyrenophora tritici-repentis* Pt-1C-BFP]	19.3878	160.284	13.6464	14.6519
108912	hypothetical protein	497.257	939.696	946.382	39.8035
109621	TOS1 [*Ajellomyces dermatitidis* ATCC 18188]	4.10121	46.9128	13.2525	12.59
109761	hypothetical protein	47.1996	15.3064	220.189	5.38889
109777	hypothetical protein	9.44393	1911.98	9.39186	17.3473
111657	CFEM domain-containing protein [*Colletotrichum orbiculare* MAFF 240422]	166.127	297.019	363.317	14.1029
106779	glucan 1,3-beta-glucosidase precursor [*Pyrenophora tritici-repentis* Pt-1C-BFP]	25.0507	10.1316	83.5794	7.08085
68922	alpha-L-arabinofuranosidase axhA-2 [*Colletotrichum higginsianum*]	127.918	13.6616	20.9847	19.4836
74252	plant senescence-associated protein [*Sphaerulina musiva* SO2202]	199.471	255.449	1726.37	279.305

Yang (2013) + Rudd (2015) + RNA-Seq (this study)

Brunner (2013) + Yang (2013) + Rudd (2015) + RNA-Seq (this study)

Brunner (2013) + Kellner (2014) + Rudd (2015) + RNA-Seq (this study)

Yang (2013) + Kellner (2014) + RNA-Seq (this study)

(continued)

23191	MFS general substrate transporter [*Sphaerulina musiva* SO2202]	692.769	25.4898	435.715	135.449	Kellner (2014) + Rudd (2015) + RNA-Seq (this study)
38075	Acyl-CoA dehydrogenase NM [*Glarea lozoyensis* ATCC 20868]	6.17573	64.1815	8.87318	12.5057	
41244	major facilitator superfamily transporter [*Colletotrichum graminicola* M1.001]	55.5397	15.4838	106.082	14.6924	
43383	salicylate hydroxylase [*Capronia coronata* CBS 617.96]	5.71817	9.524	79.1299	26.8503	
43487	Cloroperoxidase [*Sphaerulina musiva* SO2202]	77.5169	54.7066	25.1927	7.62675	
49829	sulfate transporter 4.1 [*Verticillium dahliae* VdLs.17]	3.64322	20.8392	51.7828	3.07444	
63214	acetoin reductase [*Colletotrichum fioriniae* PJ7]	281.804	17.334	298.157	582.274	
63538	oxidase [*Marssonina brunnea* f. sp. 'multigermtubi' MB_m1]	144.425	15.3304	229.88	159.872	
64595	Sugar/inositol transporter [*Macrophomina phaseolina* MS6]	25.4397	7.2431	134.895	6.67091	
70577	siderophore iron [*Colletotrichum orbiculare* MAFF 240422]	19.3624	24.3239	7.37781	65.6757	
72602	Alkylglycerol monooxygenase [*Fusarium oxysporum* f. sp. cubense race 1]	259.806	908.742	136.567	74.7064	
72846	metalloprotease [*Sphaerulina musiva* SO2202]	22.2136	10.34	45.7149	101.637	
76021	metalloprotease [*Sphaerulina musiva* SO2202]	27.8192	16.5219	91.5561	183.818	
82765	3-oxoacyl-(acyl-carrier-protein) reductase [*Pyrenophora tritici-repentis* Pt-1C-BFP]	9.03977	13.8402	66.4231	9.08397	
90843	hypothetical protein	34.9314	474.776	46.7334	103.793	
92432	hypothetical protein	62.5184	3.63322	51.358	103.758	
92901	hypothetical protein	239.979	10.0542	155.571	311.171	
99379	chitinase [*Aspergillus fumigatus*]	3.82299	8.9125	43.5275	51.5959	
100089	polyketide synthase [*Zymoseptoria tritici* IPO323]	122.627	36.0135	42.674	8.54671	
100990	Glutathione-dependent formaldehyde-activating family GFA [*Macrophomina phaseolina* MS6]	96.3046	56.2987	74.835	10.4384	
101477	Siderophore iron transporter 1 [*Penicillium roqueforti*]	39.1246	30.8716	31.1387	249.76	
101835	hypothetical protein	698.843	34.4456	630.716	136.004	
104337	Serine hydrolase FSH [*Penicillium roqueforti*]	124.204	20.1477	8.2715	3.7614	
104571	phosphatidylethanolamine-binding-like protein [*Zymoseptoria tritici* IPO323]	831.86	23.5532	2634.58	281.128	
104715	MFS peptide transporter [*Aspergillus kawachii* IFO 4308]	845.237	108.557	2089.7	2193.37	
105608	hypothetical protein	186.764	110.137	1576.14	1519.55	
106445	hypothetical protein	11.9319	110.616	14.4368	21.3639	
43176	steroid monooxygenase [*Sphaerulina musiva* SO2202]	4.57501	1.7158	17.6818	418.714	Yang (2013) + Kellner (2014) + Rudd (2015) + RNA-Seq (this study)
46257	hypothetical protein	51.8611	141.584	256.784	0	
70541	fatty acid hydroxylase superfamily protein [*Aspergillus kawachii* IFO 4308]	63.6316	128.187	35.4332	6.61076	
74298	Cloroperoxidase [*Sphaerulina musiva* SO2202]	1804.84	218.149	103.523	35.1417	
77055	hydrophobic surface binding protein B [*Aspergillus oryzae*]	461.555	15.9829	137.944	127.749	
77672	alpha/beta-hydrolase [*Aspergillus ruber* CBS 135680]	364.855	83.0221	886.896	282.197	
94368	Cloroperoxidase [*Sphaerulina musiva* SO2202]	123.594	9.42399	125.002	55.308	
96677	Cloroperoxidase [*Sphaerulina musiva* SO2202]	31.9909	18.6919	449.089	11.2813	
99917	secreted small proline-rich-protein [*Zymoseptoria tritici* IPO323]	283.194	124.143	1352.83	656.696	
101235	Cloroperoxidase [*Sphaerulina musiva* SO2202]	62.2268	357.975	86.3628	21.6137	
102956	Cu,Zn superoxide dismutase-like protein, partial [*Sphaerulina musiva* SO2202]	29.49	17.9949	338.343	206.462	
109991	hypothetical protein	6.50952	1638.52	7.05825	8.21801	
61141	Endo-1,4-beta-xylanase [*Fusarium oxysporum* f. sp. cubense race 4]	353.196	37.5712	262.466	304.144	Brunner (2013) + Rudd (2015) + RNA-Seq (this study)
65051	glycoside hydrolase family 115 protein [*Baudoinia compniacensis* UAMH 10762]	38.9354	14.9359	102.656	52.8558	
111130	alpha-L-arabinofuranosidase [*Colletotrichum higginsianum*]	461.574	39.7913	217.738	133.473	

Curriculum Vitae

Personal data

Name:	Alexander Yemelin
Date of birth:	19.10.1986
Place of birth:	Nikolaev, Ukraine
Nationality:	German

Academic education

2011 – 2017	**Research associate / Doctoral studies** (Institute of Biotechnology and Drug Research, Kaiserslautern / Johannes Gutenberg-Universität Mainz) Supervisor: Prof. Dr. Eckhard Thines; Dissertation: „Identification and characterization of novel factors involved in dimorphism and pathogenicity of fungal wheat pathogen *Zymoseptoria tritici*“
since 2012	**TU Kaiserslautern, Informatics (Bachelor study)**
2006 – 2011	**Diploma studies, Biology** (Technische Universität Kaiserslautern) Supervisor: Dr. A. J. Foster; Diploma thesis: "Identifizierung und Charakterisierung von Acr1p-abhängigen Genen im Reisbranderreger *Magnaporthe grisea*"
2005 – 2006	**TU Kaiserslautern, Mathematics (Diplom study)**

School education

1993 – 2005	**High school graduation (Abitur)** (Heinrich Heine Gymnasium, Kaiserslautern)

List of publications:

Breth, B., Odenbach, D., Yemelin, A., Schlinck, N., Schröder, M., Bode, M., Antelo, L., Andresen K., Thines, E., Foster, A. J. (2013). The role of the Tra1p transcription factor of *Magnaporthe oryzae* in spore adhesion and pathogenic development. *Fungal Genetics and Biology, 57*, 11-22.

Jacob S., Foster A., Yemelin A., Thines E. (2014). Histidine kinases mediate differentiation, stress response, and pathogenicity in *Magnaporthe oryzae*. *MicrobiologyOpen 2014*; *3*(5): 668–687.

Jacob, S., Foster, A. J., Yemelin, A., Thines, E. (2015). High osmolarity glycerol (HOG) signalling in *Magnaporthe oryzae*: Identification of MoYPD1 and its role in osmoregulation, fungicide action, and pathogenicity. *Fungal biology*, *119*(7), 580-594.

Jacob, S., & Yemelin, A. (2016). Stress Biology in Fungi and "Omic" Approaches as Suitable Tools for Analyzing Plant–Microbe Interactions. *Host-Pathogen Interaction: Microbial Metabolism, Pathogenicity and Antiinfectives*, 153-178.

Jacob, S., Yemelin, A., Bohnert, S., Andresen, K., Thines, E. (2017). The exceptionality of stress response in *Magnaporthe oryzae*: a set of "salt stress-induced" genes unique to the rice blast fungus. *Journal of Plant Diseases and Protection*, 1-4.

Matheis, S., Yemelin, A., Scheps, D., Andresen, K., Jacob, S., Thines, E., Foster, A. J. (2017). Functions of the *Magnaporthe oryzae* Flb3p and Flb4p transcription factors in the regulation of conidiation. *Microbiological Research*, *196*, 106-117.

Yemelin, A., Brauchler, A., Jacob, S., Laufer, J., Heck, L., Foster, A. J., .Antelo, L., Andresen, K. and Thines, E. (2017). Identification of factors involved in dimorphism and pathogenicity of *Zymoseptoria tritici*. *PloS one*, *12*(8).

Yemelin, A., Brauchler, A., Jacob, S., Laufer, J., Antelo, L., Andresen, K., Foster, A. J. and Thines, E. (2017). Random T-DNA insertional mutagenesis identifies two novel dimorphism-related genes as virulence factors of *Zymoseptoria tritici*. (submitted to PLoS pathogens)

Poster/talks:

"Identification of novel factors involved in dimorphism and pathogenicity of *Zymoseptoria tritici*"

(Annual Meeting of the Association for General and Applied Microbiology (VAAM), Jena (2016))
(13th European Conference on Fungal Genetics, Paris (2016))

Funding:

This work was supported by a grant from the "Stiftung Rheinland-Pfalz für Innovation".